Formation mechanisms and control of biofouling in submerged MBRs

Luo, Jinxue

2015

Luo, J. (2015). Formation mechanisms and control of biofouling in submerged MBRs. Doctoral thesis, Nanyang Technological University, Singapore.

https://hdl.handle.net/10356/62182

https://doi.org/10.32657/10356/62182

NANYANG TECHNOLOGICAL UNIVERSITY

Formation mechanisms and control of biofouling in submerged MBRs

School of Biological Sciences
Nanyang Technological University
Singapore

2015

Formation mechanisms and control of biofouling in submerged MBRs

BY

JINXUE LUO

SCHOOL OF BIOLOGICAL SCIENCES

A thesis submitted to the Nanyang Technological University in partial fulfillment of the requirement for the degree of Doctor of Philosophy

2015

Acknowledgements

I would like to express my deep gratitude to my co-supervisor, Assoc Prof. Scott A. Rice, for his continued support, supervision and guidance during the 4 years of my Ph.D program. I am indebted for his patience and kindness throughout my Ph.D project. Without his consistent and illuminating instruction, this thesis could not have reached its prese nt form.

I would like to express my deep gratitude to my supervisor, Prof. Yehuda Cohen, for his supervision and guidance during my Ph.D time. I cherish the chance that he offers to me to pursue my dream.

I would like to express my deep gratitude to my co-supervisors Prof Law Sai-Kit Alex and Prof. Guoqiang Zhuang in Chinese Academy of Sciences, for their support and encouragement for my research in Nanyang Technological University, Singapore.

I would like to express my deep appreciation to Dr. Jinsong Zhang in Singapore Membrane & Technology Center for his support and guidance in engineering aspect of my project.

I would like to express my deep appreciation to Dr. Torsten Thomas in University of New South Wales for his help in the bioinformatics. I would like also to show my appreciation to Miss Tan Xiaohui for her help in my experiments. Her assistance is greatly acknowledged.

I am grateful to my fellow laboratory mates, Chen Xi, Goh Shuwen, Manisha Mukherjee, Zhang Qiaoyun, Hu Jie, Feng Shugeng, Huang Wenhai, Stanny Ong, Grant Tan Chuan Hao, Yogananda Maspolim, Harish Venkatakrishnan and all the AEBC members for their help and providing a friendly and conducive working atmosphere.

Finally, I want to show my deep love to my wife and my parents for their love, understanding and consistent encouragement throughout my study.

Table of Contents

List of Figures

List of Tables

Abbreviations

α	Alpha
β	Beta
γ	Gamma
AHLs	*N*-acyl homoserine lactone autoinducers
AIs	Autoinducers
BAP	Biomass-associated products
C6-HSL	*N*-hexanoyl-DL-homoserine
C8-HSL	*N*-octanoyl-DL-homoserine lactone
CA	Cellulose acetate
CLSM	Confocal laser scanning microscopy
Con-A	Concanavalin A
d	Day
EPS	Extracellular polymeric matrix
FITC	Fluorescein-5-isothiocyanate
FISH	Fluorescent *In Situ* Hybridization
FTIR	Fourier transform infrared spectroscopy
HCl	Hydrochloric acid
HF	Hollow fiber
H_2O_2	Hydrogen peroxide
HRT	Hydraulic retention time
LMH	$L.m^{-2}.h^{-1}$

MBR	Membrane bioreactor
MLSS	Mixed liquor suspended sludge
NaClO	Sodium hypochlorite
NaOH	Sodium hydroxide
NMDS	Nonmetric Multidimensional Scaling
NO	Nitric oxide
O_3	Ozone
OTUs	Operation taxonomic units
PAC	Powdered activated carbon
PBS	Phosphate buffered saline
PCR	Polymerase chain reaction
PROLI NONOate	1-(hydroxy-NNO-azoxy)-L-proline, disodium salt
PVDF	Polyvinylidene fluoride
QS	Quorum sensing
r	Pearson’s correlation coefficients
rRNA	Ribosomal RNA
SEM	Scanning electron microscopy
SMP	Soluble microbial products
SNP	Sodium nitroprusside
TOC	Total organic carbon
TMP	Transmembrane pressure
UAP	Utilization-associated products

WWTP	Wastewater treatment process

Abstract

Membrane bioreactors (MBRs) are increasingly being applied in modern wastewater treatment plants. Biofouling of the MBRs represents a significant challenge in the application of membrane based technologies for water purification. Biofouling is the build-up of organic and biological cake-layers on the membranes that may block the membrane pores. The biofouling layers will reduce membrane permeability and increase the hydraulic resistance of the membrane. Thus, membrane fouling results in an increase of the trans-membrane pressure (TMP) when operated at a constant flux or a decreased flux when operated at a constant pressure. Therefore, it is necessary to identify the relative contribution of microbes and macromolecules to the biofouling process in order to develop appropriate strategies to reduce fouling and hence increase operational efficiency.

Two identical laboratory-scale MBRs were operated at a low, constant flux (13 - 15 LMH) to treat artificial synthetic wastewater (TOC of 200 mg/L). The TMP was maintained at a low pressure (3 - 15 kPa), steady state for the first 80 - 87 d of operation and then was observed to increase exponentially from 15 to 90 kPa over 30 d. The biofouling layers on the hollow fiber membrane surfaces were observed to contain significant amounts of α-polysaccharides, β-polysaccharides, proteins and microorganisms that were always present on the hollow fiber membranes, even during the early stages of MBR operation when the TMP was still in the low pressure phase (Chapter 2). Quantitative image analysis indicated that each of these components on membrane correlated positively with the TMP increase, Pearson's correlation coefficients 0.7 - 0.95. Among the four components, the proteins increased fastest when the TMP was rapidly increasing and comprised the greatest proportion of the individual components when TMP increased. This indicated that the production of proteins was more important than the two types of polysaccharides or the cells during the transition of TMP from the low to high TMP stage. Additionally, co-localization analysis revealed that approximately 50% of the EPS co-localized with 80 - 90% of the cells. The co-localization data indicated that the majority of the EPS components were closely associated with the cells, suggesting that the EPS components may be the byproducts of microorganisms on membrane rather than being randomly distributed on the membrane from the aqueous phase. Therefore, the formation of microbial biofilms on the membranes is the key driver of the biofouling process in MBRs. Thus, it is vital to develop methods to prohibit or reduce biofilm formation on the membranes *in situ* or to disperse the mature biofilms.

As part of the development of novel strategies to control biofilms on membranes, it is also

essential to determine if the biofilm is formed by a selected subset of microorganisms in the sludge community or if biofilm formation is a stochastic process. Therefore, the microbial biofilm community, including bacteria (Chapter 3) and fungi (Chapter 4), were investigated through 16S and ITS tagged pyrosequencing at different stages of the fouling process. At low TMP, the biofilms were most highly similar to the sludge and as the biofilm developed and the TMP increased, the biofilm communities diverged from the sludge. Ultimately the biofilm community appeared to be distinct from the sludge and the greatest differences were seen for the bacterial community. In contrast, the fungal communities were overall less diverse and showed only minor differences in relation to the sludge. This was mostly seen in subtle shifts in the percentage composition of individuals, while the community was still dominated by the same groups. It was noted that the correation between the richness of biofilm bacterial community and TMP increase was not evident in this study. Compared to the sludge community, the bacteria including *Burkholderiales*, *Pseudomonadales* and *Rhizobiales* and fungi including the *Archaeosporales* and *Hypocreales* were enriched in the biofilm, indicating these microorganisms were more fit when growing as biofilm compositions relative to the growth and competition in the planktonic sludge. Additionally, during the process of TMP increase, the *Alphaproteobacteria*, represented by *Rhodospirillales*, *Sphingomonadales* and *Rhizobiales* in this project, and the fungi including *Saccharomycetales* and *Hypocreales* became more dominant in the late stage biofilms, indicating these organisms may contribute more to the construction of late rather the early biofilm and may play an important role to the TMP increase in the biofouling process. These results indicated that the change of microbial community that occurred before the TMP jump may be the most important in its effect on biofouling process. It may be possible to target those organisms to ultimately delay their incorporation into the biofilm and hence delay the TMP jump.

Finally, strategies based on nitric oxide (NO) induced biofilm dispersal were tested to control biofilm formation and TMP increase in the MBR (Chapter 5). The potential for NO to control biofilms in MBR systems was tested using two distinct approaches. The first was to disperse pre-established, mature biofilms that had developed during MBR operation and the second was to prevent biofilm accumulation by applying the NO from the beginning of the MBR operation. The results showed that treatment using the NO donor PROLI NONOate resulted in a 50% (in pre-established biofilm dispersal experiment) and 28.2% (in the biofilm prevention experiment) reduction of fouling resistance. The CLSM analysis showed that, in the biofilm prevention experiment, the NO treatment also resulted in a reduction of biofilm biomass, for both cells (66.7% reduction) as well as macromolecules (e.g. 37.7% reduction for proteins).

Analysis of the community composition indicated that the bacterial Orders of *Thiotrichales*, *Gemmatimonadales* and *Xanthomonadales* and fungal Orders of *Hypocreales* and *Glomerales* were reduced in abundance after the PROLI NONOate treatment. Furthermore, the development of the community associated with the late stage biofilm was delayed, but not entirely prevented, as a consequence of the PROLI treatment. These results demonstrated that the NO donor PROLI NONOate had the potential to control biofouling in MBRs.

Chapter 1 Literature Review

1.1 Wastewater treatment process

The issue of how to best manage sewage, which refers to municipal and industrial wastewater, is increasingly challenging due to population booms, urbanization and increasing industrialization. The current wastewater treatment processes were developed in the 1920s (Porter, 2010). Generally, a complete process for wastewater treatment (Fig. 1.1) includes 4 units: physical treatment, chemical treatment, biological remediation and a final liquid-solid separation process.

A physical treatment step is applied to remove the large, biologically undigestable or recalcitrant materials (e.g. plastic bags, solid refuse and even dead animals) from the sewage. The methods in the physical treatment unit include sedimentation, floatation and skimming and barrier screening (Wang et al., 2004). Sedimentation is related to the settling of solid substances by gravity, while flotation is used to eliminate the solids with a density lower than water by dissolving air under pressure in the wastewater (J. Rubio and Rosa, 2007). Barrier screening, just as the name implies, is a technique that passes the wastewater through a filtration medium, such as sand filters or rotary dewatering screen separators, and separates the solids and water (Cantrell et al., 2007). Chemical treatment unit is a process to remove organics as well as harmful substances, such as arsenic, cyanide, phenol and household detergents and bacteria from wastewater (Wu et al., 2011). The methods in the chemical treatment process are different based on the properties of the pollutants in the wastewater, such as coagulation, adsorption, ion exchange, chlorination, ozonation and neutralization (Avsar and Batibay, 2010; Wu et al., 2011).

However, expenditure for the chemical process of wastewater is usually very high (Jangkorn et al., 2011)and the overused chemicals used may also pose an environmental risk. Therefore, an alternative method, biological treatment, was used to degrade the dissolved organics and toxic substances in the wastewater through microbial activity. The microbes, which normally form the activated sludge, utilize the organics as nutrients and convert them to the stable end products, such as carbon dioxide, water and biomass (Khan et al., 2013; Show et al., 2013). Inorganic substances in the wastewater, e.g. metals, can also be accumulated within the microorganisms (Li et al., 2013; Raja and Omine, 2012). The biological treatment for wastewater is divided into aerobic and anaerobic degradation based on the demand for dissolved oxygen. Many technologies have been designed based on the biological aerobic or

anaerobic digestion, such as oxidation ponds, lagoons, trickling filters, and activated sludge processes (Bal and Dhagat, 2001). The activated sludge process is the most prevalent in modern wastewater treatment plants.

The last step of wastewater process is liquid-solid separation. The purpose of this step is to remove the biomass or sludge from the treated wastewater before the water is released or reused. In a biological wastewater treatment process, the traditional liquid-solid separation methods are designed based on the density difference between the sludge and water, which includes sedimentation tank (Salim et al., 2013), dissolved air flotation (DAF) (Kiuru, 2001) and screening, e.g. rotary dewatering screen separators (Bergheim et al., 1993). However, the gravity based separation process requires more space and longer time and may lead to a high number of bacteria in the effluent. Thus, in order to enhance the efficiency and effluent quality, membrane filtration based liquid-solid separation technologies, e.g. membrane bioreactors, were emerged in the wastewater treatment, which is described in the following section.

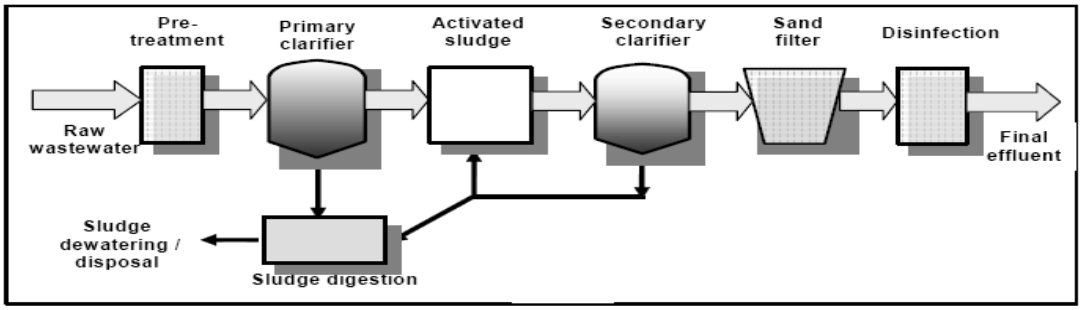

Fig. 1.1 Schematic of a typical conventional wastewater treatment technology. The Figure is adapted from Cicek et al., 2003 **(Cicek, 2003).**

1.2 Membrane Bioreactors

The membrane bioreactor (MBR) technology is a combination of the biological degradation process that utilizes a standard activated sludge for the biological removal of carbon and nutrients and a direct solid–liquid separation by membrane filtration (Fig. 1.2) (Mutamim et al., 2013). As noted above, a traditional wastewater treatment plant relies on sedimentation to separate the activated sludge from the purified water. In contrast, in the MBR plant, the separation of purified water from the biomass is accomplished by using filtration membranes instead of the settling tank. Membranes used in water purification and separation processes are defined as semipermeable films, which control the selective transfer of mass from one bulk phase to another bulk phase and separate the influent into retentate and permeate (Fig. 1.3). They can be classified into microfiltration (MF), ultrafiltration (UF), nanofiltration (NF),

and reverse osmosis (RO) membranes on the basis of pore structure and the filtration applications (Viessman et al., 2008). Pore size of MF membranes ranges from 0.1 - 100 µm. The pressure of MF membranes usually ranges from 20 - 250 kPa. The UF membranes have pore sizes ranging from 0.005 - 100 µm and can be operated between 30 - 300 kPa. NF membranes can be used to filter small organic molecules as well as dissolved ions, but have low rejection to monovalent ions, e.g. Na^+. The pressure for NF membranes is in the range of 300 – 1,000 kPa. The RO membranes have sub-nanometer pores and can be used to remove small organic molecules and dissolved ions, including the monovalent ions, e.g. Na^+. The pressure for RO membranes is very high (> 1,000 kPa). Compared to traditional wastewater treatment technique (Fig. 1.1), there are many advantages in MBRs (Fig. 1.2), including reducing the treatment space, which saves on capital expenditure, higher biomass concentration, higher quality of effluent and less sludge production (Melin et al., 2006). However, there is an intrinsic problem in MBR technology blocking its wider application in the world, which is membrane fouling.

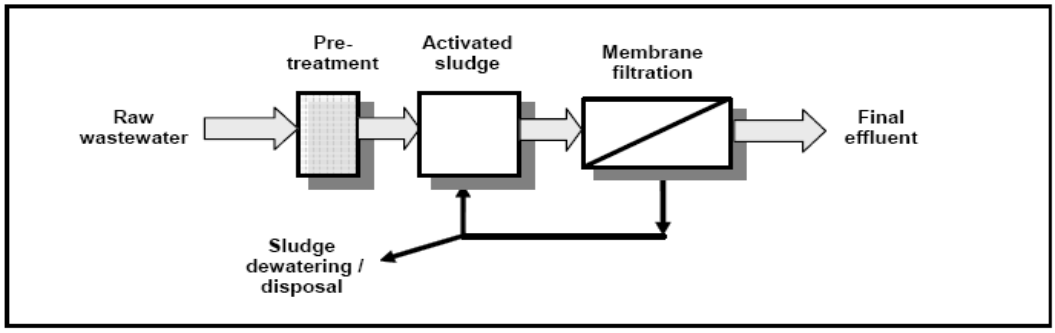

Fig. 1.2 Schematic of a typical membrane bioreactor (MBR). The Figure is adapted from Cicek, 2003 .

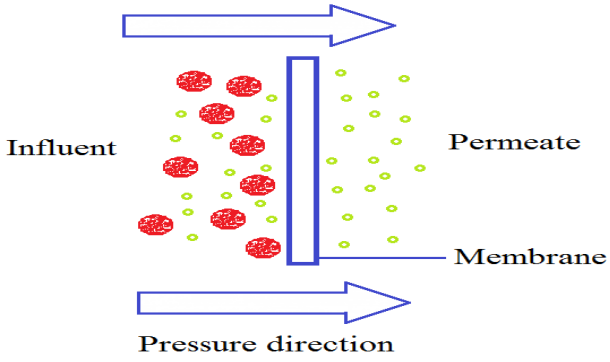

Fig. 1.3 Schematic of membrane based filtration. Arrows indicate the direction of hydrostatic pressure, from high to low. The influent is represented by water molecules and some organics with low molecule weight (small circles) and some macromolecule compounds and ions (large circles).

1.3 Membrane fouling

Membrane fouling is the deposition of substances on the membrane surface or into the membrane pores, reducing the water permeability of membranes. Based on the nature of the foulants, fouling can be classified as scaling (or precipitation fouling), colloidal fouling, and biofouling (Le-Clech et al., 2006). Scaling comes from the crystallization of solid salts, oxides and hydroxides on the membrane surface, e.g. $CaCO_3$ and $Mg(OH)_2$ (J. Moghadasi, 2007). Colloidal fouling is mediated by particles in the size range from 1 nm to 1 μm (J. Buffle, 1995). The colloidal foulants in water treatment systems include inorganic colloids (Tran T, 2007), such as clay minerals, silica, iron oxides/hydroxides, manganese oxides and aluminum, and organic macromolecules (Her et al., 2007), such as polysaccharides, proteins and humid acids. Biofouling is a term related to the undesirable deposition of a biological-layer on membrane surface. The essential process of biofouling is principally a consequence of microbial growth on the membrane surface (Vanysacker et al., 2014). It is now well understood that bacteria preferentially grow in the environment as surface associated communities which are encased in an extracellular polymeric matrix (EPS) and such a community is defined as a biofilm (Wei and Ma, 2013). Membrane fouling can be classified into three categories: removable fouling, irremovable fouling and irreversible fouling, based on their extent of attachment (Meng et al., 2009). Removable fouling, which is caused by loosely adhered precipitate, can be wiped off easily with physical cleaning, e.g. back flushing. In contrast, irremovable fouling consists of deposits within the membrane pores and is hard to remove through physical cleaning alone, and therefore requires the combination of chemical cleaning and physical methods. Irreversible fouling results from long-term operation and, as the name suggested, cannot be easily eliminated by either of the methods described above. It was reported that the long-term biofouling is a main reason for the development of irreversible fouling (Zhang et al., 2007). Membrane fouling may lead to many adverse effects on the efficient operation of the MBR, such as reduced flux or the need to increase transmembrane pressure (TMP) to maintain a constant flux rate. MBRs are usually operated at constant pressure or at constant flux. In this way, membrane fouling results in reduced productivity, increased treatment costs as well as shorter lifespan of membranes as a consequence of chemical cleaning of fouled membranes. Therefore, membrane fouling and its consequences restrict the widespread application of MBRs and it is essential to understand the fouling process in order to develop effective strategies to reduce or prevent fouling.

1.4 Biofouling in MBRs

1.4.1 Formation of biofouling in MBRs

In MBRs, as discussed above, membrane biofouling is a complicated phenomenon resulting from the aggregation and deposition of many organisms and their excretions on the membrane surface, leading to the reduction of permeation flux and rise of transmembrane pressure (TMP). Specifically, membrane biofouling is comprised of living microorganisms, extracellular polymeric substances (EPS) (Wang et al., 2009) and inorganic components that bind to the EPS and microbes. EPS consists of components such as polysaccharides, proteins, DNA and humic acids (Comte et al., 2006; Sponza, 2002), and may facilitate inorganic components of the sludge to also concentrate at the membrane surface. One of the functions of EPS is to form a matrix that helps to hold bacteria together within the biofilm (Laspidou and Rittmann, 2002). EPS can help microbes adhere to surfaces, aggregate, and acts as a protective barrier, which protects microorganisms from antimicrobials and predatory eukaryotes. The EPS matrix, by helping establish high density communities, may also facilitate interspecies interactions.

1.4.2 EPS compositions and contributions in biofouling process

As discussed above, the production of EPS is very important to the formation of biofouling formation (Rosenberger et al., 2006; Wang et al., 2009). Thus, the composition and roles of EPS have been studied extensively using a range of techniques including scanning electron microscopy (SEM), confocal laser scanning microscopy (CLSM) and Fourier transform infrared spectroscopy (FTIR) analysis (Meng et al., 2007) and chemical extraction methods (Liu and Fang, 2002). EPS is usually recognized to be either bound EPS or soluble EPS (Comte et al., 2006; Laspidou and Rittmann, 2002; Wang et al., 2009). Bound EPS is mainly composed of the microbially produced and cell surface bound polymers (Laspidou and Rittmann, 2002). Soluble EPS, as the name implies, is comprised of microbially produced soluble polymers, hydrolysis products of attached organic matter and organic molecules released into the bulk liquid phase, e.g. soluble macro-molecules, colloids and slimes (Comte et al., 2006). Recently, the soluble EPS has been renamed as soluble microbial products (SMP) (Janga et al., 2007; Laspidou and Rittmann, 2002). SMP can also be divided into two categories: substrate-utilization-associated products (UAP), which are produced as a consequence of substrate metabolism and biomass-associated products (BAP), which are released as a consequence of biomass lysis (Laspidou and Rittmann, 2002). There is a cyclic

correlation between bound EPS and SMP. Microbes acquire electrons from the electron-donor or substrate to build active biomass, in which bound EPS and utilization-associated products (UAP) are produced. Subsequently, part of the bound EPS can be hydrolyzed into biomass-associated products (BAP), while active biomass ultimately will undergo a nature death and decay process. Finally, UAP and BAP can be utilized by active biomass as recycled electron-donors substrates. It has been suggested that SMP, rather than bound EPS, associates with the biofilm first, to form the initial protective barrier (Comte et al., 2006). And in this way, it has been suggested that SMP plays a more important role in biofilm formation than bound EPS although this remains to be demonstrated. However, some studies have shown that the TMP increased and the MBR permeate was reduced when the amount of bound EPS increased (Cho et al., 2005; Wang et al., 2009). Recently, a study suggested that the bound EPS played a more significant role in the colonization of early biofouling while the SMP contributed more to the formation of late biofouling (Gao et al., 2013a). Thus, more work is needed to determine the role of the SMP and bound EPS in biofouling process.

Both the SMP and bound EPS are comprised of polysaccharides, proteins and nucleic acids (Comte et al., 2006; Meng et al., 2009). These polymers had been demonstrated to fill and block the membrane pores or to deposit on the membrane surfaces from the bulk phase, causing fouling and reducing the permeability (Rosenberger et al., 2006). However, no consensus has been agreed upon in their roles in the biofouling process. For example, there are different types of polysaccharides and it has recently been shown that *Alpha*-polysaccharides play an important function in the initial attachment of the biofilm onto the membranes, while the *Beta*-polysaccharides and proteins contributed to the construction of the mature biofilm structures (Chen et al., 2006a). However, it was also reported that the polysaccharides had a higher correlation to membrane permeability than proteins, though the proteins dominated the biofouling components (Gao et al., 2013b). Therefore, further work also needs to be done to elucidate the specific contributions of the biopolymers and bacteria involved in the fouling process.

1.4.3 Microbial community and contributions in biofouling process

As a group of biofouling components, the microbial community has also been studied extensively using fluorescence in situ hybridization (FISH) (Almeida et al., 2011) and sequencing methods, such as sanger sequencing (da Silva et al., 2014) and pyrosequencing (Liu et al., 2012), to determine their role in biofouling behavior. In a study on membrane biofouling in pilot-scale MBRs, the *Beta-*, *Gamma-*, *Delta-*, and *Alphaproteobacteria* were all

found to be associated with the biofilm and that the *Betaproteobacteria* were the most abundant bacteria groups (Miura et al., 2007). In a laboratory-scale submerged MBR, it was futher demonstrated that *Alpha-proteobacteria*, *Beta-proteobacteria* and *Bacteroidetes* were the dominant bacterial groups, while the *Nitrospira, Verrucomicrobia, Acidobacteria, Actinobacteria, Planctomycetes* and *Spirochaetes* represented the minority populations (Huang et al., 2008). Moreover, compared to the activated sludge, the *Alpha*proteobacteria and *Nitrospira* were enriched in the biofilm of this study (Huang et al., 2008). In contrast, it was reported that, in a drinking water distribution system in Shanghai, the *Betaproteobacteria* and *Gammaproteobacteria* were the key bacterial groups, though *Alphaproteobacteria*, *Bacteroides*, *Actinobacteria, Nitrospirae* and *Firmicutes* were also represented in the biofilm (Bai et al., 2010). In another study on membrane biofouling in pilot-scale MBRs, *Beta-*, *Gamma-*, *Delta-*, and *Alphaproteobacteria* were found to be associated with the biofilm and that the *Betaproteobacteria* were the most abundant bacteria groups (Miura et al., 2007). Thus, there is no consensus on the dominant bacteria in biofilms and whether there is a correlation between the increased TMP and specific microorganisms. Some dominant microbial groups in the biofouling process of MBR were summarized in Table 1.1.

In addition to bacteria, fungi are also an important group of organisms that can form the surface associated biofilms (James et al., 2011; Ramage et al., 2009). A wide spectrum of fungi has been reported to form biofilms, including *Candida* spp., *Saccharomyces* spp., *Cryptococcus* spp. and *Aspergillus* spp. (Bojsen et al., 2012; Chandrasekar and Manavathu, 2008; López-Ribot, 2005; Ravi et al., 2009). Additionally, the fungi can also form biofilms in combination with bacteria and other microbial groups. For example, investigation of the microbial biofilm community on sandstone in a Bayon temple in Cambodia showed that the biofilm microbial community was composed of bacteria, fungi, Metazoa and Alveolata (Lan et al., 2010). The fungal groups, such as Geotrichum, Penicillium and yeast and keratinophilic fungi (including *Chrysosporium* spp., *Microsporum* spp., *Trichophyton* spp. and *Aspergillus* spp.), were found to prevail in the anoxic and aerobic sludge (Awad and Kraume, 2010, 2011), indicating the fungi are a significant group of microbial community in activated sludge. It has been reported that fungi played important functions in activated sludge and MBR systems, such as phenol removal and degradation of azo dyes (Ahn et al., 2008; Hai et al., 2011; Hai et al., 2013). While much work to date has been undertaken to characterize the fungal community in the activated sludge system (Lim et al., 2012; Miura et al., 2007), more studies are required to investigate the role of the fungal community in the biofouling phenomenon in MBRs.

Table 1.1 The key microbial community in biofouling process in previous studies

Case of study	Key microbial community	material of membrane	Reference
1	Betaproteobacteria	PE	Miura et al., 2007
2	Proteobacteria (β, α subdivisions), Bacteroidetes	——	Huang et al., 2008
3	Proteobacteria (β, α, γ subdivisions)	PVDF	Muñoz et al., 2009
4	Proteobacteria (β, α and γ subdivisions) and Bacteroidetes	PA	Ivnitsky et al., 2009
5	Firmicutes, α-proteobacteria, Methanosarcinales, Methanospirillaceae	PVDF	Calderón et al., 2011
6	Gammaproteobacteria, Alphaproteobacteria, Bacteroidetes and Firmicutes	PVDF	Lim et al., 2012
7	Proteobacteria, Bacteroidetes, Planctomyces	——	Piasecka et al., 2013
8	Proteobacteria, Bacteroidetes	PVC	Ma et al., 2013
9	Proteobacteria, Bacteroidetes	PMMA	Gao et al., 2014

While it is known that EPS plays an important role in the biofouling on membranes, the contribution to biofouling of another component, microorganisms, was not clear. Currently, two hypotheses have been established to describe the process of biofouling. One hypothesis is that the deposition of biofouling layers is a consequence of filtration of extracellular polymeric substances (EPS) and microbes in the water onto the membrane to form a cake-layer (Lee et al., 2008). The alternative hypothesis is that microbes specifically attach onto the membrane to establish a biofilm and subsequently grow into EPS encased communities that ultimately block the membrane pores (Lee et al., 2008). Biofilms can be defined as populations of microorganisms attached to a surface, surrounded by an EPS matrix (O'Toole G, 2000). Biofilm formation initiates from the attachment of individual cells onto a surface. The transition of microorganisms from planktonic to the attached growth mode is influenced by the chemical nature of the environment, such as nutrient concentration or type, pH and temperature. Bacteria also express specific genetic pathways that facilitate surface attached growth, e.g. those associated with motility and adhesins. After the initial attachment, microbes will proliferate and spread on the surface. At the same time, EPS will be secreted and surround the organisms and this helps to cement the cells onto the surface. Subsequently, a flat

monolayer is formed. Finally, the mature biofilms, often with a complex 3-dimensional architecture are constructed. At this stage, the mature biofilms on MBR membranes may clog the pores and reduce the membrane permeability, resulting in the biofouling phenomenon. Thus, the result of biofilm formation on MBR membranes is the phenomenon of biofouling. At the end of the biofilm lifecycle, the microorganisms in mature biofilms may actively detach or disperse from the surface and reenter the free swimming or planktonic phase. These organisms may subsequently attach to the same or different surfaces, and in this way, microorganisms experience a repetitive cycle between planktonic and biofilm growth (Fig. 1.4) (Keener, 2004). The specific mechanism of fouling is important as it speaks directly to the types of control strategies that may be the most effective. If the biocake and fouling is solely a consequence of passive migration of materials from the bulk phase onto the membrane, then strategies designed to reduce the deposition of those components, such as more frequent backwashing, may be best suited to control biofouling. Conversely, if active biofilm development and secretion of the associated EPS is the key to the fouling process, then strategies should ideally focus on reducing biofilm growth on the membrane surface. Therefore, it is necessary to pay more attentions on the relationships of microbial community and EPS production.

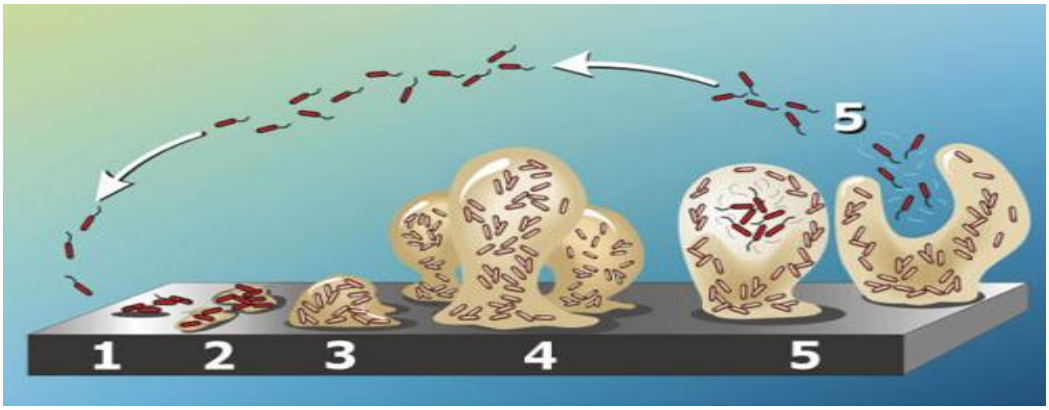

Fig. 1.4 Life cycle of biofilm associated microorganisms. The figure is adapted from Keener (Keener, 2004).

1.5 Biofouling control in MBRs

As discussed above, biofouling and its consequences for membrane performance and treatment costs are one of the key challenges to be addressed for MBRs. Therefore, strategies must be developed to control biofouling in MBRs. Currently the methods of biofouling control have focused on material modification, optimization of engineering operations,

physical and chemical cleaning and biological treatments.

1.5.1 Modification of membrane materials

Biofouling in MBRs is perceived as the deposition of microorganisms and organic substances on the membrane surface. Therefore, some efforts have focused on the modification of the membrane surface to make them toxic to the microorganisms or unsuitable for biofilm growth. It was reported that modification of polypropylene membrane surface by ozone treatment and graft polymerization with 2-hydroxy-ethyl methacrylate reduced the fouling tendency and increased the permeability of membranes (Sainbayar, 2001). For instance, the polyurethane membrane surface has been modified through the addition of the antimicrobial polymer, *N*-halamine, to make the membrane toxic to the microbes and observed a 100% reduction of the growth of *Escherichia coli* and *Staphylococcus aureus* after 2 h contact between the organisms and the membrane (Tan and Obendorf, 2007). Another study reported that modification of polypropylene membrane surface by ozone treatment and graft polymerization with 2-hydroxy-ethyl methacrylate reduced the fouling tendency and increased the permeability of membranes (Sainbayar, 2001). It was also demonstrated that coating the membranes with polyether–polyamide can make the membrane more smooth and hydrophilic to prohibit the adhesion of microbes (Louie et al., 2006). Based on the results from Louie et al. 2006, the volume of efflux through the coated membrane was 47% larger than the uncoated membrane after the operation of 100 d. However, it was reported that the modifications on membrane properties can be masked through the pre-conditioning of the membrane surface by the organic chemicals and macromolecular foulants in the water, which are the metabolites of microorganisms (Al-Juboori and Yusaf, 2012).

1.5.2 Optimization of engineering operations

Many studies have been performed to determine optimal operational parameters to reduce the biofouling in MBRs. Aeration is required in aerobic MBRs, which can provide oxygen for microbes and also results in high shear forces to remove fouling from the membrane surface, however this results in higher energy consumption. Therefore, a novel bubbling method to split air bubbles into fine bubbles for aeration and larger coarse bubbles for fouling control was developed (Phattaranawik, 2007). While intermittent permeation was reported to be a good method to control biofouling, the effluent flux in intermittent permeation is less than for continuous permeation (Itoh, 1995). Critical flux was shown as another important parameter influencing biofouling in MBRs. The critical flux is a threshold flux value in MBR, where the

TMP can be maintained at low pressure for a relatively long time if the MBR is started with a flux below the critical flux (Field et al., 1995). Previous data showed that the time for TMP to rise was prolonged when the effluent flux was reduced (Field et al., 1995). However, the setting of critical flux reduced the production of effluent and still cannot prevent the biofouling completely. Therefore, the optimal operation represents a tradeoff between increased product production, higher flux, and reduced membrane fouling, lower flux. Therefore, some techniques have been developed to remove biofilms or to kill microorganisms on membranes through the physical and chemical cleaning methods. *In situ* ultrasonication has been regarded as a promising method to remove fouling in wastewater treatment. Ultrasound waves can produce compression and expansion waves and thus causes cavitation waves. The sudden formation and collapse of the low-pressure bubbles in solutions can release energy to bombard and dislodge substances from membrane surface. It has been shown that permeation flux of a membrane was maintained during sonication treatment, whereas a decline of permeation flux occurred at the absence of sonication (Veerasamy et al., 2009). But the drawbacks of the ultrasonication treatment are the high energy demand and high expenditure of this method (Hulsmans et al., 2010).

Chemical cleaning is the most commonly used method to reduce biofouling and to maintain permeability of membranes that have already fouled. The agents used for chemical cleaning can be classified into alkaline, e.g. sodium hydroxide (NaOH) and sodium hypochlorite (NaClO); acids, such as hydrochloric acid (HCl) and citric acid; disinfectants, e.g. chlorine and dichloroisocyanurate (DCC) (Yu et al., 2013); oxidants, such as hydrogen peroxide (H_2O_2), O_3 or Potassium Permanganate ($KMnO_4$); surfactants and metal chelating agents such as Ethylene Diamine Tetra Acetic acid (EDTA) (Lin et al., 2010; Madaeni et al., 2009). These chemicals can be applied by directly immersing the fouled membrane modules into a separate tank with a high concentration the cleaning chemicals or combining them with the physical treatment, e.g. backwashing (Lin et al., 2010). It was reported that treatment with the combination of 3000 mg/L NaClO and 500 mg/L NaOH reduced 81.8% of TMP (Li et al., 2011) and treatment with 1000 mg/L citric acid recovered 90% of the membrane permeability in MBR (Yan et al., 2012). However, such compounds are not always effective since the bacterial biofilms can develop the resistance to these disinfectants (Bridier et al., 2011). Furthermore, the over application of biocides and disinfectants, which are generally toxic compounds, also represent environmental risks (Guardiola et al., 2012) and may damage the polymeric membrane structure (Puspitasari et al., 2010). Therefore, an environmentally responsible biofouling control strategy is required.

1.5.3 Biological treatment strategies

As discussed above, conventional methods, such as applying a shear force and backwashing, can delay biofilm formation but ultimately cannot prevent membrane biofouling. Chemical agents can kill microbes and remove biofilms from the membranes, but the irreversible fouling layers tend to be resistant to chemical treatments. Furthermore, the overuse of chemicals can damage the polymeric membrane structure and can also contribute to environmental pollution. Therefore, it is urgent to explore environment-friendly biological methods to control biofouling.

Quorum sensing (QS) is a mechanism used by bacteria to regulate gene expression at the population level (Miller MB, 2001). Quorum sensing bacteria usually excrete small chemical molecules, called autoinducers (AIs), into the environment. Membrane bound receptors are able to specifically bind to the AI compounds and when the receptors are activated by the binding of AIs, they will induce the transcription of specific genes, including the genes for the AI expression. Normally, the receptors are inactive when the cell density is low. But when the AI concentrations increase to a threshold concentration, which can be a reflection of population density, the autoinducer will bind to the receptor. QS has been demonstrated to be involved in the formation of biofilms and surface attachment as well as EPS production have also been shown to be controlled by quorum sensing (Nadell et al., 2008). For example, the maturation of biofilms of *Burkholderia cepacia* H111 is dependent on the CepI/R QS system (Huber, 2001). Similarly, the AhyI/R AHL QS system is involved in the biofilm maturation of *Aeromonas hydrophila* (Lynch et al., 2002). Given that biofilms, the development of which is at least in part controlled by QS, are a key component of biofouling in MBRs (Ponnusamy et al., 2010), it is not surprising that QS signaling has been associated with MBR communities. Many species within the bacterial groups that have been found to be associated with MBRs, as described in section 1.3.3 above, have also been shown to utilize QS regulation. In addition, it has been shown that QS signals can be directly isolated from MBRs. Three different *N*-acyl homoserine lactone autoinducers (AHLs), including *N*-hexanoyl-DL-homoserine (C6-HSL), *N*-octanoyl-DL-homoserine lactone (C8-HSL) and an unidentified AHL, were found in the biofilm layer on membranes (Yeon et al., 2009b). Additionally, when the concentration of the AHLs in the MBR reactor increased, the TMP was also observed to increase (Fig. 1.5), implying the QS system mediated the membrane fouling in MBRs (Yeon et al., 2009b).

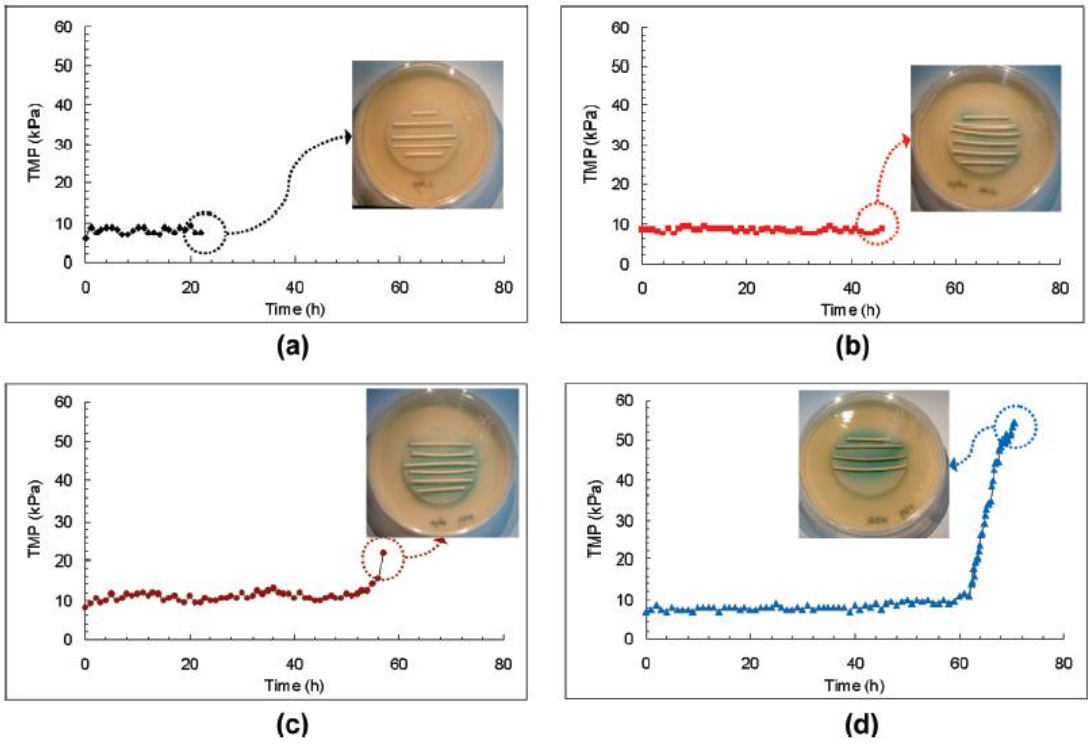

Fig. 1.5 Occurrence of AHL signals in biofilms at different TMP stages in a MBR: (a) 22 h, (b) 46 h, (c) 58 h, and (d) 72 h. The *Agrobacterium tumefaciens* QS reporter strain, which can respond the AHLs and produce blue color on the agar plate with X-gal was used to make soft agar plates onto which hollow fiber membranes were placed. The Figure is adapted from Yeon et al. (2009).

Based on this understanding of how QS operates at the molecular level, several strategies have been developed to interfere with or to disrupt the QS mediated gene expression. For example, it was shown that the production of AHLs can be reduced by addition of analogues of the substrates for AHL synthesis (Parsek, 1999). A range of natural products have been identified that bind to the QS signal receptor and prevent the AHL signal from binding to and activating the receptor. For example, garlic, penicillic acid and patulin, were found to prevent the mature biofilm formation of *Pseudomonas aeruginosa* (Rasmussen and Kristoffersen, 2005). Some studies also focused on synthesizing autoinducer analogues by modification of the native signal molecules (Reverchon, 2002). Furanones were reported to have antifouling properties in the marine macro alga *Delisea pulchra* (de Nys, 1993). These compounds, which are structurally similar to AHLs, act as signal receptor binding antagonists to disrupt the QS response and the biomass of *P. aeruginosa* PAO1 biofilms were significantly decreased when the biofilm was treated with a synthetic furanone (Hentzer et al., 2003). Similarly, furanones

were reported to prevent biofilm formation of *Bacillus subtilis* BE1500 on mild steel surfaces, where the treated biofilm was decreased in thickness and demonstrated higher cell death compared to the untreated control (Ren, 2002). In addition to signal receptor antagonists, it may also be possible to manipulate the QS system by quorum quenching methods, e.g. degrading the AHL signal, which effectively prevents the signal from accumulating to a high enough concentration to activate the receptor. Indeed, there are a number of enzymes from natural sources that have been shown to actively degrade AHLs. Porcine kidney acylase I, which can inactivate the AHL molecule by amide bond cleavage, was found to delay the TMP rise in MBR (Yeon et al., 2009b). This suggested that the QS system can be manipulated to control MBR biofouling.

Nitric oxide (NO) is an intracellular signaling molecule that has recently been shown to be involved in biofilm formation process (Barraud et al., 2006). In *P. aerugionsa*, NO is synthesised by NirS and its accumulation within biofilm microcolonies has been associated with cell death and dispersal from biofilms (Hentzer, 2005). Furthermore, a *nirS* mutant failed to undergo cell death and dispersal indicating that NO may mediate these aspects of biofilm development. The exogenous addition of NO through the addition of NO releasing compounds called NO donors, induced biofilm dispersal in *P. aerugionsa* and a range of bacteria including *E. coli, Staphyloccous epidermidis* and the yeast *Candida albicans* (Iyer et al., 2003). For example, the NO produced by sodium nitrite citric acid has the antifungal effect on the *Trichophyton* sp. (Regev-Shoshani et al., 2013), *Aspergillus* sp., *Monilinia* sp. and *Penicillium* sp. (Lazar et al., 2008). The low, sub-lethal concentrations (25 to 500 nM) of sodium nitroprusside (SNP), which is a NO donor, was reported to induce the biofilm dispersal of *P. aeruginosa* biofilms (Barraud et al., 2006). Another NO donor compound, PROLI NONOate, was also reported to induce the dispersal of *P. aeruginosa* PAO1 biofilms at concentrations of 5 - 80 μM (Barnes et al., 2013). In addition to the PAO1 wild-type, the biofilms formed by the *P. aeruginosa* PAO1 Δalg and Δpel mutants can also be dispersed by the PROLI NONOate exposure (Barnes et al., 2014). Since the NO has the potential to disperse the biofilm, it may be valuable to control biofouling phenomenon through applying NO to MBR to reduce the formation of biofilm on membrane. However, to date, no previous study tested its effect on MBR membranes to control biofouling.

1.6 Overview and objectives of this project

The objective of this PhD project was to study the biofouling process and to develop an effective strategy to control MBR biofouling by interfering with key steps in the biofilm

development process. In addition, the project has developed a detailed understanding of the process of biofilm formation in the MBR system and the relationship between the fouling community and the increase in TMP. Investigation of key species of microorganisms was undertaken at different stages of MBR operation and the biofilm community was compared with the sludge community to determine if specific organisms were associated with the biofilm rather than the sludge that may be involved in the fouling process. Furthermore, the architecture and composition of the biofilm was investigated. Specifically, the spatial organization of microbial aggregates and their relationship with EPS components was investigated. Subsequently, biological methods of biofouling control were tested using NO to determine if the application of NO donors can reduce microbial fouling and significantly delay the TMP increase associated with the biofouling process.

Chapter 2 Characterization of biofouling components on HF membrane in MBR

2.1 Introduction

To date, the components contributing to biofouling have been studied extensively, but few reports have investigated the correlation between the different biofouling components and the TMP increase to define their role in this process (Juang et al., 2010; Meng et al., 2010). To date, two hypotheses have been established to describe the process of biofouling. One hypothesis is that the deposition of biofouling layers is a consequence of filtration of EPS and microbes in the water onto the membrane to form a cake-layer. The alternative hypothesis is that microbes specifically attach onto the membrane to establish a biofilm and subsequently grow into EPS encased communities that ultimately block the membrane pores. The specific mechanism of fouling is important as it speaks directly to the types of control strategies that may be the most effective. If the biocake and fouling is solely a consequence of filtration of materials onto the membrane, then strategies designed to reduce the deposition of those components, such as more frequent backwashing, may be best suited to control biofouling. Conversely, biofilm development and the associated EPS secretion is the key to the fouling process, then a strategy should ideally focus on reducing biofilm growth on the membrane surface. Therefore, this study aimed to investigate the relationships between each of the biofouling components and the increase in TMP. To better understand the process of biofouling in terms of specific components as well as the timing of their deposition on the membranes, it is essential to investigate the accumulation of these biofouling components on the MBR membranes during the MBR operation. Therefore, the α-polysaccharides, β-polysaccharides, proteins and microorganisms were differentially stained and quantified using high resolution imaging based on confocal laser scanning microscopy (CLSM), to define the timing and spatial distributions of these biofouling components (Chen et al., 2007).

2.2 Methods and materials

2.2.1 MBR system and operation

Two identical, laboratory scale MBR systems, each composed of an anoxic sludge tank, an aerobic sludge tank and a membrane module inside the aerobic sludge tank, were operated to treat the artificial synthetic wastewater, total organic carbon (TOC) of 200 mg/L (Fig. 2.1a). The artificial wastewater was composed of glucose (320 mg/L), beef extract (60 mg/L),

peptone (80 mg/L), KH_2PO_4 (7 mg/L), $MgSO_4 \cdot 7H_2O$ (14 mg/L), $FeSO_4 \cdot 7H_2O$ (7.3 mg/L) and sodium acetate (90 mg/L). The effective volumes for the anoxic tank and aerobic tank were 2 L and 5 L respectively. A "curtain" style membrane module was used, which consisted of 100 pieces of hollow fiber (HF) PVDF membranes (ZeeWeed 500, kindly provided by GE Singapore). The average length of each membrane piece was 10 cm and the total area for each membrane module was 565 cm^2. One end of the membrane piece was sealed and hung down into the sludge tank, which were the free ends. The other ends of the membranes were open and sealed into a chamber that was connected to the suction pump (Fig. 2.1b).

The activated sludge was collected from the Ulu Pandan wastewater treatment plant in Singapore and acclimated in artificial synthetic wastewater for 60 d before the start of experiments. While running, the synthetic wastewater from the feedwater tank passes through the anoxic tank and aerobic tank and is degraded by the sludge biomass in the two tanks. The wastewater is then recycled from the aerobic tank to the anoxic tank to be further degraded. The purified water is subsequently separated from the sludge by the membrane module. The two MBRs were run at a constant flux, 13 - 15 $L.m^{-2}.h^{-1}$ (LMH). The hydraulic retention time and sludge retention time for each MBR were maintained at approximately 10 h and 25 d respectively for the two MBRs. The concentration of the mixed liquor suspended sludge (MLSS) was maintained at 3 - 5 g/L. Both MBRs were run at a room-temperature of 25 - 28 ^oC. The TMP was monitored automatically using a digital pressure gauge (Ashcroft). The TOC of the influents and permeates was measured using a multi N/C® 2100s (AnalytikJena) to monitor the performance of MBRs.

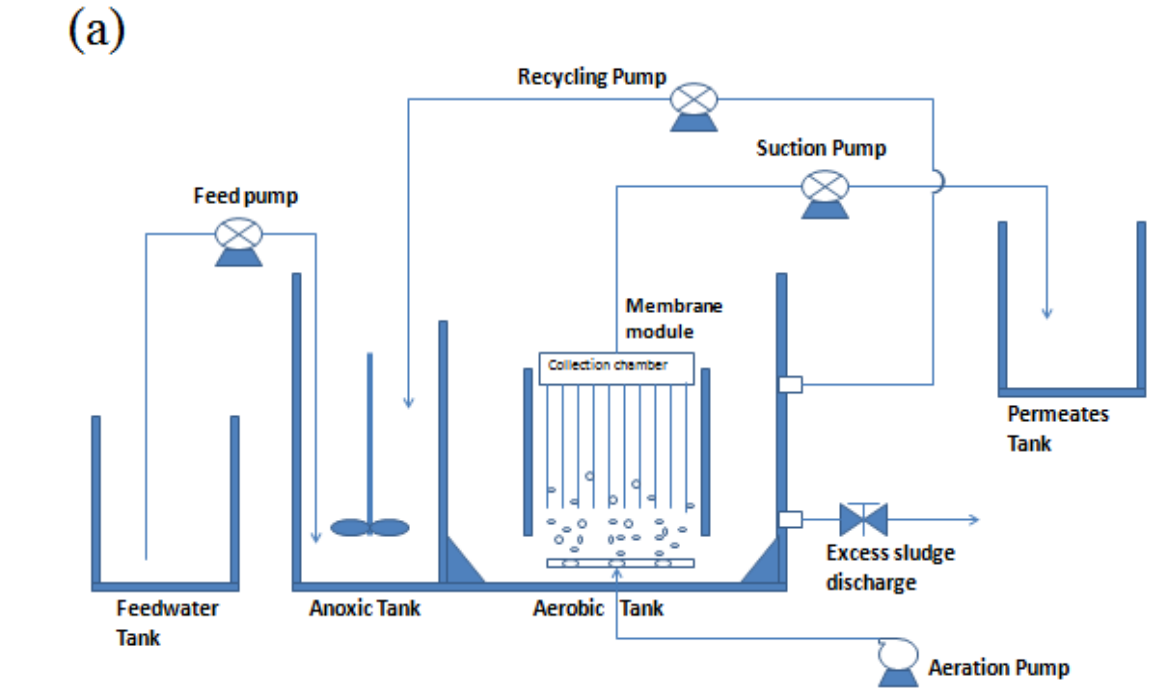

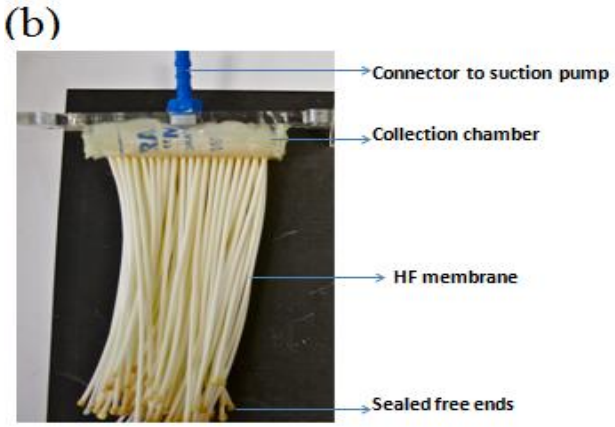

Fig. 2.1 The MBR system used in this project. (a) The schematic view of the internal submerged MBR. (b) The configuration of the "curtain" style HF membrane module.

2.2.2 Staining of biofilm samples

Membrane pieces were collected to analyze biomass by CLSM at different points along the transmembrane pressure (TMP) curve. Three replicate HF membranes were cut from the free ends of membrane module at every time point, immersed in 20 μM SYTO 63 red fluorescent nucleic acid stain solution (Molecular Probes, Invitrogen) and incubated at room temperature for 30 min to stain the DNA in the microbial cells. The membranes were then removed from the SYTO 63 staining solution and soaked in 500 μL fluorescein-5-isothiocyanate (FITC 'Isomer I', Molecular Probes, Invitrogen) staining solution (1 mg/mL) for 1 h to stain the proteins for imaging. The membranes were then immersed in freshly prepared 0.2 mg/mL concanavalin A-tetramethylrhodamine (Molecular Probes, Invitrogen) staining solution for 30 min which stains the α-mannopyranosyl and α-glucopyranosyl sugar residues. Finally, the membranes were stained with 1 g/L calcofluor white solution (Sigma) for 30 min to label the

β-D-glucopyranose polysaccharides (Chen et al., 2007). All of the staining procedures were performed at room temperature, 25 - 28 oC, in the dark. After staining, the samples were immersed into phosphate buffered saline (PBS, pH 7.2) for 10 min twice to remove excess stain.

2.2.3 CLSM imaging

After staining, the HF samples were put onto glass slides for observation using an inverted confocal laser scanning microscope (CLSM, LSM 710, Carl Zeiss). Four channels were used to scan the biofouling samples. The calcofluor white was excited at 405 nm and detected using the emission range of 410 - 480 nm. FITC stained samples were excited at 488 nm and observed at 500 - 540 nm for emission. The tetramethylrhodamine conjugated concanavalin A was detected via excitation at 543 nm and emission at 550 - 600 nm. The SYTO 63 was excited at 633 nm and captured at 650 - 700 nm (Chen et al., 2007). For each membrane piece, a minimum of 3 - 5 images were collected. Therefore, a minimum of 9 - 15 images were collected for the triplicate membrane samples at every time point.

2.2.4 Analysis to the 3D images

Three dimensional reconstructions of the biofilms were produced using the software ZEN-2009 light edition (Carl Zeiss) by the "3D" process. Images were processed using the "maximum intensity projection (MIP)" to convert the 3D image into integrated 2D images. The MIP 2D images were split into different channels in the "x" and "y" directions to separately observe the differently stained components. The orthographic projection was also performed to the 3D images by "Ortho" process to convert the 3D image to 2D images at the "xy", "xz" and "yz" directions.

The quantitative analysis of the 3D CLSM images was performed using IMARIS (Version 7.3.1, Bitplane). The biovolume of each channel in the 3D CLSM images was calculated by applying the "surface" function to the 3D images and calculating the volume of surfaces. The co-localization analysis performed using the "Coloc" function (IMARIS). The Pearson correlation coefficient and Mander colocalization coefficient were calculated for the image data to determine correlations between biofilm components for each sample.

2.2.5 EPS extraction and quantification

The EPS in the activated sludge mixture was extracted based on the NaOH-formaldehyde

protocol (Liu and Fang, 2002). Ten mL of sludge liquor was centrifuged at 4000 *g* at 4 ^{o}C for 10 min and the supernatant was collected into a clean tube for quantification of the soluble EPS. To extract the bound EPS, the cell pellet was re-suspended in 5 mL 0.85% NaCl and 0.22% formaldehyde solution at 4 ^{o}C for 1 h after which, 5 mL of 1 M NaOH was added and incubated at 4 ^{o}C for 3 h. The sludge solution was centrifuged at 13000 *g* for 20 min. The supernatant solution containing the extracted, bound EPS was transferred to a clean tube. The soluble and bound EPS were both filtrated through 0.45 μm membrane filters (PALL, Product No.: 4614). The concentration of carbohydrates in the soluble and bound EPS was determined by the phenol-sulphuric acid method using glucose to generate a standard curve (DuBois et al. 1956). The concentration of proteins in the EPS was quantified by the Coomassie (Bradford) Protein Assay Kit (Pierce, Product No.: 23200) using bovine serum albumin as the standard (Bradford 1976).

2.3 Results and analysis

2.3.1 Two-stage TMP increasing curve in MBRs

The MBR systems were operated at a constant flux of 15 L.m^{-2}.h^{-1} for approximately 115 d and the TMP was monitored continuously. It was observed that the two MBRs, which had separate sludge tanks as well as separate membrane modules, exhibited similar TMP profiles over the entire study period (Fig. 2.2). Both were observed to operate at a steady TMP at approximately 5 - 15 kPa for the first 80 - 87 d. From day 87 onwards, the two MBRs showed a rapid increase in TMP, from 20 to 90 kPa by 115 d, which was the maximum pressure of the system. It was noted that MBR-2 showed a slightly faster rate of increase to reach its maximum pressure by 110 d.

Based on these observations, the TMP curve was divided into two stages. The first phase was characterized as a long-term, low TMP stage, in which TMP was maintained between 3 - 15 kPa (Fig. 2.2). The two MBR modules differed slightly as they made the transition into stage 2, the TMP jump phase. For MBR-1, the transition occurred after the first 82 d while for MBR-2, it occurred after 87 d. The average rate of TMP increase (dTMP/dt) was 0.183 kPa/d and 0.172 kPa/d at the low TMP stage in MBR-1 and 2 respectively. The second stage was characterized by a rapid TMP increase in a short span of time, and is referred to here as the TMP jump, which has been reported previously (Cho and Fane, 2002; Ognier et al., 2002;

Tardieu et al., 1998). The average rate of TMP increase, which occurred between 15 kPa to 90 kPa, was 2.143 kPa/d for MBR-1 and 2.778 kPa/d for MBR-2. Compared to the low TMP stage, the rate of TMP increase was almost 15 fold faster in the TMP jump phase relative to the low TMP stage. There was no further increase in TMP as the MBRs had reached the maximum pressure at the end of the jump stage.

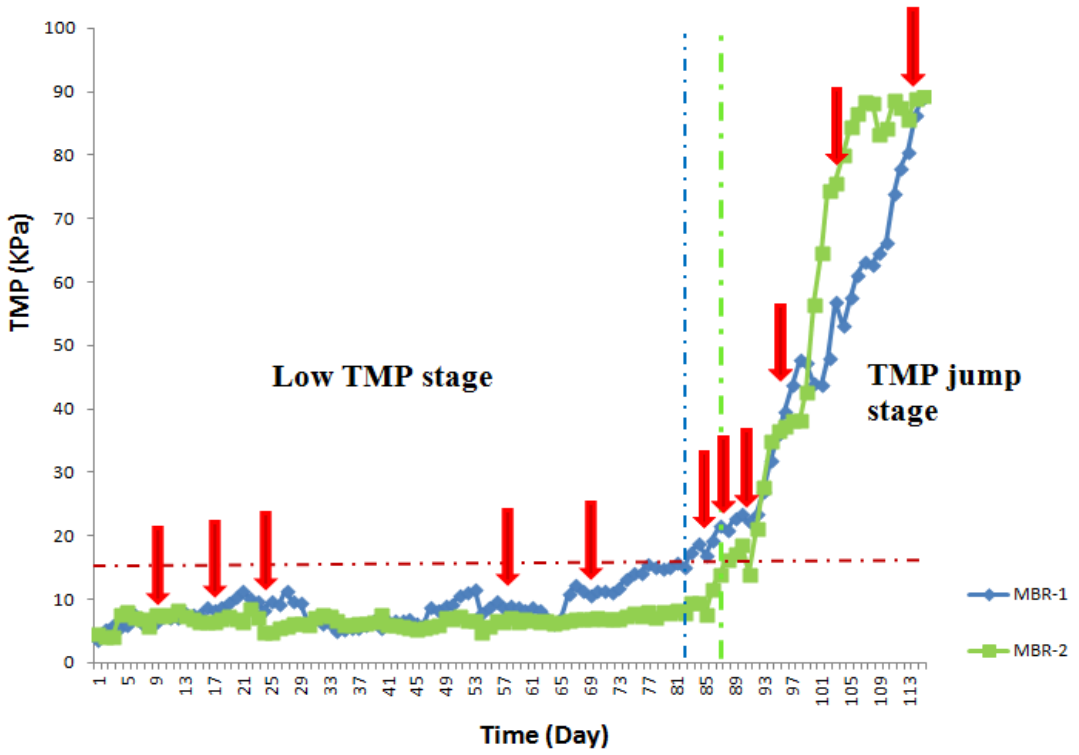

Fig. 2.2 TMP profiles and sampling time points for the analysis of biofouling components in the two replicate MBRs. The TMP curves were divided into the low TMP stage and TMP jump stage by 15 kPa, indicated by the red horizontal dashed line and the vertical dashed lines. The fouled membrane samples were collected at different time points, indicated by the red arrows.

2.3.2 Determination and heterogeneous distribution of biofouling components

To visualize and quantify the biological components associated with the different stages of MBR operation, the membrane samples were stained with the specific fluorescent dyes and observed by CLSM. The biofilm samples were collected based on the TMP increase (Fig. 2.2). For MBR-1, five samples were collected when the TMP was between 3 - 15 kPa, three samples were taken between the TMP of 15 - 30 kPa, one sample was collected when the TMP was between 30 - 60 kPa and two samples were taken when the TMP increased from 60 kPa to 90 kPa. For MBR-2, six samples were collected when TMP was between 3 - 15 kPa, one sample was collected at the TMP between 15 - 30 kPa, one sample was taken between the

TMP of 30 - 60 kPa and two samples were collected between the TMP of 60 - 90 kPa (Table 2.1). It should be noted that for each sampling point, three replicates were collected for the hollow fiber membranes.

Table 2.1 The time and TMP when hollow fiber membranes were collected for analysis

Time frame of sample (days)	Sampling TMP (kPa) (MBR-1, MBR-2)	Number of Samples (MBR-1, MBR-2)
1 - 87	3-15 , 3-20	5, 6
87 - 94	15-30, 20-30	3, 1
95 - 102	30-60, 30-60	1, 1
102 - 115	60-90, 60-90	2, 2

Four fluorescent dyes that are separately specific for α-polysaccharides, β-polysaccharides, proteins and microorganisms were applied to the membranes collected from the MBRs. All four components were observed in the biofouling layers in the two MBRs at both the low TMP (3 - 15 kPa) and high TMP stages (15 - 90 kPa) (Figs. 2.3 and 2.4), suggesting that all the four components may contribute to the biofouling process. The general pattern of biofouling, based on image visual observation, is presented here and the detailed analysis and correlation of the individual components is presented in subsequent sections below.

(a)

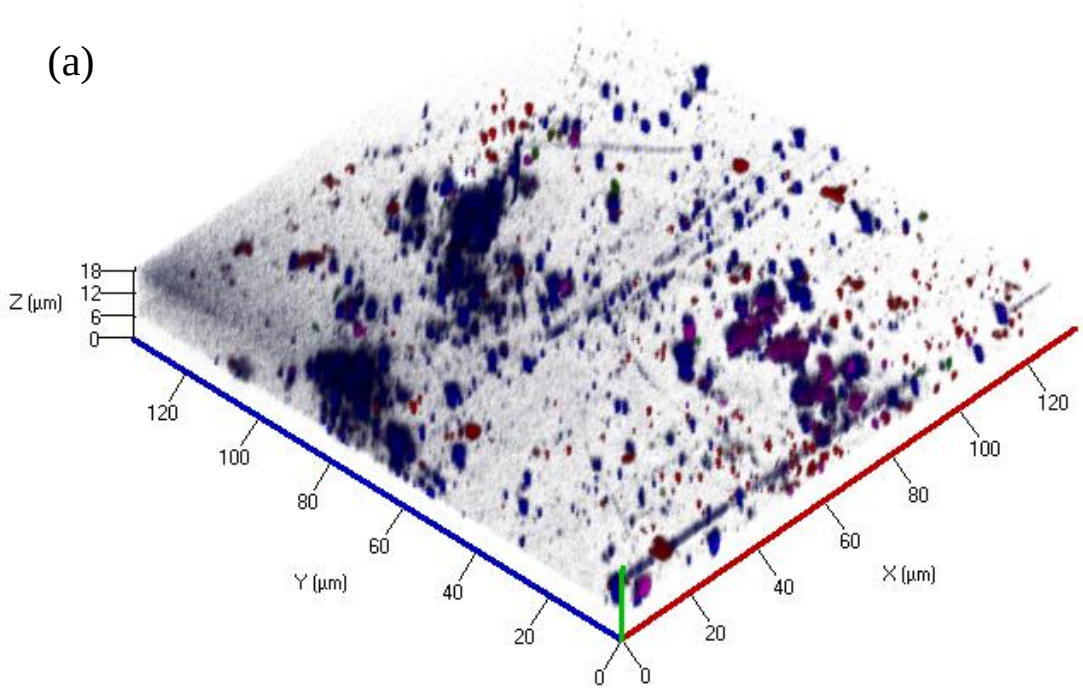

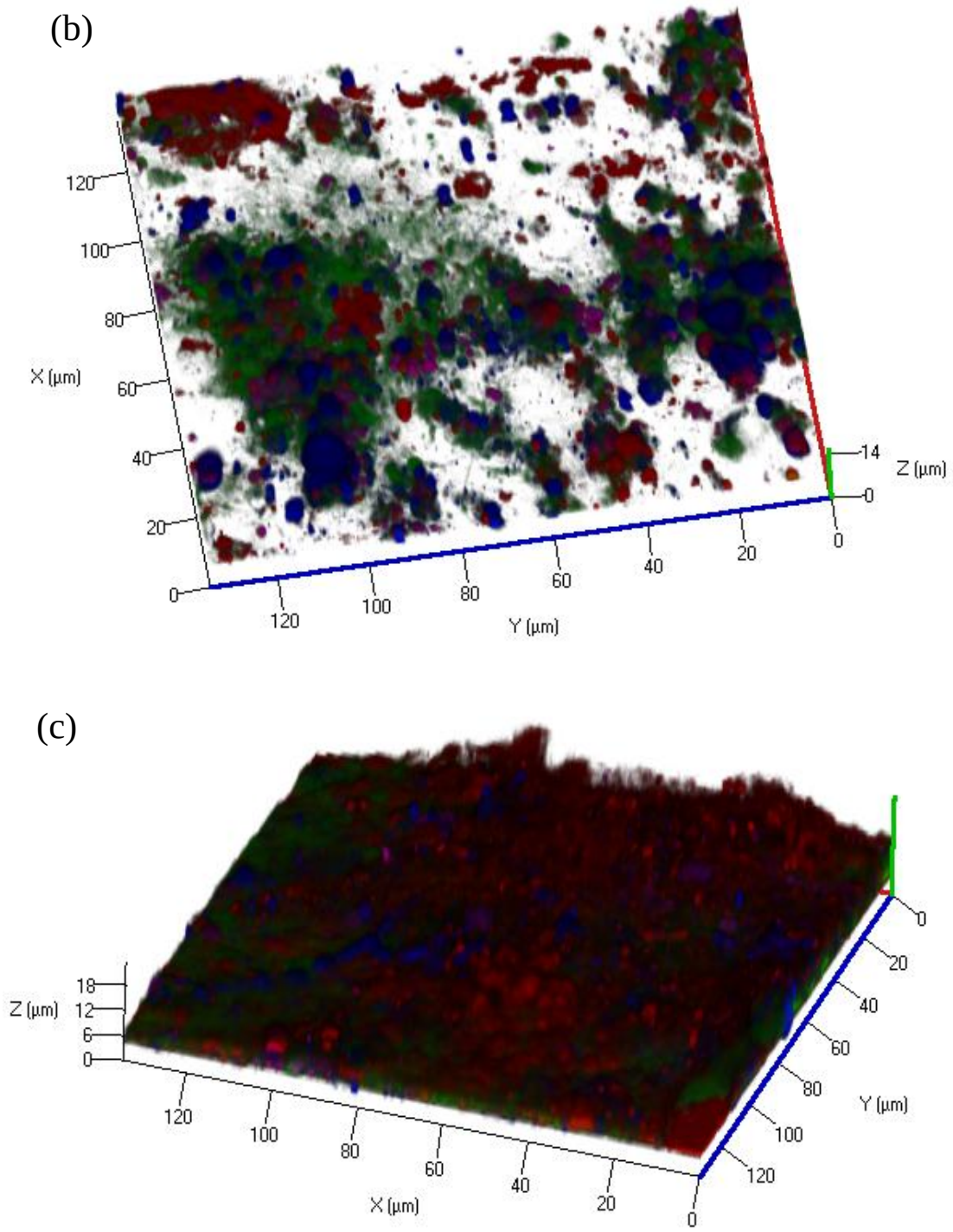

Fig. 2.3 (Continued from the previous page) Three dimensional images of the biofouling layers on hollow fiber membranes from MBR-1. The biofouling layers formed at (a) 5 - 10 kPa, (b) 10 - 20 kPa and (c) 60 - 90 kPa. All images are top down projects of 3-D reconstructions of the biofilm. The total magnification for the images was 630×. The red color in the images shows the α-polysaccharides, the blue color shows the β-polysaccharides, the green color shows the proteins and the purple color shows the microbes.

(a)

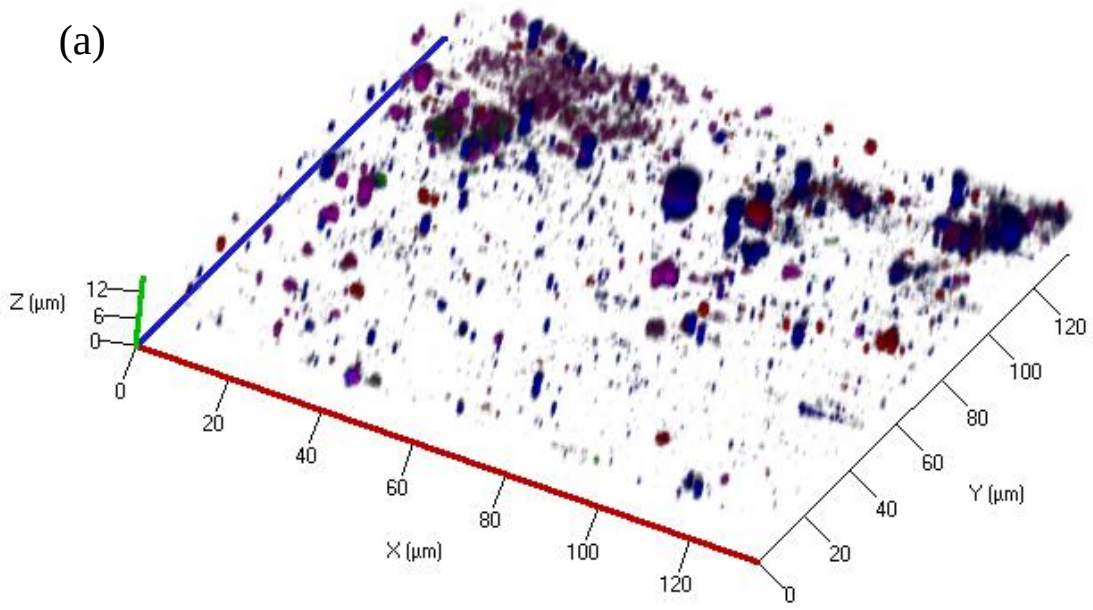
Z (µm)
12
6
0
0
20
40
60
80
100
120
X (µm)
0
20
40
60
80
100
120
Y (µm)

(b)

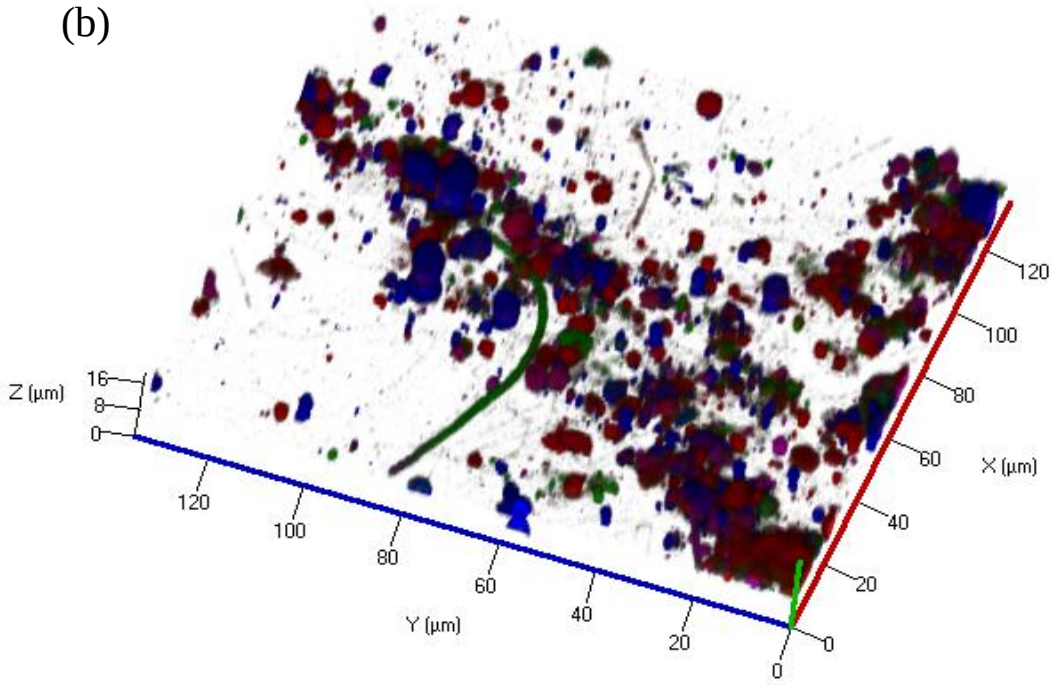
Z (µm)
16
8
0
120
100
80
60
40
20
0
Y (µm)
0
20
40
60
80
100
120
X (µm)

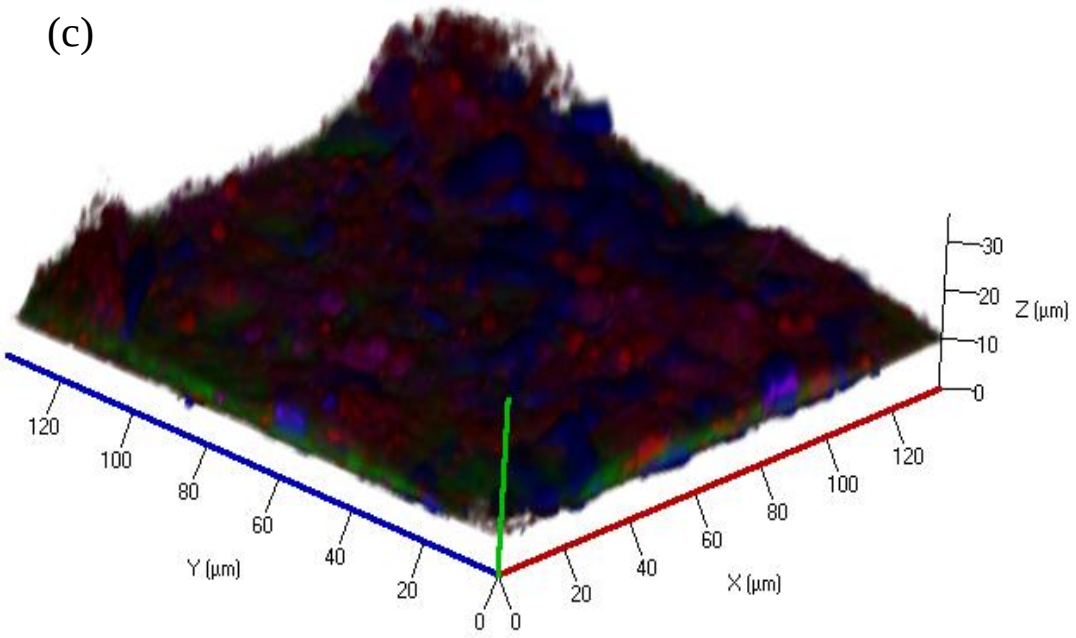

Fig. 2.4 (Continued from the previous page) Three dimensional images of the biofouling layer on hollow fiber membranes from MBR-2. The biofouling layer formed at (a) 5 - 10 kPa, (b) 10 - 20 kPa and (c) 60 - 90 kPa. All images are top down projects of 3-D reconstructions of the biofilm. The total magnification for the images was 630×. The red color in images shows the α-polysaccharides, the blue color shows the β-polysaccharides, the green color shows the proteins and the purple color shows the microbes.

The distribution of microorganisms and biomolecules was analyzed on the membrane surface by quantitative image analysis. After 10 d (TMP 5 kPa), the biofouling layers were observed to be distributed as small clusters on the membranes from both MBRs (Figs. 2.3a and 2.4a) and empty spaces were observed between these small clusters. The thickness for the clusters ranged from 1 - 5 μm (Fig. 2.5a). When the TMP was 10 - 20 kPa, clusters were again observed and these were also surrounded by empty spaces (Figs. 2.3b and 2.4b). The clusters were larger than those observed at 5 kPa, where their thickness increased to 1 - 10 μm (Fig. 2.5b). In the TMP jump phase, 60 - 90 kPa, the biofilm was observed to be a continuous layer on the membrane surface and there were less open spaces observed (Figs. 2.3c and 2.4c). While uniformly spread across the surface, the thickness of the biofilm was heterogenous. For example, the thickness at 60 - 90 kPa varied from 5 to 20 μm (Figs. 2.4c and 2.5c). In addition to the observation that, at low TMP, the biofilm was comprised of small clusters of unevenly distributed material across the membrane surface, or that, at high TMP, the biomass was a confluent mat of variable thickness, it was also observed that the individual components,

including proteins, polysaccharides and cells, were also not evenly distributed. Therefore, the individual components of the biofouling layers were characterized separately.

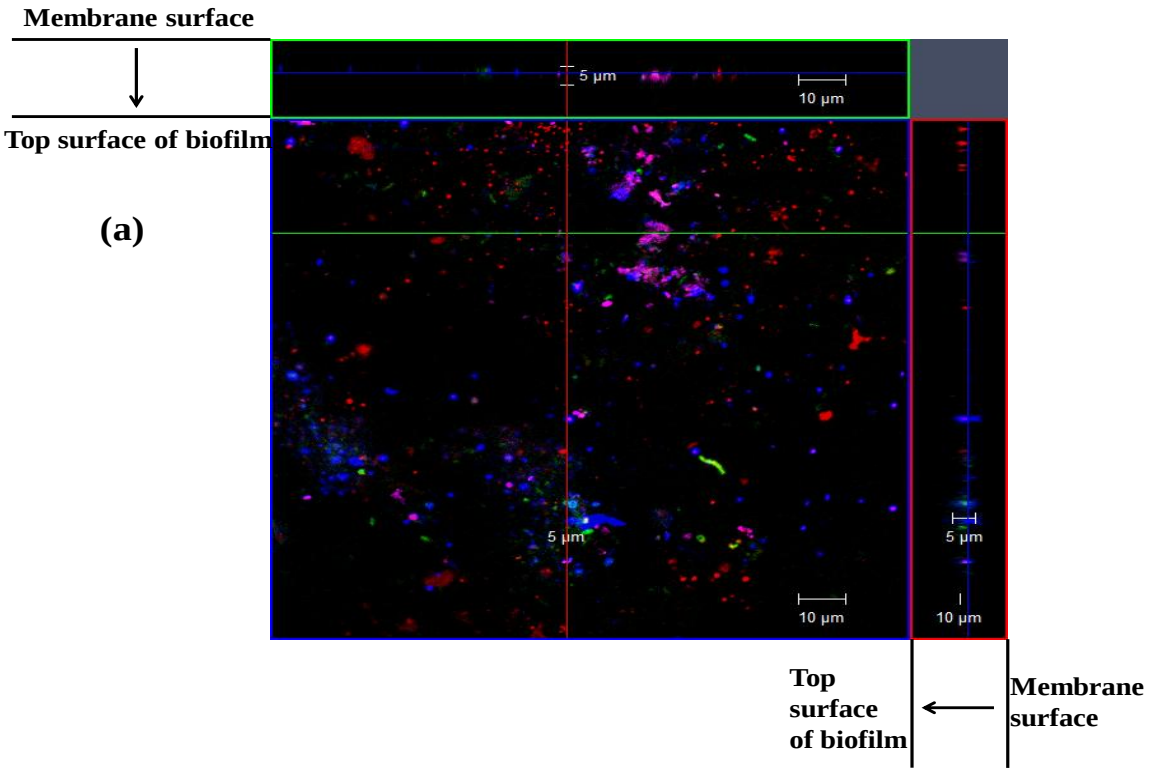

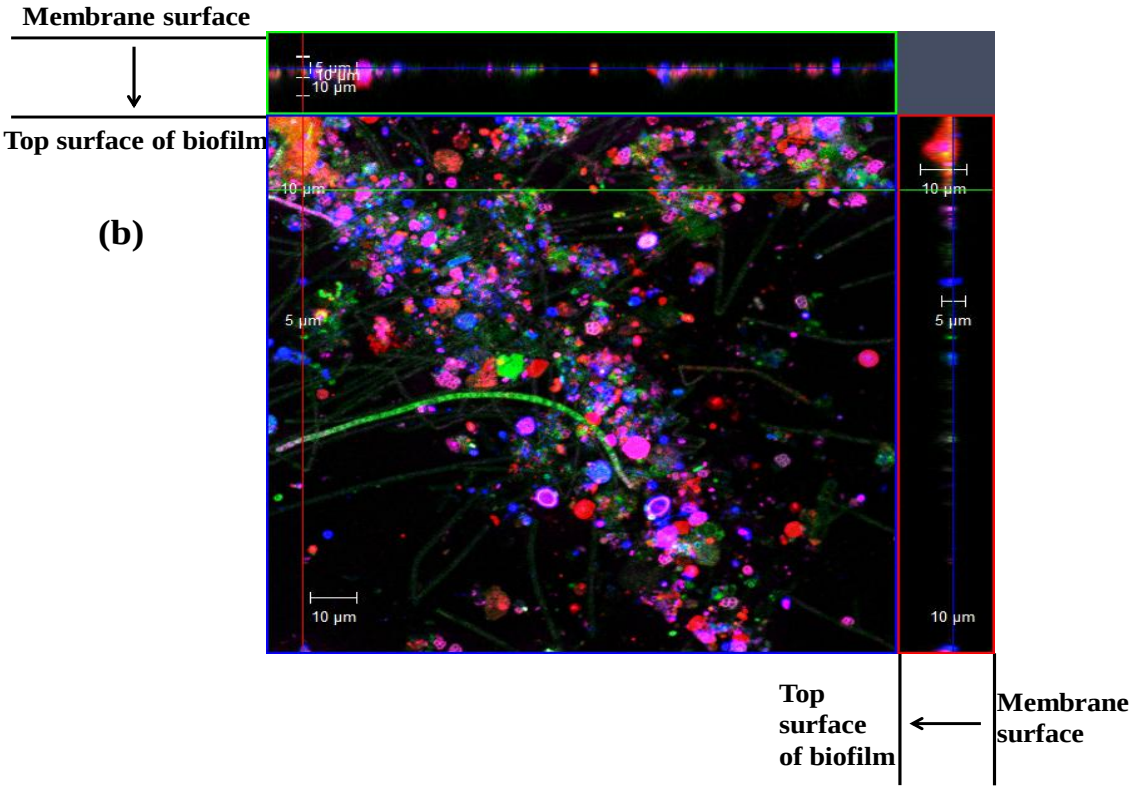

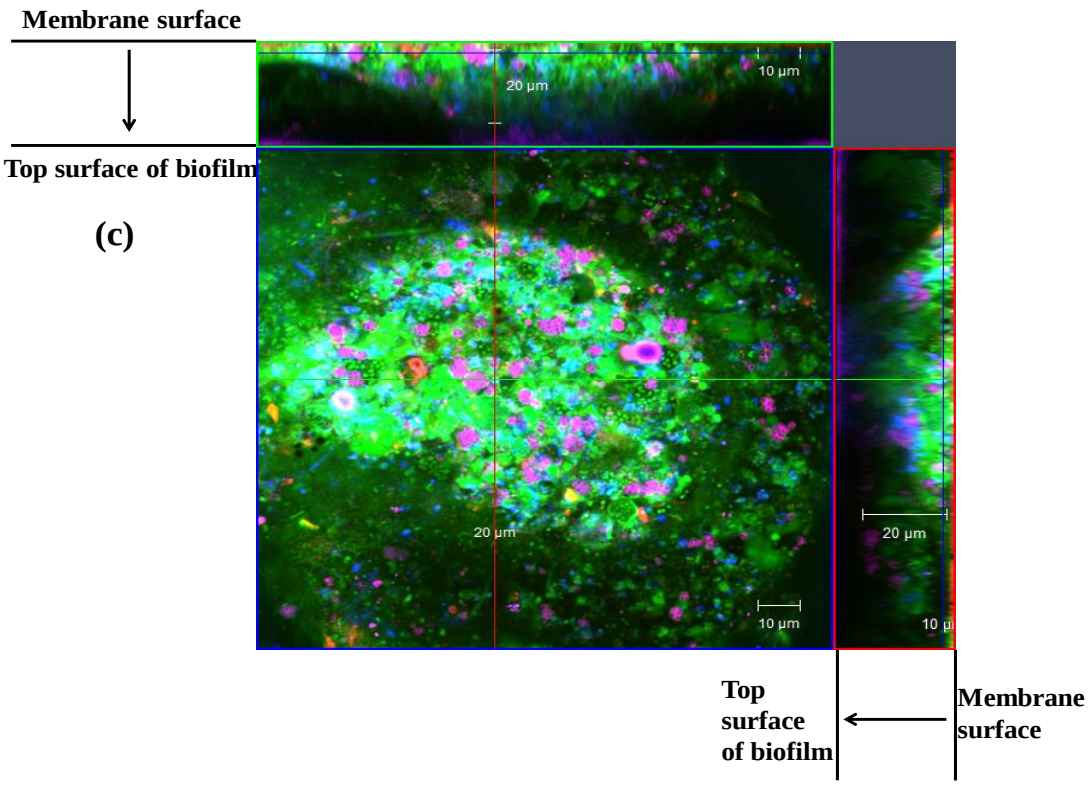

Fig. 2.5 (Continued from the previous page) The orthographic projection of the biofilm on HF membranes. The biofouling layer formed at 3 - 10 kPa (a), 10 - 20 kPa (b) and 60 - 90 kPa (c). The total magnification for the images was 630×. The α-polysaccharides (red), β-polysaccharides (blue), proteins (green) and cells (purple) were separately stained and imaged in different fluorescent channels for these composite images.

2.3.3 Contributions of biofouling components to the biofouling process

While it is understood that the α-polysaccharides, β-polysaccharides, proteins and microorganisms are important factors for the biofouling process, it remains unclear as to their specific contribution to fouling and whether the TMP rise is attributed to one specific class of macromolecules or the microbial cells. To elucidate these questions, the variation of the biovolumes of the four biofouling components was determined by quantitative image analysis at each time point.

2.3.3.1 α-polysaccharides

The α-polysaccharides were determined by staining of tetramethylrhodamine conjugated concanavalin A. There was a heterogeneous distribution of the α-polysaccharides on the membrane. In the low TMP stage, 3 - 10 kPa, the α-polysaccharides were observed to be distributed in small clusters on the membrane surface with empty spaces between the clusters (Fig. 2.6a). At higher TMP, the α-polysaccharide clusters were bigger and covered more

surface area on the membrane (Figs. 2.6c and 2.6d).

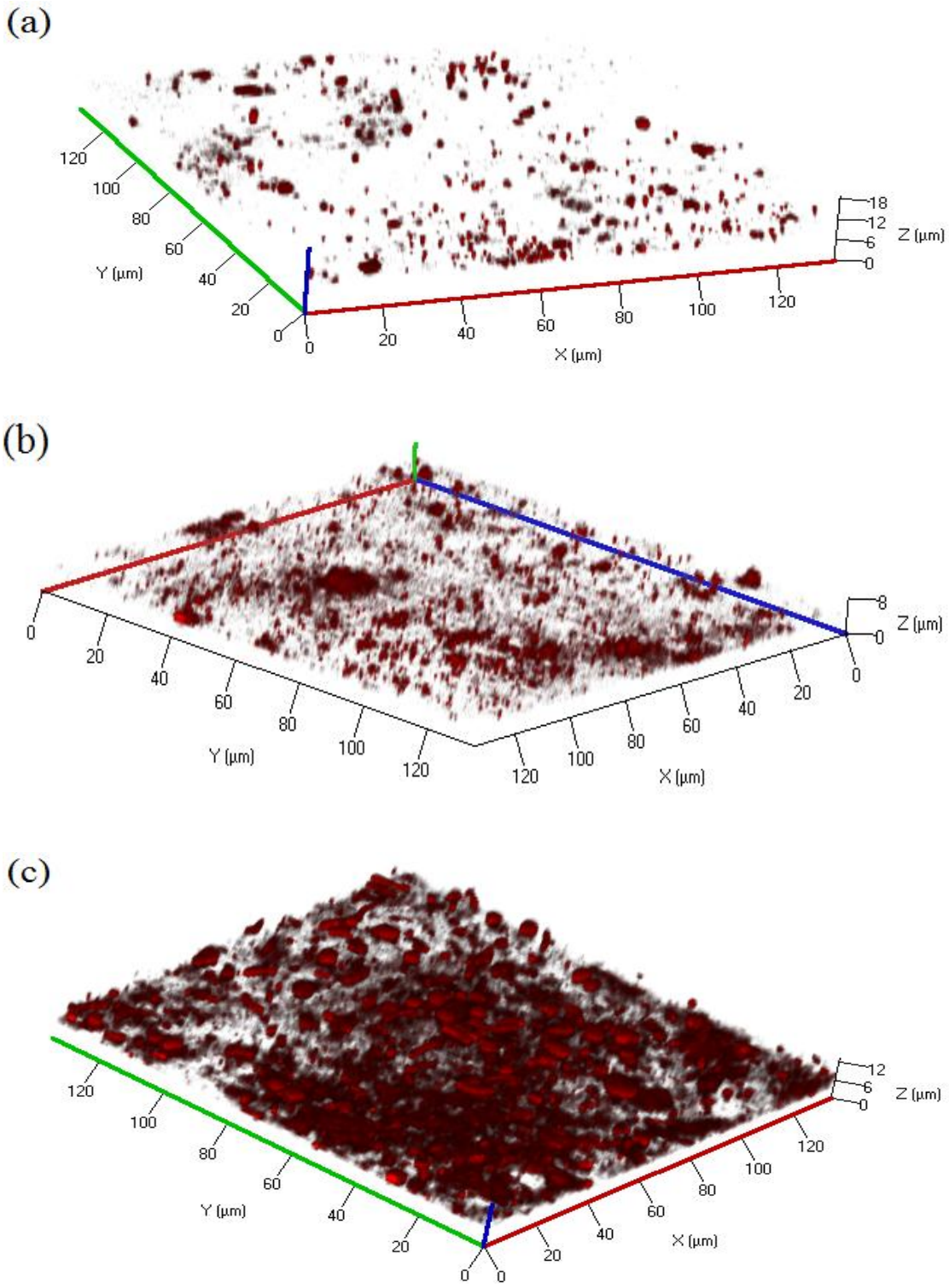

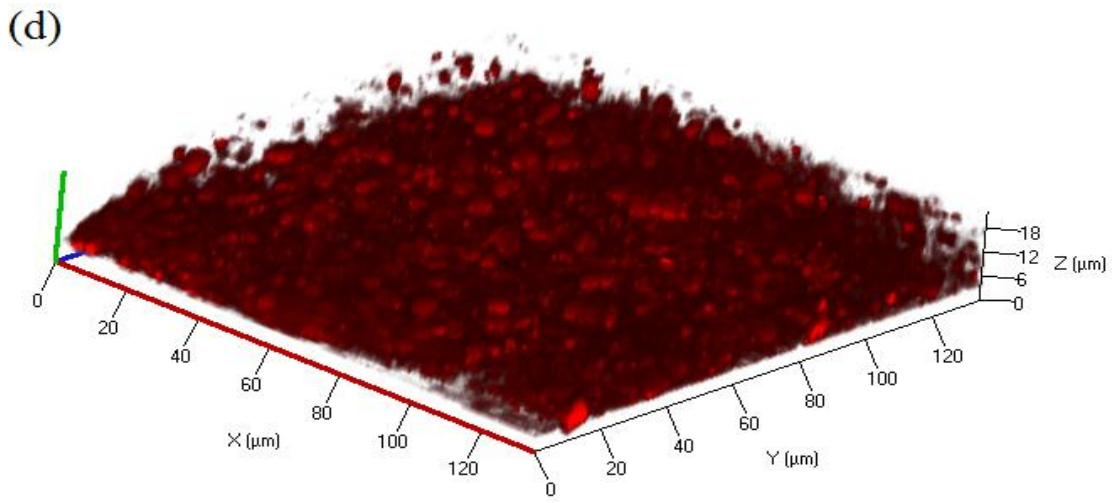

Fig. 2.6 (Continued from the previous page) Three dimensional images of α-polysaccharides on hollow fiber membranes in a submerged MBR. The α-polysaccharides layer formed at (a) 3 - 10 kPa, (b) 10 - 15 kPa, (c) 15 - 30 kPa and (d) 30 - 60 kPa. All images were top down projections of 3-D reconstructions of the α-polysaccharides layer. The total magnification for the images was 630×.

The biovolumes of α-polysaccharides were observed to increase on the membrane across the changing TMP profile (Fig. 2.6). Specifically, when the TMP was between 3 - 15 kPa, the biovolume of the α-polysaccharides ranged from 0.04 - 0.44 $\mu m^3/\mu m^2$ in MBR-1 and 0.06 - 0.25 $\mu m^3/\mu m^2$ in MBR-2. After the TMP increased to 15 - 30 kPa, the α-polysaccharides were observed to occupy 0.25 - 0.8 $\mu m^3/\mu m^2$ (MBR-1) and 0.25 - 0.42 $\mu m^3/\mu m^2$ (MBR-2). When the TMP continued to rise, the biovolume of the α-polysaccharides increased dramatically to 0.42 - 0.71 $\mu m^3/\mu m^2$ (MBR-1) and 0.42 - 1.05 $\mu m^3/\mu m^2$ (MBR-2) at a TMP of 30 - 60 kPa, and 1.18 - 1.77 $\mu m^3/\mu m^2$ in MBR-1 and 0.47 - 1.47 $\mu m^3/\mu m^2$ in MBR-2 at TMP of 60 - 90 kPa (Fig. 2.7). The Pearson's correlation coefficient (r) was 0.794 and 0.743 in MBR-1 and MBR-2 respectively between the TMP values and the biovolume of the α-polysaccharides (Table 2.2), indicating that the TMP rise was moderately correlated with the increase of biovolume of α-polysaccharides.

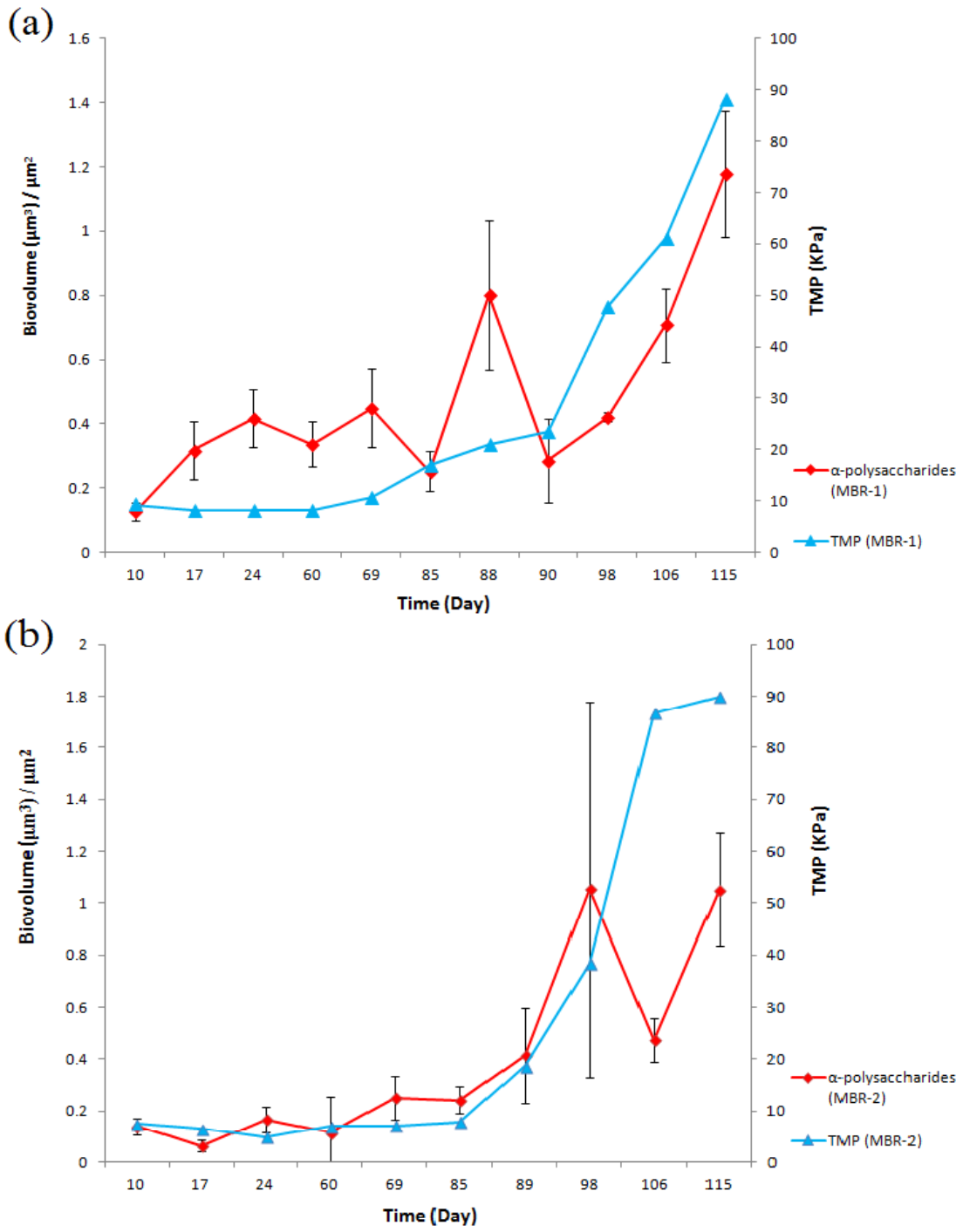

Fig. 2.7 The biovolumes of the α-polysaccharides in biofilms on hollow fiber membranes during the operation of (a) MBR-1 and (b) MBR-2. The biovolume of the α-polysaccharides (red) are shown relative to the TMP curve (cyan) during MBR operation. The biovolume is presented as the volume (μm^3) of the α-polysaccharides per area of hollow fiber membrane (μm^2). The data points were the average values of the 10-15 replicate images. The error bars are the standard error of the mean (n=10-15).

Table 2.2 Correlation between the biofilm components and TMP increase in MBRs

	α-polysaccharide (MBR-1, MBR-2)	β-polysaccharide (MBR-1, MBR-2)	Protein (MBR-1, MBR-2)	Microbes (MBR-1, MBR-2)	#Biofilms (MBR-1, MBR-2)
Pearson Correlation (r) with TMP	0.794, 0.743	0.94, 0.656	0.952, 0.959	0.921, 0.772	0.966, 0.903
*Significance (p >)	0.003, 0.009	0.0001, 0.028	0.0001, 0.0001	0.0001, 0.005	0.0001, 0.0001

*: Correlation was significant at the 0.05 level (2-tailed).

#: The biofilm represents the biovolume as determined from the merged images integrating all four components together into a single image for analysis.

2.3.3.2 β-polysaccharides

The β-polysaccharides were visualized by calcofluor white staining. Similar to the α-polysaccharides, the β-polysaccharides were also observed to be heterogeneously distributed on the membrane, where the distribution pattern was in small clusters at low TMP and as a continuous mat or large clusters at high TMP (Fig. 2.8).

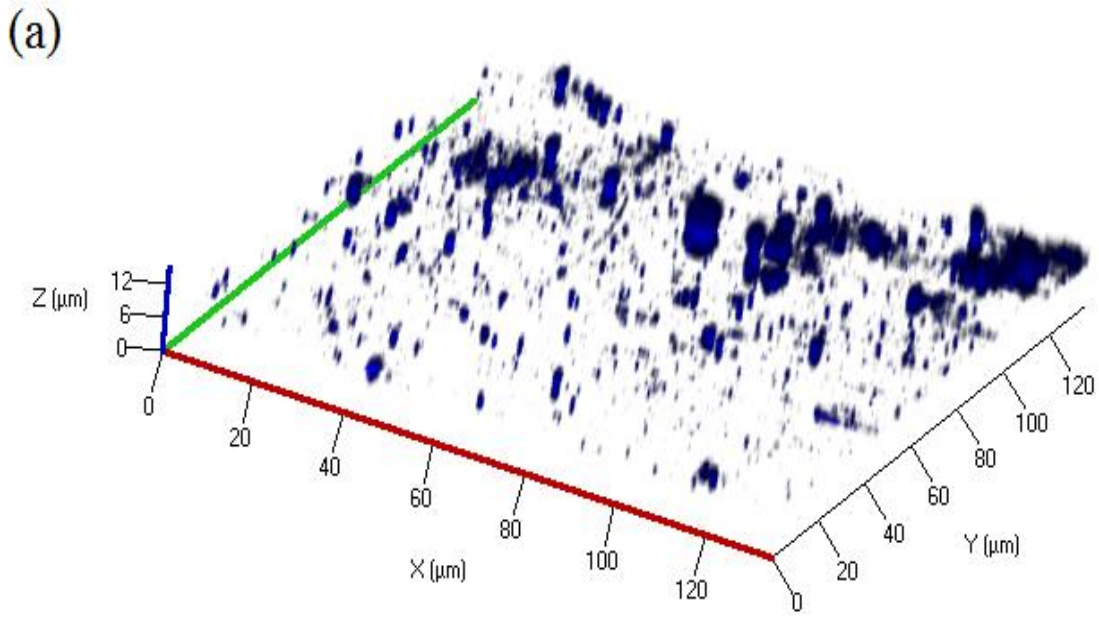

(b)

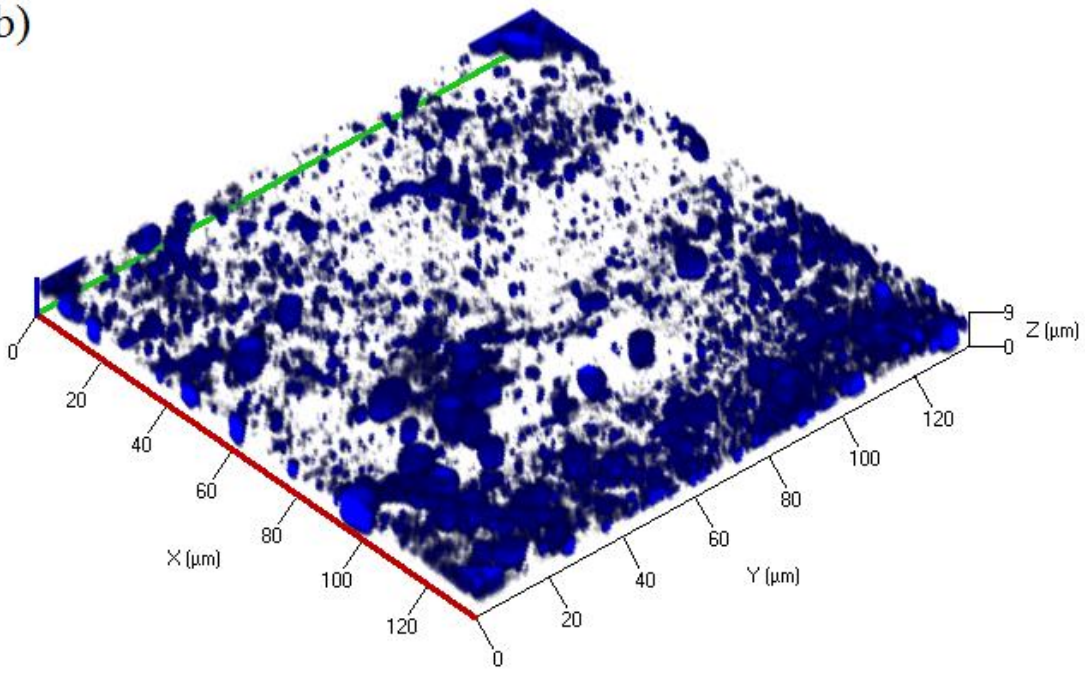
0
20
40
60
80
100
120
X (µm)
0
20
40
60
80
100
120
Y (µm)
9
0
Z (µm)

(c)

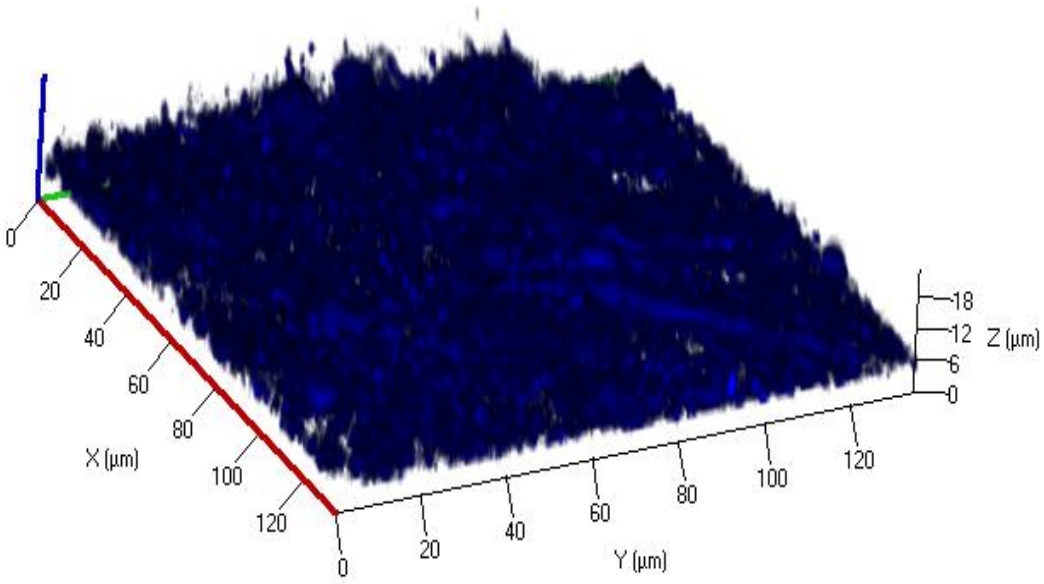
0
20
40
60
80
100
120
X (µm)
0
20
40
60
80
100
120
Y (µm)
18
12
6
0
Z (µm)

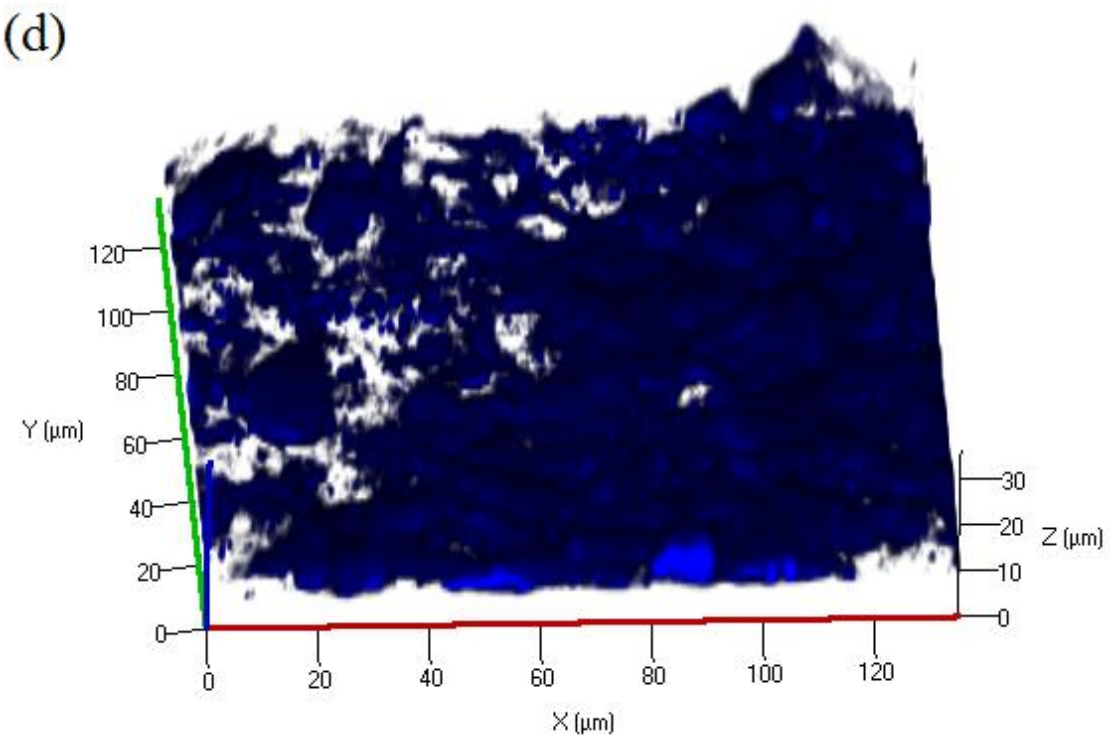

Fig. 2.8 (Continued from the previous page) Three dimensional images of β-polysaccharides on hollow fiber membranes in a submerged MBR. The β-polysaccharides layer formed at (a) 3 - 10 kPa, (b) 10 - 15 kPa, (c) 15 - 30 kPa and (d) 30 - 60 kPa. All images were top down projects of 3-D reconstructions of the β-polysaccharides layer. The total magnification for the images was 630×.

The β-polysaccharides were found to increase in biovolume on the membrane surface as the TMP increased in MBR-1 (Fig. 2.9). The volumes of the β-polysaccharides varied from 0.03 - 0.46 μm^3 /μm^2 when TMP was between 3 - 15 kPa. When the TMP increased to 15 - 30 kPa, the volume of the β-polysaccharides varied from 0.33 to 0.5 $\mu m^3/\mu m^2$. The volume of the β-polysaccharide increased to 0.5 - 0.8 $\mu m^3/\mu m^2$ when the TMP reached 30 - 60 kPa. When the TMP continued to rise to 60 - 90 kPa, the volume of the β-polysaccharides increased further and was between 0.8 - 2.2 $\mu m^3/\mu m^2$, with an average volume of 1.67 $\mu m^3/\mu m^2$. The Pearson's correlation coefficient (r) was 0.94 for the comparison between the TMP values and biovolumes of β-polysaccharide in MBR-1 (Table 2.2), indicating the TMP rise correlated strongly with the increase in β-polysaccharide biovolume.

Analysis of the β-polysaccharide accumulation in MBR-2 showed a similar pattern of increase, where the biovolume increased in accordance with the TMP, ranging from 0.05 - 0.7 $\mu m^3/\mu m^2$

(3 - 15 kPa), 0.7 - 0.76 $\mu m^3/\mu m^2$ (15 - 30 kPa), 0.7 - 1.25 $\mu m^3/\mu m^2$ (30 - 60 kPa) and 0.71 - 2.69 $\mu m^3/\mu m^2$ (60 - 90 kPa) (Fig. 2.9). The correlation coefficient (r) between the TMP and β-polysaccharides was 0.656 (Table 2.2), which indicated a moderate correlation between the two factors and was not as strong as observed for MBR-1, however, there remains a positive correlation in the two separate MBRs between the TMP rise and β-polysaccharide accumulation.

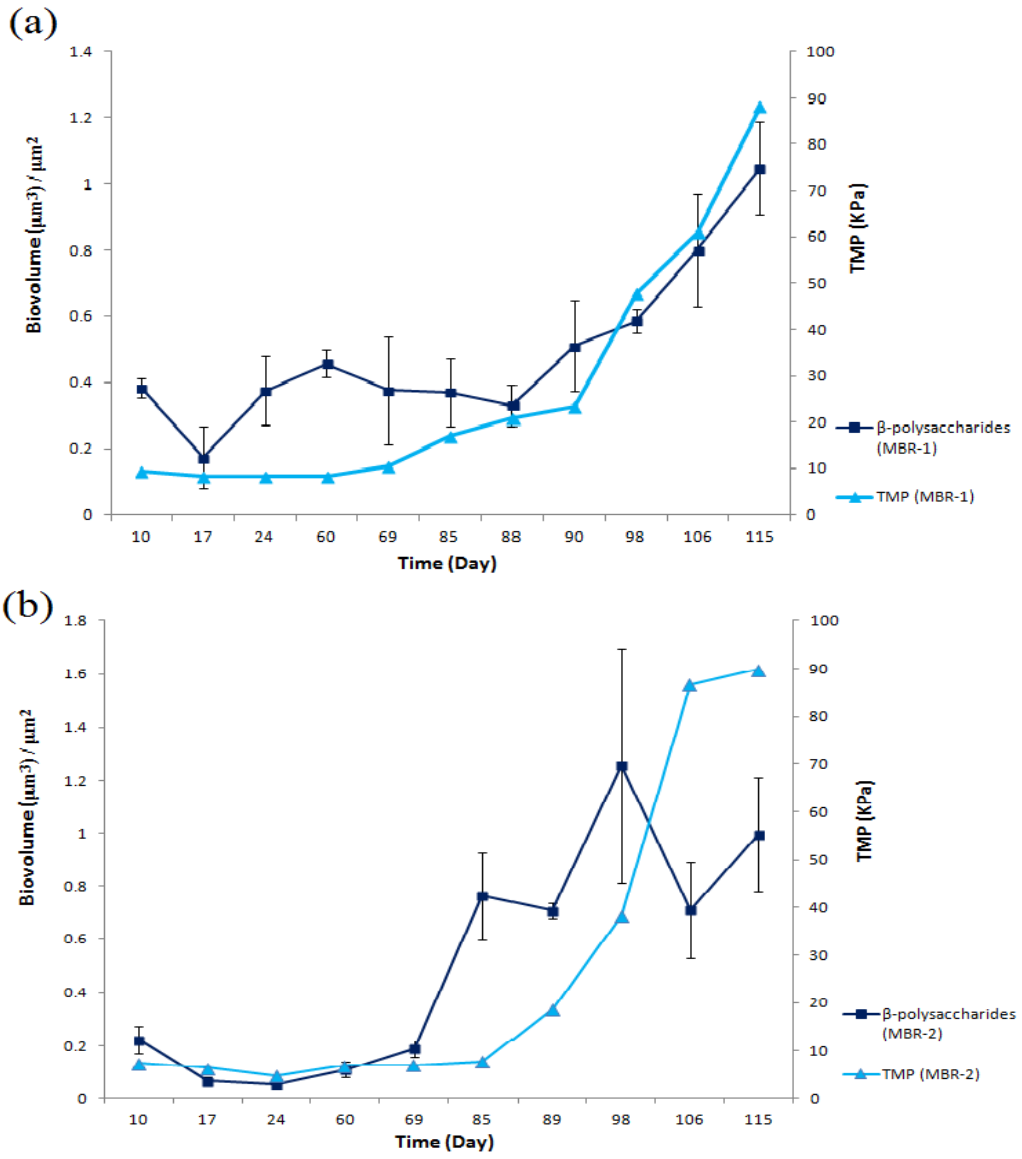

Fig. 2.9 The biovolumes of the β-polysaccharides in biofilms on hollow fiber membranes during the operation of (a) MBR-1 and (b) MBR-2. The biovolume of the β-polysaccharides (blue) are shown relative to the TMP curve (cyan) during MBR operation. The biovolume is presented as the volume (μm^3) of the β-polysaccharides per area of hollow fiber membrane (μm^2). The data points were the average values of the 10-15 replicate images. The error bars are the standard error of the mean (n=10-15).

2.3.3.3 Proteins

Similar to the polysaccharides (α and β), the proteins were also observed to be unevenly distributed on the membrane surface. The amount of protein observed was much lower in the initial stages of operation and they were present as very small clusters (Fig. 2.10a). These small protein clusters were observed to increase in size and surface coverage as the experiment progressed (Fig. 2.10b). The proteins were also observed to be distributed as a continuous layer, covering almost the entire membrane area even when TMP was still low (10 - 15 kPa) (Fig. 2.10c). After the TMP exceeded the threshold of 15 - 20 kPa, the protein layer became thicker and the thickness increased in proportion to the TMP increase (Fig. 2.10 d, e, f).

The protein biomass was observed to increase on the membrane surface during the MBR operation (Fig. 2.10). The biovolumes ranged from 0.026 to 0.63 $\mu m^3/\mu m^2$ in MBR-1 and 0.06 to 0.96 $\mu m^3/\mu m^2$ in MBR-2 when the TMP was between 3 - 15 kPa. At a TMP of 15 - 30 kPa, the volumes of proteins were from 0.58 to 1.02 $\mu m^3/\mu m^2$ in MBR-1 and 0.82-0.96 $\mu m^3/\mu m^2$ in MBR-2. Further, the volume of proteins increased to 1.53 - 1.69 $\mu m^3/\mu m^2$ in MBR-1 and 1.59 $\mu m^3/\mu m^2$ in MBR-2 when the TMP was between 30 kPa to 60 kPa. The protein volumes further increased to 3.01 $\mu m^3/\mu m^2$ in MBR-1 and 2.62-2.65 $\mu m^3/\mu m^2$ in MBR-2 when the TMP jumped to approximately 90 kPa (Fig. 2.11). The Pearson's correlation coefficient (r) was calculated and indicated a strong correlation between the protein accumulation and TMP rise, 0.952 for MBR-1 and 0.959 for MBR-2 (Table 2.2).

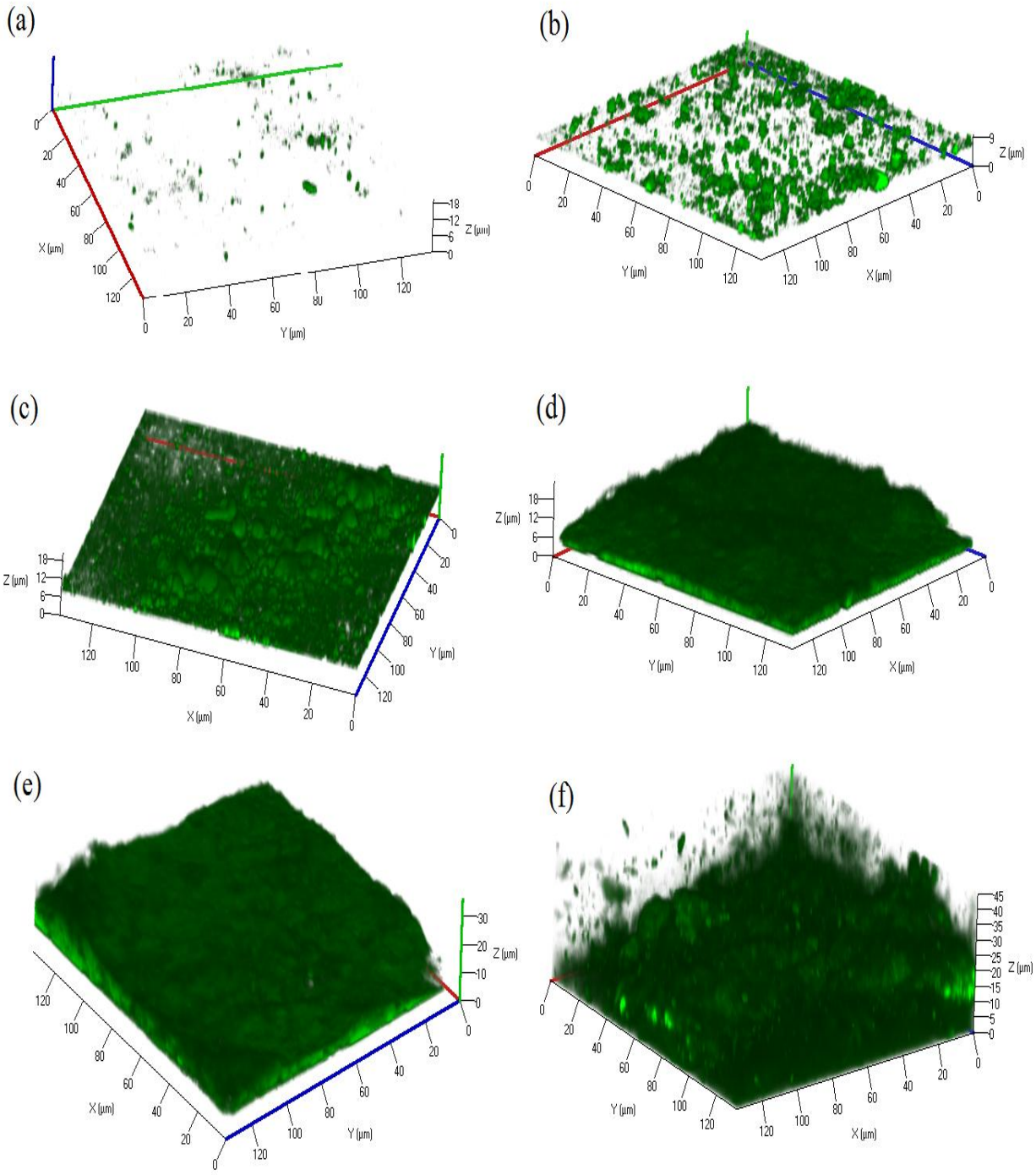

Fig. 2.10 Three dimensional images of proteins on hollow fiber membranes in a submerged MBR. The protein layer formed at (a) 3 - 8 kPa, (b) 8 - 10 kPa, (c) 10 - 15 kPa, (d) 15 - 30 kPa, (e) 30 - 60 kPa and (f) 60 - 90 kPa. All images were top down projects of 3D reconstructions of the protein layer. The total magnification for the images was 630×.

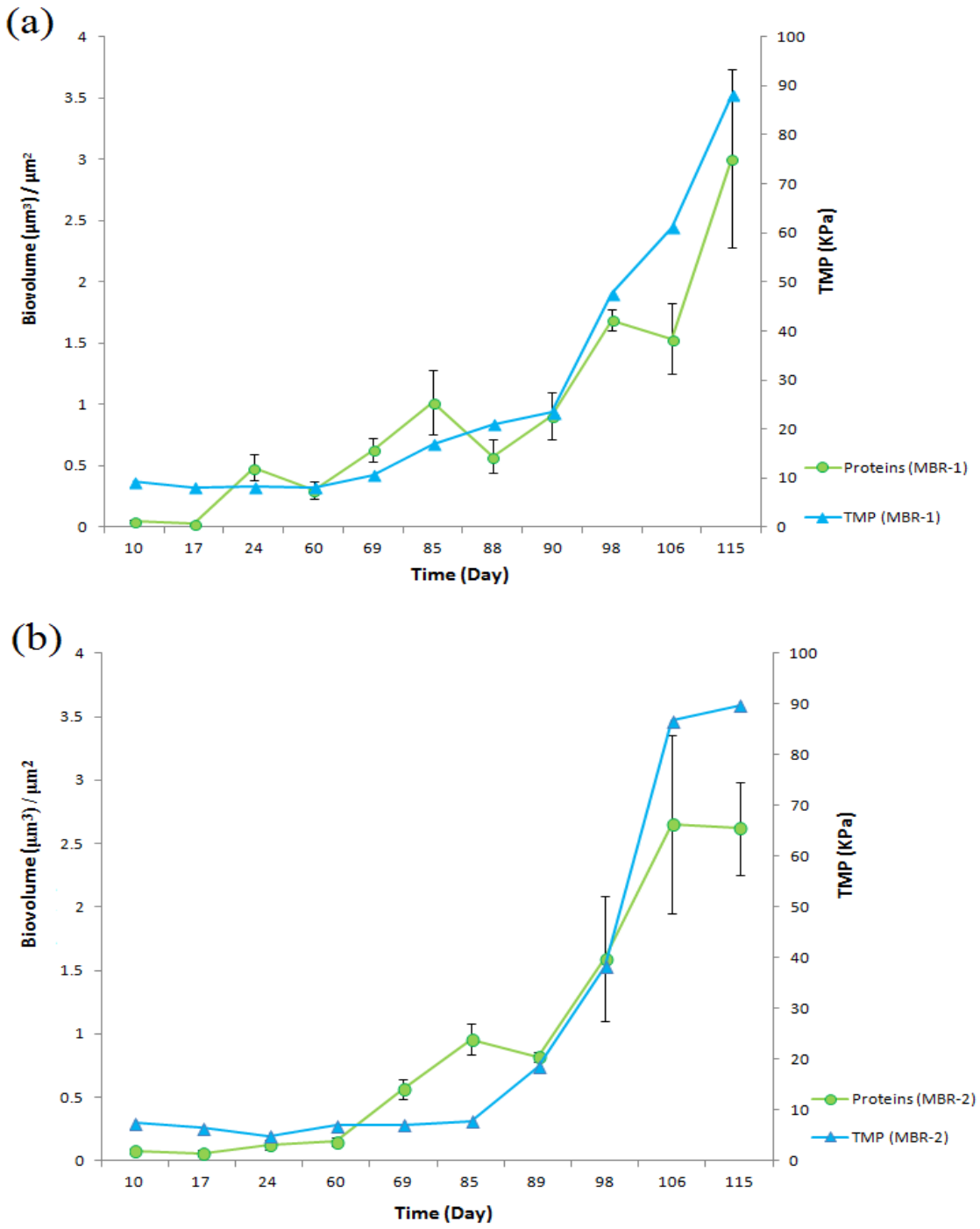

Fig. 2.11 The biovolumes of the proteins on hollow fiber membranes during the operation of (a) MBR-1 and (b) MBR-2. The biovolume of the proteins (green) are shown relative to the TMP curve (cyan) during MBR operation. The biovolume is presented as the volume (μm^3) of the proteins per area of hollow fiber membrane (μm^2). The data points were the average values of the 10 - 15 replicate images. The error bars are the standard error of the mean (n=10 - 15).

2.3.3.4 Distribution of cells on membrane

The attachment of microbes was also observed to be heterogeneous on membrane surface. In the first 10 d, only a few microorganisms were attached on the membranes and they distributed in very small clusters. The small microbial clusters increased in size across time while the MBRs were at the low TMP stage. When the TMP increased to 40 - 60 kPa, larger clusters of microorganisms were observed and these formed a continuous microbial mat on the membranes at 80 - 90 kPa (Fig. 2.12).

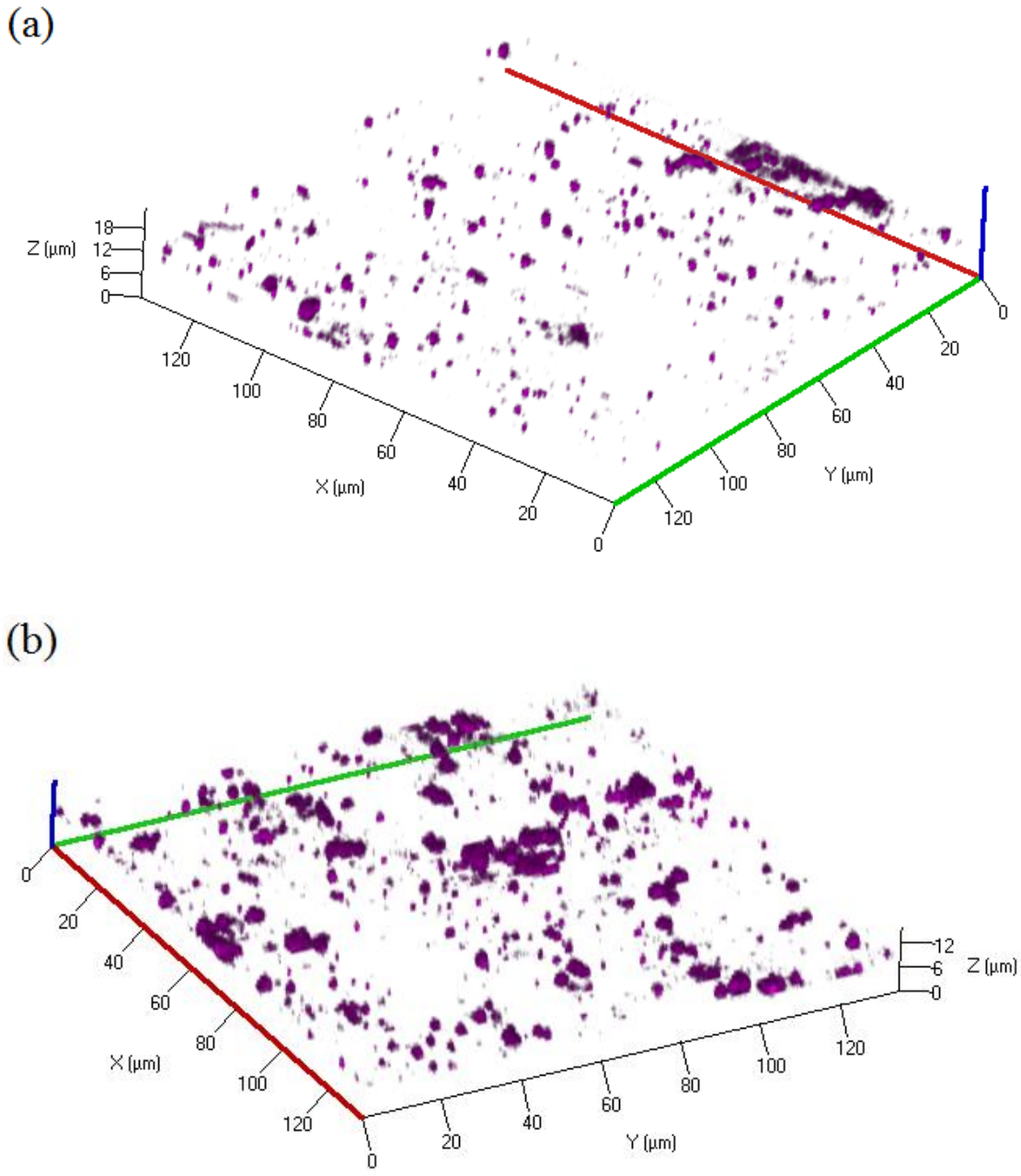

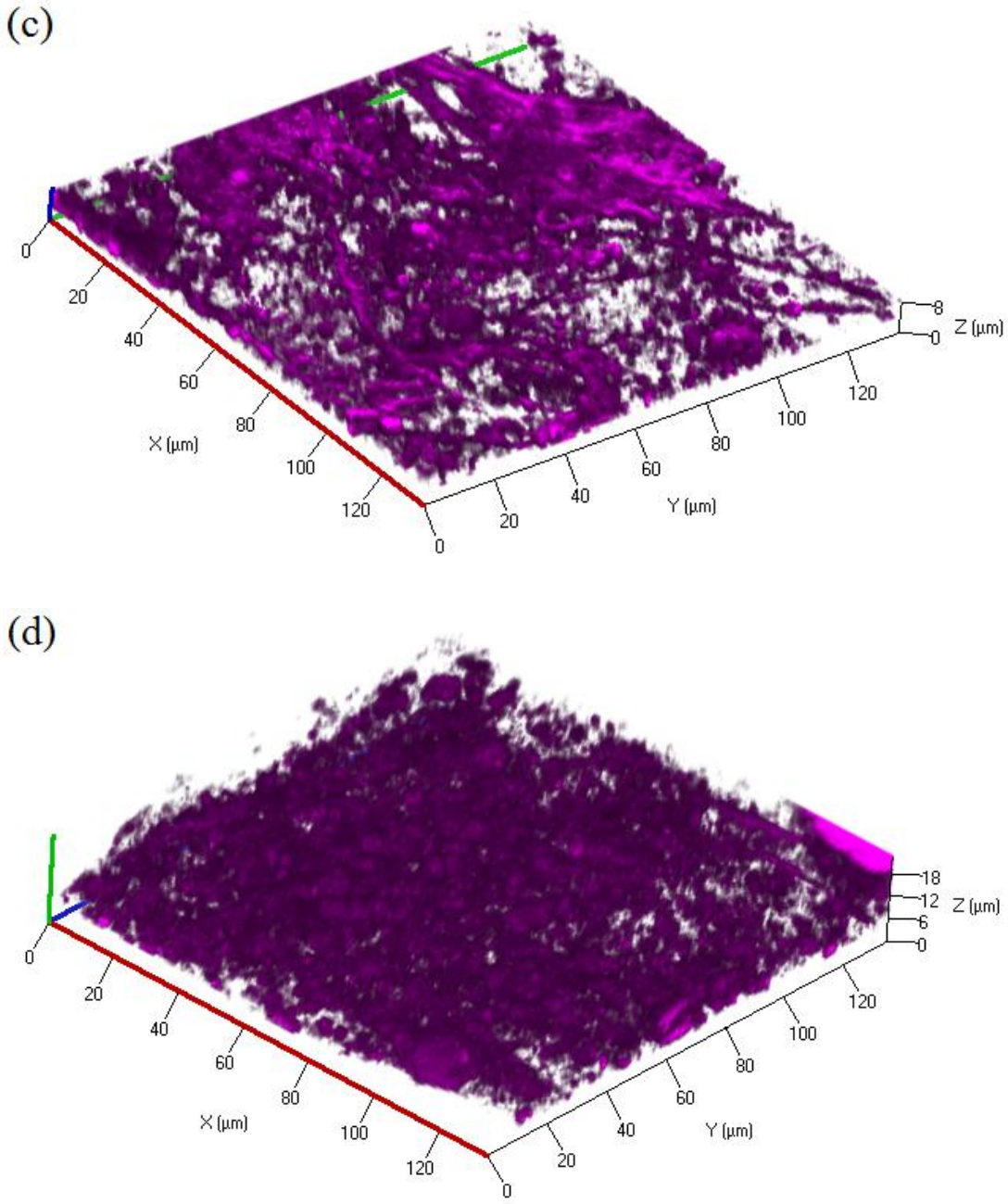

Fig. 2.12 Three dimensional images of microorganisms on hollow fiber membranes in a submerged MBR. The microbial layer formed at (a) 3 - 10 kPa, (b) 10 - 15 kPa, (c) 15 - 30 kPa and (d) 30 - 60 kPa. All images were top down projects of 3-D reconstructions of the microbial layer. The total magnification for the images was 630×.

At a TMP of 3 - 15 kPa, the microbial volume varied from 0.01 - 0.24 $\mu m^3/\mu m^2$ in MBR-1 and 0.04 - 0.28 $\mu m^3/\mu m^2$ in MBR-2. When the TMP increased to 15 - 60 kPa, the biovolumes for the microbes were between 0.27 - 0.6 $\mu m^3/\mu m^2$ in MBR-1 and 0.4 - 0.97$\mu m^3/\mu m^2$ in MBR-2. Finally, when the TMP reached the maximum level, 80 - 90 kPa, the microbial volume grew

to 0.9 $\mu m^3/\mu m^2$ in MBR-1 and 1.37 $\mu m^3/\mu m^2$ in MBR-2 (Fig. 2.13). The Pearson's correlation coefficients (r) between the TMP change and variation of microbial volume were 0.921 for MBR-1 and 0.772 for MBR-2 (Table 2.2), which implied the TMP rise was strongly correlated to the number of microorganisms in MBR-1 and also had a moderate correlation to the microbial volume in MBR-2.

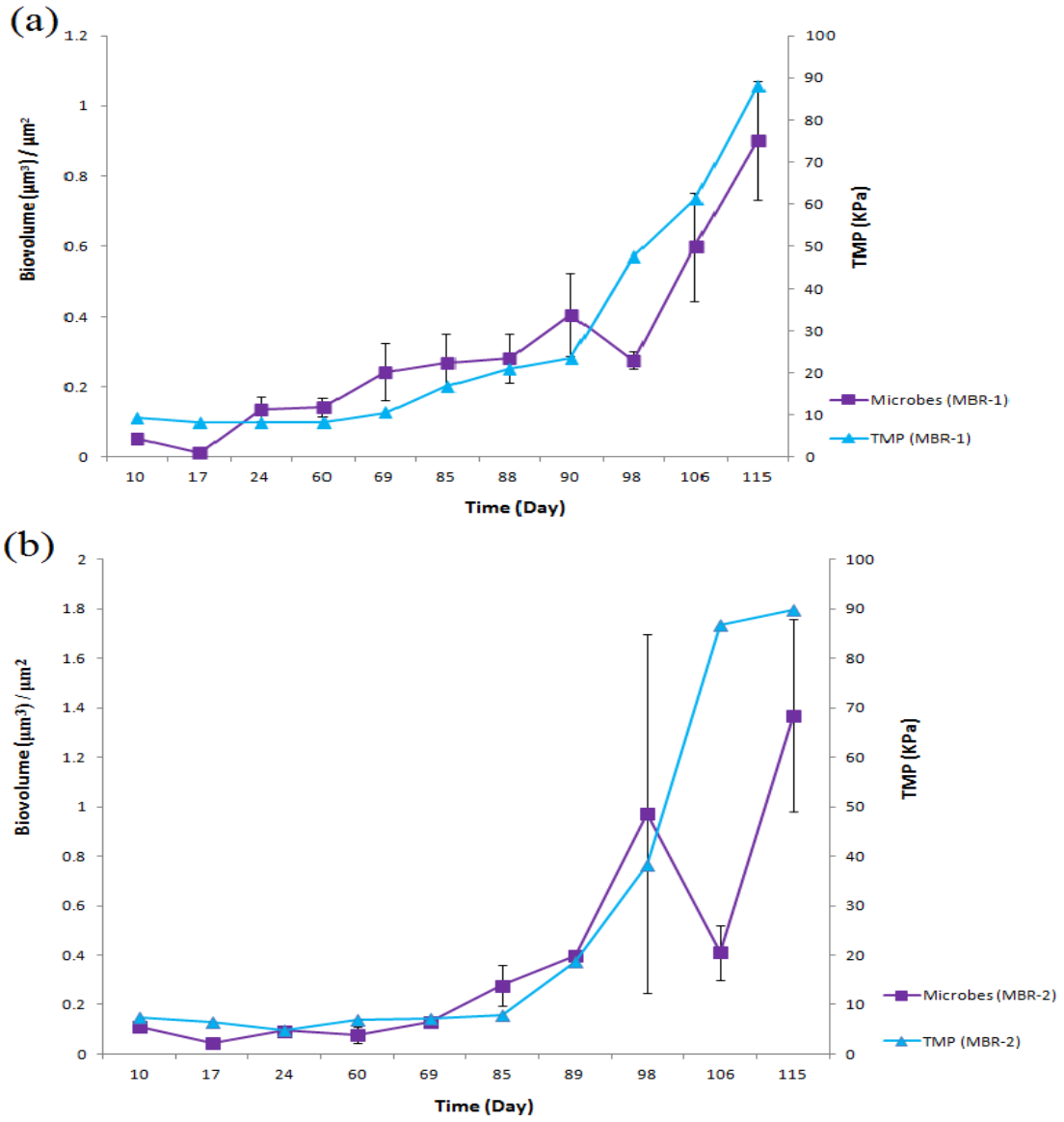

Fig. 2.13 The biovolumes of the microorganisms on hollow fiber membranes during the operation of (a) MBR-1 and (b) MBR-2. The biovolume of the microorganisms (purple) are shown relative to the TMP curve (cyan) during MBR operation. The biovolume is presented as the volume (μm^3) of the microorganisms per area of hollow fiber membrane (μm^2). The data points were the average values of the 10 - 15 replicate images. The error bars are the standard error of the mean (n=10 - 15).

2.3.3.5 The correlation between the total biovolume and TMP increase

Based on the analysis above, all of the four biofilm components, including α-polysaccharide, β-polysaccharide, protein and microorganisms, were shown to all have a positive correlation to the TMP rise, even though some components were strongly correlated to the TMP increase while others were only moderately correlated to the TMP jump. The biovolumes of the four biofouling components can be added together to determine the total biofilm volume and can be used to determine the relationship between the total biovolume and the TMP change. The data showed that the total biovolume ranged from 0.3 - 1.7 $\mu m^3/\mu m^2$ at a TMP of 3 - 15 kPa (MBR-1), and increased to 1.91 - 2.11 $\mu m^3/\mu m^2$ at a TMP of 15 - 30 kPa, 2.97 - 3.64 $\mu m^3/\mu m^2$ at TMP of 30 - 60 kPa, and reached 6.13 $\mu m^3/\mu m^2$ at a TMP of approximately 90 kPa (Fig. 2.14a). In MBR-2, the total biovolume was 0.24 - 2.24 $\mu m^3/\mu m^2$ at a TMP of 3 - 15 kPa, which increased to 2.34 $\mu m^3/\mu m^2$ at a TMP of 18.6 kPa and was 4.24 - 6.03 $\mu m^3/\mu m^2$ when the TMP jumped to approximately 90 kPa (Fig. 2.14b). The Pearson's correlation coefficients (r) between the TMP increase and biofilm accumulation were 0.966 and 0.903 for MBRs 1 and 2 respectively (Table 2.2), which indicated a significant correlation between the TMP rise and biofilm growth.

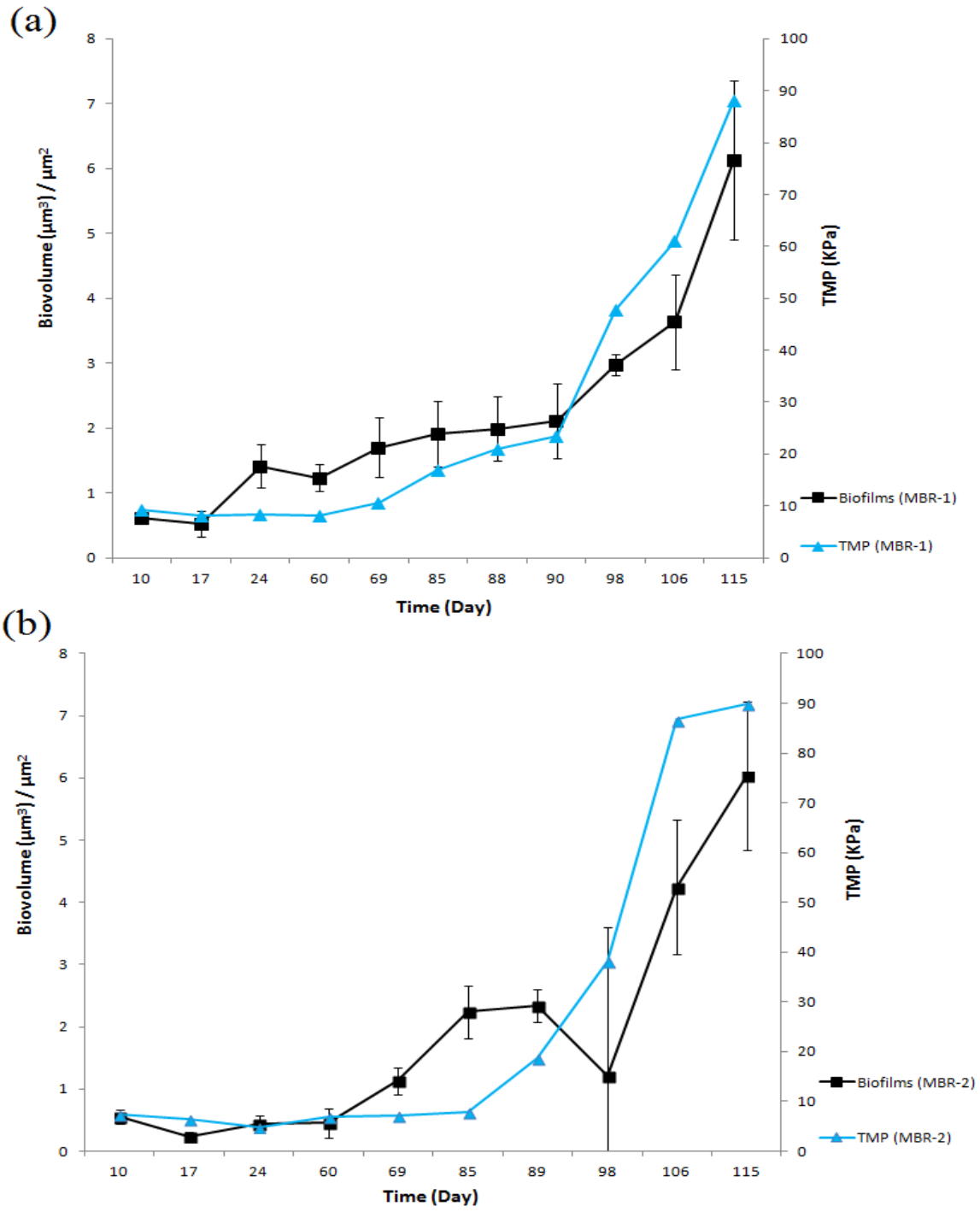

Fig. 2.14 The biovolumes of the biofilms (integration of the 4 components) on hollow fiber membranes during the operation of (a) MBR-1 and (b) MBR-2. The biovolume of the biofilms (black) are shown relative to the TMP curve (cyan) during MBR operation. The biovolume is presented as the volume (μm^3) of the biofilms per area of hollow fiber membrane (μm^2). The data points were the average values of additive biovolume of the four components on membrane. The error bars are the standard error of the mean (n=10 - 15).

2.3.4 Role of protein in TMP increase

The TMP curve was described above to be comprised of two distinct stages (Section 2.3.1), and it was observed that once the TMP reached 15 - 20 kPa, the pressure profile rapidly progressed to the jump stage. In contrast, the TMP was relatively stable at less than 15 kPa for up to 80 d preceding the jump stage. Therefore, the TMP of 15 - 20 kPa was determined here to be a threshold for the subsequent TMP jump stage. While there was a strong positive correlation of the various biofilm components to the TMP rise in the MBRs, it remains unclear which of the components were the most important factor to drive the sudden TMP jump. This was investigated by examining the change in the biofouling components before the TMP exceeded the threshold stage.

2.3.4.1 Increase rate of biofouling components

To study the increase of each biofouling component, the biovolume was normalized to its initial value measured at day 10, which was the first sampling time. For MBR-1, the volume of proteins was found to increase 6.5 - 13.6 fold by day 69, when the TMP was approximately 10 kPa, and increased 22 fold by day 85 when the TMP was 17 kPa. In comparison, the volumes of the α-polysaccharides, β-polysaccharides and microorganisms increased more slowly. When the TMP was 17 kPa at day 85, the biovolume of the α-polysaccharides, β-polysaccharides and microorganisms had only increased 1.99 fold, 1 fold and 5.19 fold respectively relative to the volume at day 10. This indicated that the proteins increased faster than the α- and β-polysaccharides and microorganisms when the TMP reached the threshold TMP stage (15 - 20 kPa). Further, after the TMP exceeded the threshold stage, this trend was maintained for the four components, where the protein volume increased 33 - 36 fold overall when the TMP was between 40 - 60 kPa and 65 fold when the TMP jumped to 88 kPa, while the α-polysaccharides, β-polysaccharides and microorganisms increased only 9.33, 2.73 and 17.35 fold respectively when the TMP jumped to 88 kPa at day 115 (Fig. 2.15a).

The same trend was observed for MBR-2, where the biovolumes of α-polysaccharides, β-polysaccharides and microorganisms increased more slowly than the proteins. When the TMP rose to the 18 kPa at day 89, the biovolumes of α-polysaccharides, β-polysaccharides and microorganisms increased 2.99, 3.19 and 3.61 fold respectively while the volume of proteins had increased 10.63 fold. Additionally, when the TMP increased to 87 kPa at day 106, the biovolumes of the α-polysaccharides, β-polysaccharides and microorganisms increased 3.41, 3.2 and 3.74 fold respectively while the proteins had increased 34.34 fold (Fig. 2.15b).

Therefore, in the both MBRs, the proteins were shown to increase the fastest as the TMP rose to and passed through the threshold stage.

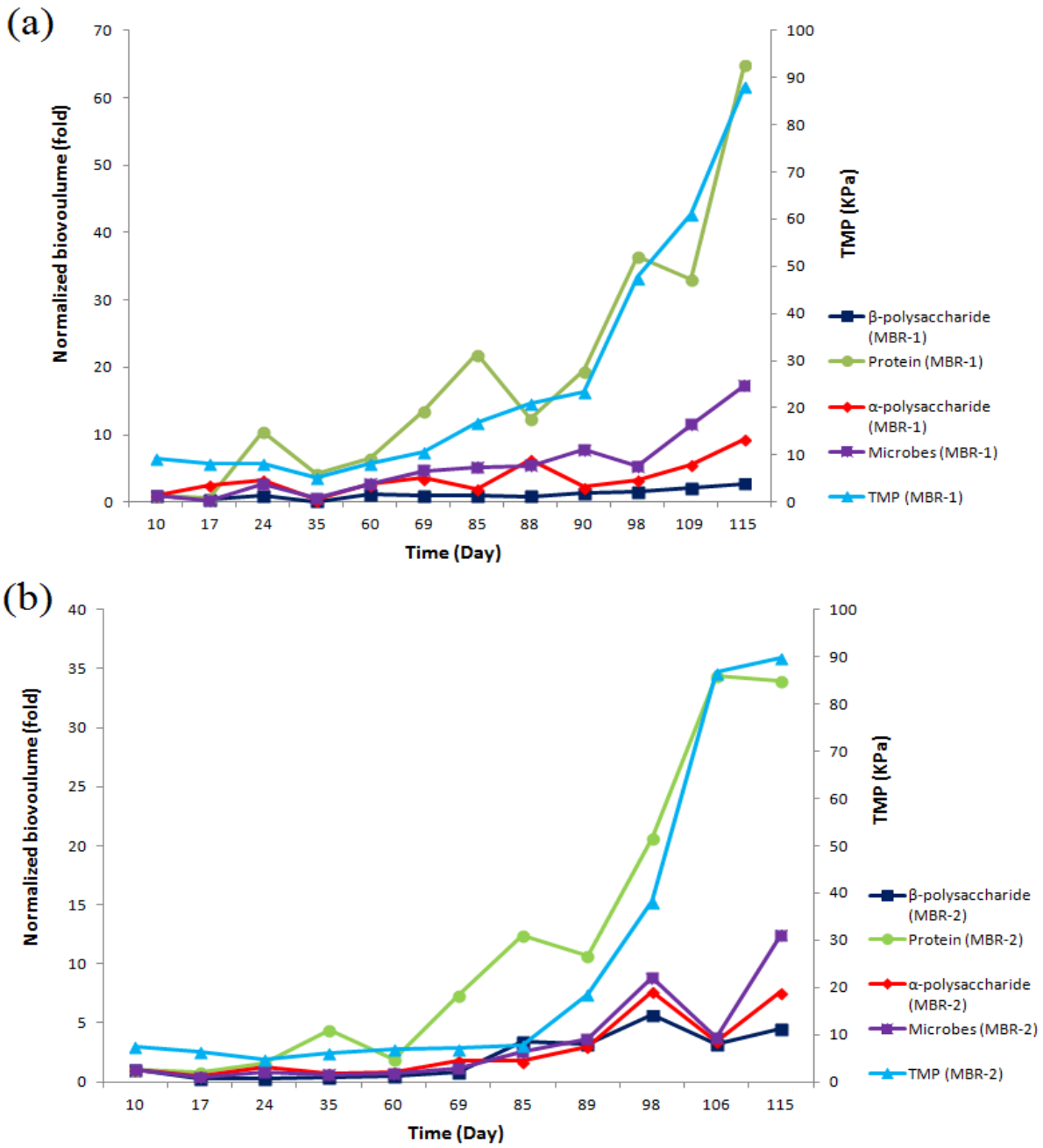

Fig. 2.15 Normalized biovolume (fold increase) for the four biofouling components in MBR-1 (a) and MBR-2 (b). The left "y" axis shows the normalized volume (fold change) as normalized to the initial value measured on day 10 and the right "y" axis shows the TMP (kPa).

2.3.4.2 Changes in abundance of biofilm composition

As indicated above, all four components investigated were positively correlated with the TMP

rise. Therefore, to better define the role of the different components in the fouling process, their relative percentages of each component was determined from the image data. The α-polysaccharides and β-polysaccharides were observed to be the dominant components of the biofilm on the membranes during the initial stages of the biofouling process (Fig. 2.16). For MBR-1, the α- and β-polysaccharides accounted for 63.09% and 20.76% respectively of the total biomass at 6 kPa on day 10. And at day 17, the percentages for the α- and β-polysaccharides were 32.61% and 60.22% respectively when the TMP was approximately 6 kPa. In contrast, the proteins and microorganisms accounted for only 7.61% and 8.54% respectively on day 10, and 5.06% and 2.12% on day 17. Similarly, the α- and β-polysaccharides also dominated the initial biofouling layers in MBR-2, where the percentages for the α- and β-polysaccharides were 40.5% and 25.31% respectively at 6 kPa (day 10), while the proteins and microbes accounted for only 14.11% and 20.07%. Thus, the α-polysaccharides and β-polysaccharides were found to be dominant macromolecules during the early stages of fouling.

However, the proteins were observed to significantly increase in percent composition in the later stages of the MBR operation (Fig. 2.16). In MBR-1, the percentage of protein increased to 34.33% at day 24 and 37.07% at day 69, when the TMP was between 8 - 12 kPa, while the abundance of α-polysaccharides, β-polysaccharides and microorganisms were 26.53%, 29.45% and 9.69% respectively at day 24, and 22.15%, 26.5% and 14.29% at day 69. When the TMP rose to 17 kPa at day 85, the proteins were found to account for 53.38% in the total biomass, whereas the other components were present at lower levels, 19.33% (α-polysaccharides), 13.19% (β-polysaccharides) and 14.1% (microorganisms). The abundance of proteins from day 24 onwards was between 40% - 60% for MBR-1. Similarly, the proteins also became dominant in MBR-2 (Fig. 2.16b), where their abundance increased to 57% at day 35 (6 - 7 kPa) while the abundance of the α-polysaccharides, β-polysaccharides and microorganisms were 15.7%, 15.6% and 11.68% respectively. Thus, the proteins were the predominant biomolecules in the biofilms for both MBRs, even when the pressure was still low (3 - 15 kPa) and continued to be the dominant macromolecule for the duration of the experiment.

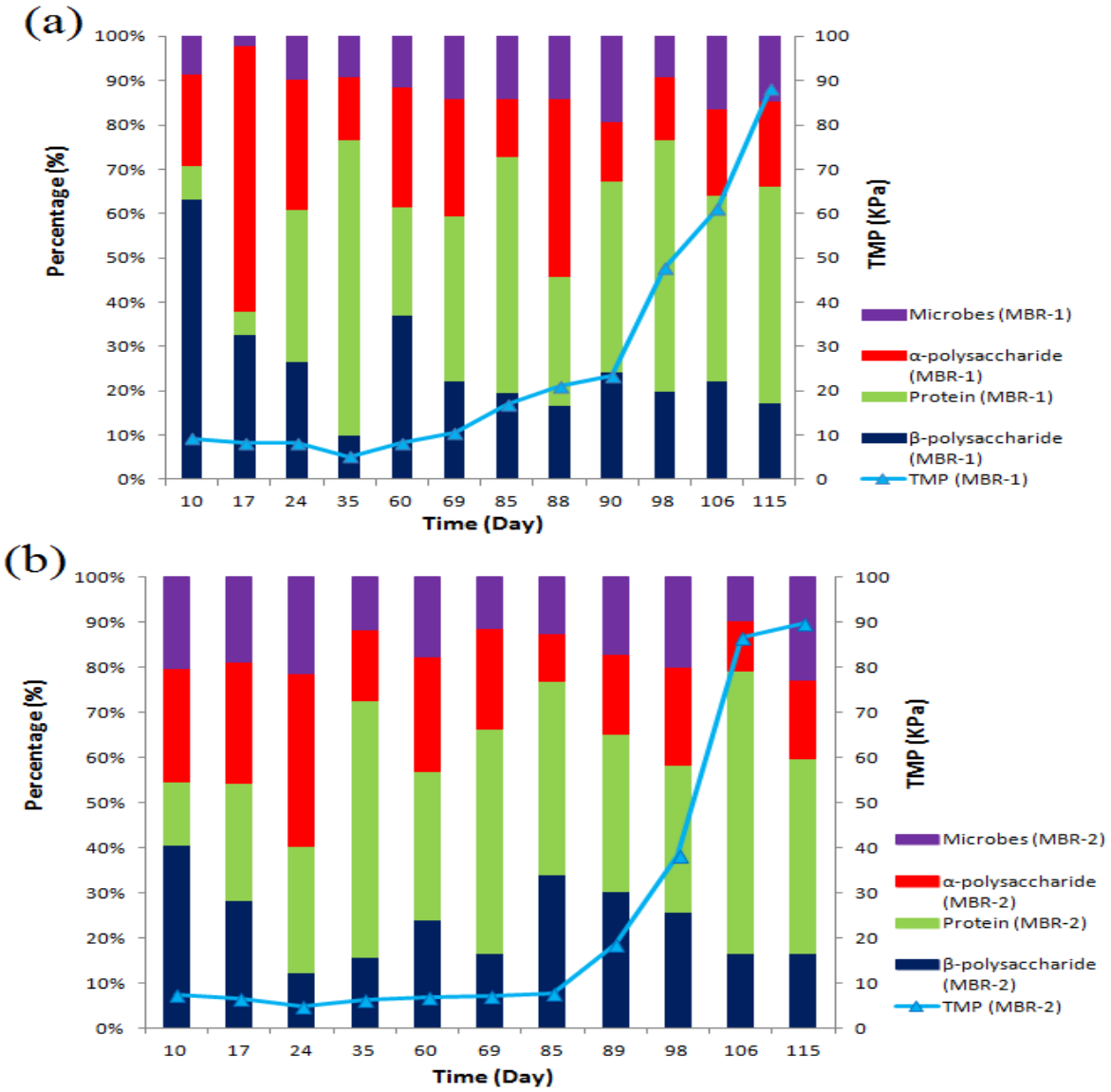

Fig. 2.16 The relative percentage of each biofilm component during operation of the MBRs. The "x" axis shows the time (day). The left "y" axis shows the relative percentage for each biofouling component. The percentage for different components was calculated by dividing the volume of each component by the total volume of the four components. The right "y" axis shows the TMP.

2.3.5 Correlation of sludge EPS components and TMP increase

The data above have presented the relative abundance of different biopolymers in the biofilm. In particular, it was apparent from the data above that the proteins were enriched in the biofilm relative to the cells and other biopolymers. One possible source of the proteins and polysaccharides is from the sludge or the bacteria in the sludge. Therefore, to determine if the

enrichment of proteins in the biofilm could be due to a concomitant enrichment in the sludge and therefore deposition into the biofilm, the EPS components in activated sludge were quantified at different stages of operation. It should be noted that the goal was not to make a quantitative comparison of the EPS components in the biofilm and the sludge, but rather to determine the relative abundance of different polymers in the sludge for comparison to their relative abundance in the biofilm and how these ratios changed over time. As described above, the EPS in sludge was divided into two components, soluble EPS (sEPS) and bound EPS (bEPS), where the total carbohydrates (polysaccharides) and proteins were quantified.

For both MBRs, there were no significant changes in the protein or carbohydrate concentrations in the sEPS component of the sludge (Fig. 2.17). Similarly, the protein concentrations did not vary in the bEPS across the TMP curve. In contrast, the concentrations of the carbohydrates in the bEPS were observed to increase at a steady rate for both systems, increasing from 60 μg mL^{-1} at the low TMP stage to 120-160 μg mL^{-1} at the high TMP stage (Fig. 2.17). Despite showing an increase in concentration across the TMP profile, there was no significant correlation of the carbohydrate concentration in the bEPS and the TMP rise (Table 2.3).

Table 2.3 The correlation of sludge EPS components and TMP increase

	Carbohydrates in sEPS (MBR-1, MBR-2)	Carbohydrates in bEPS (MBR-1, MBR-2)	Proteins in sEPS (MBR-1, MBR-2)	Proteins in bEPS (MBR-1, MBR-2)
Pearson Correlation (r) with TMP	-0.311, 0.408	0.573, 0.56	-0.43, 0.067	0.025, -0.462
*Significance (p)	0.549, 0.422	0.235, 0.248	0.395, 0.9	0.963, 0.356

*: Correlation was significant at the 0.05 level (2-tailed).

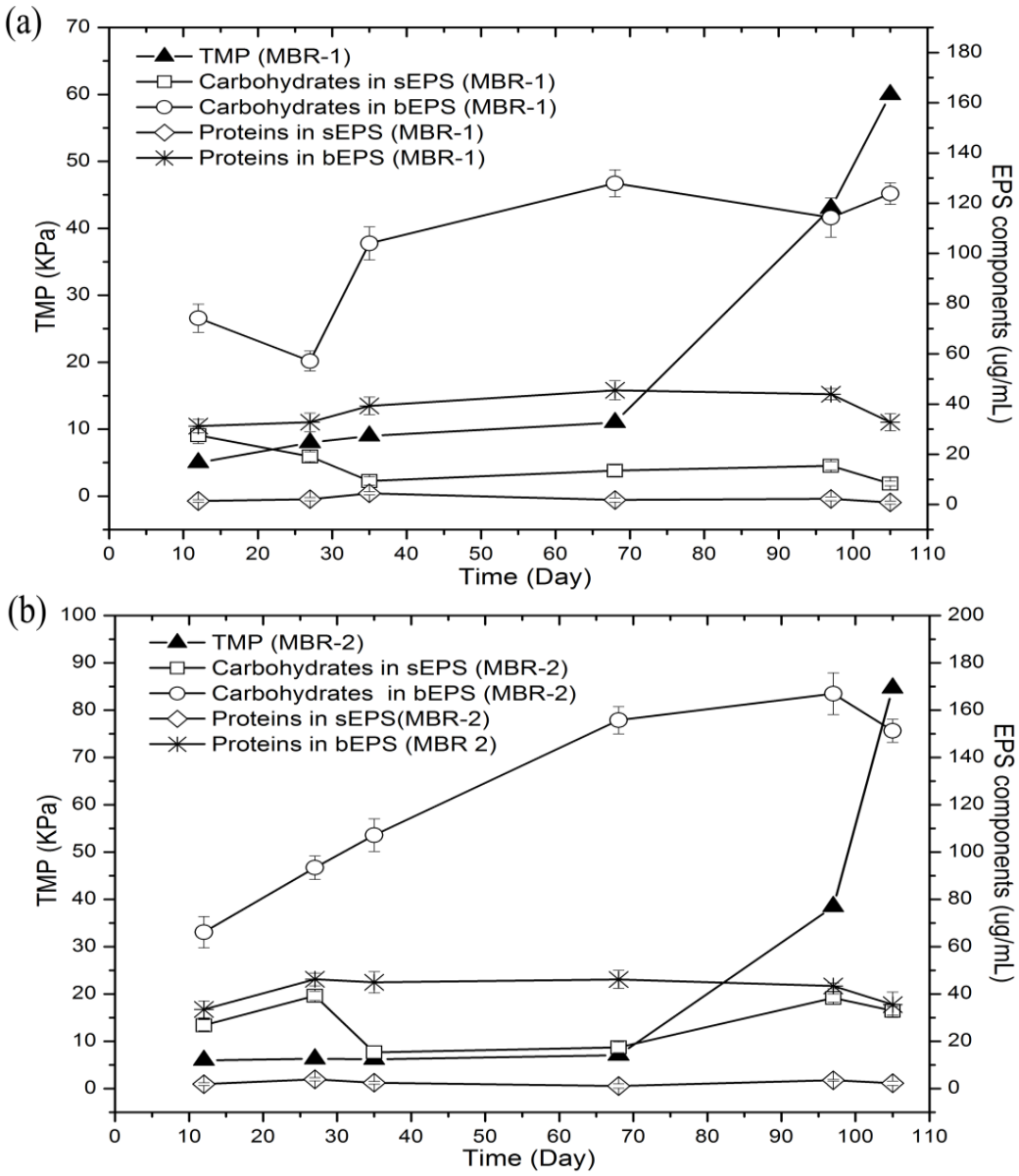

Fig. 2.17 The concentration of carbohydrates and proteins in the sludge for MBR-1 (a) and MBR-2 (b). The TMP at each test point (solid triangles) are shown to the left *y* axis. The carbohydrates in the soluble EPS (sEPS) (open squares), carbohydrates in the bound EPS (open circles), proteins in sEPS (open diamonds) and proteins in bEPS (stars) are shown to the right *y* axis. The data points are the average values of EPS components in sludge. The error bars are the standard errors of the mean (n=3).

2.3.6 Relations between microbes and other biofouling components

The α-polysaccharides, β-polysaccharides, proteins and microorganisms were demonstrated above to correlate positively to the TMP increase during the biofouling process. Proteins were also shown to increase the most dramatically during the increase in TMP. In order to develop

strategies to control fouling, it is important to know the source of these components. They can either be derived from the soluble EPS compounds in the sludge, which become attached to the membrane as a consequence of the filtration process or they can be produced at the membrane surface by the bacteria attached onto the membrane. To address this question, image based analysis was used to characterize the localization of the EPS components. The hypothesis is that if the compounds are filtered onto the membrane surface from the soluble components in the sludge, e.g. the soluble EPS, they should be randomly distributed on the membrane. Conversely, if they were produced by the bacteria growing on the membrane surface, e.g. the bound EPS, then they would be expected to co-localize with the bacterial cells on the membrane. Therefore, the relationships between the biopolymers and cells were assessed through the distribution, production and co-localization of EPS components and microbial cells.

2.3.6.1 Correlation in biovolume of microorganisms and EPS components

To determine the relationship between the individual fouling components, the Pearson correlation coefficient between the EPS fractions and microbes was calculated. Comparison of the biofilm compositions across the TMP curve indicated that the biovolume of α-polysaccharides was positively correlated to the increase in cells for both MBR-1 and MBR-2 (Fig. 2.18), where the Pearson's correlation coefficients (r) were 0.926 and 0.850 in MBR-1 and MBR-2 respectively (Table 2.4). Similar positive correlations were also found for the β-polysaccharides and microbes, Pearson's correlation coefficients (r) 0.822 (MBR-1) and 0.971 (MBR-2), and for proteins and bacteria, Pearson's correlation coefficients (r) 0.923 (MBR-1) and 0.795 (MBR-2) (Table 2.4). The high Pearson's correlation coefficients indicated that the EPS components increased proportionally in relation to the change in the biovolume of cells in the biofilms.

Table 2.4 Correlation of EPS components and the microorganisms in biofouling layers.

	α-polysaccharide (MBR-1, MBR-2)	β-polysaccharide (MBR-1, MBR-2)	Protein (MBR-1, MBR-2)
Pearson Correlation coefficient (r) to microorganisms	0.926, 0.850	0.822, 0.971	0.923, 0.795
*Significance (p)	0.0001, 0.002	0.002, 0.0001	0.0001, 0.006

*: Correlation is significant at the $p < 0.05$ level (2-tailed).

2.3.6.2 The co-localization of EPS components and microorganisms

To determine if the macromolecules were closely associated with the microbial cells, images were analyzed by Mander's coefficient in quantitative co-localization analysis (Figs. 2.18 and 2.19) (Dunn et al., 2011; Zinchuk and Zinchuk, 2001). This method can be used to determine whether two or more fluorescent signals occupy the same pixels in the same section in confocal microscopic images. The Mander's coefficient ranges from 0-1, in which 0 indicates that none of the pixels in the selected channel co-localize with another channel and 1 indicates that 100% of the pixels in the selected channel co-localize with the signals from the first channel.

At the TMP of 3-10 KPa, an average of 47.8(±18.3)% of *Alpha*-polysaccharides in biofouling colocalized with 78.8(±12.6)% of microbial cells on membrane in the two MBRs (Table 3). Similarly, 41.3(±13.7)% of *Beta*-polysaccharides in biofouling colocalized with 81.3(±16.6)% of microbial cells while 50.8(±15.2)% of proteins colocalized with 69.2(±23.7)% of microbial cells (Table 3). When the TMP increased to the threshold 15-20 KPa, more EPS components were found to colocalize to the microorganisms (68.5(±15.9)% of *Alpha*-polysaccharides vs. 83.8(±15.4)% microorganisms, 62.6(±12.1)% of *Beta*-polysaccharides vs. 73.6 (±8.3)% microorganisms, 59.7(±9.5)% of proteins vs. 86.2(±0.6)% microorganisms). When the TMP continued to rise to the 60-90 KPa, the trend of colocalization between the EPS components and microorganisms was maintained on membrane, where there were 59(±11.5)% of *Alpha*-polysaccharides, 59.7(±16.1)% of *Beta*-polysaccharides and 57.1(±15.2)% of proteins in biofouling colocalized with 90-97.3% of microorganisms (Table 2.5). This suggested a strong overlap of the EPS components with the microbial cells on membrane.

Table 2.5 The co-localization coefficients between the EPS components and microbial cells on the hollow fiber membrane in MBR-1 (a) and MBR-2 (b).

(a)

Time (d)	TMP (KPa)	*Alpha*-polysaccharides (αs) vs. Microbes (M)		*Beta*-polysaccharides (βs) vs. Microbes (M)		Proteins (Pr) vs. Microbes (M)	
		Mander_αs	Mander_M	Mander_βs	Mander_M	Mander_Pr	Mander_M
10	5	0.600	0.598	0.395	0.970	0.615	0.371
17	8.2	0.283	0.770	0.267	0.589	0.376	0.385
24	9.5	0.244	0.813	0.232	0.999	0.259	0.889
60	9.7	0.440	0.928	0.349	0.808	0.515	0.853
69	10.6	0.729	0.926	0.496	0.987	0.646	0.867
88	20.5	0.844	0.992	0.747	0.819	0.692	0.868
106	60.9	0.723	0.929	0.521	0.988	0.673	0.977
115	89	0.511	0.999	0.658	0.951	0.537	0.999

(b)

Time (d)	TMP (KPa)	*Alpha*-polysaccharides (αs) vs. Microbes (M)		*Beta*-polysaccharides (βs) vs. Microbes (M)		Proteins (Pr) vs. Microbes (M)	
		Mander_αs	Mander_M	Mander_βs	Mander_M	Mander_Pr	Mander_M
10	4.5	0.786	0.771	0.725	0.949	0.756	0.691
17	6.5	0.411	0.587	0.352	0.637	0.611	0.339
24	7.3	0.350	0.924	0.401	0.668	0.362	0.738
60	7.8	0.385	0.710	0.434	0.887	0.474	0.941
69	9.5	0.549	0.848	0.477	0.632	0.463	0.849
88	16.3	0.525	0.683	0.505	0.653	0.502	0.856
106	75.8	0.479	0.941	0.419	0.806	0.370	0.949
115	89.4	0.647	1.000	0.789	0.872	0.704	0.966

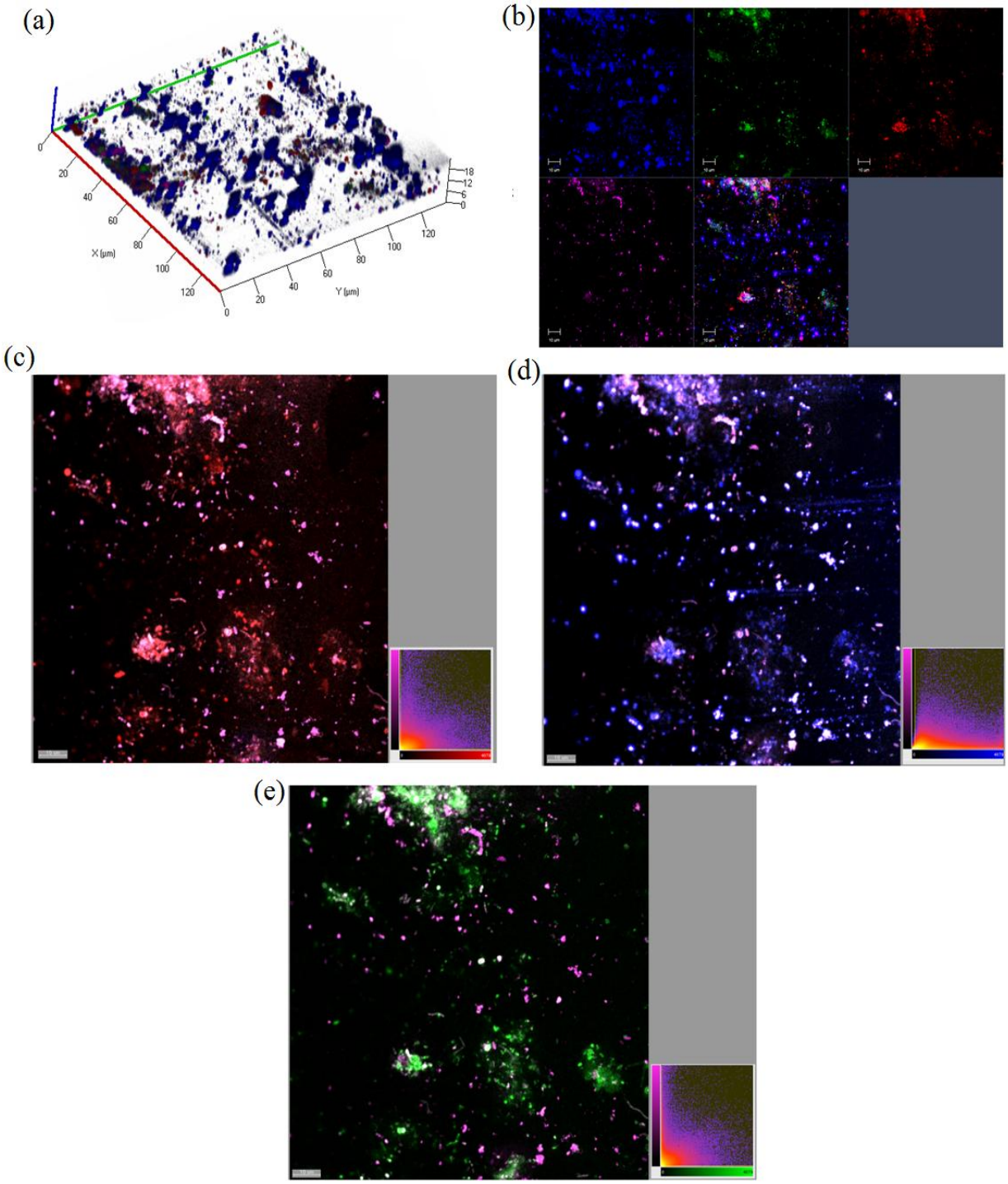

Fig. 2.18 The co-localization analysis of the 3D image of biofouling layer at 5-10 kPa. The 3D image of the biofouling layer (a) was processed using the "Maximum Intensity Projection" function in ZEN-2009 light edition (Carl Zeiss) to convert images into 2D images and were split to show the relative distribution of biofouling components (b). The co-localized pixels (white) were displayed between the α-polysaccharides (red) and microbes (purple) (c), β-polysaccharides (blue) and microbes (purple) and proteins (green) and microbes (purple). The scatter plot graphs next to the co-localized images in c, d, e show the intensity distribution of pixels.

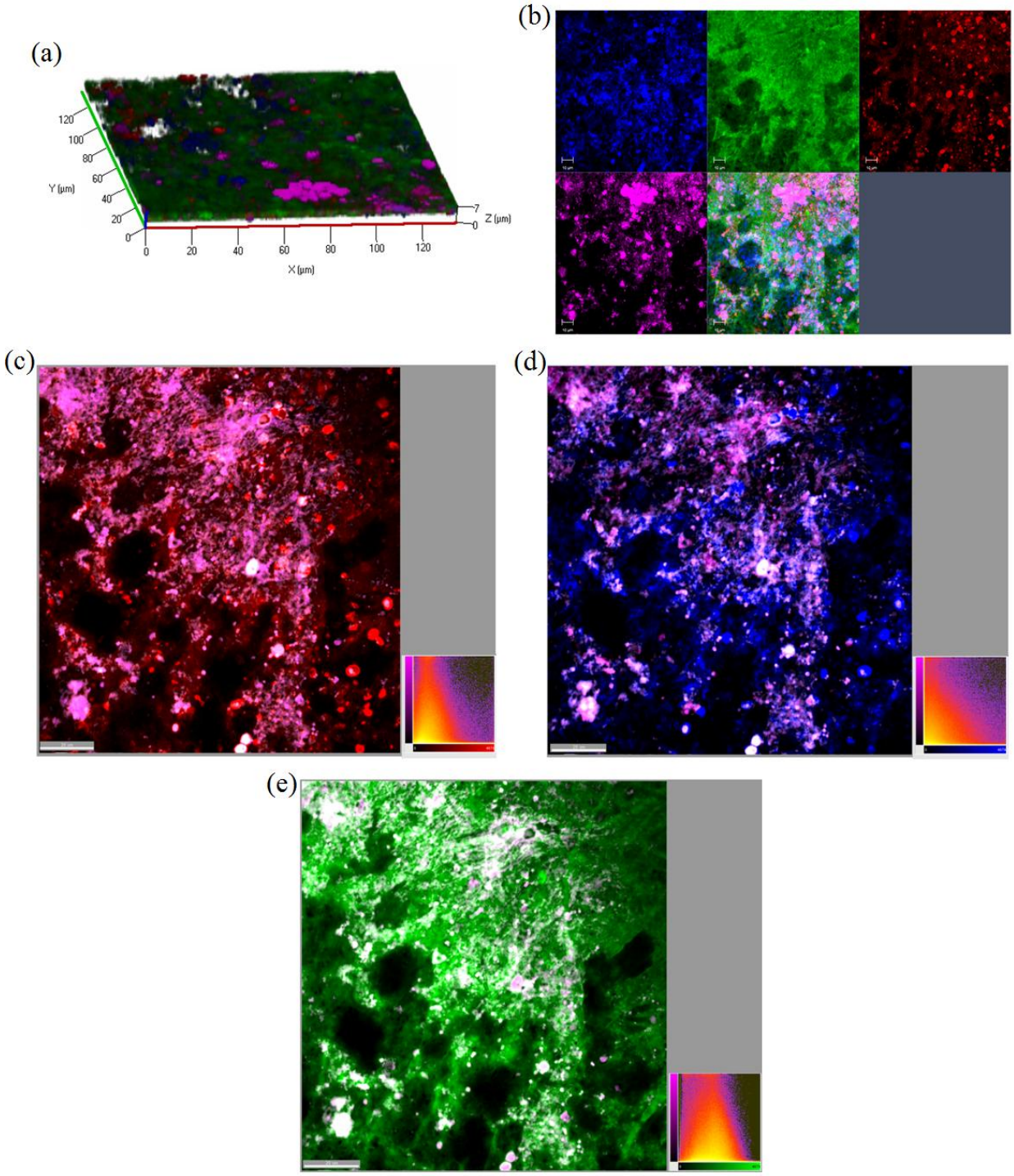

Fig. 2.19 The co-localization analysis of the 3D image of biofouling layer at 30-90 kPa. The 3D image of the biofouling layer (a) was processed using the "Maximum Intensity Projection" function in ZEN-2009 light edition (Carl Zeiss) to convert images into 2D images and were split to show the relative distribution of biofouling components (b). The co-localized pixels (white) were displayed between the α-polysaccharides (red) and microbes (purple) (c), β-polysaccharides (blue) and microbes (purple) and proteins (green) and microbes (purple). The scatter plot graphs next to the co-localized images in c, d, e show the intensity distribution of pixels.

2.4 Discussion

The biofouling phenomenon, which leads to the TMP jumping, is a crucial problem for the wider application of MBRs (Nguyen et al., 2012). In this project, the TMP increase was observed to occur in two distinct phases. The first phase was defined as a steady TMP stage, where the TMP was maintained between 3 - 15 kPa for 85 to 90 d. The second phase was characterized by a rapid TMP increase, where the TMP reached the maximum pressure, 80 - 90 kPa, in less than 20 d. The rate of increase for this stage was significantly greater, dTMP/dt of 2.143 - 2.778 kPa/day, than the rate of change for the constant pressure phase dTMP/dt of 0.172 - 0.183. This rapid TMP increase has been previously observed and has been termed the TMP jump phase (Cho and Fane, 2002). For example, it was also reported that the TMP changed in two distinct stages and that the increasing rate of TMP (dTMP/dt) was below 10^{-2} Pa/s (equal to 0.864 kPa/day) in the first stage and approximately 1 Pa/s (equal to 86.4 kPa/day) in the second stage, when the MBR was operated at a constant flux of 10 $L.m^{-2}.h^{-1}$ (Ognier et al., 2002). Similarly, a three-stage TMP curve was described in MBRs operated at a constant flux of 10 $L.m^{-2}.h^{-1}$ to 30 $L.m^{-2}.h^{-1}$, where the TMP increased from approximately 1 kPa to 2 kPa quickly in the first 1 h (stage 1), then increased slowly to 7-8 kPa over a period of 200 h (stage 2) and entered into an abrupt jump stage in stage 3 [96, 97]. Examination of the 3 phase TMP curve on a daily basis indicated that it had features which were consistent with the TMP curve reported here, where there was a long-term, low TMP stage followed by a rapid TMP increase stage.

The key question remains as to what component of the microbial biofilm contributes most to the change in TMP or loss of system performance. It seems clear that the increase in TMP is in part a consequence of the increased resistance of the biocake or biofilm that forms on the membrane (Hwang et al., 2012). To determine the relationship between the TMP rise and the biofilm formed on the membranes, quantitative image analysis was performed and it was observed that the biofilm was heterogeneously distributed across the membrane surface. This was particularly obvious for the low TMP stage, where the biofilm appeared as small clusters of cells and EPS. Over time, these small clusters increased in size and at the time when the TMP was at its highest, 60 - 90 kPa, most of the membrane surfaces were covered by the biofilms as large clusters or as a continuous film on the membrane. It has been proposed that the transition of TMP from a slow to a fast rate of increase, as observed during the TMP jump, may be a consequence of the heterogeneous distribution of the fouling layer (Cho and Fane, 2002). The hypothesis is that some, but not all, parts of membrane would become colonized or

fouled and this would lead to a local reduction in permeability and flux for those regions. Therefore, when a MBR is operated at a constant average flux, this would require the flux through unfouled or less fouled portions of the membrane to increase to maintain that flux. Previous work has demonstrated that increased flux is associated with an increased rise in the TMP (Le Clech et al., 2003). This process would lead to a self accelerating process of fouling on the rest of the membrane, with a concomitant increase in the TMP required to push water across the less fouled portions of the membrane. In this way, the heterogeneous biofilm distribution observed here may lead to the rapid TMP jump observed.

While the accumulation of the biofilm on the membrane seems to be a driver of the increase in TMP, the biofilm is composed of many different macromolecules as well as cells and it remains possible that much of the fouling issue is specific to the accretion of a specific biofilm component, e.g. the EPS or cells. Previous studies have investigated the different biofilm components in an attempt to answer this question and most have concluded that EPS components are important for the TMP rise. For example, it has previously been suggested that the polysaccharide component of biofilms formed by *Micrococcus luteus* was a key factor in fouling of the membranes (Lei et al., 2009). In contrast, proteins were determined as the main EPS component in another work, although the EPS also contained significant amounts of plolysaccharides (Meng et al., 2007). Recently, it was reported that over production of the alginate polysaccharide was associated with an accelerated TMP jump (Chen et al., 2013). It was presented in this study that the two types of polysaccharides investigated (α and β), proteins and microbial cells were all present in the biofilm at both low and high TMP stages in MBR. This was consistent with the previous publications (Chen et al., 2007; Chen et al., 2006b), showing the α-polysaccharides, β-polysaccharides, proteins and microorganisms were all involved in the biofouling process and should be considered together when the biofouling mechanisms are investigated.

The α-polysaccharides, β-polysaccharides, proteins and microorganisms were all positively correlated, Pearson Correlation coefficients between 0.7 - 0.95, with the TMP increase. The integrated biovolumes of the four components were also positively correlated with the TMP increase (Pearson correlation coefficient 0.9 - 0.97). This indicated that the combined effect of the individual components may be the factor that leaded to the increased TMP. Among the four components, proteins were shown to increase faster than the cells or either of the two polysaccharide types monitored. Indeed, on a percentage basis relative to the total biomass biovolume, the proteins were present in the highest proportion, especially at the TMP jump

stage. By comparison, the polysaccharides represented the highest proportion of the four components when the TMP was relatively stable and that both the α- and β-polysaccharides made relatively similar contributions. In comparison, it was reported that the α-polysaccharides were the dominant EPS components while proteins and β-polysaccharides were minor components during the initial stages of biofilm formation in MBRs (Chen et al., 2006a). The higher protein biomass observed in this study was consistent with other published work showing that proteins accumulated preferentially in the biofouling layers of the MBR (Tian et al., 2012). It was noted that studies by Lei et al., 2009 and Chen et al., 2013 used pure bacterial cultures, *Micrococcus luteus* and *Pseudomonas aeruginosa*, respectively to foul the membrane, while datas from Meng et al., 2007 and this study used the sludge cultures, which are highly species to study the fouling process. This may explain why two different conclusions were acquired. Collectively, the data suggested that the production of proteins was more important than the two types of polysaccharides or the cells during the transition of from the low to high TMP stage under the conditions used for this study. This may also suggest that strategies that target proteins may be suitable to control the biofouling process in MBRs. In one previous study, the protein composition of the EPS was reported to be significantly different from the cellular proteome in biofilms formed by acid mine drainage microbial community, where the histone-like DNA binding protein and cold shock protein were overrepresented in the EPS (Jiao et al., 2011). In studies with pure cultures, the surface proteins, such as Bap protein, Esp protein and LapA protein, were identified in the biofilm matrix (Latasa et al., 2006). Therefore, future studies may focus on the compositions and diversity of the proteome of biofilm matrix.

The results indicated that the distribution of the biofilm on the membrane surface and the higher ratio of proteins to other biofilm components may be linked to the TMP rise. The protein and other components may either accumulate on the membrane as a consequence of being filtered onto the membrane from the sludge or they may be secreted by the microbial cells that settle and attach to the membrane. In soluble EPS, the protein biomass as well as the polysaccharides remained relatively constant across all stages of MBR operation. This finding is supported by another study, where the biofilm exhibited a higher filtration resistance than the bulk sludge cake layer (Wang et al., 2007). The surface associated biofilm is likely to be the source of biopolymers responsible for the reduction in MBR performance. To investigate the source of the different components, the relationships between the EPS compositions, including α-polysaccharides, β-polysaccharides and proteins, and the microbial cells were characterized. This was performed by quantitatively describing the co-localization of the

different components, with the expectation that if they accumulate randomly from the sludge, there should be weak or little co-localization. Conversely, if the EPS components are produced by the cells, then there should be a strong, positive correlation in their co-localization with the cells. Interestingly, the EPS components were found to correlate positively with the microorganisms, where the Pearson correlation coefficients were 0.24 - 0.35 between the three EPS macromolecules and the microbes. The Pearson correlation co-efficients were not very high, and this may be due to the shape of the microbial cells and the relative site of production of the EPS components. For example, if the EPS is secreted from the cell, then it would surround the cell and would not occupy identical pixels as the cells. To address this, the images were analyzed using the Mander co-localization coefficient, which revealed that approximately 50% of the EPS co-localized with 80 - 90% microbial cells. The polysaccharides and proteins usually had larger biovolumes and enveloped the microbes, which would be consistent with their production and secretion by the microbes. While it remains a possibility that the EPS components in the sludge could preferentially adhere to the bacterial cells, the data suggests that the fouling components are present on the membrane largely as a consequence of attachment of bacteria to the membrane surface and initiating biofilm development, complete with the secretion of EPS.

It is important to determine the relationships between the EPS macromolecules and microorganisms in the biofouling layers, which may relate to the strategy to control the biofouling phenomenon in MBRs, e.g. to reduce soluble EPS components or to target biofilm development and the production of EPS by the microbial biofilm community. Based on the results presented here, it appears that the EPS components may be the byproducts of microorganisms, indicating the biofilm growth on the membranes is the key driver of the biofouling process. Therefore, to control biofouling, it is vital to develop a method to prohibit or reduce biofilm formation on the membranes *in situ* or to disperse the mature biofilms.

Chapter 3 Correlation between the Bacterial Community and MBR Performance

3.1 Introduction

Microorganisms have been determined to be one of the most important factors in the biofouling phenomenon (Chen et al., 2007; Meng et al., 2010). The attachment of microorganisms onto a surface, e.g. membrane, has also been revealed as a trigger for the formation of biofilms (Abbas et al., 2013; Tuson and Weibel, 2013). In order to control the biofouling phenomenon in MBRs, it is necessary to understand the microbial communities attached on the membrane and their relationship to the TMP increase. Several studies have investigated the microbial communities involved in the fouling process of MBRs. For example, the microbial diversity in biofouling layers was investigated in a municipal wastewater MBR using a combination of 16S rRNA clone library sequencing and Fluorescent In Situ Hybridization (FISH), and found that the *Betaproteobacteria* comprised the majority of the biofilm community (Miura et al., 2007). Similarly, it was also found that the *Beta-proteobacteria* were the predominant bacteria in the membrane biofilms (Zhang et al., 2008). In contrast, recently, microbial communities in a submerged MBR were studied using 16S rRNA gene sequencing by pyrosequencing (Lim et al., 2012). The fouling process was divided into two separate stages, the initial fouling stage and the late fouling stage, where the TMP was 6 - 13 KPa in the initial fouling stage and 13 - 30 KPa in the late fouling stage. In this study, the *Gammaproteobacteria* were found to be the dominant bacteria in biofilms in both the initial and late fouling stages. Additionally, the *Bacteroidetes* and *Firmicutes* displayed a higher abundance in the biofilms than in the activated sludge. The *Bacteroidetes* have also been reported to be the dominant organisms in membrane biofilms (Ivnitsky et al., 2007). In a similar study on the species succession in the biofilms at different TMPs, it was observed that the *Gammaproteobacteria* and *Actinobacteria* were the two most abundant bacteria in both the low and high TMP stages (Lim et al., 2012). Thus, there is no consensus on the dominant bacteria in biofilms and whether there is a correlation between the increased TMP and specific microorganisms. This is crucial in the development of novel strategies to control membrane biofilm formation. Therefore, in this study, the biofilm communities on hollow fiber membranes and in the activated sludge in the MBR tanks were characterized through high throughput metacommunity sequencing based on tagged 16S rRNA gene sequencing.

3.2 Methods and materials

3.2.1 MBR set-up and operations

Three experiments using two different laboratory-scale submerged MBRs were performed to compare biofilm development with MBR performance. All three experiments were operated using artificial synthetic wastewater, total organic carbon (TOC) of 200 mg/L. MBR-1 (experiment 1) was an external submerged MBR, which was composed of an anoxic sludge tank, an aerobic sludge tank and a filtration tank where a membrane module was installed (Fig. 3.1a). Experiments 2 and 3, which were performed in parallel, utilized internal submerged MBRs, where each MBR was composed of an anoxic sludge tank, an aerobic sludge tank, and a membrane module inside the aerobic sludge tank (Fig. 3.1b). The membrane modules for all three MBRs consisted of 100 pieces of hollow fiber (HF) PVDF membranes (ZeeWeed 500, kindly provided by GE Singapore) and were assembled as a "curtain" style module. The average length of each hollow fiber membrane was 10 cm and the total area for each membrane module was 565 cm^2. One end of the membrane was sealed with epoxy glue and hung down into the sludge tank, which were the free ends. The other ends of the membranes were open and sealed into a chamber that was linked to a suction pump (Fig. 3.1c).

Artificial wastewater, composed of glucose (320 mg/L), beef extract (60 mg/L), peptone (80 mg/L), KH_2PO_4 (7 mg/L), $MgSO_4 \bullet 7H_2O$ (14 mg/L), $FeSO_4 \bullet 7H_2O$ (7.3 mg/L) and sodium acetate (90 mg/L) was used to supply nutrients to the MBR community. For each experiment, fresh activated sludge was collected from the Ulu Pandan wastewater treatment plant in Singapore and acclimated in artificial synthetic wastewater for 60 d before the start of each experiment. While running, the synthetic wastewater from the feed tank passed through the anoxic tank and aerobic tank and was degraded by the sludge biomass in the two tanks. The wastewater was then recycled from the aerobic tank to the anoxic tank to be further degraded. The purified water was subsequently separated from the sludge by the membrane module. The MBRs were operated at constant flux, 15 - 17 Liters /m^2 h (LMH) for MBR-1 and 13 - 15 $L.m^{-2}.h^{-1}$ for MBR-2 and MBR-3. The hydraulic retention time and sludge retention time for the three MBRs were maintained at approximately 10 h and 25 d, which were operated at room temperature, 25 - 28 ^oC. The TMP was monitored automatically using a digital pressure gauge (Ashcroft). The TOC of the influent and permeate was measured by multi N/C® 2100s (AnalytikJena) to monitor the performance of MBRs.

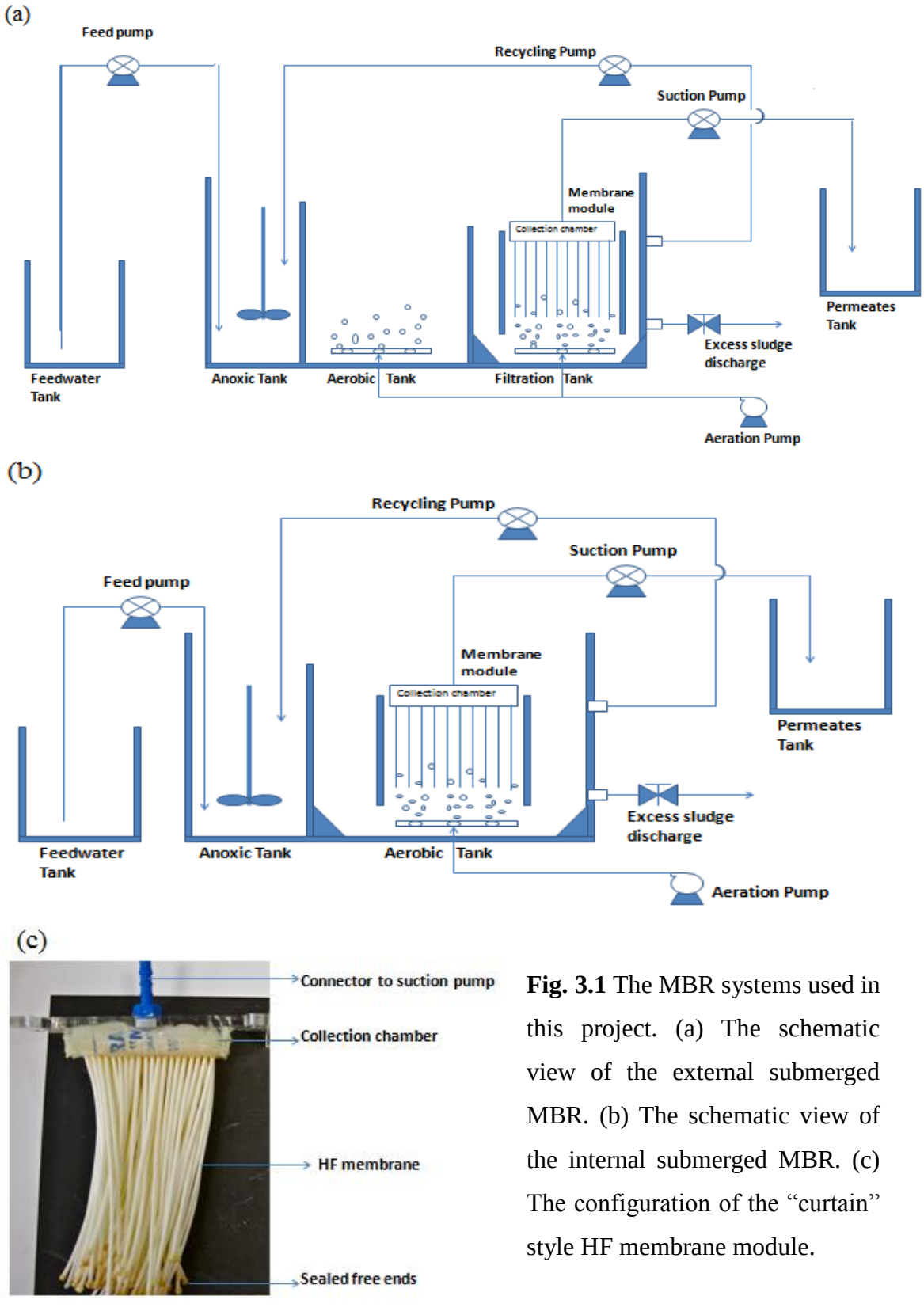

Fig. 3.1 The MBR systems used in this project. (a) The schematic view of the external submerged MBR. (b) The schematic view of the internal submerged MBR. (c) The configuration of the "curtain" style HF membrane module.

3.2.2 DNA extraction

Total DNA from the biofouling community growing on the HF membranes as well as from the activated sludge was separately extracted by a modified CTAB-PEG protocol (Griffiths et al.,

2000; Paithankar and Prasad, 1991). For each sample point, three independent sludge samples or hollow fibers were collected for replicates. Briefly, all solutions, including of 5% CTAB in 120 mM phosphate buffer (pH 8), phenol/chloroform/isoamyl alcohol (25:24:1), chloroform/isoamyl alcohol (24:1), 30% (w/v) PEG solution (i.e. Polyethylene glycol 6000 or 8000) dissolved in 1.6 M NaCl, 70% ice-cold ethanol and DNase-free water were prepared fresh before extraction. DNA was extracted from 0.5 g wet sludge collected by centrifugation of mixed liquor suspended sludge at 17, 000 *g* for 5 min. To extract the surface bound community, the HF membrane pieces were cut into small pieces and put into lysing matrix tubes (MP Biomedicals, USA). Subsequently, 0.5 mL of 5% CTAB and 0.5 mL phenol/chloroform/isoamyl alcohol (25:24:1) were added. The tubes were placed in Fast-Prep bead beater (FastPrep-24, M.P. biomedicals, USA) and shaken at speed setting 5.5 for 30 s. Afterwards, the tubes were centrifuged at 17,000 *g* for 5 min. The top aqueous layer was transferred to a clean 2 mL tube. Then, RNase was added at a final concentration of 10 µg/mL and incubated at 37˚C for 30 min. After RNA digestion, 0.5 mL phenol/chloroform/isoamyl alcohol (25:24:1) was added. The samples were vortexed briefly and the tubes were centrifuged at 17,000 *g* for 5 min. The top aqueous layer was transferred into clean 2 mL tubes and mixed well with 2 volumes of a 30% PEG solution and incubated at 4˚C overnight to precipitate the DNA. The following day, the samples were centrifuged at 17,000 *g* for 15 min and the supernatant was discarded. The DNA pellets were washed with 70% ice cold ethanol three times and air-dried for 30 min. Finally, the dry DNA pellets were dissolved in DNase and RNase free distilled water and the concentration was quantified using a NanoDrop spectrophotometer (Thermo Scientific). The aqueous DNA samples were stored at -80˚C.

3.2.3 Pyrosequencing

The DNA was sequenced by the "454" pyrosequencing method (Research and Testing Laboratory, Texas, US) (Handl et al., 2011). The primers selected for the bacterial PCR were Gray28F (5'-GAG TTT GAT CNT GGC TCAG-3') and Gray519R (5'-GTN TTA CNG CGG CKG CTG-3') (Baker et al., 2003). The number of reads for every sample was approximately 3,000.

3.2.4 Sequence processing

The pyrosequencing data was processed using the MOTHUR software (http://www.mothur.org/wiki/Main_Page) based on the Costello analysis pipeline (Costello et al., 2009; Schloss et al., 2009). The sequences were sorted by the barcodes to generate groups

of data for the samples. The sequence packets were trimmed and the barcodes and primers were removed from the sequences. The sequences that had poor quality, below 25, were removed from the dataset. Next, the size of data packets was reduced to facilitate the analysis through the process of "unique". The chimeric sequences were identified and removed from the datasets. Finally, the sequences were aligned with the SILVA bacterial 16S rRNA sequence database and assigned to taxonomic groups based on the SILVA bacterial taxonomic reference (Pruesse et al., 2007). The criterion for the sequence classification (similarity to the reference sequence) were Species (> 97%), Genus (94% - 97%), Family (90% - 94%), Order (85% - 90%), Class (80% - 85%), and Phylum (75% - 80%) (Lim et al., 2012). Sequences with similarities below these criteria were classified into unidentified groups for each taxonomic rank. Finally, a shared phylotype file was generated through the command "make.shared" for all the samples.

3.2.5 Plot of rarefaction curve

The rarefaction curve was plot based on the OTUs or phylotypes acquired and the number of sequences pooled. The relationship between the phylotypes and sequences was calculated by MOTHUR using the command of "rarefaction. single".

3.2.6 Phylotype-based analysis with PRIMER 6

The richness, evenness and diversity of the phylotypes were calculated with PRIMER 6 (PRIMER-E) (Clarke and Gorley, 2006). The Margalef's index was selected for the assessment of richness, using the formula $I_{Margalef} = (S - 1) / \ln(N)$, where S is the number of species in the sample, and N is the total number of individuals in the sample. The pielou's index was chosen to describe community level evenness and was calculated using the formula J = H'/ln(S) where H' is Shannon diversity and S is the total number of species in the sample. The Shannon index was used to indicate the diversity of the phylotypes. The formula for the Shannon diversity is as below:

$$H = \sum_{i=1}^{S} - (P_i * \ln P_i)$$

H is the Shannon diversity index, P_i is the fraction of the entire population made up of phylotype I, S is the total numbers of the phylotypes in the samples, and ∑ here presents the sum of the phylotype 1 to phylotype S.

Phylogenetic trees and Nonmetric Multidimensional Scaling (NMDS) plot were created between the samples based on the Bray-Curtis similarity of phylotype compositions in the different groups (Clarke, 1993). The similarity or dissimilarity between the samples or groups was calculated by the operation "SIMPER" in Primer E (Clarke, 1993). And the contributions of the phylotypes to the similarity or dissimilarity were calculated based on the different abundances of phylotypes between the samples and the effluences of phylotype to the community change. The bacteria that contributed $\geq$ 0.5% to the similarity or dissimilarity were considered to be relevant to the community composition.

3.3 Results

3.3.1 Biofouling behavior and sampling time-points

The correlation between the microbial community and MBR fouling was determined in three replicate experiments. For each of the three experiments, the TMP profiles were similar over the entire study period and were observed to have a steady TMP stage at approximately 3 - 15 kPa for the first 70 to 90 d of operation (Fig. 3.2). For experiment 1, which was run at the constant flux of 15 - 17 $L.m^{-2}.h^{-1}$, the TMP rose from 3 kPa to 15 kPa over a 70 d period. For experiments 2 and 3, which were run at a constant flux of 13 - 15 $L.m^{-2}.h^{-1}$, the system required 80 - 87 d to for the TMP to increase from 3 kPa to 15 kPa. After the TMP exceeded 15 kPa, the TMP was found to increase exponentially in all three experiments, termed here as the 'jump stage' or 'TMP jump' and reached approximately 90 kPa, which was the maximum pressure for the MBRs. The TMP jump stage required 29, 36 and 28 d for experiments 1, 2 and 3 respectively. Based on these observations, the experimental TMP phases are described as two stages, the steady state and TMP jump phases.

Based on these profiles, which were consistent with previously reported TMP profiles for laboratory scale systems (Cho and Fane, 2002; Ognier et al., 2002; Tardieu et al., 1998), samples were collected from the sludge and the membranes at 7 kPa, 10 kPa, 30 kPa and 60 kPa in experiment 1, 6 kPa, 10 kPa, 20 kPa, 55 kPa and 90 kPa for experiment-2, and 5 kPa, 7 kPa, 15 kPa, 80 kPa and 90 kPa in experiment 3 to characterize the microbial communities in the two stages of MBR operation (Fig. 3.2).

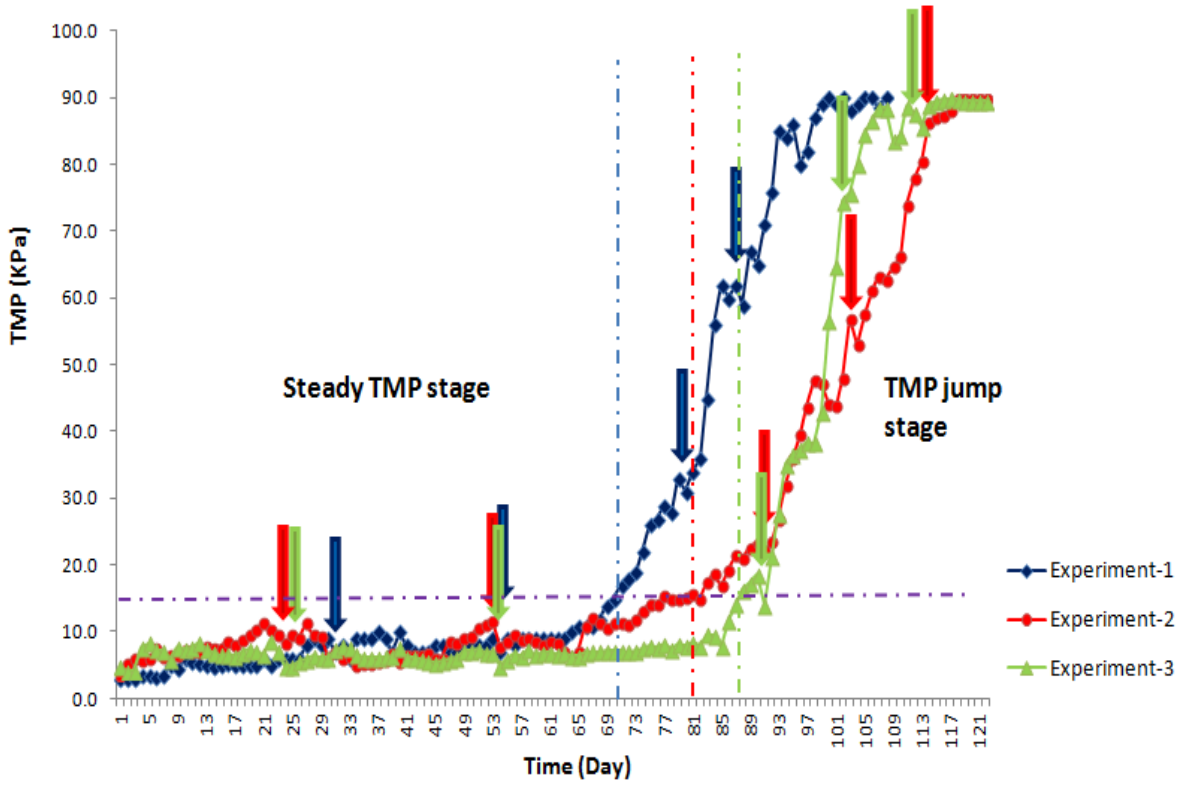

Fig. 3.2 TMP profiles and sampling time points for microbial community analysis in three replicate MBRs, experiment 1 (blue), experiment-2 (red) and experiment-3 (green). The TMP curves were divided into two stages, steady TMP stage (< 15 kPa) and the TMP jump stage (> 15 kPa). The horizontal dashed line (purple) indicates the threshold TMP and the vertical dashed line separates the two TMP stages. The samples, including biofilms on the membranes and the sludge biomass, were collected at different time points, indicated by the arrows.

3.3.2 Community analysis

After removing sequences of poor quality, experiments 1 - 3 respectively had 92,413 sequences for 18 samples, 22,4616 sequences for 27 samples and 265,869 sequences for 30 samples. The average number of sequence reads were 5,130 per sample (experiment-1), 8,319 per sample (experiment-2) and 8,860 per sample (experiment-3). After sample processing, the read lengths for the 16S rRNA genes were 300 - 500 bp (Fig. S3.1). The phylotypes for the bacterial communities were classified at multiple taxonomic ranks based on these sequencing results. At the species level, most OTUs were unclassified, while it was possible to classify most of the sequences at the Genus level. Therefore, the genus level was used as the starting point to analyze the bacterial communities.

The rarefaction curves were investigated for these individual samples to check the coverage of

phylotypes (Fig. S3.2). At the Genus level, the coverage of phylotypes for all samples was 97.5% - 99.43% for experiment-1, 94.77% - 99.6% in experiment-2 and 91.55% - 98.66% for experiment-3 (Fig. 3.3). Therefore, the sequencing reads for both the biofilms and the sludge, covered almost all the bacterial genera in the MBRs. For the higher taxonomic ranks, the phylotype coverage was higher. The high coverage of phylotypes provided confidence in the sequencing depth and the sampling size and that the data are an accurate reflection of the true bacterial communities of the MBRs.

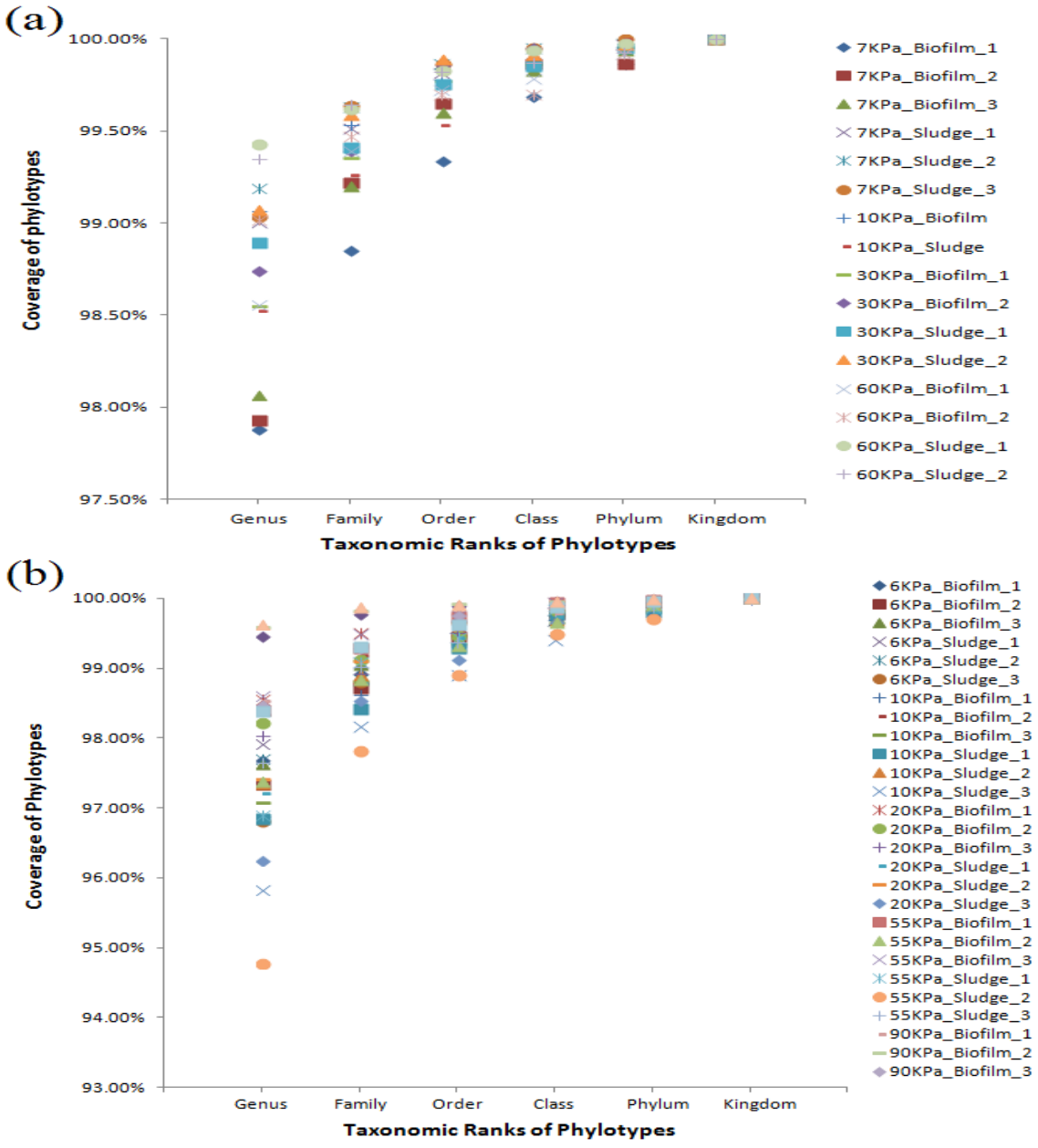

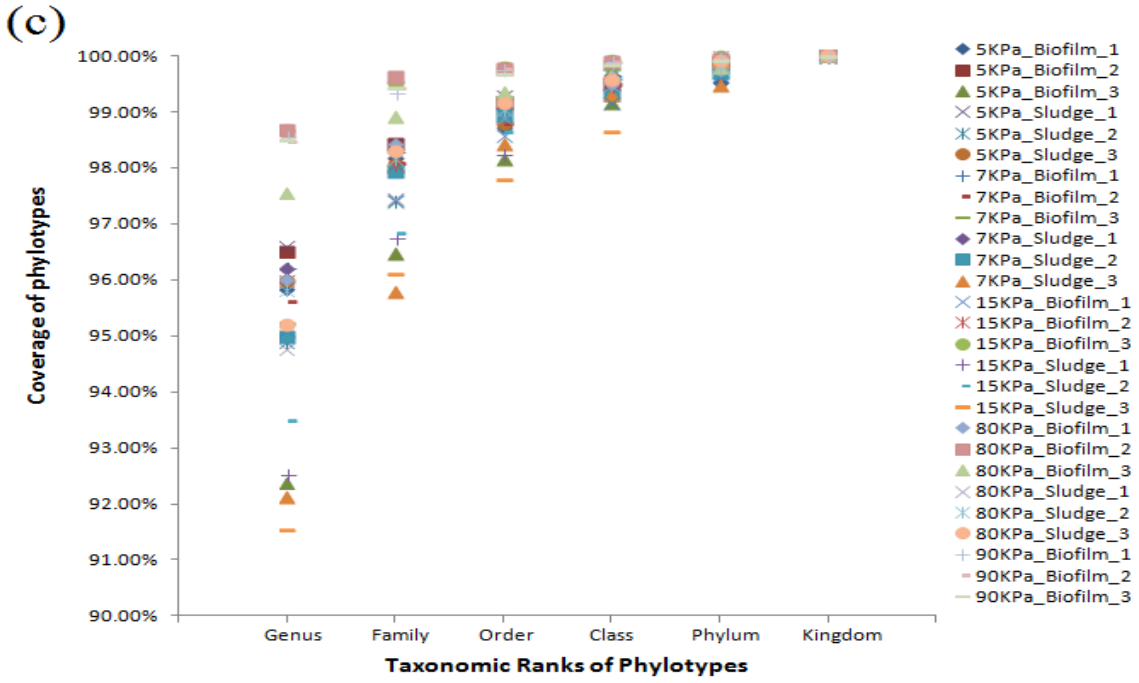

Fig. 3.3 (Continued from previous page) The coverage of bacterial phylotypes at different taxonomic ranks for experiment-1 (a), experiment-2 (b) and experiment-3 (c).

3.3.3 Bacterial diversity in biofilms and activated sludge

3.3.3.1 Richness of bacterial communities in MBRs

The Margalef's richness indices were determined in order to investigate the number of bacterial genera in the activated sludge and biofilm communities. The richness of the bacterial communities was found to be lower in the early biofilm samples than in the activated sludge when the TMP was low (Fig. 3.4). For example, at a TMP of 7 kPa, the Margalef's richness index for bacteria was 20.33 for the biofilm community on the membrane compared to 23.75 for the sludge community in experiment-1 (Fig. 3.4a). Similar levels of diversity were observed in experiment-3, where the Margalef's index was 20.13 for the biofilm and 27.55 in the activated sludge at 5 kPa. The difference in community richness at the low TMP was less marked in experiment-2, where the membrane biofilm richness was 25.91, which was similar to the richness, 26.73, in the activated sludge at a TMP of 6 kPa. However, the general trend was for a lower richness on the membranes in the initial samples relative to the activated sludge at low TMP.

This relationship changed over time and across the TMP curve where the richness of the bacterial communities was observed to decrease in the activated sludge and to increase in the

biofilms extracted from the membranes, resulting in a higher richness in the biofilms than in the sludge at high TMP (Fig. 3.4). For example, the richness of the sludge community decreased (experiment-1) from 23.75 (7 kPa) to 15.96 (60 kPa). In contrast the biofilm richness was relatively unchanged across the same time frame, 20.33 (7 kPa) to 21.02 (60 kPa). Similarly, in experiment-3, the Margalef's index decreased from 27.55 at 5 kPa to 19.58 at 80 kPa for the sludge community but increased from 20.13 at 5 kPa to 34.47 at 80 kPa for the biofilm community. The microbial community for both the membrane biofilms as well as the sludge community showed the same pattern of change for experiment-2, where there was an initial peak in diversity for the 10 kPa sample and then the community diversity returned to approximately the starting level of diversity at 20 and 55 kPa.

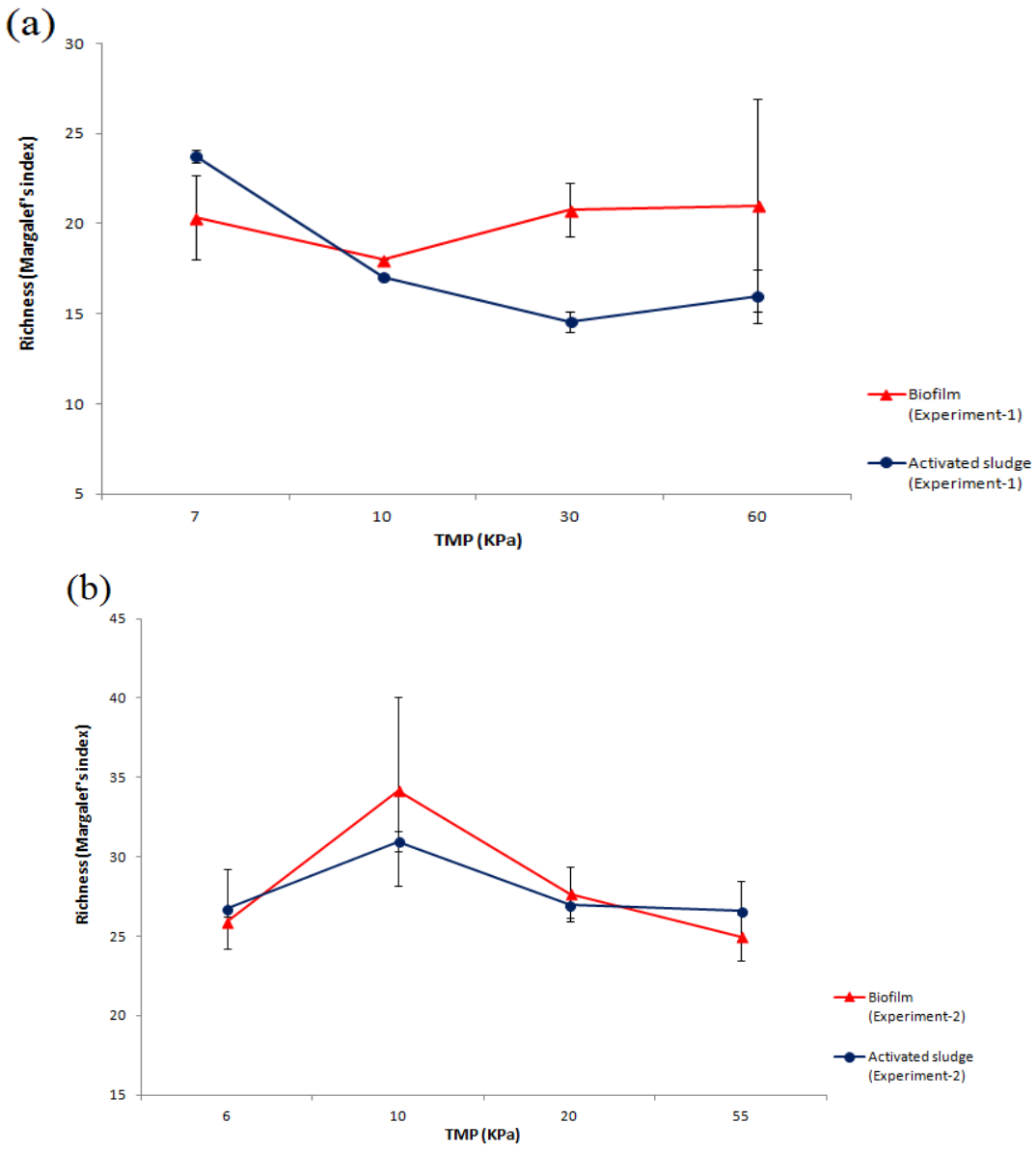

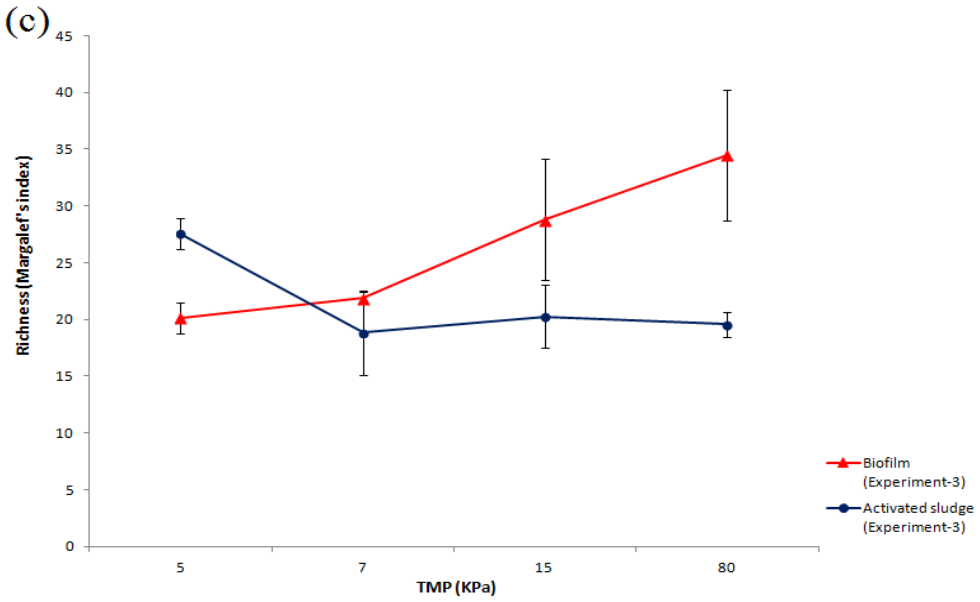

Fig. 3.4 (Continued from previous page) Richness of bacterial communities at the Genus level for the biofilm and sludge samples in experiment-1 (a), experiment-2 (b) and experiment-3 (c). The data points are the average Margalef index from triplicate samples at each TMP value. The error bars are the standard errors of the mean (n=3).

3.3.3.2 Diversity of bacterial communities in MBRs

While the measure of richness is useful to describe overall diversity (richness) of the community, the relative contribution of organisms to the community (evenness) is not considered. Therefore, to get a detailed understanding of the true diversity of the community, the Shannon diversity index was used as a measurement combining the richness and evenness. A high Shannon diversity index number suggests a community with high diversity.

The Shannon diversity indices were calculated for samples collected at the different TMPs for both the biofilm and activated sludge samples. For experiments 1 and 2, the diversity of the sludge community was observed to remain relatively stable across the different TMP stages, while for experiment 3, the diversity showed considerable variability between all samples (Fig. 3.5). The diversity index for the biofilm samples generally increased for experiments 2 and 3 as the TMP increased, but showed a slight overall decrease over time in experiment 1. The clearest trend was that the diversity index for the membrane biofilms was higher in all three experiments relative to the sludge once the TMP had entered the jump stage.

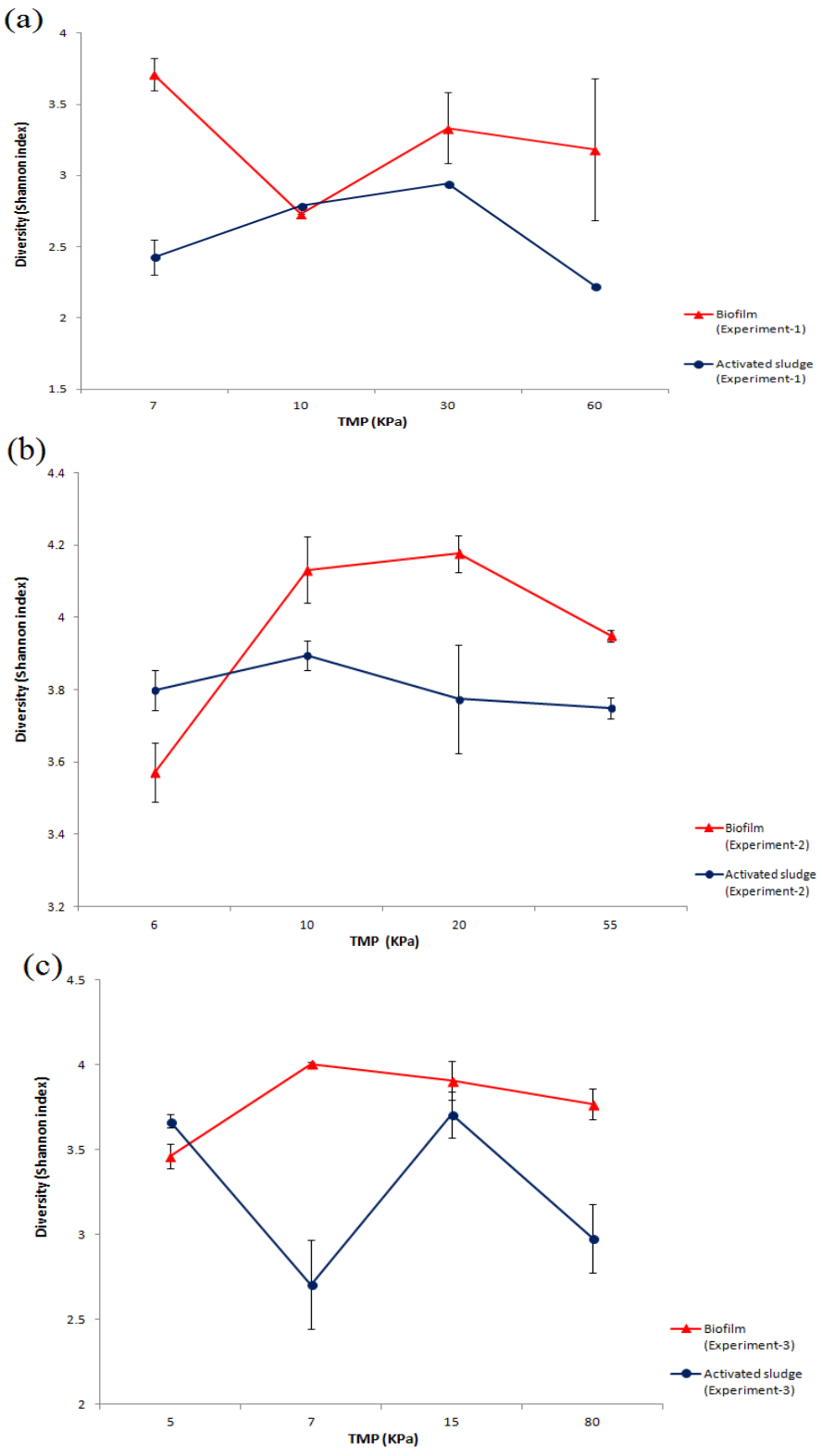

Fig. 3.5 The diversity of bacterial communities at the Genus level for the membrane biofilm and sludge samples in experiment-1 (a), experiment-2 (b) and experiment-3 (c). The error bars are the standard errors of the mean (n=3).

3.3.4 Relationship between bacterial biofilm and sludge communities

The data presented above suggest that the richness of the biofilm community was low at the beginning of the experiment and that the overall diversity of the biofilm community, while initially lower than in the sludge, ultimately became more diverse than the sludge community at the high TMP stages. The measures described above suggest that the biofilm community changes dramatically as the TMP goes from low to high. However, the analysis does not provide a detailed description of how the community changes over time nor does it determine if the TMP is correlated with specific organisms or is more generally a function of general biofilm formation on the membranes. Therefore, the relationships among all samples were studied using the Bray-Curtis similarity method at the taxonomic level of Order. Due to the potential for PCR and pyrosequencing bias, the dominant species may be more readily amplified than rare organisms and hence may artificially exaggerate differences in the community (Pinto and Raskin, 2012). Transformation of the raw data may reduce the influence of the PCR and pyrosequencing bias (Fowler et al., 1998) and hence the community variation was analyzed using both the square root transformed community data (Figs. 3.6 and 3.7) as well as the raw community data respectively (Figs. S3.3 and S3.4). To facilitate the analysis, the construction of phylogenetic trees and NMDS plots was performed using a Bray-Curtis resemblance matrix.

3.3.4.1 A specific subset of sludge bacteria form biofilms on the membranes

The microorganisms in the activated sludge would logically have to be the source of the communities that eventually form on the membranes. If the biofilm communities are specifically selected for, then the community composition would be expected to be dramatically different in composition relative to the sludge but should be consistent across experiments. If there is no selection, the biofilm community would be expected to be more similar to the sludge or that the biofilm would differ from the sludge, but the community would be a random assortment of sludge organisms.

The NMDS plots, constructed based on the Bray-Curtis similarity at the Order level, showed that the membrane biofilm communities were generally different from the activated sludge communities for all three experiments (Figs. 3.6 and 3.7). This was apparent based on the observation that the biofilm samples formed separate, distinct branches relative to the sludge. This was particularly clear at high TMP for experiments 2 and 3, where all of the biofilm samples, except for the first time point, 6 kPa and 5 kPa, clustered together. And this was also

observed in experiment-1, e.g. samples at 10, 30 and 60 kPa. Even for the bacterial communities at the lowest TMP in all the 3 experiments, the biofilms were also separated from the sludge at the same pressure. Specifically, the biofilms at 6 kPa displayed 30% dissimilarity to the sludge at 6 kPa in experiment-2 (Fig. 3.7b), indicating a subset of the community was selected from the sludge to form the biofilm on the membrane. Therefore, the community data suggests that the biofilm initially resembles the activated sludge community and subsequently diverges from the sludge to establish a community with a distinct relative composition.

3.3.4.2 Change in bacterial community composition in biofilms from low to high TMP

As indicated above, the bacterial communities in biofilms were different from the sludge at all TMP stages. But the communities within the biofilms were also observed to vary at different TMP values. This was particularly obvious in experiment-1 (Fig. 3.7a), where the biofilm at 7 kPa was closer in composition to the sludge (65% similarity) but was less similar to the biofilms at 30 kPa and 60 kPa (55% similarity). This trend was also observed in experiments 2 and 3 (Figs. 3.7b and c), where the biofilms at the lowest TMP clustered in one group while the biofilms at higher TMPs clustered into another group. These observations suggest that the membrane biofilm community changes as the pressure increased from the low TMP to high TMP stages in the MBRs.

3.3.4.3 Changes in bacterial community composition occurred before the TMP jump

The cluster analysis suggested that the biofilm community changed in accordance with the increase in TMP. This could indicate that the community composition changes as a consequence of the TMP change, or alternatively, the changing community could cause the TMP jump. Based on the analysis above, the TMP curve was separated by a threshold TMP (15 kPa) into a long-term, low TMP stage and a short-term, high TMP stage (also referred to here as the jump stage) and the relationships between biofilms were compared at low TMP and high TMP. If the bacterial community changes in response to the TMP, then it would be expected that the changes in the community composition would lag behind the TMP increase. If the community changes first and is followed by the TMP jump, then the majority of the community shift would be expected to occur or be complete before the TMP increased.

The NMDS plots showed that the bacterial succession was completed before the TMP exceeded the threshold 15 kPa (Fig. 3.7). This was particularly clear in experiment-2, where

the biofilms at 20 kPa, 55 kPa and 90 kPa clustered in one group, while the biofilms at 6 kPa and 10 kPa clustered into two separate groups, as the biofilm group at 10 kPa showed a closer relationship to the biofilms at 55 kPa and 90 kPa. This indicated that the biofilms at high TMP was quite similar to the biofilms at the late phase of low TMP. This phenomenon was also observed in experiment-1 and experiment-3. In experiment-1, the biofilms at 60 kPa was quite similar to the biofilms at 10 kPa (70% similarity). Even in experiment-3, the biofilms at 80 kPa had 80% similarity to the biofilms at 15 kPa and 75% similarity to the biofilms at 7 kPa. Collectively, these findings suggested that the succession of bacterial communities in biofilms occurred prior to the point at which the TMP exceeded the threshold and entered the jump stage.

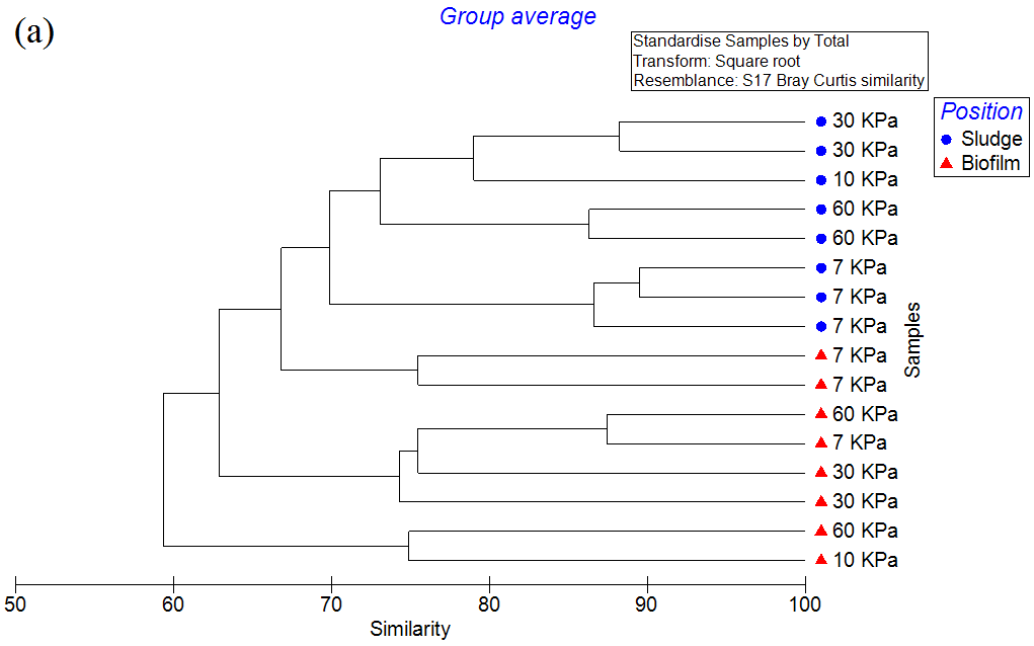

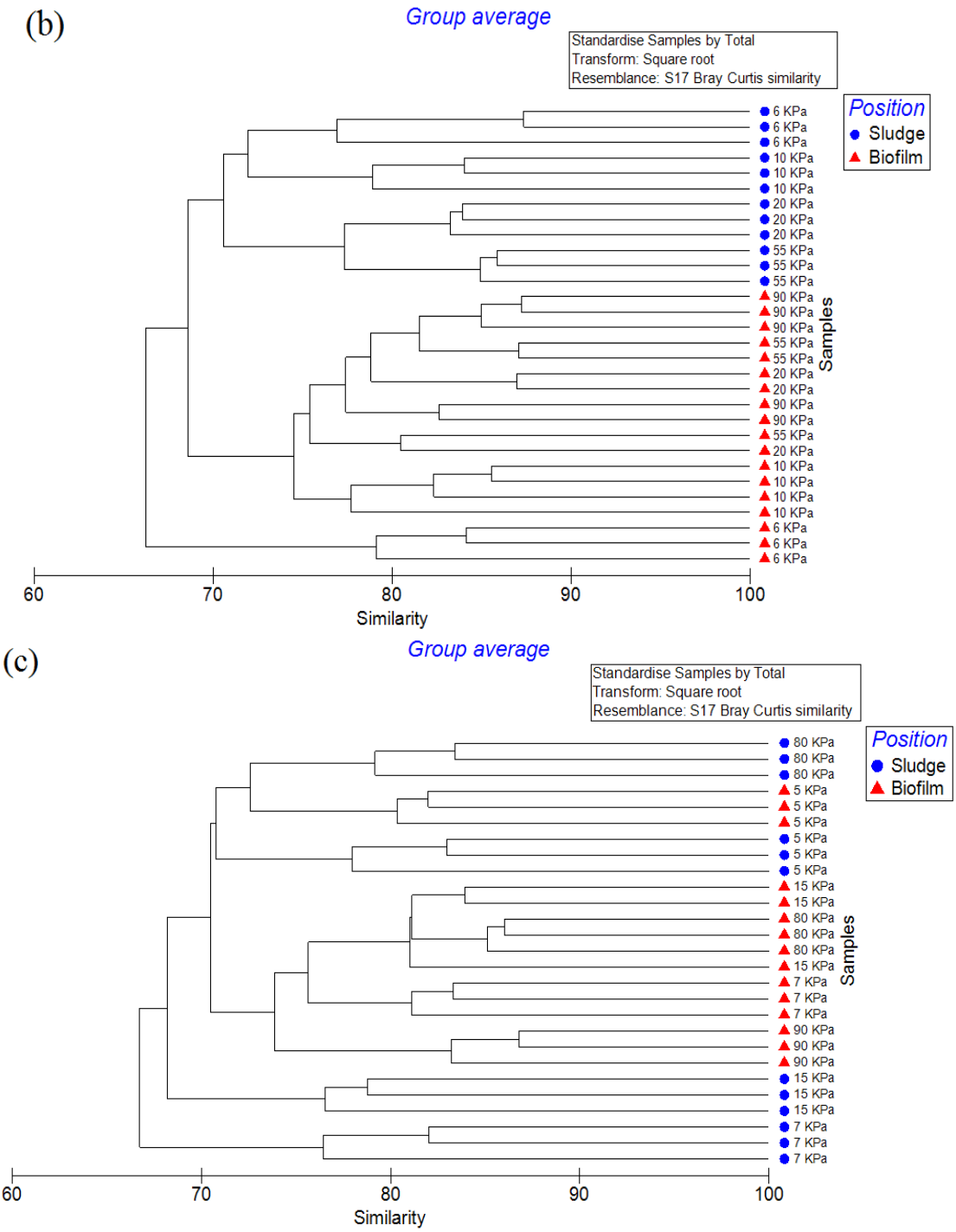

Fig. 3.6 (Continued from previous page) The phylogenetic tree at the Order level for biofilms and activated sludge samples in the experiment-1 (a), experiment-2 (b) and experiment-3 (c). The transformation of square root was performed on all samples.

(a)

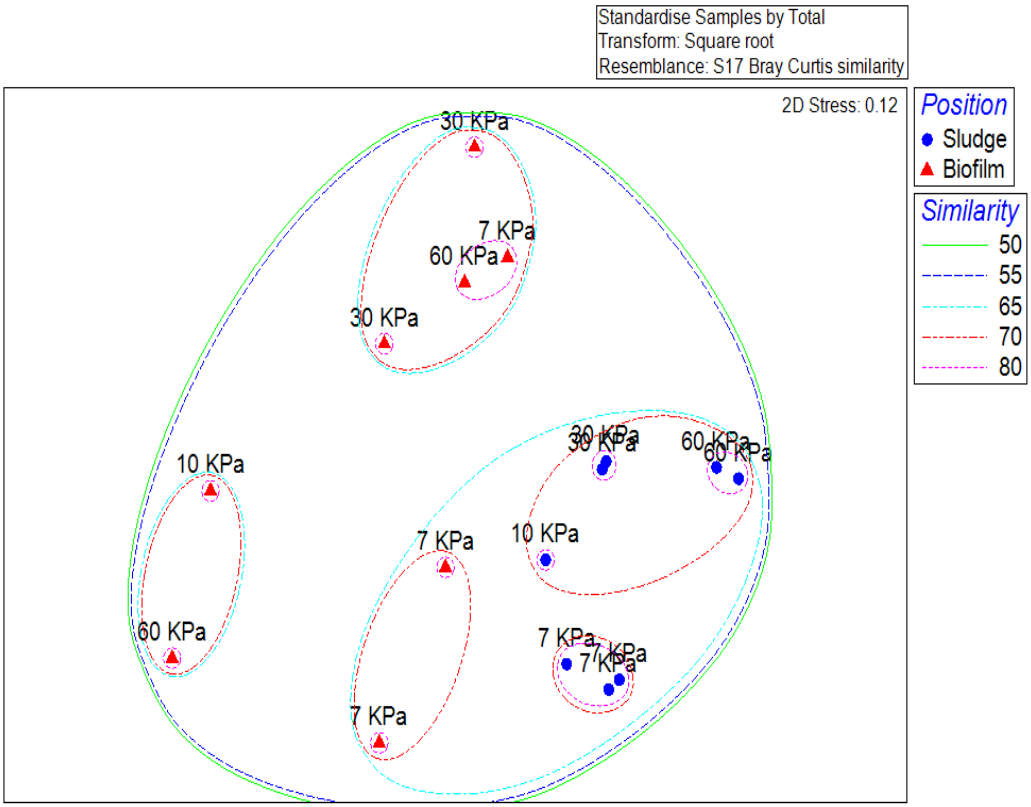
Standardise Samples by Total
Transform: Square root
Resemblance: S17 Bray Curtis similarity
2D Stress: 0.12
Position
Sludge
Biofilm
Similarity
50
55
65
70
80
30 KPa
7 KPa
60 KPa
30 KPa
10 KPa
60 KPa
7 KPa
10 KPa
7 KPa
7 KPa

(b)

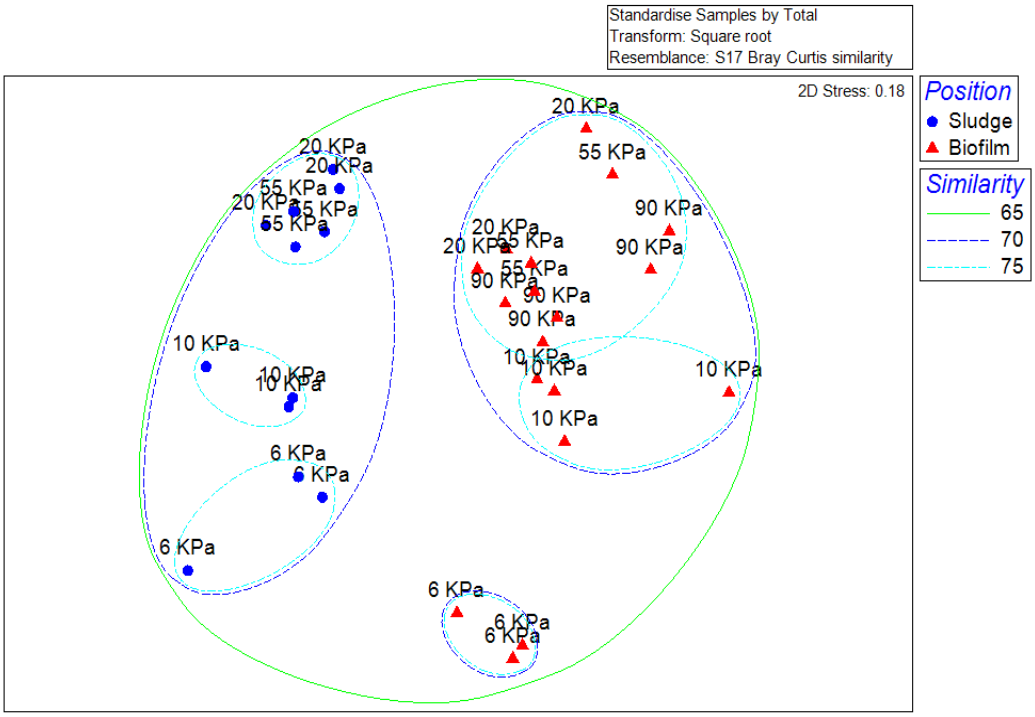
Standardise Samples by Total
Transform: Square root
Resemblance: S17 Bray Curtis similarity
2D Stress: 0.18
Position
Sludge
Biofilm
Similarity
65
70
75
20 KPa
55 KPa
90 KPa
10 KPa
6 KPa

(c)

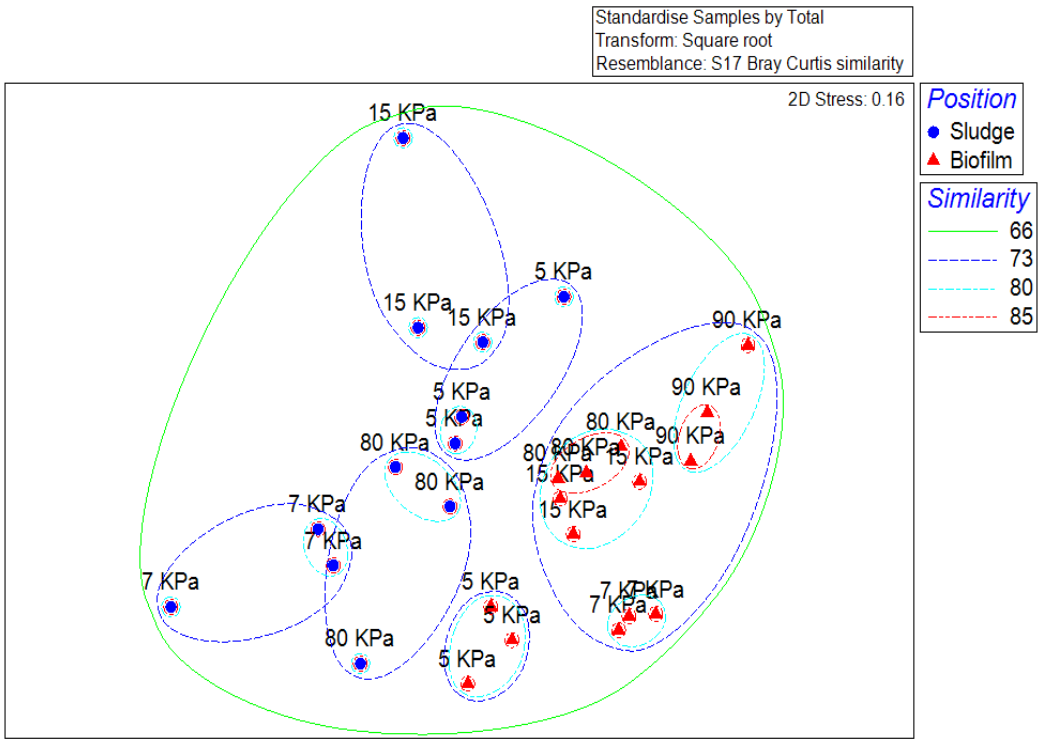

Fig. 3.7 (Continued from previous page) NMDS plots at the Order level for biofilms and activated sludge samples for experiment-1 (a), experiment-2 (b) and experiment-3 (c). The data were square root transformed for analysis. The blue circles represent the bacterial communities in sludge, and the red triangles represent the bacterial communities in biofilms. The dotted lines show the average Bray-Curtis similarities between samples, where the colored lines indicate different percentage similarities.

3.3.5 Compositions of bacterial communities in sludge and biofilms in MBRs

While the sludge community must be the source of bacteria to form the biofilm on the membranes, the data presented above suggests that the overall composition of the biofilms were different from the sludge community (Fig. 3.7). To better understand the specific organisms that contribute to the differences in community composition, the relative abundances of the bacteria that contribute most to the dissimilarity, or difference, between the sludge and biofilm communities were investigated.

3.3.5.1 Compositions of bacterial communities in seed activated sludge at low TMP stage

As a microbial reservoir in the MBR, the bacterial communities of the seed sludge, taken at the start of experiment, were investigated for all three experiments. The sludge communities in experiments 2 and 3 showed a closer relationship (79% similarity) than with the sludge in

experiment-1 (Fig. 3.8b). This would be expected since experiments 2 and 3 were run in parallel. Despite being run at different times, the three sludge communities still showed 65.59% similarity. Specifically, the activated sludge in the three experiments was dominated by members of the same five bacterial Orders. These included *Rhodocyclales* (64.59% in abundance in experiment-1, 24.4% in abundance in experiment-2, 19.26% in abundance in experiment-3), *Sphingobacteriales* (abundances were 10.61% for experiment-1, 18.97% for experiment-2 and 27.96% for experiment-3), *Burkholderiales* (5.27% in abundance in experiment-1, 9.19% in abundance in experiment-2, 7.63% in abundance in experiment-3), *Myxococcales* (2.94% in abundance in experiment-1, 9.12% in abundance in experiment-2, 2.96% in abundance in experiment-3) and *Actinomycetales* (2.19% in abundance in experiment-1, 2.41% in abundance in experiment-2, 2.13% in abundance in experiment-3), which composed 85.96%, 64.09% and 59.94% of the bacterial communities in sludge at low TMP stage in the experiments 1, 2 and 3 respectively (Fig. 3.8a).

The biggest difference in the sludge from experiment 1 vs. experiments 2 and 3 was in the *Rhodocyclales* and *Flavobacterales*. The *Rhodocyclales* were the most abundant bacteria in the sludge in experiments 1 and 2 and the second most abundant bacteria of sludge in experiment-3. However, the abundance for *Rhodocyclales* in experiment-1 was almost 3 fold (64.59%) more than in experiment-2 (24.4%) and experiment-3 (19.26%). Another difference was in the abundance of the *Flavobacterales*, which were the dominant sludge bacteria in experiment-2 (8.76%) and experiment-3 (9.94%) but were rare bacteria in the sludge in experiment-1 (0.46%).

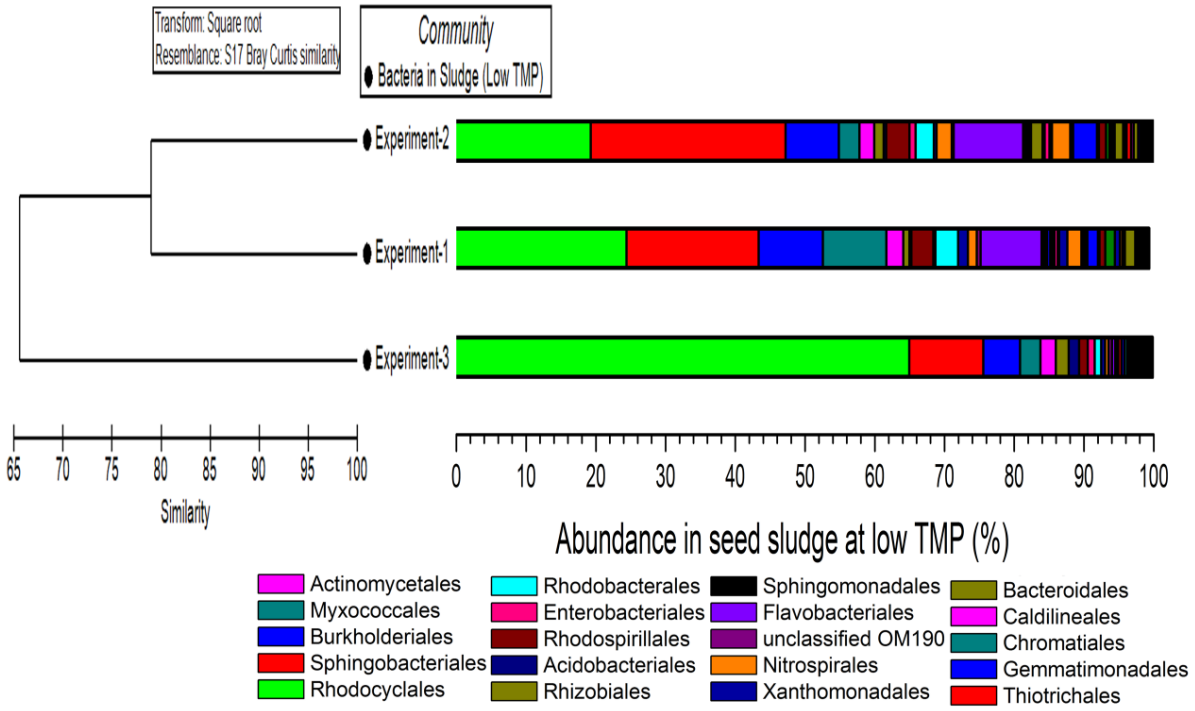

Fig. 3.8 The bacterial communities in activated sludge at the low TMP stage. The phylogenetic tree for the bacterial communities in the sludge from three experiments was based on the Bray-Curtis similarity.

3.3.5.2 Compositions of bacterial communities in biofilms at the low TMP stage

3.3.5.2.1 Dominant bacteria in the early biofilms

The biofilms formed at the low TMP stage were observed to have different community structures in the three experiments (Fig. 3.9). In experiment-1, 16 Orders of bacteria were observed to dominate the early biofilms, which comprised 90.69% of the whole bacterial community. The five most abundant bacterial groups were *Sphingobacteriales* (28.55%), *Rhodocyclales* (16.38%), *Burkholderiales* (8.39%), *Actinomycetales* (8.24%) and *Myxococcales* (5.71%). In experiment-2, 18 Orders of bacteria comprised 93.22% of the bacterial communities in the low TMP stage biofilms. The top five most abundant were *Sphingobacteriales* (32.68%), *Burkholderiales* (25.4%), *Rhodocyclales* (9.84%), *Pseudomonadales* (6.94%) and *Actinomycetales* (2.91%). For experiment-3, 21 Orders of bacteria contributed 94.89% of the bacterial community in biofilms at the low TMP stage, where the top five most abundant groups were *Rhodocyclales* (24.67%), *Sphingobacteriales* (20.03%), *Burkholderiales* (15.53%), *Opitutales* (12.07%) and *Bacteroidales* (2.41%).

The communities for all three experiments were found to share 59.75% similarity at the low TMP stage (Fig. 3.9). Five Orders of bacteria were found to be the dominant groups in all three experiments (Fig. 3.9). They contributed 80.1% to the total similarity among the three bacterial communities at the low TMP stage and were *Sphingobacteriales* (28.55% in experiment-1, 32.68% in experiment-2, 20.03% in experiment-3), *Rhodocyclales* (16.38% in experiment-1, 9.84% in experiment-2, 24.67% in experiment-3), *Burkholderiales* (8.39% in experiment-1, 25.4% in experiment-2, 15.53% in experiment-3), *Actinomycetales* (8.24% in experiment-1, 2.91% in experiment-2, 2% in experiment-3) and *Flavobacteriales* (1.17% in experiment-1, 1.97% in experiment-2, 2.09% in experiment-3). They comprised 62.73%, 72.8%, 64.32% of the bacterial community in biofilms at the low TMP in experiments 1, 2 and 3 respectively, indicating they dominated the community in biofilms at the low TMP stage in all three experiments.

Interestingly, the biofilm communities in experiments 2 and 3 were more closely related to each other than the biofilms characterized in experiment-1 at the low TMP stage, where the similarity of the bacterial community was 73.04% between experiment-2 and experiment-3. This phenomenon was also observed for the bacterial community in the sludge, where the bacterial communities in the parallel experiments 2 and 3 were most closely related to each other relative to experiment-1.

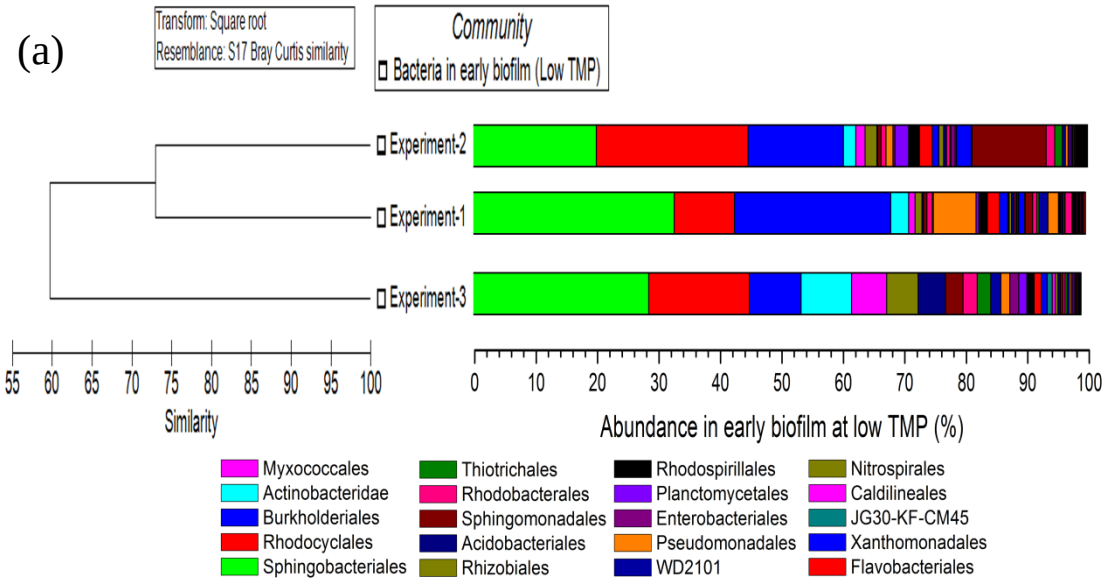

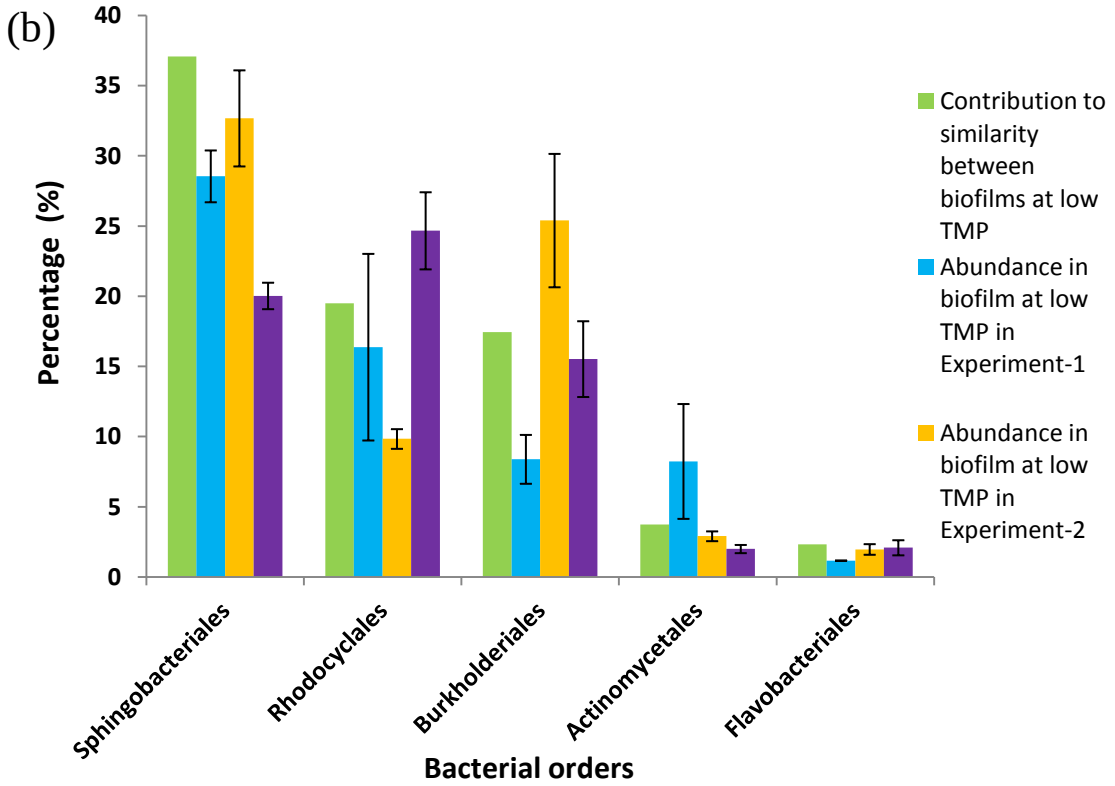

Fig. 3.9 (Continued from previous page) The bacterial communities at the Order level in membrane biofilms at the low TMP stage. (a) The abundance and phylogenetic tree for the bacterial communities in biofilms from three experiments. (b) The common dominant bacteria in biofilms at the low TMP stage in three experiments. The error bars are the standard error of the mean (n=3).

3.3.5.2.2 Selection for a biofilm community at the low TMP stage

Based on their relative abundance in biofilms and sludge, a group comprised of three Orders of bacteria, including *Burkholderiales*, *Pseudomonadales* and *Rhizobiales*, were enriched in the biofilms in all the three experiments (Fig. 3.10). Interestingly, for all three experiments, the *Pseudomonadales* were present in the sludge at very low abundance (0.14% in experiment-1, 0.25% in experiment-2, 0.05% in experiment-3), but were some of the dominant organisms in the early biofilms (1.46% in experiment-1, 6.94% in experiment-2, 1.12% in experiment-3, all $p<0.05$ by T test). This may suggest that there is strong selection for those bacteria to form biofilms on the membranes and that biofilm formation favors their proliferation.

Two Orders of bacteria, *Rhodocyclale*s and *Sphingobacteriales*, were particularly interesting in this comparison. They were the top two most abundant bacteria in the sludge at the low TMP stage in all three experiments (Fig. 3.8a). However, in the early biofilms, they exhibited a different trend (Fig. 3.10). In experiments 1 and 2, *Sphingobacteriales* were found to have a higher abundance in the early biofilms than in the sludge in experiment-1 (10.61% in sludge vs. 28.55% in the low TMP biofilm for experiment-1, 18.97% in sludge vs. 32.68% in the low TMP biofilm for experiment-2, both $p<0.05$ by T test), while Rhodocyclales had a lower abundance in the early biofilms than in the sludge (64.95% in sludge vs. 16.38% in early biofilms for experiment-1, 24.4% in sludge vs. 9.84% in early biofilm for experiment-2, both $p<0.05$ by T test). This may suggest that the *Sphingobacteriale*s were more fit during biofilm development than *Rhodocyclales*, even though they were both dominant components of the low TMP biofilms. However, in experiment-3, *Sphingobacteriales* were observed to have a lower abundance in the low TMP biofilms than in the sludge (27.96% in the sludge vs. 20.03% in the biofilm, $p<0.05$ by T test), while the *Rhodocyclales* had a higher abundance in the biofilm than in the sludge (19.26% in the sludge vs. 24.67 % in the biofilm, $p<0.05$ by T test).

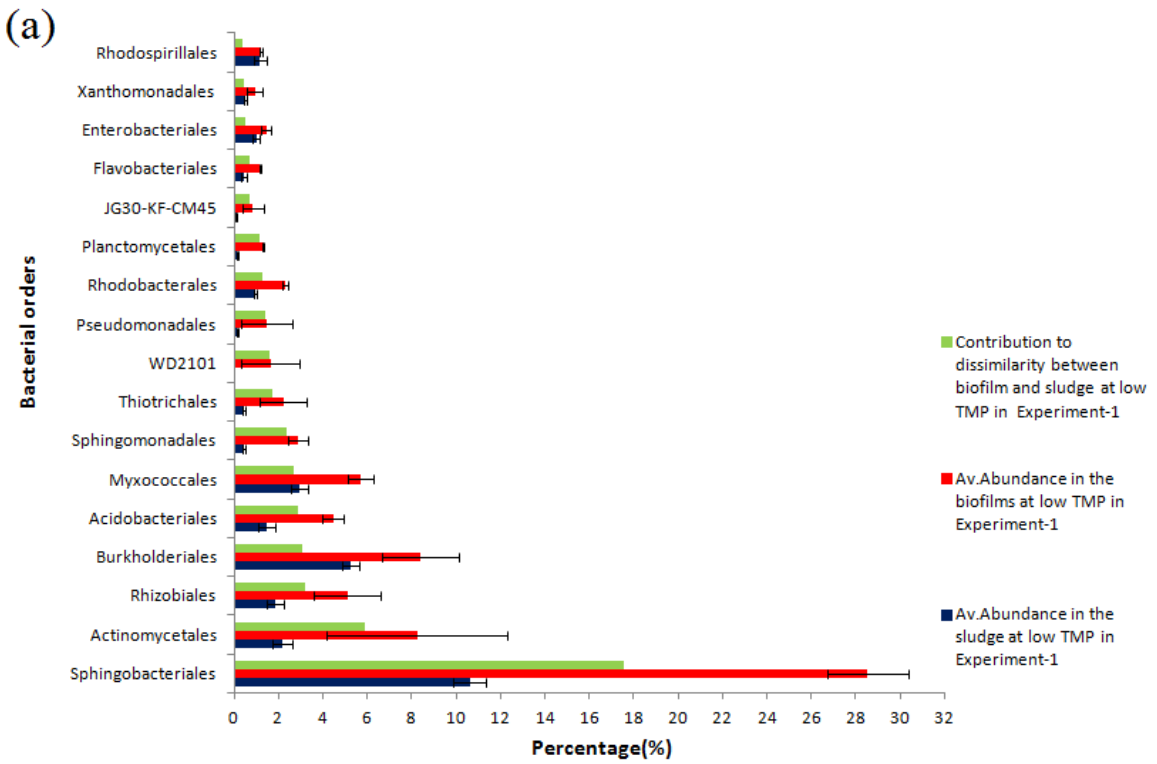

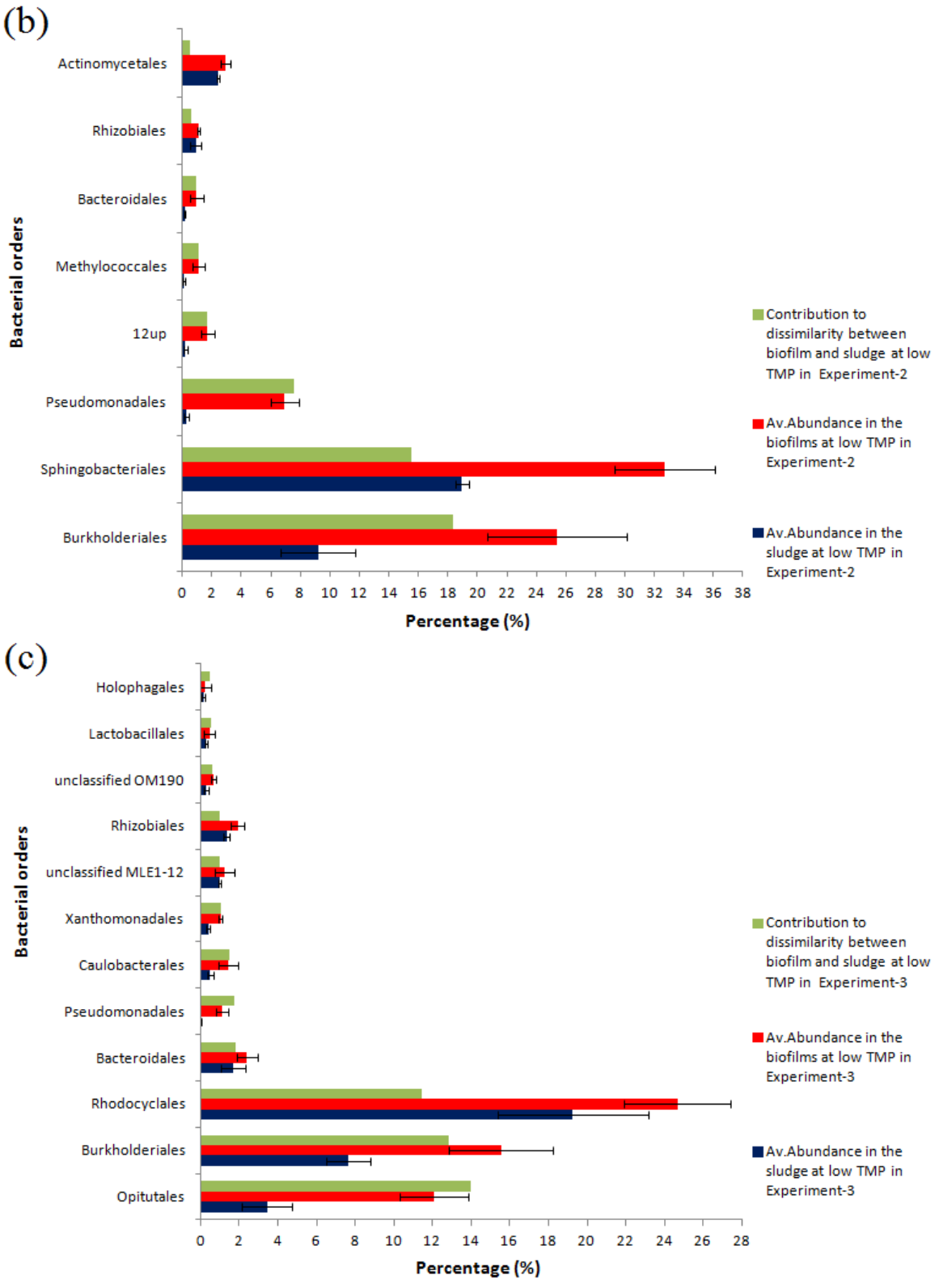

Fig. 3.10 (Continued from previous page) Enrichment of specific bacteria in the membrane biofilms at the low TMP stage, (a) experiment-1, (b) experiment-2, and (c) experiment-3. The data points were the average values of the triplicate samples at low TMP. The error bars are the standard error of the mean (n=3).

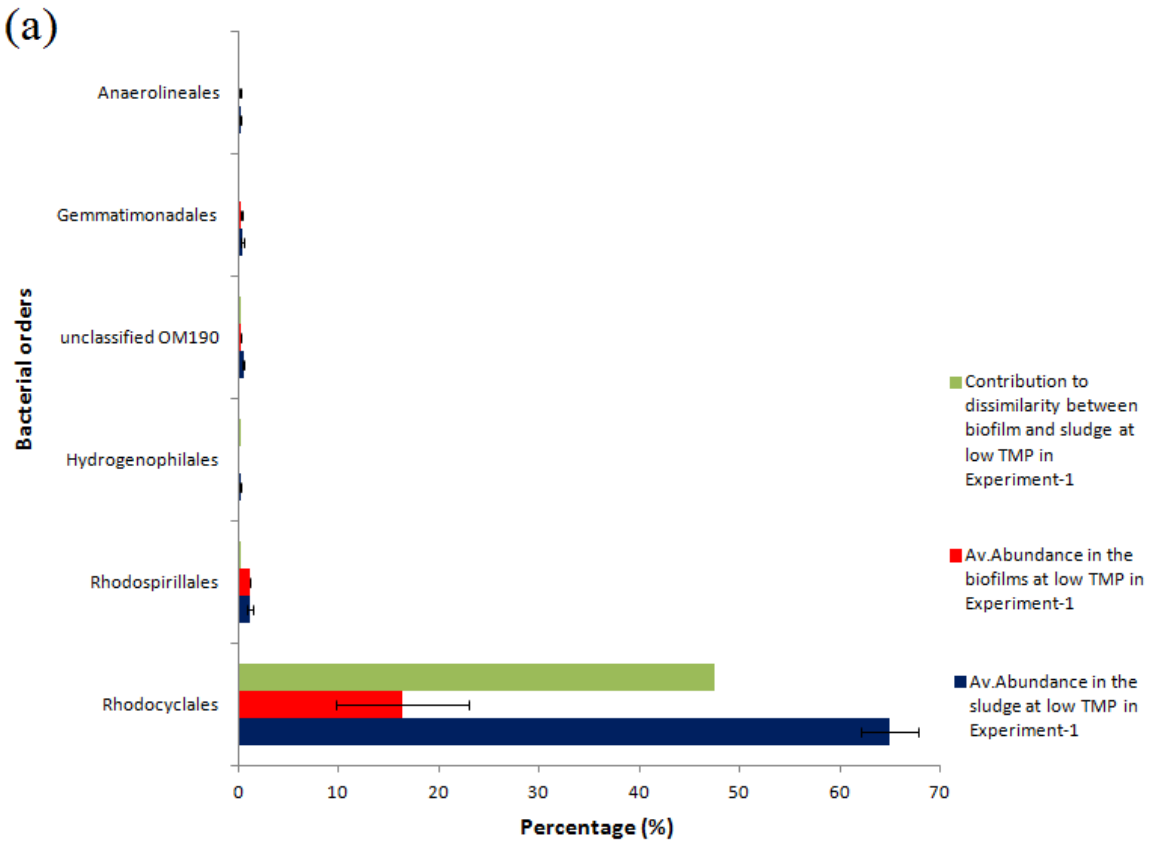
(a)
Anaerolineales
Gemmatimonadales
unclassified OM190
Hydrogenophilales
Rhodospirillales
Rhodocyclales
Bacterial orders
0
10
20
30
40
50
60
70
Percentage (%)
Contribution to dissimilarity between biofilm and sludge at low TMP in Experiment-1
Av.Abundance in the biofilms at low TMP in Experiment-1
Av.Abundance in the sludge at low TMP in Experiment-1

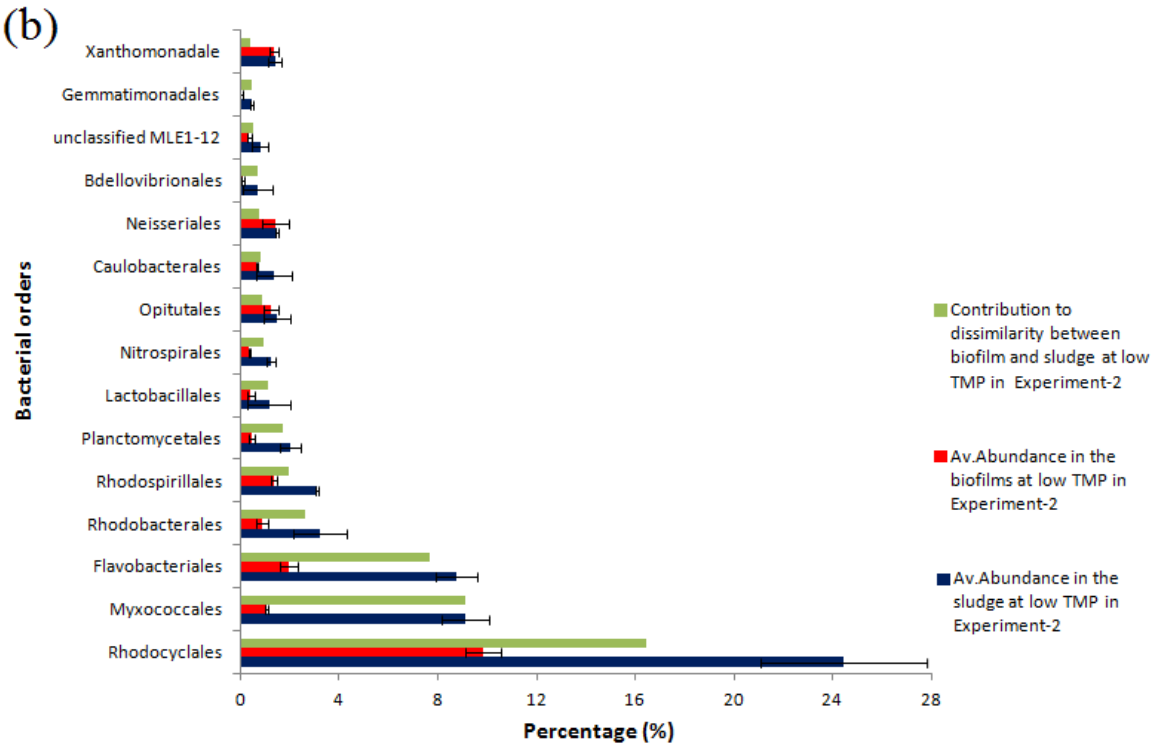
(b)
Xanthomonadale
Gemmatimonadales
unclassified MLE1-12
Bdellovibrionales
Neisseriales
Caulobacterales
Opitutales
Nitrospirales
Lactobacillales
Planctomycetales
Rhodospirillales
Rhodobacterales
Flavobacteriales
Myxococcales
Rhodocyclales
Bacterial orders
0
4
8
12
16
20
24
28
Percentage (%)
Contribution to dissimilarity between biofilm and sludge at low TMP in Experiment-2
Av.Abundance in the biofilms at low TMP in Experiment-2
Av.Abundance in the sludge at low TMP in Experiment-2

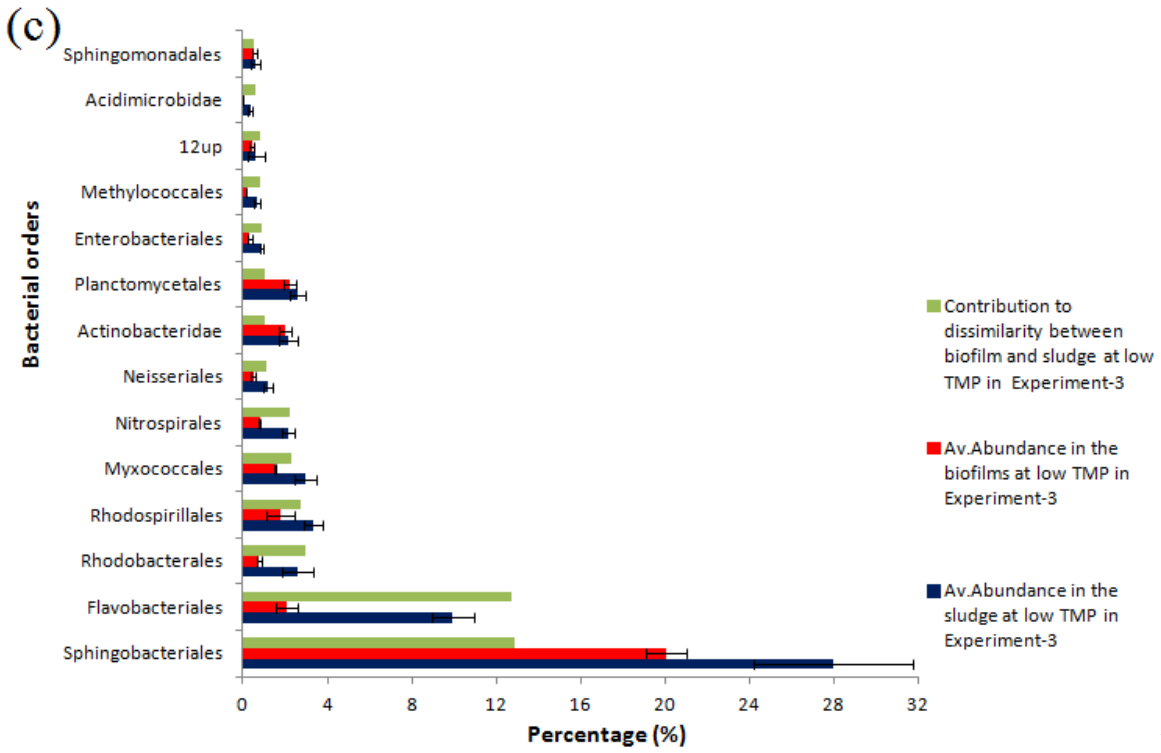

Fig. 3.11 (Continued from previous page) Preferential growth of bacteria in the sludge relative to the membrane biofilms (a) experiment-1, (b) experiment-2, and (c) experiment-3. The data points were the average values of the triplicate samples collected from the low TMP stage. The error bars are the standard error of the mean (n=3).

3.3.5.3 The composition of the bacterial biofilm community at the high TMP stage

Additionally, it was of interest to determine if the biofilm communities that developed on the membranes at the high TMP stage were similar to each other or if they were distinct. Therefore, the biofilm communities at the high TMP stages (30 - 90 kPa) were compared with each other.

3.3.5.3.1 Dominant bacteria in late biofilms

In experiment-1, 16 Orders of bacteria were the dominant groups in the biofilms at 30 kPa and 90 kPa (Fig. 3.12a), where they comprised 91.28% of the community. The five most abundant bacteria were *Sphingobacteriales* (29.11%), *Burkholderiales* (12.19%), *Chlorobiales* (10.24%), *Rhodocyclales* (6.42%) and *Rhodospirillales* (5.01%). For experiment-2, a group of 23 Orders of bacteria were observed to dominate the biofilm community at 55 kPa and 90 kPa, where they comprised 96.37% of the bacterial biofilm communities (Fig. 3.12a). The top five

most abundant bacteria were *Sphingobacteriales* (21.7%), *Burkholderiales* (10.65%), *Rhodocyclales* (9.3%), *Actinomycetales* (7.83%) and *Sphingomonadales* (7.24%). In experiment-3, 19 Orders of bacteria dominated the bacterial biofilm communities at 80 kPa and 90 kPa (Fig. 3.12a). They represented 91.21% of the whole bacterial community and the top five most abundant bacteria were *Sphingobacteriales* (37.36%), *Burkholderiales* (14.13%), *Rhodocyclales* (9.45%), *Actinomycetales* (3.73%) and *Rhodospirillales* (3.63%).

Comparison of the bacterial communities for the three MBRs indicated that they had 67.47% similarity at the high TMP stages (Fig. 3.12b). Five different bacterial Orders were found to be the dominant organisms in all three experiments (Fig. 3.12c). They contributed 71.61% to the total similarity among the bacterial communities at the high TMP stage. These five Orders were *Sphingobacteriales* (29.11% in MBR-1, 21.7% in MBR-2, 37.36% in MBR-3), *Burkholderiales* (12.19% in MBR-1, 10.65% in MBR-2, 14.13% in MBR-3), *Rhodocyclales* (6.42% in MBR-1, 9.3% in MBR-2, 9.45% in MBR-3), *Rhodospirillales* (5.01% in MBR-1, 2.64% in MBR-2, 3.63% in MBR-3) and *Rhizobiales* (2.54% in MBR-1, 6.99% in MBR-2, 2.68% in MBR-3). They comprised 55.27%, 51.28% and 67.25% of the bacteria in biofilms at high TMP in experiments 1 - 3 respectively, indicating they dominated the biofilm community at high TMP in all three experiments.

As was observed for the biofilm community at low TMP, the bacterial communities in experiments 2 and 3 were found to have a higher similarity (74.44% similarity) than with the biofilm community in experiment-1 (68.9% similarity) (Fig. 3.12b). Therefore, as was observed for the early biofilms, the bacterial biofilm community at high TMP was also affected by the initial bacterial community composition in the sludge.

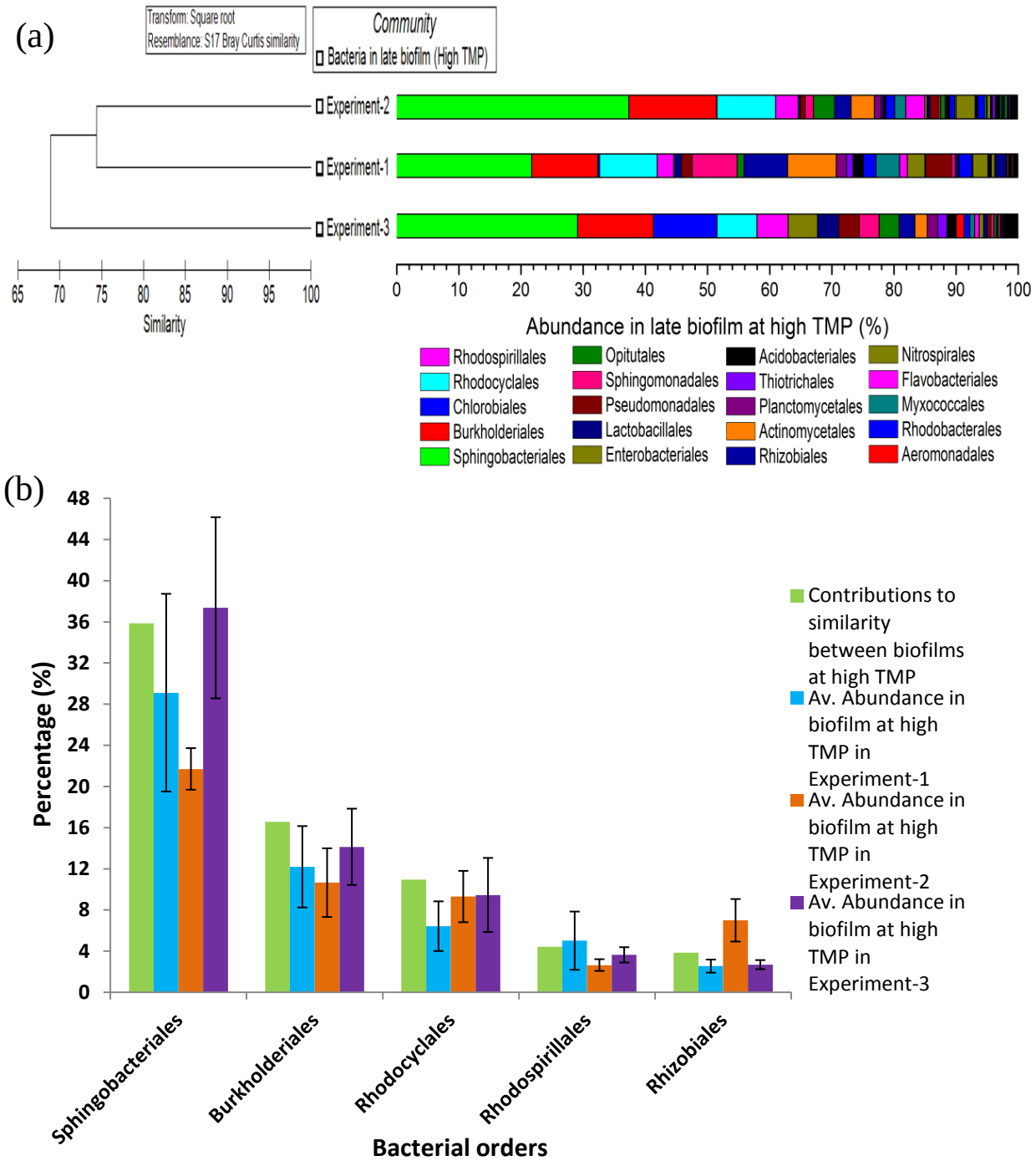

Fig. 3.12 The bacterial communities at the Order level in biofilms at the high TMP stage. (a) The abundance and phylogenetic tree for the bacterial communities in the high TMP biofilms in three separate experiments. (b) The common, dominant bacteria in high TMP biofilms in three experiments. The bacteria were selected by their contribution to the group similarity between the late biofilms in the three experiments. The error bars are the standard error of the mean (n=3).

3.3.5.4 Succession of biofilm communities from the low to high TMP stage

It was noted above that not only the biofilm communities were distinct compared to the sludge community, but also that the biofilm communities also fell into distinct clusters, depending on the specific TMP stage at which they were collected (Fig. 3.7). This suggests that the biofilm communities changed over time or during operation of the MBR. The following sections show in detail how those biofilm communities changed over time, with respect to either the increase or decrease in abundance of specific organisms.

3.3.5.4.1 Increase in abundance of specific bacteria as the TMP increased over time

Bacteria of the Orders *Rhodospirillales* and *Sphingomonadales* were observed to increase in abundance in biofilms as the TMP increased in all three experiments (Fig. 3.13). The *Rhodospirillales* accounted for 1.18%, 1.37% and 1.75% of the bacterial communities at the low TMP stage biofilms for experiments 1, 2 and 3 respectively. In contrast, at the high TMP stage, the abundance for *Rhodospirillales* increased to 5.01%, 2.64% and 3.63% for experiments 1, 2 and 3 respectively (all $p<0.05$ by T test). Similarly, the abundance of *Sphingomonadales* was 2.88%, 0.55% and 0.56% in the low TMP biofilms but increased to 3.21%, 7.24% and 1.36% in the high TMP biofilms for experiments 1, 2 and 3 respectively (all $p<0.05$ by T test). This general increase in abundance may indicate that these bacteria play an important role in building the later stage biofilms.

Additional Orders of bacteria were found to increase in biofilm abundance across the TMP increase in both experiment-2 and 3. These bacteria included *Rhizobiales*, *Actinomycetales*, *Bacteroidales* and *Rhodobacterales*. The *Rhizobiales* and *Actinomycetales*, were already the dominant biofilm bacteria at low TMP (1 - 2% in abundance for *Rhizobiales* and 2 - 3% in abundance for *Actinomycetales*) and became more dominant in biofilms at high TMP (2.7 - 7% in abundance for *Rhizobiales* and 3.7 - 7.8% in abundance for *Actinomycetales*, both $p<0.05$ by T test). For *Rhodobacterales*, they were the rare bacteria in biofilms at low TMP, where the abundance was 0.89% in experiment-2 and 0.78% in experiment-3. However, when TMP increased (80 - 90 kPa), the abundance for *Rhodobacterales* increased to 2.01% ($p<0.05$ by T test) and 1.44% ($p<0.05$ by T test) in experiment-2 and 3 respectively.

3.3.5.4.2 Decreased biofilm abundance of specific bacteria as the TMP increased over time

Bacteria of the order *Rhodocyclales* decreased in abundance in the biofilms as the TMP

increased (Fig. 3.13). In the biofilms at the low TMP stage, the *Rhodocyclales* was present at 16.38% (exp-1), 9.84% (exp-2) and 24.67% (exp-3) in the bacterial communities, while in the high TMP biofilms, its abundance decreased to 6.42% (exp-1, $p<0.05$ by T test), 9.3% (exp-2, $p>0.05$ by T test) and 9.45% (exp-3, $p<0.05$ by T test). Despite this decreased abundance, the *Rhodocyclales* were still the dominant bacteria in biofilms at high TMP. This could suggest a role for the *Rhodocyclales* in establishment of biofilms during the low TMP operation.

3.3.5.4.3 Dominant biofilm bacteria

Some bacteria were clearly the dominant organisms in the biofilms across all TMPs, irrespective of whether their relative abundance increased or decreased as the TMP increased. This was particularly obvious for the *Sphingobacteriales*, *Burkholderiales*, *Actinomycetales* and *Rhizobiales*. The *Sphingobacteriales* were consistently present in the biofilm between 20 - 37% in abundance for all time points tested. Similarly, the bacteria of Order *Burkholderiales* were present in the biofilms at abundances that ranged from 10 - 25%. Based on their consistent, high abundances, these organisms may be the key organisms responsible for biofilm formation on the MBR membranes.

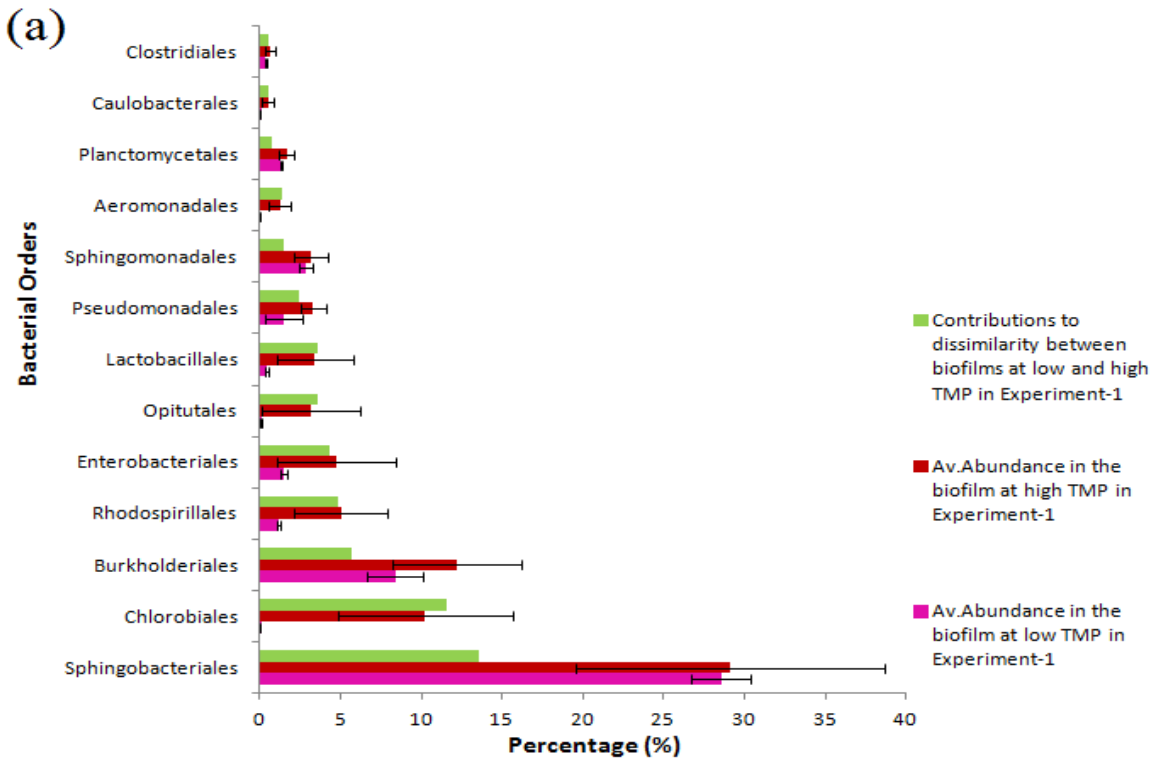

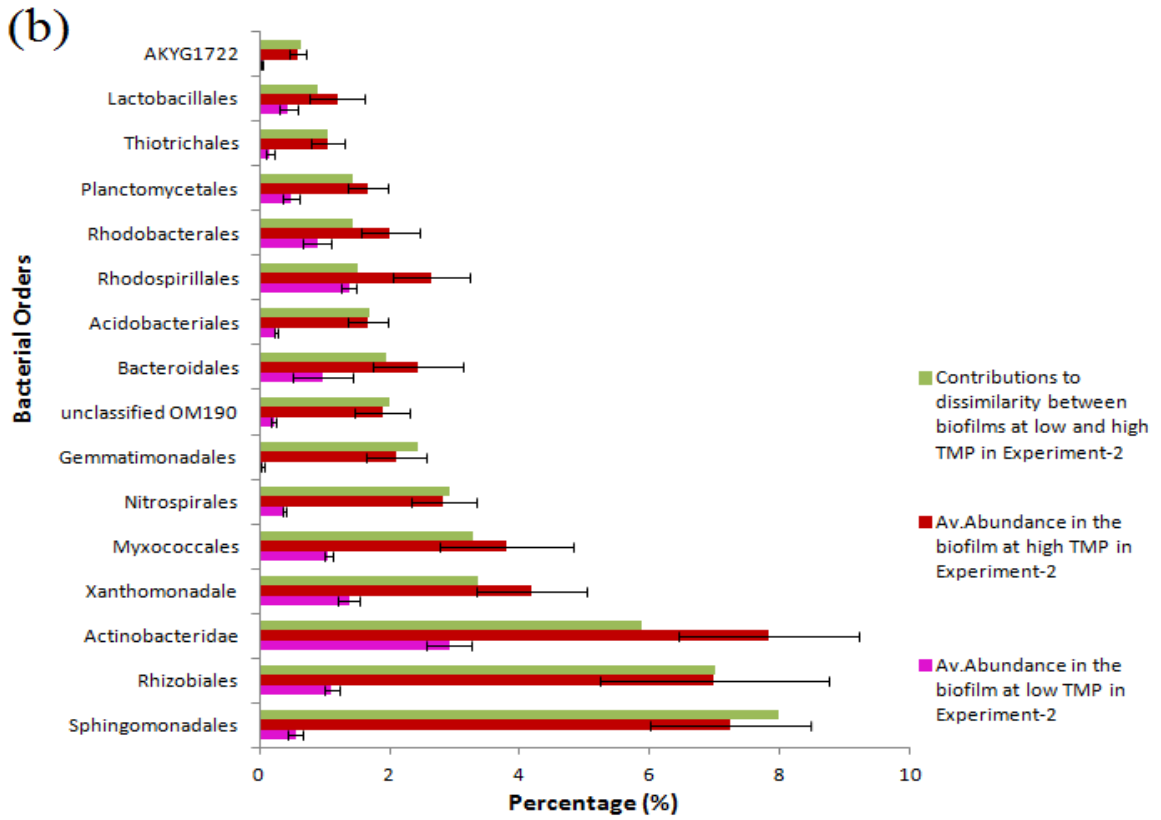

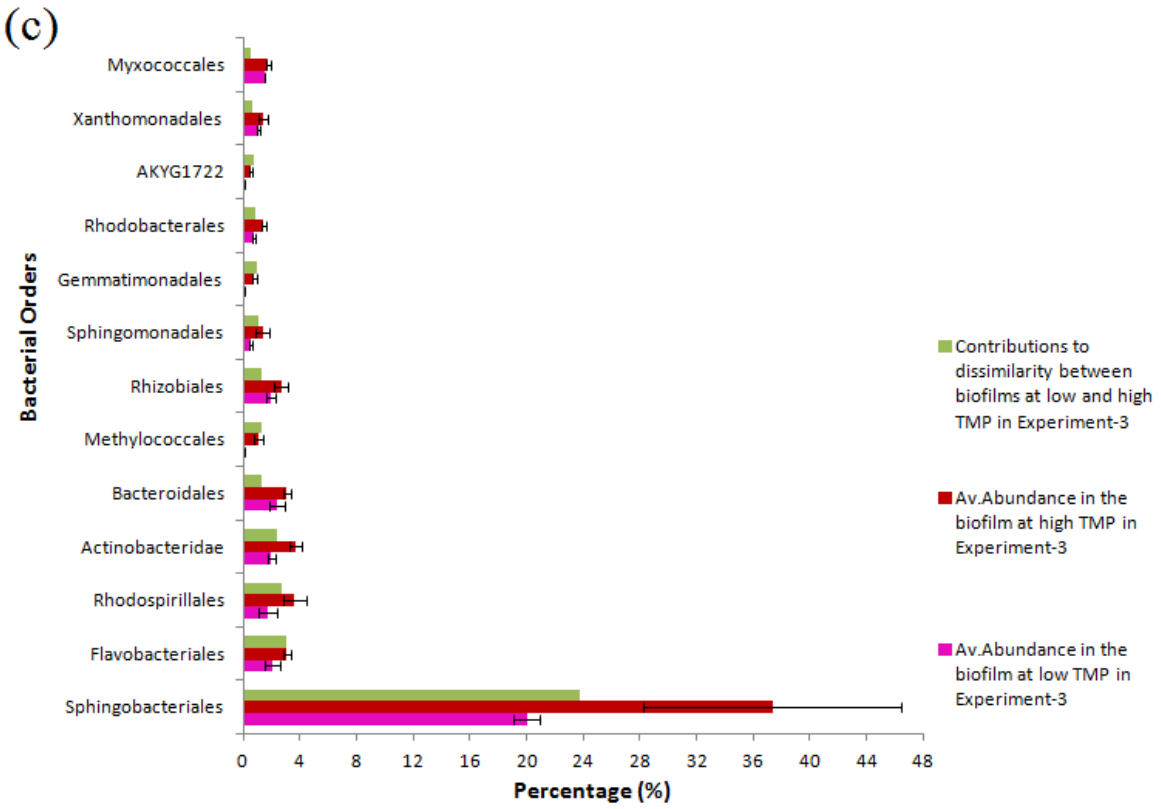

Fig. 3.13 (Continued from previous page) Increased abundance of specific bacteria in the high TMP biofilms, (a) experiment-1, (b) experiment-2, (c) experiment-3. The data points were the average values of the triplicate samples at low or high TMP. Error bars are the standard error of the mean (n=3).

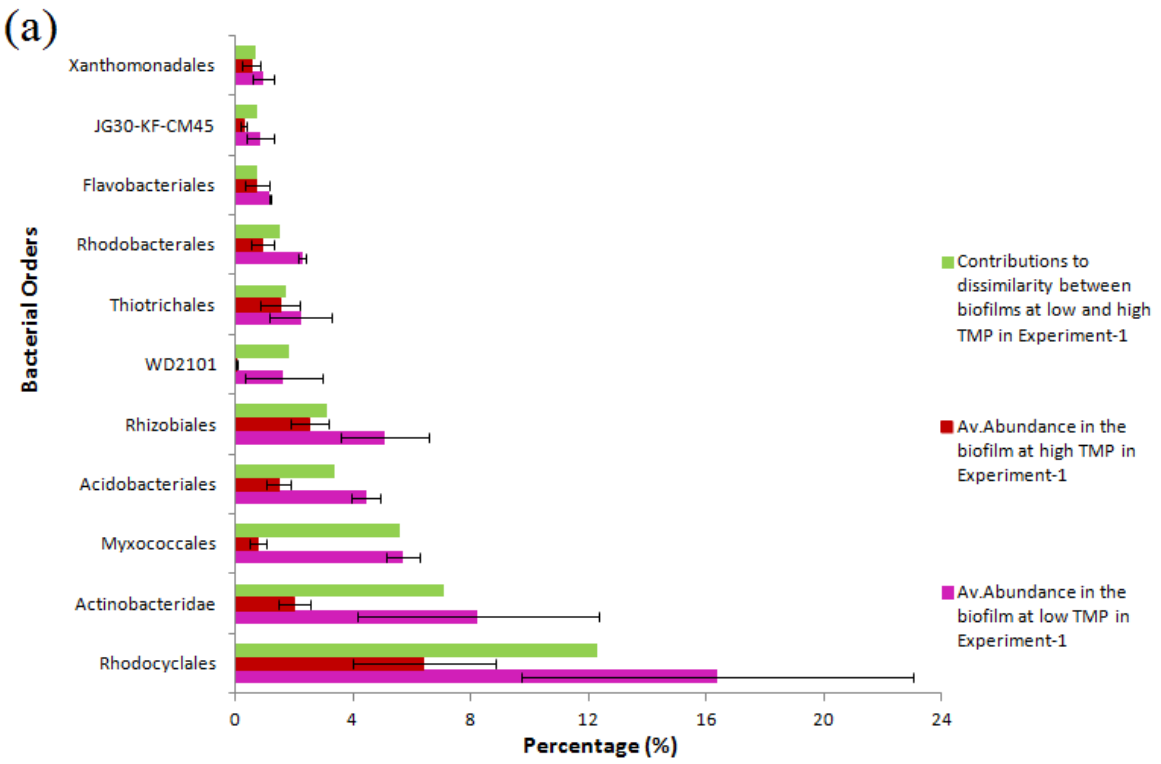
(a)
Xanthomonadales
JG30-KF-CM45
Flavobacteriales
Rhodobacterales
Thiotrichales
WD2101
Rhizobiales
Acidobacteriales
Myxococcales
Actinobacteridae
Rhodocyclales
Bacterial Orders
0
4
8
12
16
20
24
Percentage (%)
Contributions to dissimilarity between biofilms at low and high TMP in Experiment-1
Av.Abundance in the biofilm at high TMP in Experiment-1
Av.Abundance in the biofilm at low TMP in Experiment-1

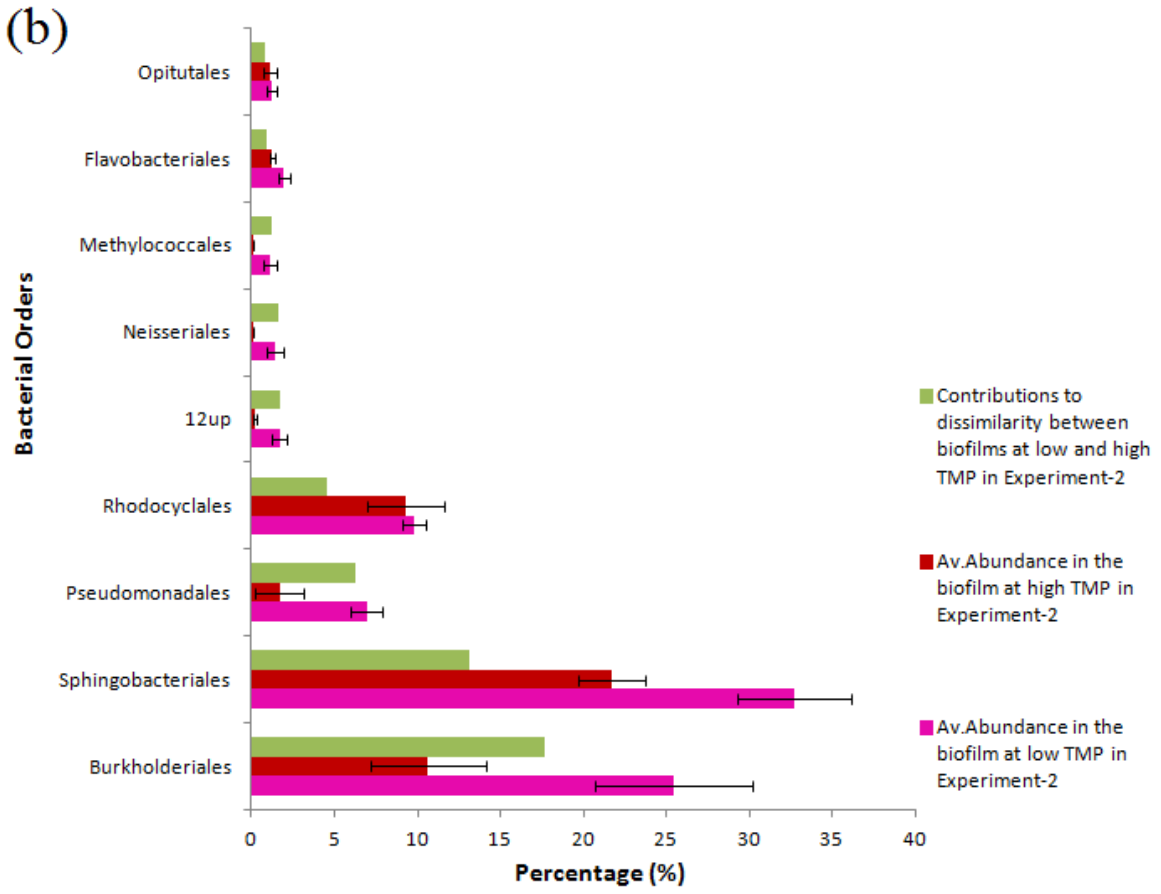
(b)
Opitutales
Flavobacteriales
Methylococcales
Neisseriales
12up
Rhodocyclales
Pseudomonadales
Sphingobacteriales
Burkholderiales
Bacterial Orders
0
5
10
15
20
25
30
35
40
Percentage (%)
Contributions to dissimilarity between biofilms at low and high TMP in Experiment-2
Av.Abundance in the biofilm at high TMP in Experiment-2
Av.Abundance in the biofilm at low TMP in Experiment-2

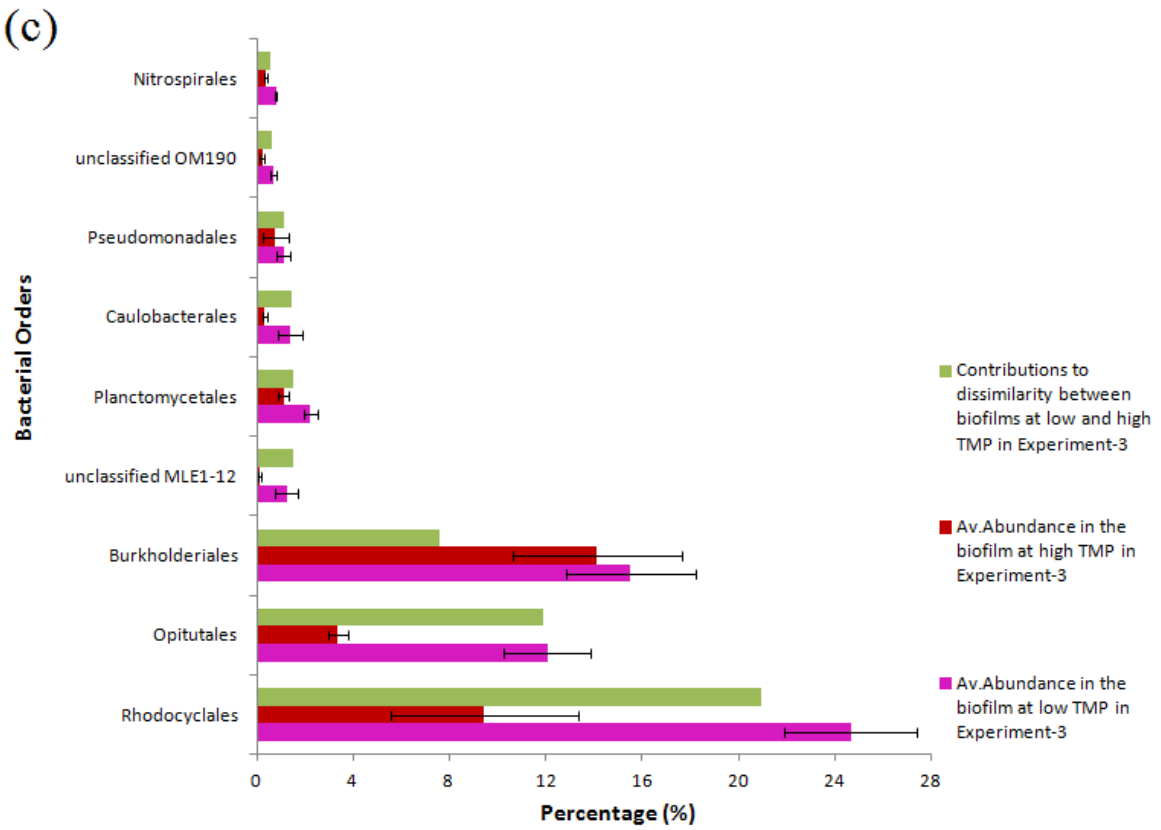

Fig. 3.14 (Continued from previous page) Decreased abundance of specific bacteria in the high TMP biofilms, (a) experiment-1, (b) experiment-2, (c) experiment-3. The data points were the average values of the triplicate samples at low or high TMP. Error bars are the standard error of the mean (n=3).

3.4 Discussion

One crucial step of biofilm formation is the attachment of microorganisms onto the membrane surface, which is followed by the proliferation of microorganisms and secretion of EPS. In this project, biofilm and sludge samples were collected at low TMP (3 - 15 kPa) and high TMP (15 - 90 kPa) stages, and the bacterial communities associated with the biofilm and sludge were determined by 16S rRNA tagged pyrosequencing.

The correlation between the richness of biofilm bacterial community and TMP increase was not evident in this study. The experiments 1 and 3 showed the increasing trend of biofilm bacterial community and TMP increase while the experiment 2 displayed a different trend. However, the richness of the biofilm at the low TMP stage was considerably reduced relative to the sludge at the same time point in all the 3 experiments suggesting that only a subset of

the bacterial species in the sludge can adhere onto the membrane. When the TMP increased, the richness of biofilm bacterial community increased in experiments 1 and 3 but were relatively stable in experiment 2. As the TMP reached its maximum, the biofilms had a higher richness than the sludge in experiments 1 and 3. It was interesting to observe that the sludge community in experiments 1 and 3 decreased in diversity over time and this may suggest that the community is experiencing some stress. If the decreased sludge diversity is a consequence of stress induced selection, then it may not be surprising that the biofilm community does not similarly decrease in diversity as it has been previously shown that the biofilms had an intrinsically higher resistance to stress than planktonic bacteria (Bernier et al., 2013; Kubota et al., 2009; Ramage et al., 2012).

The increase in biofilm diversity might also suggest that biofilm formation is initiated by a specific subset of the sludge community and those organisms subsequently facilitate the settlement of other species onto the growing biofilm. Thus, biofilm formation may not be random, but rather may occur in an ordered fashion. This is supported by the NMDS plots which show that the biofilms were more similar to each other than to the sludge community. These results were similar to the observations published comparing biofilm and activated sludge samples, where it was observed that the bacterial community in biofilm differed from the community in sludge during the operation from day 1 to day 31 in a flat-sheet membrane MBR (Piasecka et al., 2012).

Specifically, at low TMP stage, the bacterial communities on the membrane were comprised of *Sphingobacteriales*, *Rhodocyclales*, *Burkholderiales*, *Actinomycetales* and *Flavobacteriales* in all three experiments. Of these, four Orders of bacteria, *Rhodocyclales*, *Sphingobacteriales*, *Burkholderiales* and *Actinomycetales,* were also the predominant bacteria in the sludge. Similar results were previously reported where it was observed that *Bacteroidetes* and *Burkholderiales* were the co-dominant bacteria in biofilms on membranes and in activated sludge (Ivnitsky et al., 2007). It was similarly reported that the *Proteobacteria* (such as *Rhodocyclales* and *Burkholderiales*) and *Bacteroidetes* (which includes *Sphingobacteriales* and *Flavobacteriales*) were prevalent in biofilms (Huang et al., 2008; Lim et al., 2012; Miura et al., 2007; Zhang et al., 2008), although at least in one case, the dominant biofilm forming bacteria were *Gammaproteobacteria* in contrast to the results presented in this chapter indicating that the *Betaproteobacteria* were more prevalent (Lim et al., 2012). The differences in dominant bacterial community members may be related to experimental differences. For example, in the previously published work (Lim et al., 2012), the synthetic waste water

medium contained glucose at 1,000 mg/L and peptone at 50 mg/L, while the concentrations used here were 320 mg/L of glucose and 80 mg/L of peptone. Compared to the sludge community, the *Burkholderiales*, *Pseudomonadales* and *Rhizobiales* were enriched in the early biofilms at low TMP. Interestingly, while the *Pseudomonadales* were not in the top five most abundant biofilm bacteria, they were none the less present in the biofilm at higher abundance than that was observed for the sludge. Characterization of the microbial community growing on an air-diffusion biocathode in a microbial fuel cell system indicated that members of the groups *Rhizobiales* and *Pseudomonadales* were present in higher proportions in the biofilms relative to the sludge (Wang et al., 2013). Further, the *Rhizobiales* and *Burkholderiales* were also determined to be the major populations in biofilms formed in drinking water distribution systems and hence these groups may be good general biofilm forming organisms found in water systems (Liu et al., 2012). It has already been reported that the cell wall of one species under *Burkholderiales* was enveloped in a polysaccharide capsule (Moxon and Kroll, 1990). Also, the *Pseudomonadales* usually produce the exopolysacchrides, such as alginate, Psl and Pel, as the cell matrix in their biofilm formation (Ma et al., 2012). This is consistent with the results in chapter 2, where the polysaccharides were the dominant EPS component during the attachment of bacteria and the formation of early biofilms, and can also be used to explain why these organisms were selected to construct the early biofouling layer.

At the high TMP stage, the Orders of *Sphingobacteriales*, *Burkholderiales, Rhodocyclales, Rhodospirillales* and *Rhizobiales* were the top five most abundant bacteria in the biofilm, which comprised 50 - 70% of the biofilm community in all three experiments. Compared to the biofilm at low TMP, the *Alpha-proteobacteria* (represented here by *Rhodospirillales*, *Sphingomonadales* and *Rhizobiales*) became the most dominant groups in late biofilms at high TMP. Similarly, it was also reported that the *Alpha-proteobacteria* increased in abundance in late biofilms in an MBR system (Lim et al., 2012). It has been suggested that members of the *Sphingomonadales* were pioneer bacteria to initiate biofilm formation and flourished in the late biofilm in microfiltration and ultrafiltration based MBR systems (Calderón et al., 2011; Huang et al., 2008; Pang and Liu, 2006), due to their swarming and twitching motile ability and polysaccharides secreting ability (Pang et al., 2005). This was consistent with the results presented in this thesis which showed the *Sphingomonadales* were present but were not highly abundant in the biofilm at low TMP while they became more prevalent in the biofilm at high TMP. The *Rhodocyclales* have been reported to be a significant components of the sludge community in wastewater treatment systems (Yang et al., 2011) and were also proposed to be

important in biofouling of MBRs (Xia et al., 2010). While the data presented here indicated that the *Rhodocyclales* were a significant component of the biofilm community, they were present at lower abundance when the TMP was highest, indicating the *Rhodocyclales* may contribute more to the initial biofilm establishment. One phenomenon needs to be noted that the *Sphingomonadales* were able to secret many AHLs signals (Huang et al., 2013), which are required for the formation of biofilm for many species. Similarly, the *Rhodospirillales* can also produce and respond to the AHL signals in environment (Sant'Anna et al., 2011). The synthesis and response functions of QS signal molecules for the *Rhodospirillales* and *Sphingomonadales* may be the why how these organisms impact the formation of late biofilm formation. This may also be the reason why they became more dominant in biofouling layer at the high TMP.

It was particularly interesting to observe that the biofilm communities could be divided into two groups, where those associated with the low TMP stage (5 - 7 kPa) were most similar to each other, whilst the biofilm communities for all other samples in all three experiments formed a separate cluster. Similarly, the TMP profile can be used to divide the experiments into two stages, the low TMP stage (3 - 15 kPa) which was observed for up to 70-90 d of operation and the high TMP stage (15 - 90 kPa) where the TMP jumped to the maximum pressure in a shorter time frame (25 - 35 d). Based on these results, it is proposed that there was a threshold pressure, 15 kPa, above which the system entered into the 'jump' phase. Since the greatest change in biofilm community composition occurred prior to this threshold pressure, this would indicate that change in the bacterial community that occurred before the TMP jump may be the most relevant in relation to its effect on system performance. Based on the changes in biofilm community presented here, it is proposed that the most important bacterial groups associated with this transition stage were *Rhodospirillales* and *Sphingomonadales*, which were observed to increase in abundance in biofilms from the low to high TMP stages.

In conclusion, the bacterial community was compared for both sludge and biofilm samples and the changes in community composition were related to changes in MBR performance, as determined by the change in TMP. The results suggested that the biofilm initiated from a specific group of bacteria and that this community changed in composition as the TMP increased. Further, the biofilm community associated with the low pressure operation phase was significantly different from the community associated with the membranes at the time the TMP exceeded the threshold pressure which was followed by an exponential, jump phase

where the pressure rapidly reached its maximum for the system. Given that the biofilm initiates from a specific subset of bacteria present in the sludge, it may be possible to target those organisms to ultimately delay their incorporation into the biofilm and hence delay the TMP jump. It will also be particularly interesting to understand the mechanism that results in the subtle community shift that is associated with the TMP jump.

Chapter 4 Correlation between the Fungal Community and MBR Performance

4.1 Introduction

In addition to bacteria, fungi are also an important group of organisms that can form surface associated communities, known as biofilms (James et al., 2011; Ramage et al., 2009). A wide spectrum of fungi have the ability to form biofilms, including *Candida* spp., *Saccharomyces* spp., *Cryptococcus* spp. and *Aspergillus* spp. (Bojsen et al., 2012; Chandrasekar and Manavathu, 2008; López-Ribot, 2005; Ravi et al., 2009). Additionally, the fungi can also form biofilms in combination with bacteria. For example, investigation of the microbial biofilm community on sandstone in a Bayon temple in Cambodia, showed that the microbial community was composed of bacteria, fungi, Metazoa and Alveolata (Lan et al., 2010). The fungal community consisted of Basidiomycota, Ascomycota and Chytridiomycota in both fresh and old biofilms. Not surprisingly, fungi have been shown to be a significant component of activated sludge, where Geotrichum, Penicillium and yeast can be prevalent in the both anoxic and aerobic sludge (Awad and Kraume, 2010). Additionally, keratinophilic fungi, including *Chrysosporium* spp., *Microsporum* spp., *Trichophyton* spp. and *Aspergillus* spp., were also found in the anoxic and aerobic sludge (Awad and Kraume, 2011a). In activated sludge and MBR systems, fungi contribute important functions, such as phenol removal and degradation of azo dyes (Ahn et al., 2008; Hai et al., 2011; Hai et al., 2013). While much work to date has been undertaken to characterize the bacterial community involved in the biofouling process (Lim et al., 2012; Miura et al., 2007), few studies have investigated the role of the fungal community in the biofouling phenomenon in MBRs. Therefore, in this study, the fungal component of biofilm communities on hollow fiber membranes and in the activated sludge in the MBR tanks were characterized through metacommunity sequencing based on 18S rRNA gene sequencing. The fungal phylotypes were determined and correlated with TMP rise and fouling of the membranes. Furthermore, the compositions and succession of fungal communities in the biofilms and sludge were studied during the operation of the MBR.

4.2 Methods and materials

4.2.1 MBR set-up and operation

Three experiments were conducted, using two different laboratory scale submerged MBRs that were operated to treat artificial synthetic wastewater, total organic carbon (TOC) of 200

mg/L as described in Chapter 3. The MBR set-up and operational parameters were the same as Chapter 3.

4.2.2 DNA extraction

All samples collected were the same as those described in Chapter 3 for the bacterial community assessment. Total DNA from the biofouling community growing on the HF membranes as well as from the activated sludge was separately extracted by a modified CTAB-PEG protocol (Griffiths et al., 2000; Paithankar and Prasad, 1991), which was same as described in Chapter 3.

4.2.3 Pyrosequencing

The DNA was sequenced using the "454" pyrosequencing method (Research and Testing Laboratory, Texas, US) (Handl et al., 2011). The primers selected for the fungal PCR were forward funSSUF (5'-TGGAGGGCAAGTCTGGTG-3') and reverse funSSUR (5'-TCGGCATAGTTTATGGTTAAG-3') (Foster et al., 2013). The number of reads for every sample was approximately 3,000.

4.2.4 Fungal sequence processing

The pyro-sequencing data was processed using the MOTHUR software (http://www.mothur.org/wiki/Main_Page) based on the Costello analysis pipeline (Costello et al., 2009; Schloss et al., 2009). The sequences were sorted by the barcodes to generate groups of data for the samples. Firstly, the sequence packets were trimmed and barcodes and primers were removed from the sequences. The sequences that had poor quality, below 25, were removed from the dataset and the size of data packets was reduced to facilitate the analysis through the process of "unique". The chimeric sequences were identified and removed from the datasets using the "chimera.slayer". The reference was set to be self and the sequences were subsequently aligned with the SILVA eukaryotic 18S rRNA sequence database and assigned to taxonomic groups based on the SILVA eukaryote taxonomic reference (Pruesse et al., 2007). The criterion for the sequence classification (similarity to the reference sequence) were Species (> 97%), Genus (94% - 97%), Family (90% - 94%), Order (85% - 90%), Class (80% - 85%), and Phylum (75% - 80%) (Lim et al., 2012). Sequences with similarities below these criteria were classified into unidentified groups for each taxonomic rank. Finally, a shared phylotype file was generated through the command "make.shared" for all the samples. The coverage of phylotypes was calculated based on the phylotypes acquired and the number

of sequences pooled. The relationship between the phylotypes and sequences was calculated by MOTHUR using the command of "summary.single".

4.2.5 Phylotype-based analysis with Primer 6

Phylogenetic trees and Nonmetric Multidimensional Scaling (NMDS) plot were created between the samples based on the Bray-Curtis similarity of phylotype compositions in the different groups (Clarke, 1993). The similarity or dissimilarity between the samples or groups was calculated by the operation "SIMPER" in Primer 6 (PRIMER-E) (Clarke, 1993). The contributions of the phylotypes to the similarity or dissimilarity were calculated based on the relative abundances of phylotypes between the samples. The fungi that contributed 0.5% or more to the similarity or dissimilarity were determined to be the key organisms influencing the composition of the community.

4.3 Results

4.3.1 Biofouling behavior and sampling time-points in MBRs

The correlation between the fungal community and MBR fouling was determined in three replicate experiments, as described in Chapter 3. For each of the three experiments, the TMP profiles were similar over the entire study period and were observed to have a steady TMP stage operating between 5 - 15 kPa for the first 70 to 90 d (Fig. 3.2). For experiment-1, which was run at the constant flux of 15 - 17 $L.m^{-2}.h^{-1}$, the TMP rose from 5 kPa to 15 kPa over a 70 d period. For experiments 2 and 3, which were run at a constant flux of 13 - 15 $L.m^{-2}.h^{-1}$, the system required 80 - 87 d to for the TMP to increase from 5 kPa to 15 kPa. After the TMP exceeded 15 kPa, the TMP was found to increase exponentially, termed here as the 'jump stage' or 'TMP jump' and reached approximately 90 kPa, which was the maximum pressure for the MBRs. The TMP jump stage required 29, 36 and 28 d to reach the maximum pressure for experiments 1, 2 and 3 respectively. Based on these observations, the experimental TMP phases are described as two stages, the steady state and TMP jump phases. As described for Chapter 3, samples were collected from the sludge and the membranes at the low and high TMP stages (Fig. 4.1).

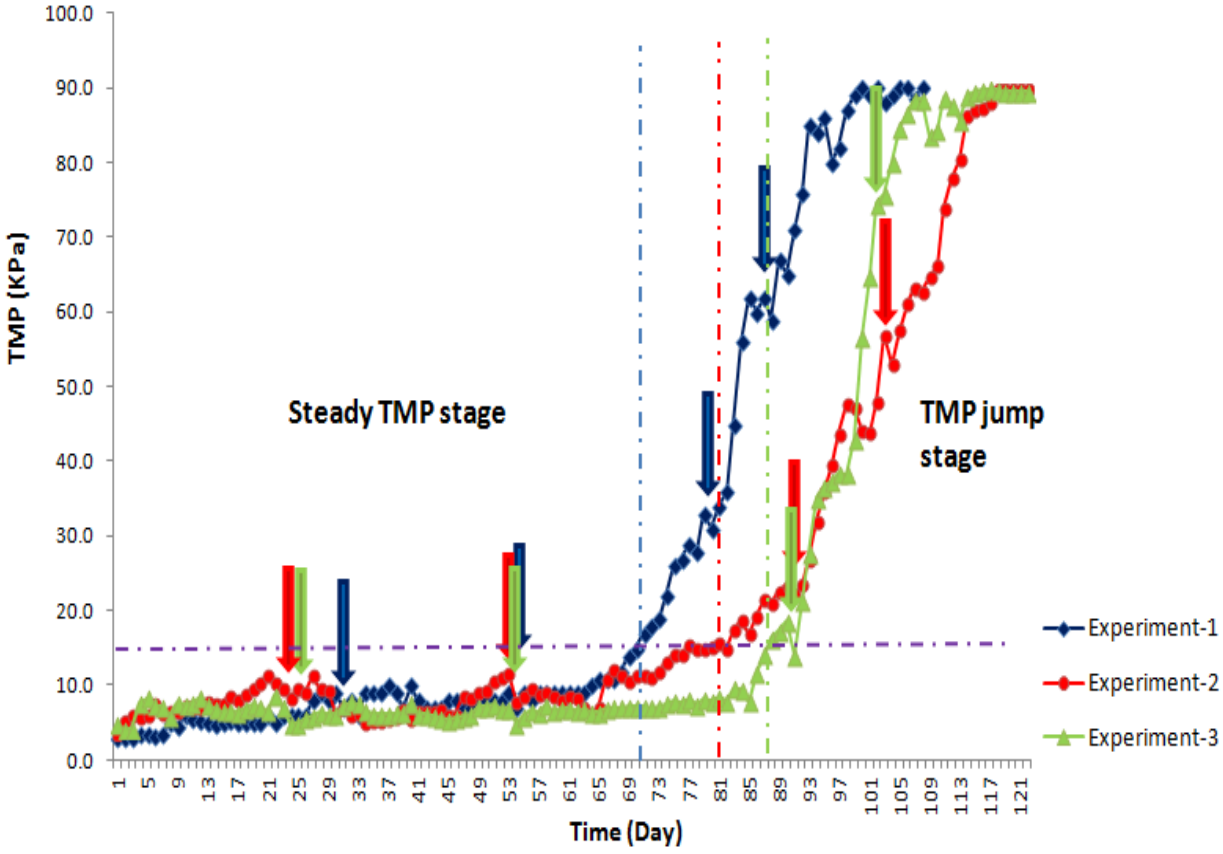

Fig. 4.1 TMP profiles and sampling time points for fungal community analysis in three replicate MBRs, experiment 1 (blue), experiment-2 (red) and experiment-3 (green). The TMP curves were divided into steady TMP stage (< 15 kPa) and the TMP jump stage (> 15 kPa). The biofilms and sludge samples were collected at different time points, indicated by the arrows.

4.3.2 Community analysis for samples

The same DNA samples used for assessing the bacterial communities described in Chapter 3 were also used to characterize the fungal community here. After removing sequences of poor quality, experiments 1 - 3 respectively had 25,575 sequences for 16 samples, 6,2187 sequences for 24 samples and 7,9427 sequences for 24 samples (Fig. S4.1). The average sequence read lengths were 450 bp in experiment-1, 395 bp in experiment-2 and 389 bp in experiment-3. The phylotypes for the fungal communities were classified at multiple taxonomic ranks based on these sequencing results. At the species level, most OTUs were unclassified, while it was possible to classify most of the sequences at the Genus level. Therefore, the genus level was used to analyze the fungal communities.

The coverage of phylotypes was calculated at different taxonomic ranks for the samples based on the relationship between the number of phylotypes and sequences. At the Genus level, the coverage of phylotypes for all samples was 95.3% - 99.8% in experiment-1, 96.1% - 99.7% in experiment-2 and 97.8% - 99.6% in experiment-3 (Fig. S4.2). For the higher taxonomic ranks, the phylotype coverage was higher, and thus the sequencing reads for both the biofilms and the sludge covered almost all of the fungal community in the MBRs. The high coverage of phylotypes provided confidence in the sampling size and that the data are an accurate reflection of the true fungal communities of the MBRs.

4.3.3 Relationship between of fungal communities in biofilms and activated sludge

4.3.3.1 The fungal biofilm community

4.3.3.1.1 Comparison of the fungal biofilm and sludge community diversity

Analysis of the diversity of the fungal community (Shannon index) showed that the biofilm community had lower diversity than the sludge at high TMP (50 - 90 kPa) in all the three experiments, where the Shannon diversity for the fungal sludge community was 1.73 - 2.1 but was only 1.13 - 1.6 for the biofilm (Fig. S4.3 in Appendix B). This also indicated that a subset of the fungal community was selected from the sludge to form the biofilm at high TMP.

Additionally, based on the Shannon diversity comparison, the fungal community appeared to have a lower diversity than the bacterial community (Chapter 3) in both the sludge and biofilms for the three experiments. In sludge, the Shannon diversity was 1.5 - 2.3 for the fungal community compared to 2.4 - 3.9 for the bacterial community in the three experiments. Similarly, the Shannon indices of diversity were 1.1 - 2.1 for the fungal biofilm community while the bacteria had higher diversity (2.7 - 4.1) in the biofilms.

4.3.3.1.2 The dissimilarity of fungal community between the biofilm and sludge

Since the sludge is the microbial source and reservoir in the MBR, the relationship between the fungal communities in the sludge and the biofilms was studied. Selection of specific fugal community members from the sludge was observed during the process of biofilm formation, based on the Bray-Curtis similarity of fungal communities (Figs. S4.3-S4.6). At low TMP, in experiment-1, the fungal biofilm communities at 7 kPa had 71.4% similarity with the sludge community. In experiments 2 and 3, which were operated in parallel, the similarity of the biofilm and sludge communities was 69.5% and 62.68% respectively (Fig. 4.2). Therefore,

approximately 30% dissimilarity was found between the biofilms and sludge at the low TMP stage, indicating that most, but not all fungi in the sludge may contribute to the establishment of biofilms at low TMP.

At high TMP, the similarity of the fungal communities in the biofilm and sludge was observed to decrease in experiments 1 and 2 when the TMP increased. In experiment-1, at 60 kPa the biofilms showed 47.21% similarity to the sludge and 40.2% similarity to the seed sludge at 7 kPa. In experiment-2, the biofilms and sludge communities also had a higher similarity at the low TMP stage (69.5% at 6 kPa) but the similarity decreased at high TMP (50.67% at 55 kPa). The dissimilarity increased to approximately 50% between the biofilms and sludge at high TMP, indicating a further selection for specific fungal communities as the biofilms adapted to the high TMP in experiments 1 and 2. For experiment-3, the similarity of fungal communities between biofilms and sludge was observed to be 62.68% at 5 kPa and 65.29% at 80 kPa and thus did not appear to change as the TMP increased.

4.3.3.2 Successional change of the fungal biofilm community at increasing TMP

The data presented above suggested that the fungal biofilm communities were generally more different from the sludge at the high TMP stage than at the low TMP stage. When the fungal biofilm communities were compared across the different TMPs, it was similarly observed that the fungal biofilm communities at the low and high TMP stages were as distinct from each other. For example, in experiment-1, the fungal biofilm community at 60 kPa displayed 53.31% dissimilarity to the 7 kPa biofilms (Fig. 4.2). In experiments 2 and 3, this phenomenon was more clear, where the high TMP biofilms (55 kPa in experiment-2 and 80 kPa in experiment-3) were found to cluster into one group and the low TMP biofilms (6 kPa in experiment-2 and 5 kPa in experiment-3) clustered into another group (Fig. 4.3).

Further, it was observed that the majority of the change in the fungal biofilm communities occurred before the TMP exceeded the threshold stage and entered the exponential jump stage. This was particularly clear in experiment-3 (Fig. 4.3c), where the fungal biofilms communities at 15 kPa were found to have a closer relationship to the biofilms at 80 kPa (67.84% similarity) than to the biofilms at 5 kPa (55.93% similarity). Additionally, in experiment-1 (Fig. 4.3a), the biofilms at 10 kPa also had a higher similarity to the biofilms at 30 kPa (68.21% similarity) than to the biofilms at 7 kPa (62.14% similarity).

(a)

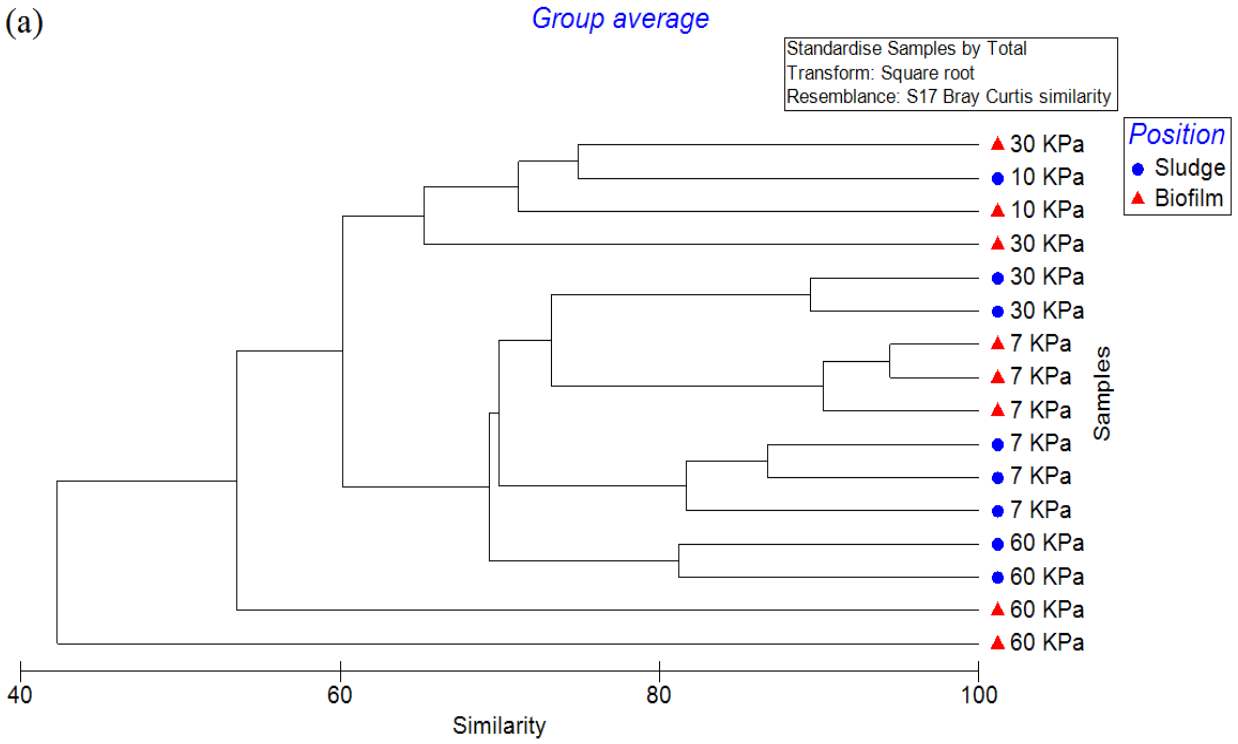
Group average
Standardise Samples by Total
Transform: Square root
Resemblance: S17 Bray Curtis similarity
Position
Sludge
Biofilm
30 KPa
10 KPa
10 KPa
30 KPa
30 KPa
30 KPa
7 KPa
7 KPa
7 KPa
7 KPa
7 KPa
7 KPa
60 KPa
60 KPa
60 KPa
60 KPa
Samples
40
60
80
100
Similarity

(b)

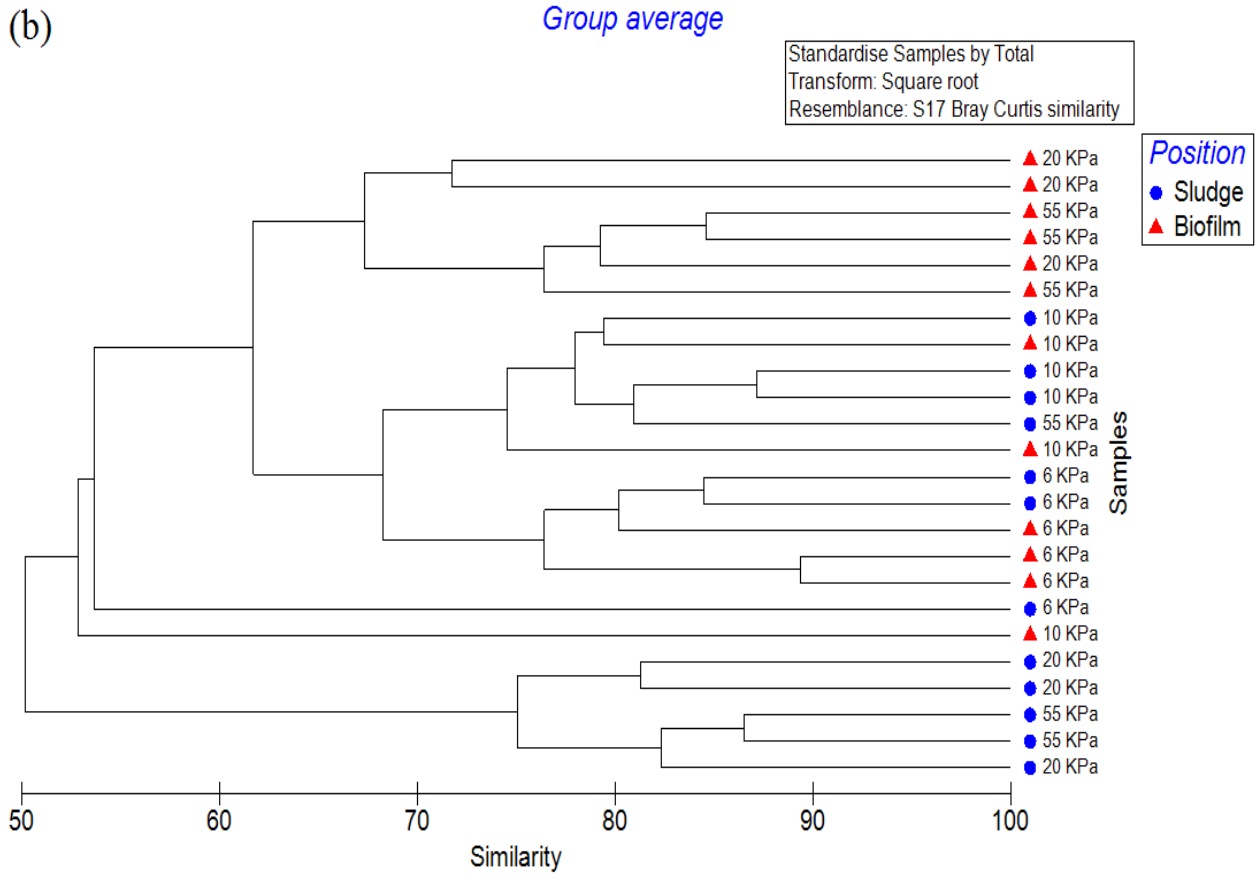
Group average
Standardise Samples by Total
Transform: Square root
Resemblance: S17 Bray Curtis similarity
Position
Sludge
Biofilm
20 KPa
20 KPa
55 KPa
55 KPa
20 KPa
55 KPa
10 KPa
10 KPa
10 KPa
10 KPa
55 KPa
10 KPa
6 KPa
6 KPa
6 KPa
6 KPa
6 KPa
6 KPa
10 KPa
20 KPa
20 KPa
55 KPa
55 KPa
20 KPa
Samples
50
60
70
80
90
100
Similarity

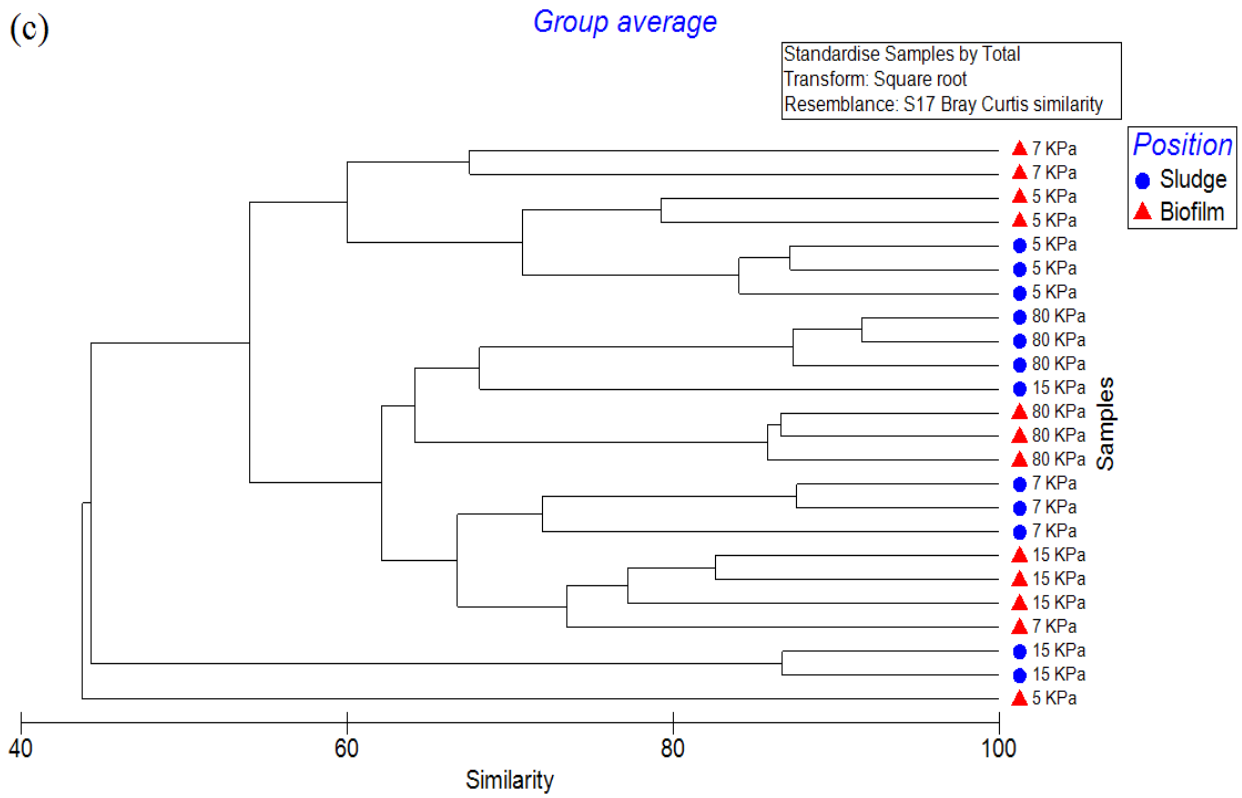

Fig. 4.2 (Continued from previous page) The phylogenetic tree at the Order level for fungi identified in the MBR system in experiment-1 (a), experiment-2 (b) and experiment-3 (c). The transformation of square root was performed on all samples. The blue circles represent the fungal communities in the sludge, and the red triangles represent the fungal communities in the biofilms. The relationships amongst samples were displayed based on the Bray-Curtis similarity between fungal communities.

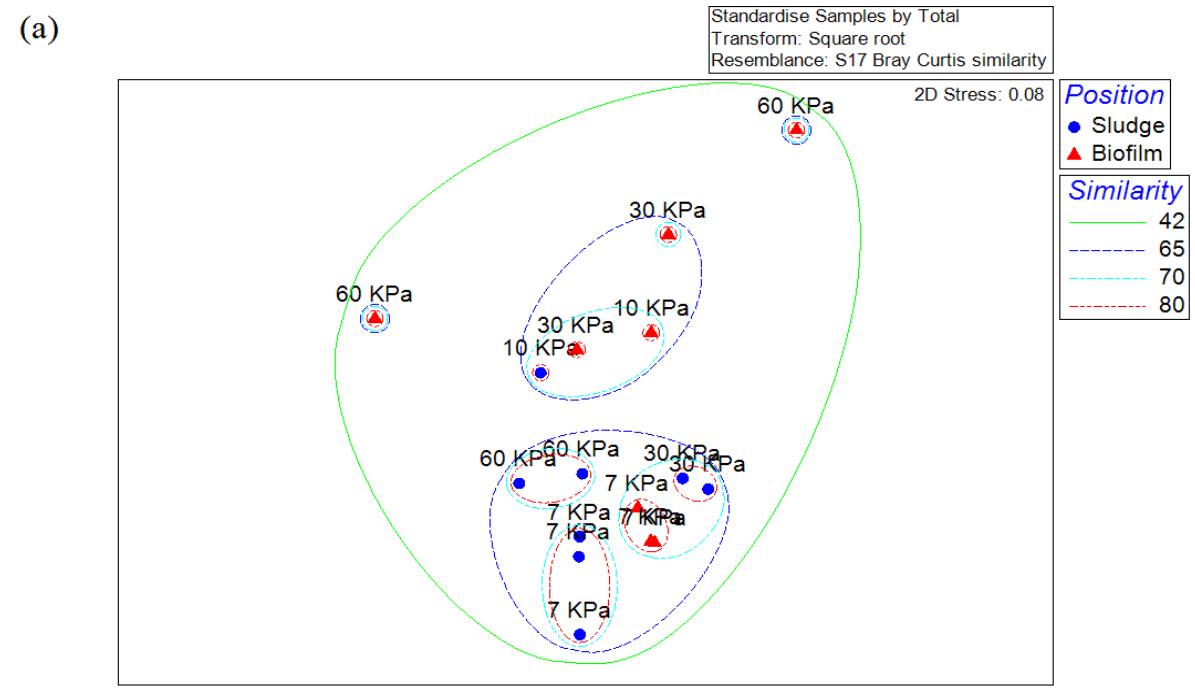

(b)

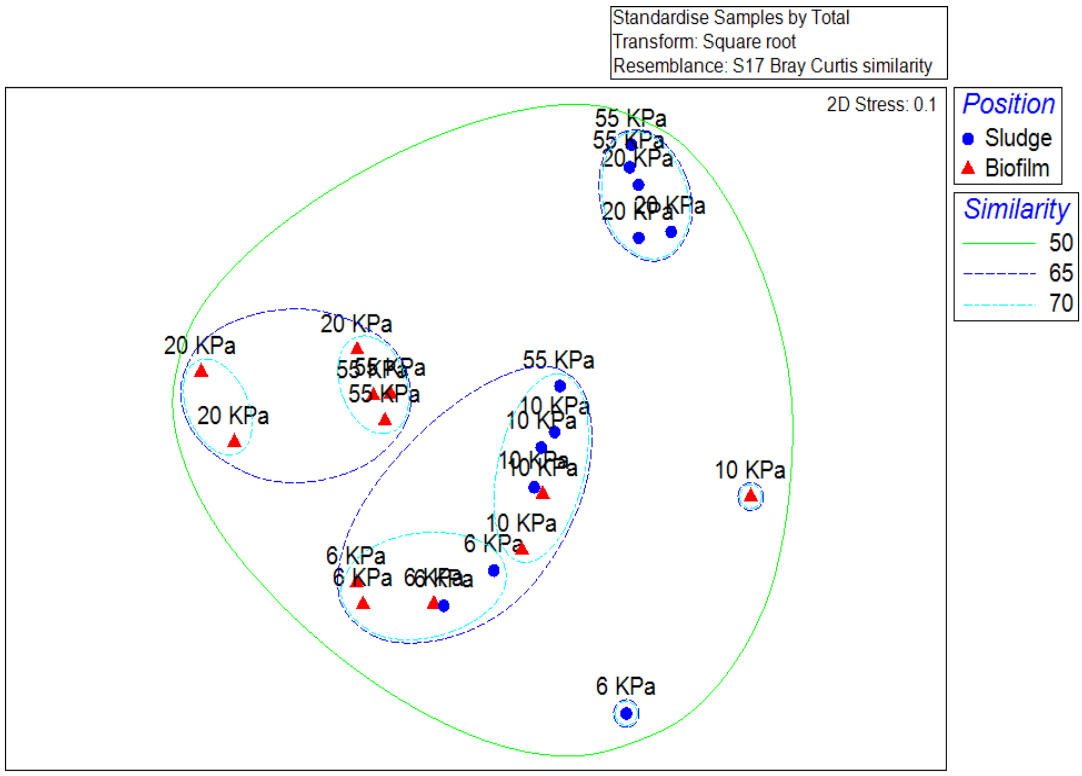

(c)

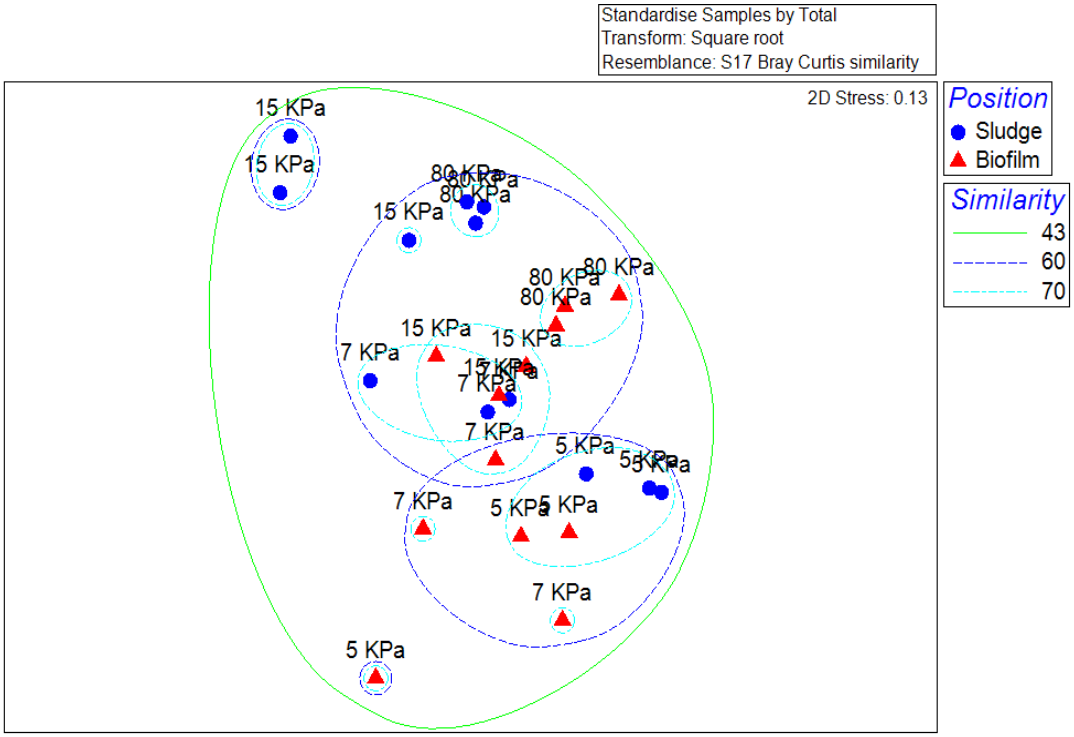

Fig. 4.3 (Continued from previous page) NMDS analysis at the Order level for biofilms and activated sludge samples the experiment-1 (a), experiment-2 (b) and experiment-3 (c). The data were square root transformed for all samples. The blue circles represent the fungal communities in the sludge, and the red triangles represent the fungal communities in biofilms. The samples were grouped by the average Bray-Curtis similarity, which was indicated by the colored lines.

4.3.4 Compositions of fungal communities in sludge and biofilms in MBRs

4.3.4.1 Compositions of fungal communities in seed sludge at low TMP

When the seed sludge, used to inoculate the reactors was examined, a total of 17 Orders of fungi were identified in experiment-1, while 25 and 36 Orders of fungi were identified respectively in the twin experiments, 2 and 3. When the Bray-Curtis similarity of the fungal communities in the seed sludge was calculated, it was observed that the sludge communities displayed 51.64% similarity in all three experiments (Fig. 4.4). The parallel reactors, experiments 2 and 3, showed a closer relationship (69.96% similarity) than with experiment-1 for the fungal sludge communities (Fig. 4.4).

Exploration of the community structure in detail revealed that five Orders of fungi constituted the dominant organisms in the seed sludge in all three experiments, based on their contributions to the overall similarity in all fungal communities (Fig. 4.4). The top three fungi were the *Glomerales*, *Saccharomycetales* and *Diversisporales*, which contributed 20 - 30% to the overall similarity between the fungal communities in the seed sludge (Fig. 4.4). However, the distribution of these Orders was not consistent for the three experiments. The Order *Glomerales* was the most abundant fungal group (58.02%) in experiment-3, while *Diversisporales* were the most dominant fungi (54.47%) in experiment-1. Members of the Order *Saccharomycetales* were the highest in abundance in experiment-2 (28.68%) and the second highest in abundance for experiment-3 (20.08%), but they only accounted for only 3.93% if the sludge community in experiment-1. Additionally, the dominant fungi also included *Mycocaliciales* and *Archaeosporales*, which contributed 13.56% and 10.2% respectively to the overall similarity of fungal communities in the seed sludge.

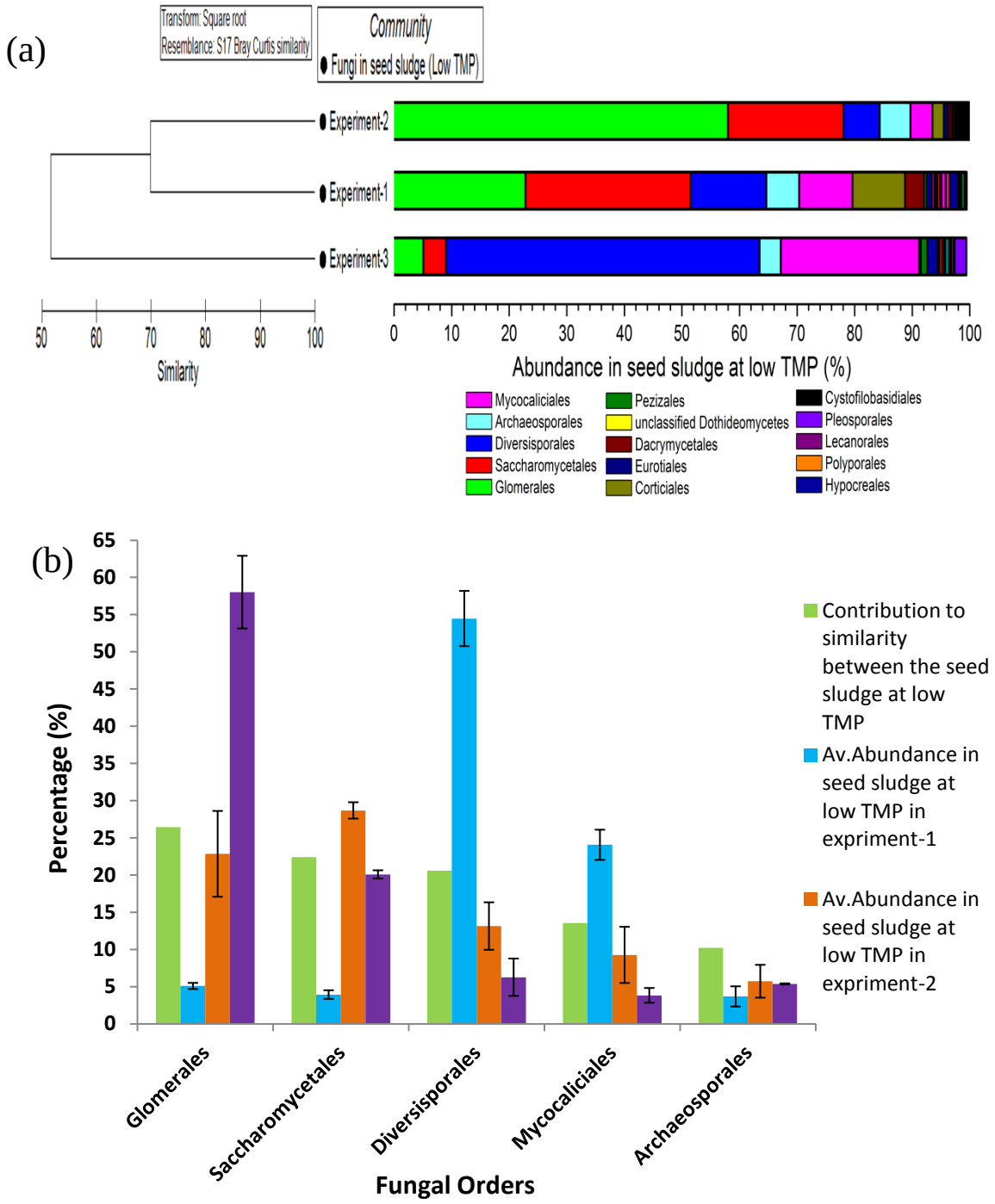

Fig. 4.4 The fungal communities in the seed sludge at the low TMP stage in the triplicate experiments. (a) The fungal community composition and relationship in the seed sludge in each experiment. (b) The common dominant fungi in early biofilms in all three experiments. The error bars are the standard errors of the mean (n=3).

4.3.4.2 Composition of fungal biofilm communities at low TMP

4.3.4.2.1 Dominant fungi at low the TMP stage

A total of 22 Orders of fungi were identified in low TMP biofilms for both experiment 1 and 2, while 31 Orders of fungi were identified in experiment-3 (Fig. 4.5). When examined using the Bray-Curtis similarity matrix for the fungal communities, 56.57% similarity was observed for these biofilms in all three experiments. Although the richness of the fungal biofilms were the same in experiments 1 and 2, the fungal communities in experiment-2 were found to have a closer relationship (63.36% similarity) to the communities in experiment-3 (Fig. 4.5). This may not be surprising since experiments 2 and 3 were performed simultaneously.

Five fungal Orders were observed to dominate the biofilm communities at the low TMP stage in all experiments (Fig. 4.5). Among these, the *Glomerales* contributed most to the group similarity, accounting for 14.46%, 38.01% and 16.55% of the fungal communities in experiments 1-3 respectively. The *Mycocaliciales* were the second dominant fungi in these early biofilms, where they had abundances of 48.46%, 7.08% and 17.2% in experiments 1, 2 and 3 respectively. The *Saccharomycetales* accounted for only 0.87% of fungal communities in low TMP biofilms in experiment-1 but had abundances of 22.22% and 22.66% in experiments 2 and 3. The *Diversisporales* and *Archaeosporales* also represented dominant fungi in low TMP biofilms in all experiments. These five fungal groups accounted for 96.28%, 94.04% and 73.85% of the biofilm communities for the three experiments, indicating they were always present in the biofilms during the biofouling process.

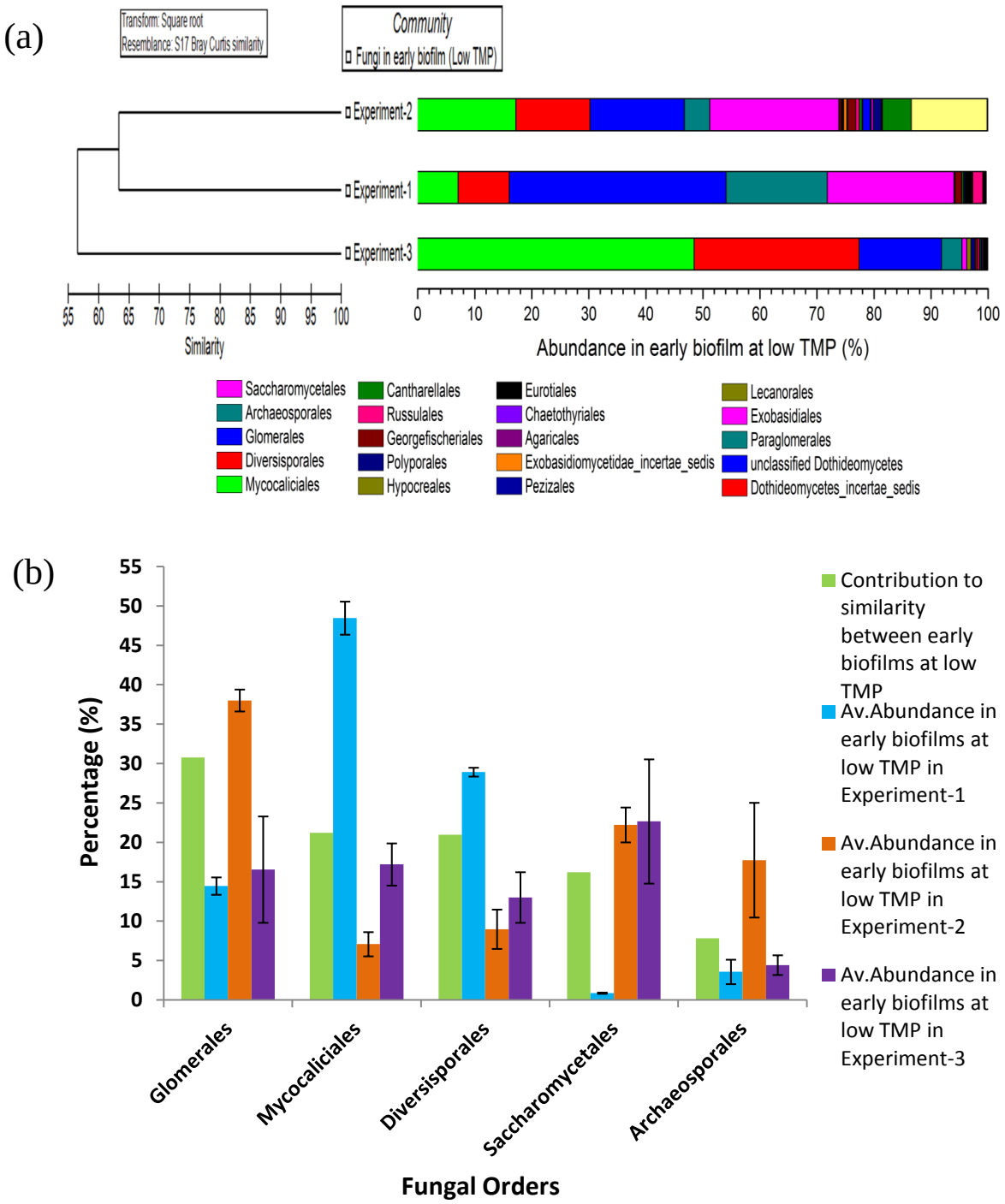

Fig. 4.5 The fungal communities in early biofilms at the low TMP stage in the triplicate experiments. (a) The compositions and relationships of fungal biofilms at the low TMP stage in each experiment. (b) The common dominant fungi in the low TMP biofilms in all three experiments. The data points of abundance are the average values for each fungal Order in different MBRs. The error bars are the standard error of the mean (n=3).

4.3.4.2.2 Comparison of fungal communities between the seed sludge and early biofilms

Compared to the fungal communities in the seed sludge, there was no clear pattern of fungi

establishing themselves into the developing biofilm. For example, the abundance of *Glomerales* was 5.09% in experiment-1 and 22.84% in experiment-2 in the seed sludge and were enriched in the low TMP biofilms 14.46% (experiment 1, $p<0.05$ by T test) and 38.01% (experiment 2, $p<0.05$ by T test). In contrast, the *Glomerales* were present in the biofilm at a lower abundance (16.55%) than in the sludge (58.02%, $p<0.05$ by T test) for experiment 3. This phenomenon was also observed for the *Diversisporales*, where there was no clear increase in its biofilm abundance relative to the sludge composition. Indeed, the data show that the dominant fungi in biofilms at low TMP were also the dominant fungal communities in the seed sludge at low TMP (Fig. 4.4c and Fig. 4.5c). This may suggest that, in contrast to the bacteria (Chapter 3), there was not a specific subset of fungi that was selected for during establishment of the biofilm. Thus, the composition of the fungal sludge community determined the composition of the fungal biofilm community.

4.3.4.3 Composition of fungal communities at high TMP

4.3.4.3.1 Composition of fungal communities in biofilms at the high TMP stage

When the TMP jumped from low to high pressure, a total of 23, 33 and 35 Orders of fungi were identified in the biofilms at high TMP, and there was 55.48% similarity between the fungal communities in all three experiments (Fig. 4.6). However, unlike the communities at low TMP, the fungal communities at high TMP showed a higher similarity between experiments 1 and 2 (71.03% similarity) than with experiment-3, even though the experiments 2 and 3 were performed simultaneously.

Representatives of five fungal Orders were observed to be the dominant fungi in the high TMP biofilms in all three experiments, including *Saccharomycetales*, *Archaeosporales*, *Glomerales*, *Diversisporales* and *Hypocreales*. The *Saccharomycetales* contributed most (34.89%) to the overall similarity in the fungal communities (Fig. 4.6). The *Archaeosporales* were the second major contributor to the group similarity of the high TMP biofilm communities (28.41%). The abundance of *Archaeosporales* was 42.34%, 31.56% and 2.74% in fungal communities in experiments 1, 2 and 3 respectively. The presence of these fungi in all three experiments indicated they may be the dominant biofilm associated fungi at the high TMP stage. Members of the *Hypocreales* were observed to be the dominant fungi (organisms present at > 1% abundance) in the high TMP biofilms in all experiments. However, the distribution of these fungi was not consistent. In experiment-3, they accounted for 58.12% of the fungal biofilm community, while their abundance was just 1.73% and 1.59% in

experiments 1 and 2 respectively.

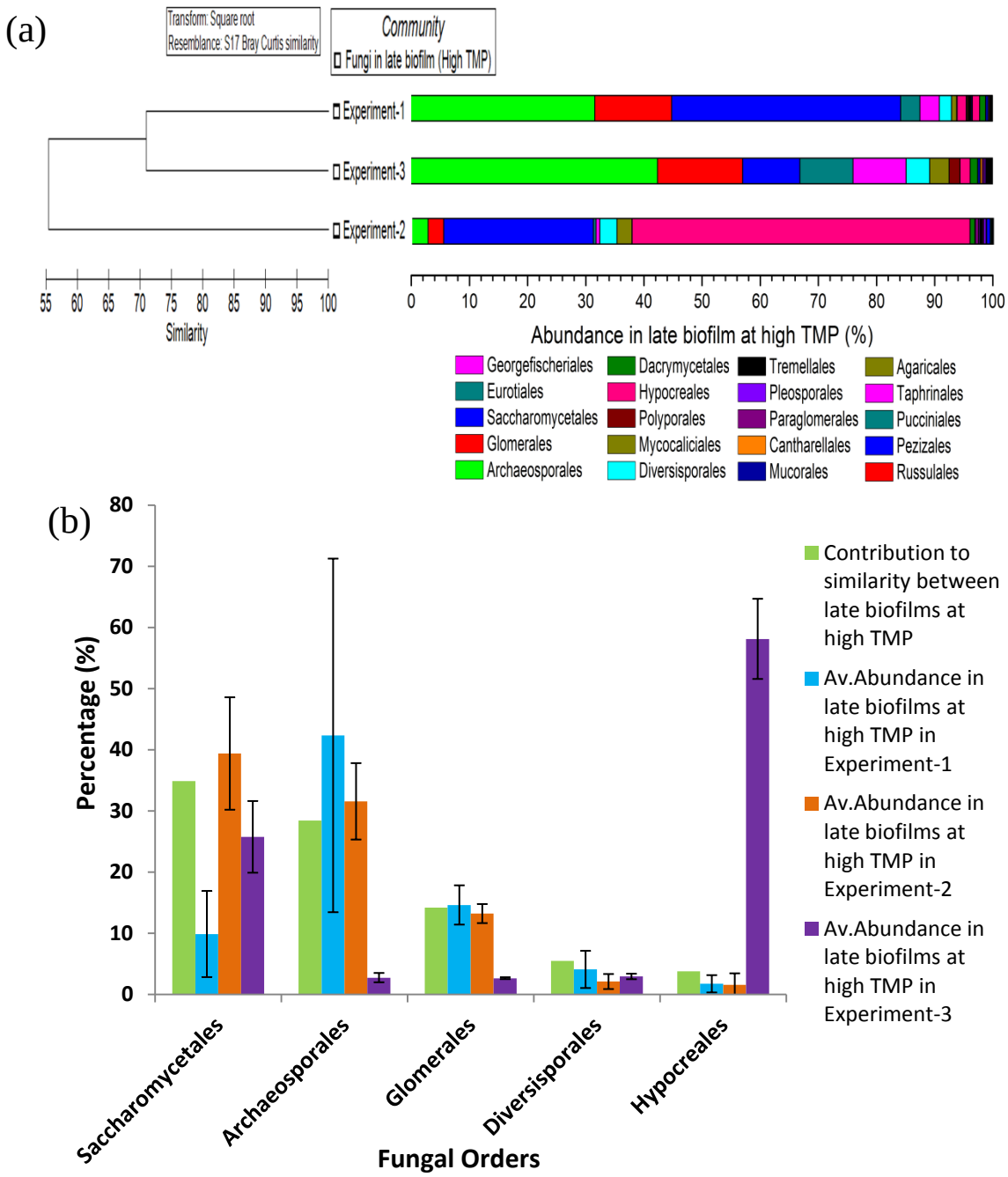

Fig. 4.6 The fungal biofilm communities at high TMP in the triplicate experiments. (a) The fungal biofilm composition and relationships at high TMP in each experiment. (b) The common, dominant fungi in late biofilms in all three experiments. The error bars represent the standard error of the mean (n=3).

4.3.4.3.2 Comparison of fungal sludge and biofilm communities at the high TMP stage

Compared to the high TMP fungal sludge communities (Fig. 4.7), the *Archaeosporales* and *Hypocreales* were present in the biofilms at higher abundances in all three experiments (Fig. 4.8). Specifically, the *Archaeosporales* were observed to account for 4.26% of the fungi in the sludge but had a higher abundance, 42.34%, in biofilms at 60 kPa (experiment-1, $p<0.05$ by T test). In experiments 2 and 3, the *Archaeosporales* were rare organisms in the sludge, with abundances of only 0.34% (experiment-2) and 0.02% (experiment-3). In contrast, they became the dominant biofilm associated fungi, accounting for 31.56% ($p<0.05$ by T test) and 2.74% ($p<0.05$ by T test) of the fungal biofilm communities at high TMP. The *Hypocreales* were the dominant organisms in the sludge at high TMP in experiments 1 and 3, where they accounted for 1.36% and 24.32% of fungi. This group increased in relative abundance in the biofilms to 1.73% and 58.12% ($p<0.05$ by T test) in experiments 1 and 3 respectively. In contrast, the *Hypocreales* were rare fungi in the sludge (0.4%) in experiment-2 but increased dramatically in the biofilm (1.59%, $p<0.05$ by T test) at high TMP. These findings suggest that the *Archaeosporales* and *Hypocreales* may have a competitive advantage or a higher fitness when forming biofilms relative to the other community members.

Additionally, some fungi were observed to have a lower relative abundance in the biofilm compared to the sludge at high TMP. Members of the *Saccharomycetales* had a lower abundance in the biofilm than in the sludge in all three experiments (Fig. 4.9). In sludge, they accounted for 16.54%, 88.96% and 48.5% of fungi at high TMP for experiments 1-3 respectively. While the abundance of *Saccharomycetales* in biofilms was 9.87%, 39.38% and 25.75% for experiments 1-3 respectively. It should be noted that while their overall relative abundances decreased in all three biofilms, the *Saccharomecetales* were one of the most dominant fungi in both the sludge and biofilms.

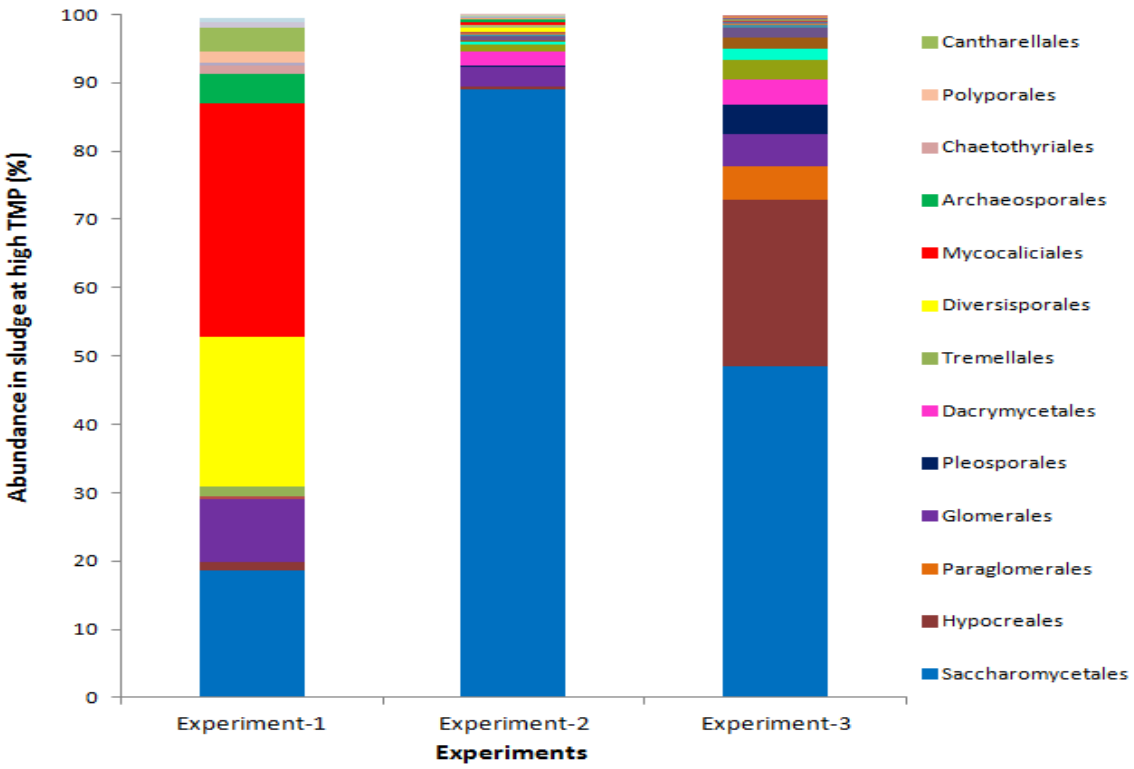

Fig. 4.7 The fungal communities of sludge at high TMP in the three MBRs. The y- axis shows the abundance of specific fungal orders in the sludge at high TMP.

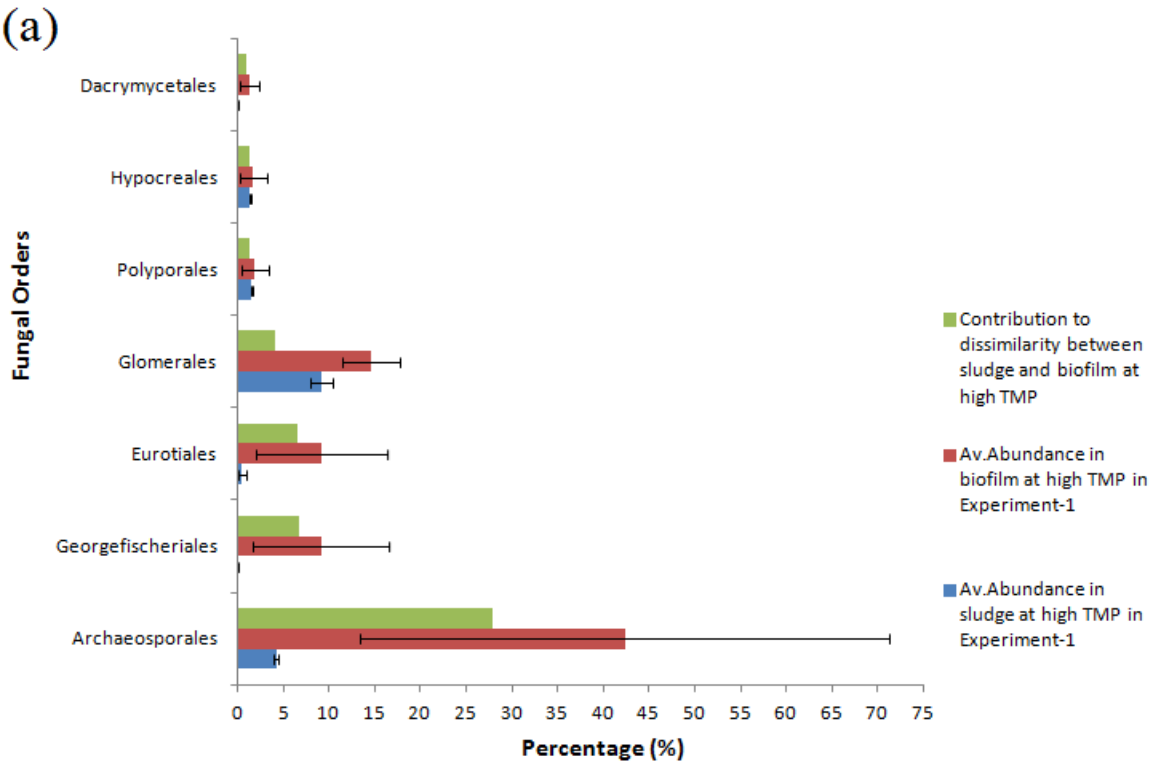

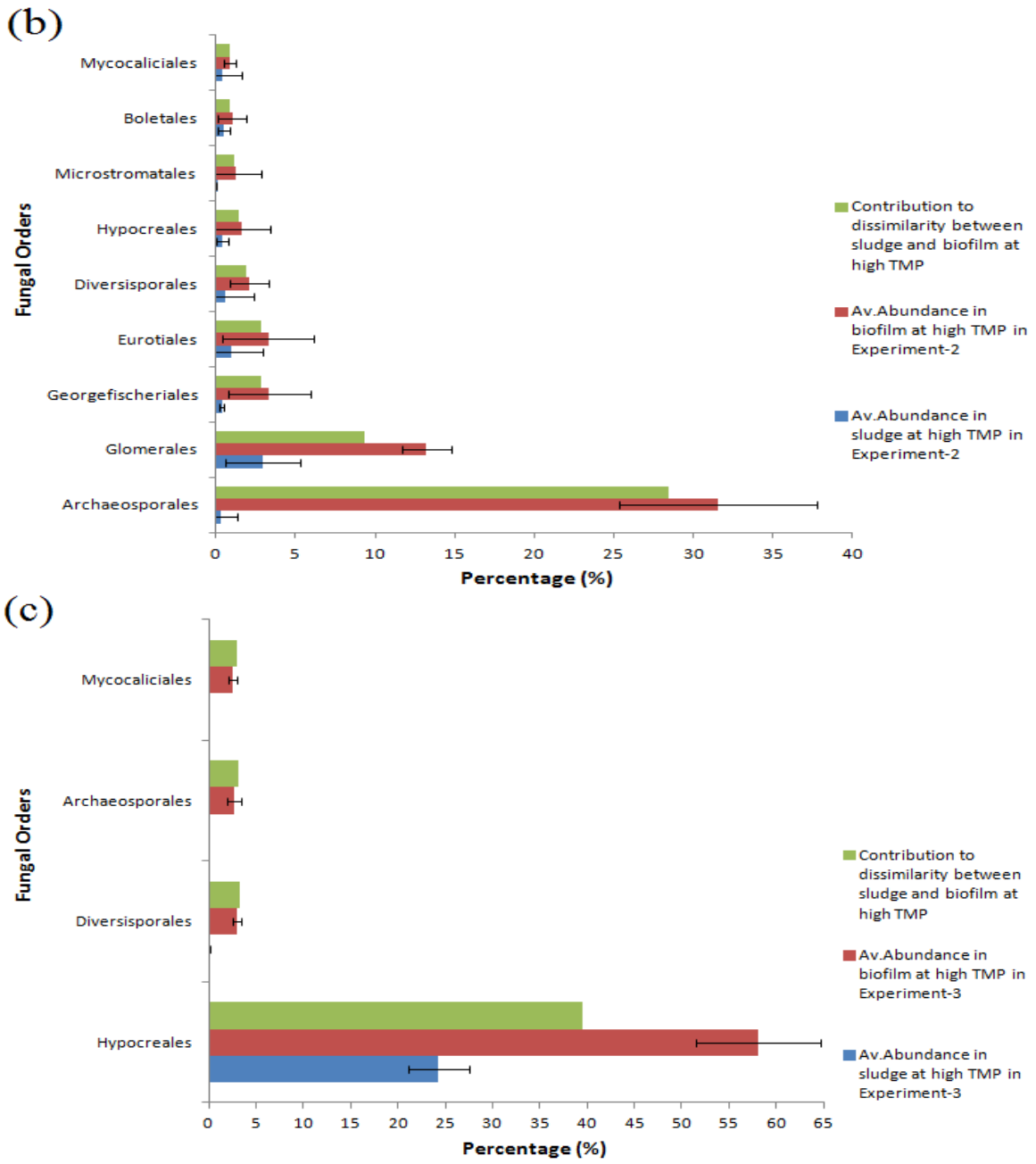

Fig. 4.8 (Continued from previous page) Enrichment of specific fungi in the membrane biofilms at the high TMP stage, (a) experiment-1, (b) experiment-2 and (c) experiment-3. The data points represent the average values of the triplicate samples at low TMP. Error bars are the standard error of the mean (n=3).

(a)

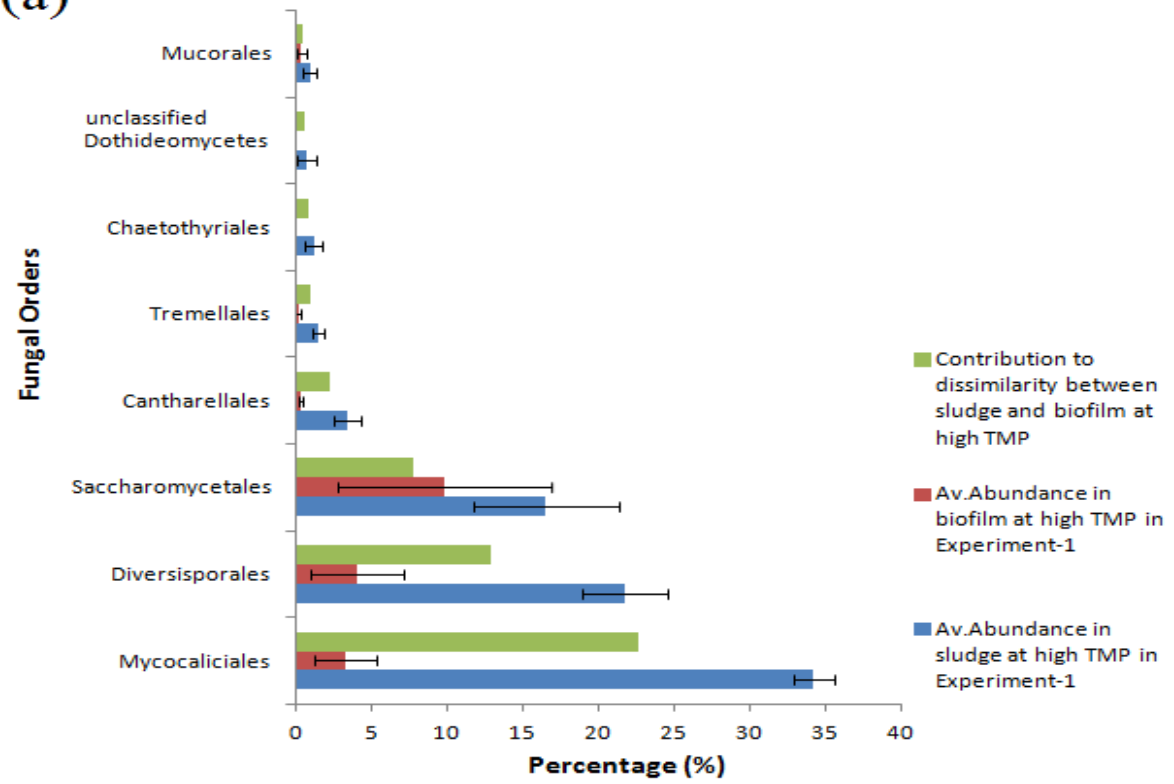
Mucorales
unclassified Dothideomycetes
Chaetothyriales
Tremellales
Cantharellales
Saccharomycetales
Diversisporales
Mycocaliciales
Fungal Orders
0
5
10
15
20
25
30
35
40
Percentage (%)
Contribution to dissimilarity between sludge and biofilm at high TMP
Av.Abundance in biofilm at high TMP in Experiment-1
Av.Abundance in sludge at high TMP in Experiment-1

(b)

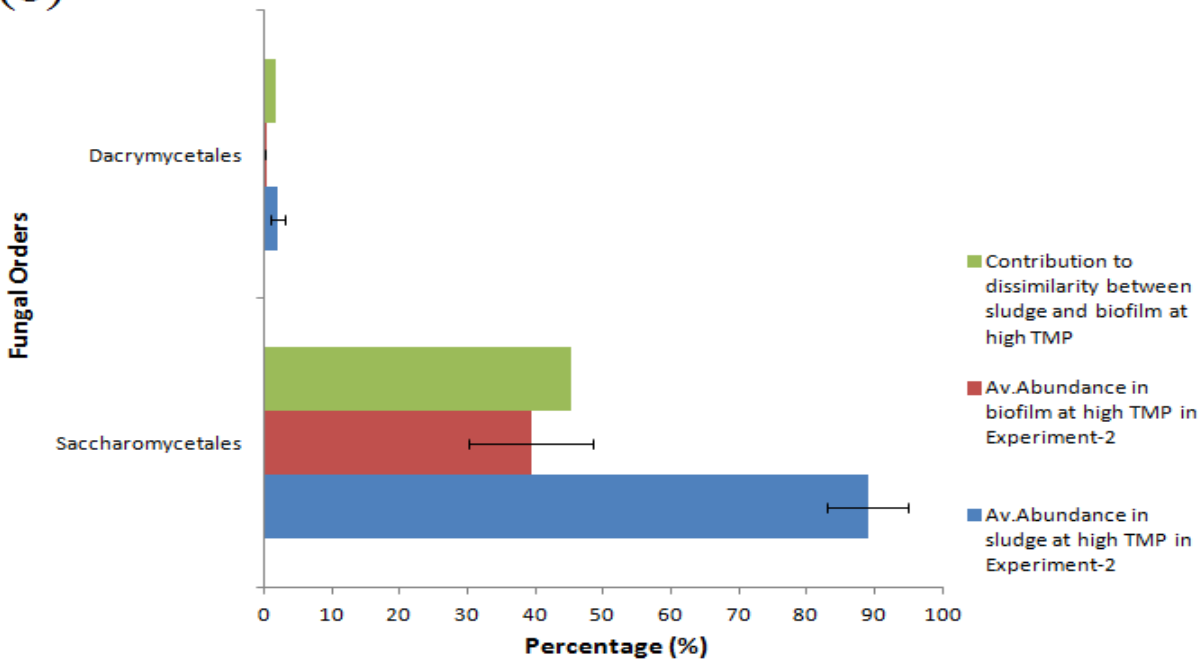
Dacrymycetales
Saccharomycetales
Fungal Orders
0
10
20
30
40
50
60
70
80
90
100
Percentage (%)
Contribution to dissimilarity between sludge and biofilm at high TMP
Av.Abundance in biofilm at high TMP in Experiment-2
Av.Abundance in sludge at high TMP in Experiment-2

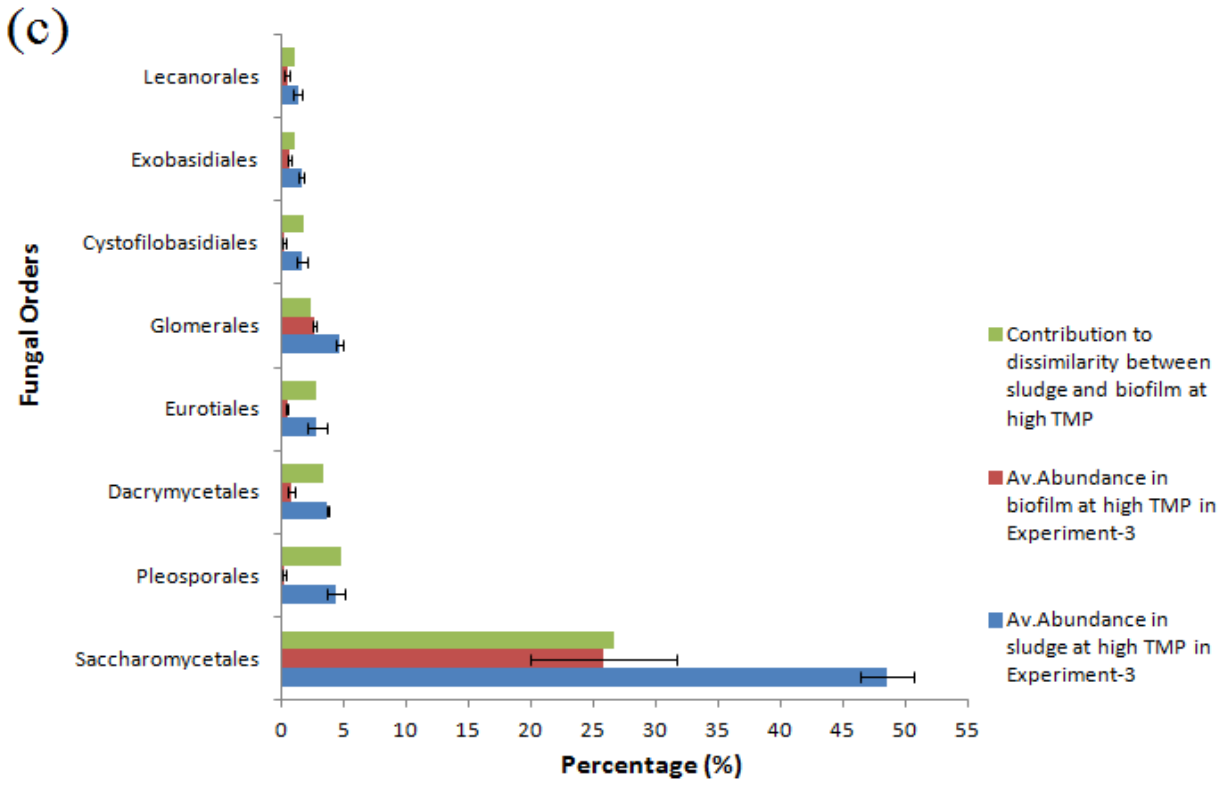

Fig. 4.9 (Continued from previous page) Preferential growth in the sludge relative to the membrane biofilms at high TMP stage in (a) experiment-1, (b) experiment-2, and (c) experiment-3. The data points represent the average values of the triplicate samples at low TMP. The error bars are the standard error of the mean (n=3).

4.3.4.4 Succession within fungal biofilms communities as the TMP increases

4.3.4.4.1 Some fungi increased in abundance in biofilms as the TMP increased

The Orders of *Saccharomycetales* and *Hypocreales* were observed to be enriched in the biofilms as the TMP increased in all experiments (Fig. 4.10). For example, in experiment-1, the *Saccharomycetales* accounted for only 0.87% of the fugal biofilm communities at low TMP (7 kPa), while their abundance increased to 9.87% in the high TMP biofilms (60 kPa, $p<0.05$ by T test). They also increased in abundance from 22.22% at 5 kPa to 39.38% ($p<0.05$ by T test) at 55 kPa in experiment-2 and from 22.66% at 6 kPa to 25.75% ($p<0.05$ by T test) at 80 kPa in experiment-3. Similarly, the *Hypocreales* were rare fungi in the early biofilms at low TMP, which accounted for only 0.74%, 0.06% and 0.03% of the community in experiments 1-3 respectively. Nevertheless, their abundance increased to 1.73% ($p<0.05$ by T test) and 1.59% ($p<0.05$ by T test) in experiments 1 and 2 and even jumped to 58.12%

(p<0.05 by T test) in biofilms in experiment-3, when the TMP increased to a high level. Another fungal Order, *Archaeosporales*, were also observed to increase in biofilm abundance in experiments 1 and 2, where they changed from 3.57% and 17.75% at low TMP to 42.34% (p<0.05 by T test) and 31.56% (p<0.05 by T test) at high TMP (Fig. 4.10a, b).

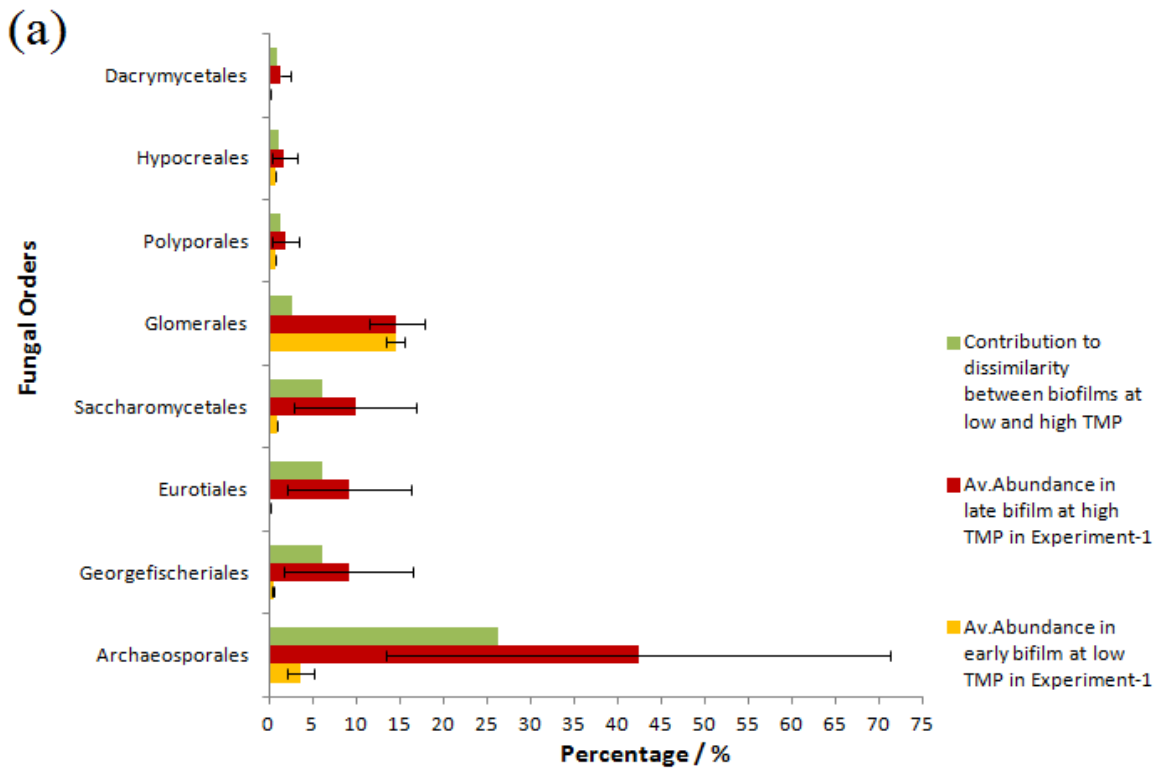

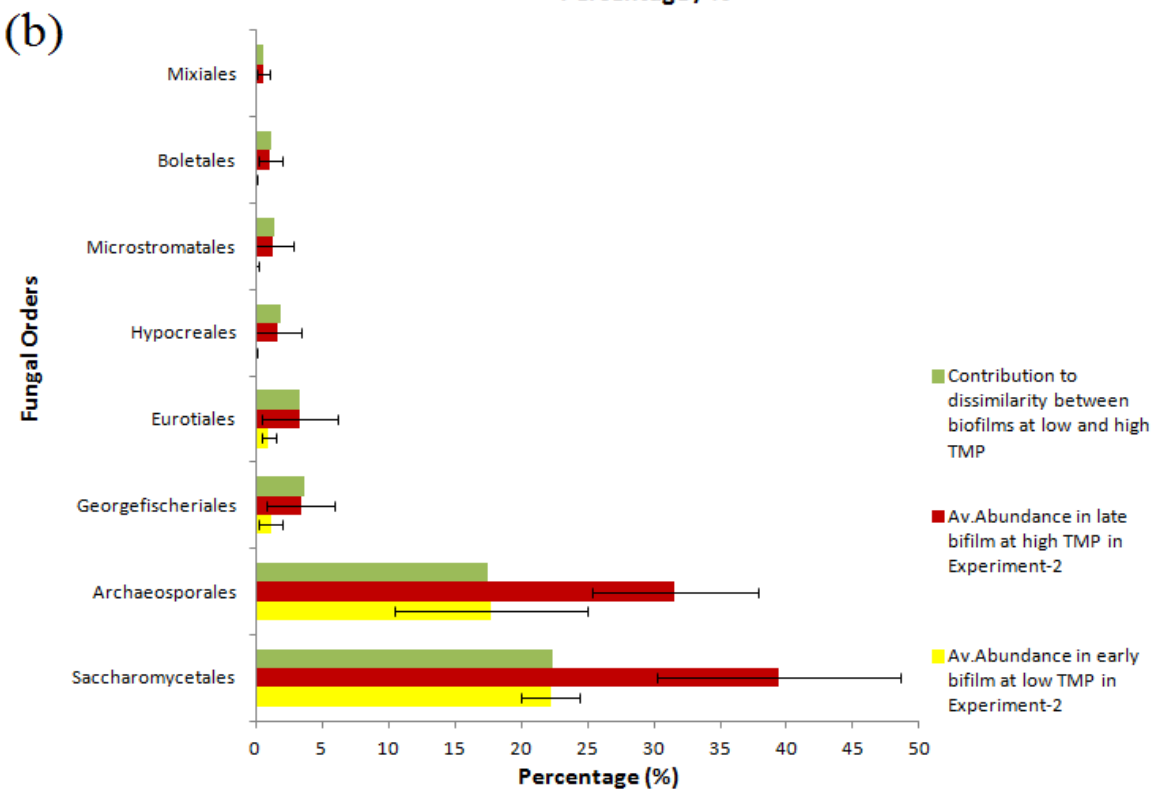

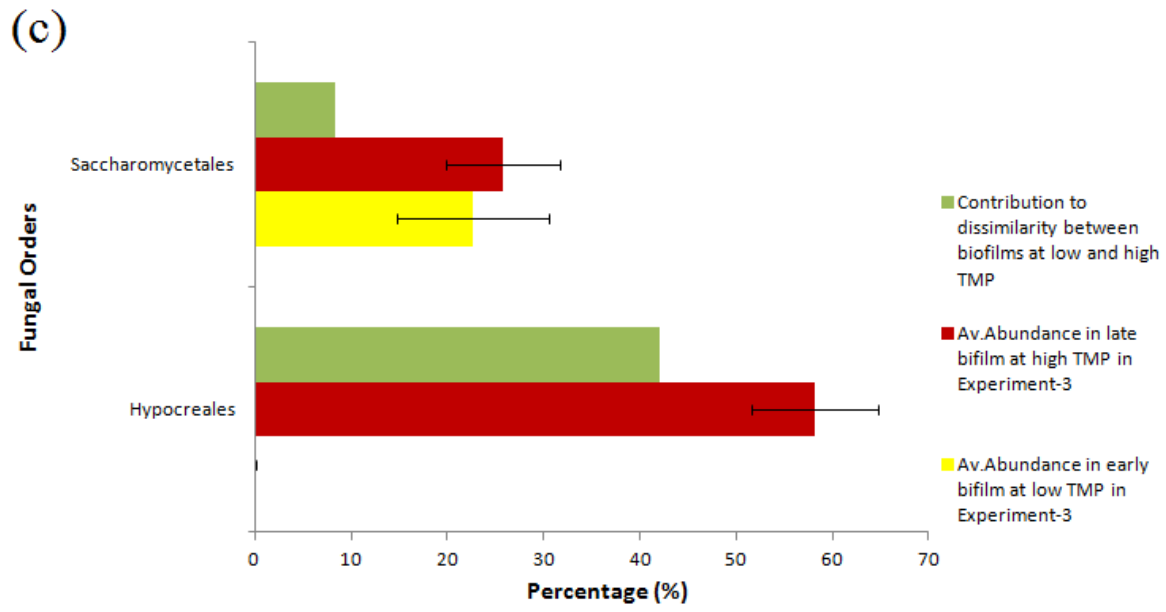

Fig. 4.10 (Continued from previous page) Increased abundance of specific fungi in the high TMP biofilms, (a) experiment-1, (b) experiment-2, (c) experiment-3. The data points represent the average values of the triplicate samples at low or high TMP. The error bars are the standard error of the mean (n=3).

4.3.4.4.2 Some fungi decreased in abundance in biofilms at high TMP

Members of the *Mycocaliciales* and *Diversisporales* were observed to decrease in biofilm abundance as the TMP increased (Fig. 4.11). The *Mycocaliciales* were the primary fungi present in the low TMP biofilms (5 - 10 kPa), with abundances of 48.46%, 7.08% and 17.2% for experiments 1, 2 and 3 respectively. However, their abundance decreased to 3.33%, 2.87% and 2.59% in experiments 1 - 3 respectively (all $p<0.05$ by T test), when the TMP jumped to the high pressure stage (50 - 80 kPa). Similar changes were also observed for the *Diversisporales*, which had higher abundance (28.92%, 8.98% and 13.01% for experiments 1 - 3 respectively) in biofims at low TMP but a lower abundance (4.08%, 2.1% and 2.93% experiments 1 - 3 respectively, all $p<0.05$ by T test) in high TMP biofilms.

The biofilm abundance of *Glomerales* was also observed to decrease at the high TMP stage for experiments 2 and 3, where they accounted for 38.01% and 16.55% in at low TMP but decreased to 13.21% and 2.65% at high TMP (both $p<0.05$ by T test). However, no decrease was observed in the abundance of *Glomerales* in biofilms in experiment-1, where the *Glomerales* accounted for 14.46% in early biofilm and 14.62% in the late biofilm. Combining

the 3 experiments, one conclusion was that the *Glomerales* were dominant fungi in biofilms at both low and high TMP but may play a more important role in the formation of early biofilms.

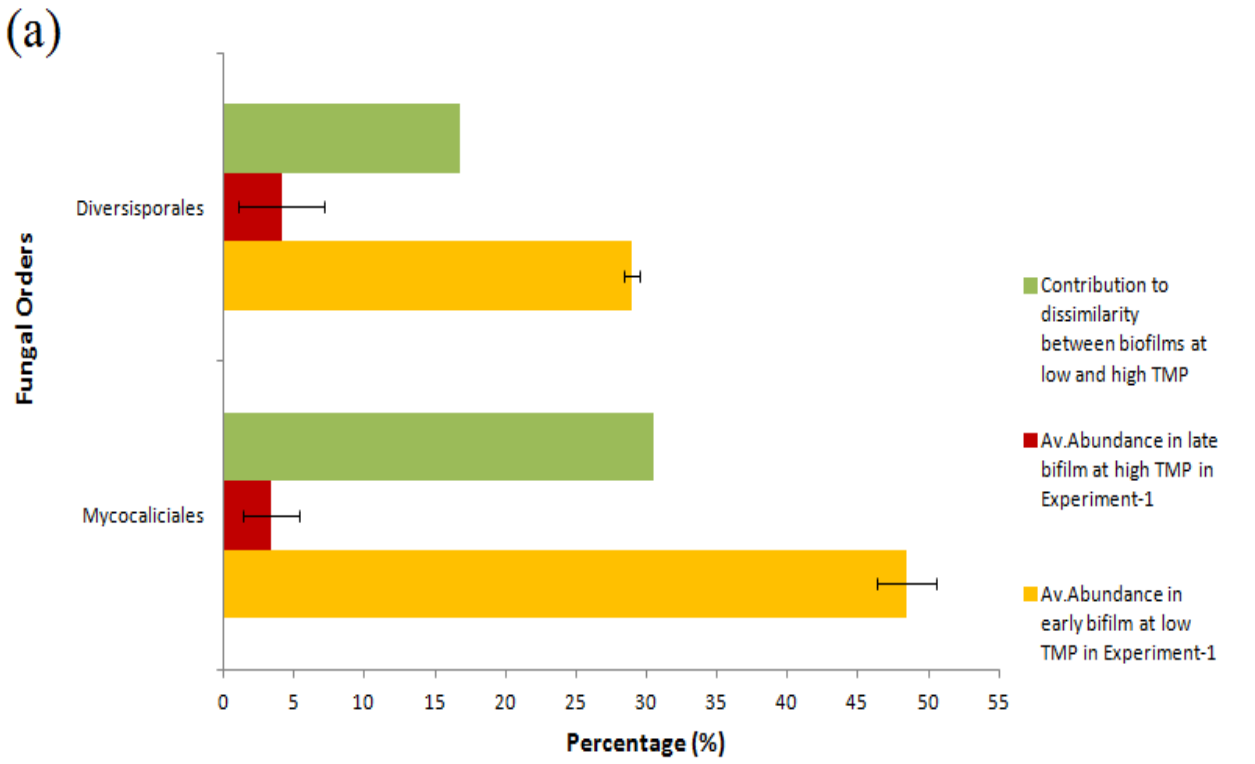

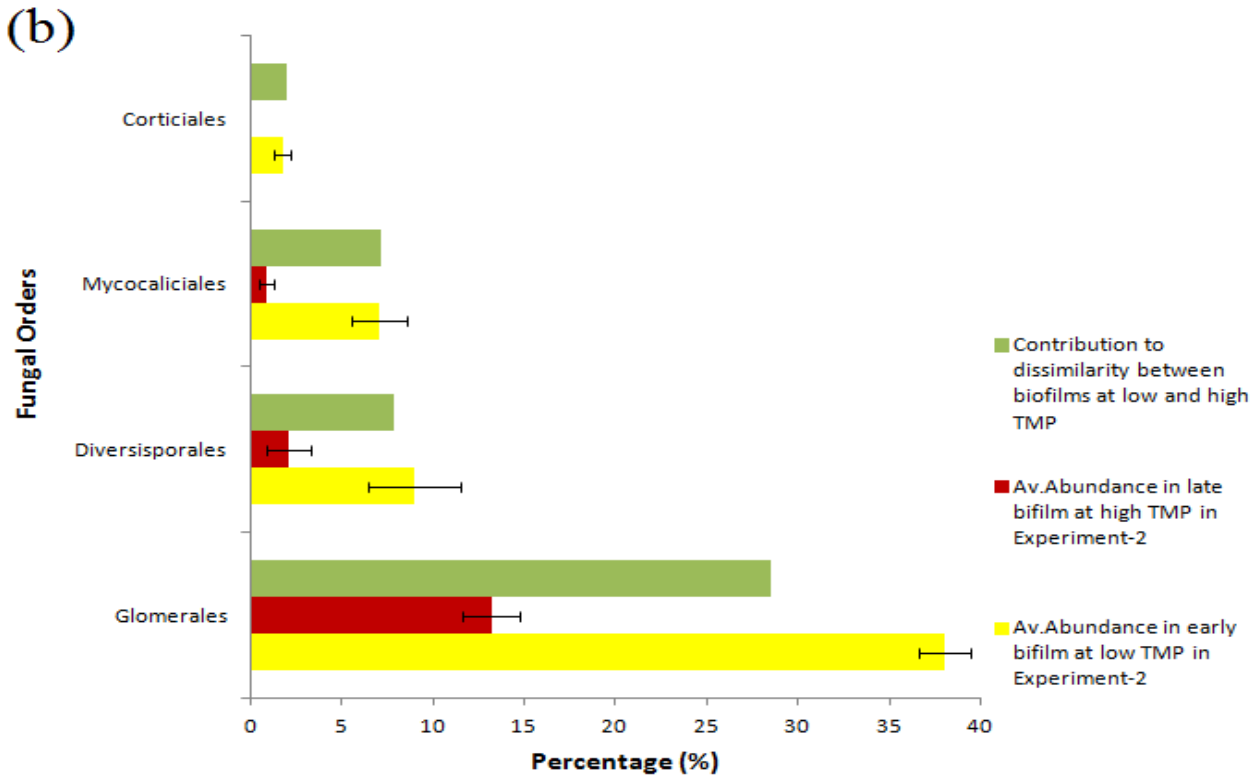

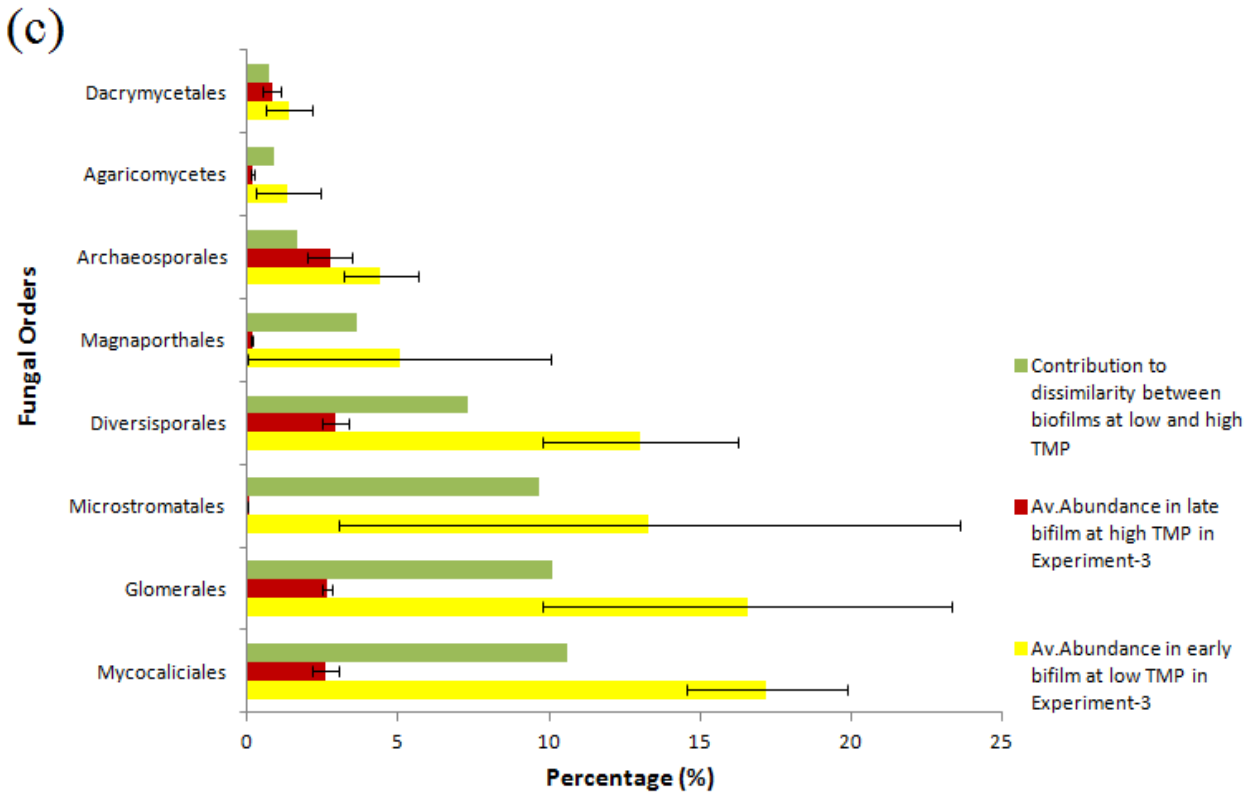

Fig. 4.11 (Continued from previous page) Decreased abundance of specific bacteria in the high TMP biofilms in (a) experiment-1, (b) experiment-2, (c) experiment-3. The data points represent the average values of the triplicate samples at low or high TMP. The error bars are the standard error of the mean (n=3).

4.3.4.4.3 Common dominant fungi in biofilms at low and high TMP

Although variations in the abundance, increase or decrease, were observed in the fungal communities in biofilms, some fungi were always the dominant organisms in biofilms at both low TMP and high TMP in MBRs. These fungi included *Mycocaliciales*, *Diversisporales*, *Glomerales*, *Archaeosporales* and *Saccharomycetales*, indicating they were fundamental components of biofilms on membrane across the whole process of the biofouling phenomenon.

4.4 Discussion

Fungi represent a ubiquitous microbial group in the activated sludge in MBRs. A broad spectrum of fungi have been reported to form biofilms, including *Candida* spp.,

Saccharomyces spp., *Cryptococcus* spp. and *Aspergillus* spp. (Bojsen et al., 2012; Chandrasekar and Manavathu, 2008; López-Ribot, 2005; Ravi et al., 2009) as well as other fungi, such as Basidiomycota, Ascomycota and Chytridiomycota (Lan et al., 2010). However, few studies have been published to date on the role of the fungal community in the biofouling process. Therefore, to better define their role in this process, the fungal communities in sludge and on hollow fiber membranes were investigated here. At low TMP (3 - 7 kPa), approximately 30% dissimilarity in the fungal community was observed between the biofilms and sludge while a higher dissimilarity (35% - 50% dissimilarity) was observed for biofilms and sludge when the TMP increased (50 - 80 kPa). This indicated that a subset of fungi present in the sludge was associated with biofilm formation at low TMP and as the TMP increased, the biofilm and sludge communities diverged. Such distinctions in the sludge and biofilm communities has been previously shown (Piasecka et al., 2012), indicating that this process may be commonplace during biofilm formation in MBR systems.

Specifically, at low TMP, the fungal biofilm community was dominated by *Glomerales*, *Mycocaliciales*, *Diversisporales*, *Saccharomycetales* and *Archaeosporales*, comprising 96.28%, 94.04% and 73.85% of the fungi in all three experiments. The *Glomerales*, *Diversisporales* and *Archaeosporales* belong to the Phylum of Glomeromycota while the *Mycocaliciales* and *Saccharomycetales* belong to the phylum of Ascomycota. Interestingly, the Ascomycota as well as the Basidiomycota have also been reported to represent significant components of biofilms found in acid mine drainage communities (Baker et al., 2009).

At low TMP, the same fungal groups dominated both the sludge and biofilm communities. This contrasted with the bacterial community, where the biofilms at the low TMP stage were comprised of organisms that were not strongly represented in the sludge community. When the TMP increased, the fungal biofilm community was dominated by *Saccharomycetales*, *Archaeosporales*, *Glomerales*, *Diversisporales* and *Hypocreales*. This was consistent with the biofilm composition at low TMP, indicating the *Ascomycota* and *Glomeromycota* were always the predominant fungi in biofilms. Compared to the sludge fungal community at high TMP, the *Archaeosporales* and *Hypocreales* were found to have a higher abundance in the biofilms, while the *Saccharomycetales* had a lower abundance in the biofilm than in the sludge. This indicated that selection of specific fungi from sludge to form the biofilm occurred mainly at the later phase of the biofouling process. It has been reported that the fungi under the Order *Saccharomycetales*, such as *Saccharomyces* sp. *Pichia* sp. and *Candida* sp., can form biofilms in groundwater treatment facilities (Gillings et al., 2006). Based on the findings presented

here, the *Saccharomycetales* decreased the abundance in biofilm at high TMP, even though they were the dominant fungi in both sludge and membrane biofilms in MBR, indicating that the *Saccharomycetales* may be less competitive during biofilm formation on membranes relative to the *Archaeosporales* and *Hypocreales*.

Based on the NMDS analysis, the fungal communities at high TMP were distinct from the fungal group at low TMP. Furthermore, the fungal biofilm communities observed at the threshold TMP (15 - 20 kPa) and high TMP stages were more similar to each other (68 - 70% similarity) than they were to the community at low TMP (5 - 7 kPa, 55 - 60% similarity). This may indicate that the major changes in the fungal community occur before the TMP jump stage. This was similar to the changes observed for the bacterial biofilm community in Chapter 3, where the bacterial biofilm community at the threshold TMP were more similar to community at high TMP (50 - 90 kPa) than to the community at low TMP (5 - 7 kPa). Collectively, the change of microbial community members in biofilms, including bacteria and fungi, occurred prior to the point where the TMP exceeded the jump threshold, suggesting that the succession of microbial community may be important for the biofouling behavior.

Specifically, compared to the biofilms at low TMP, Orders of *Saccharomycetales* and *Hypocreales* were observed to be enriched in the biofilms as the TMP increased, while Orders of *Mycocaliciales* and *Diversisporales* were found to decrease in their abundance in biofilms as the TMP increased, indicating the *Saccharomycetales* and *Hypocreales* may contribute more to the construction of late biofilms while the *Mycocaliciales* may contribute mainly to the building of early biofilms in MBR. Of note were the *Saccharomycetales*, which have been reported to be an ubiquitous biofilm associated fungal group (Ramage et al., 2009). In this study, the *Saccharomycetales* were dominant organisms in both sludge and biofilm at low and high TMP, although the abundance in biofilm was lower than in sludge at high TMP. Moreover, the *Saccharomycetales* were enriched in the biofilm as the TMP increased, leading to the *Saccharomycetales* became the most prevalent fungi in biofilm at high TMP. These findings suggested that the *Saccharomycetales* may be the most important fungi related to the biofouling phenomenon.

Although changes in the fungal biofilm community were observed as the TMP increased, some fungi were always the dominant component of the biofilm at both low TMP and high TMP. These fungi included *Mycocaliciales*, *Diversisporales*, *Glomerales*, *Archaeosporales* and *Saccharomycetales*. This was consistent with what was observed for the bacterial biofilm communities, where the *Sphingobacteriales*, *Burkholderiales*, *Actinomycetales* and

Rhizobiales were always prevalent in the biofilm. These findings indicated that some microbial groups, such as the *Saccharomycetales* and *Archaeosporales* and the *Sphingobacteriales* and *Burkholderiales* were common biofouling associated organisms.

Taken together, the TMP increase in the MBR was related to the formation of stable fungal community on membrane. Some fungal groups, such as *Archaeosporales* and *Glomerales*, were consistently present on the membrane and had higher proportions in the biofilm than in the free living sludge. Some specific fungal groups, such as *Saccharomycetales* and *Hypocreales*, increased in abundance in biofilm as the TMP increased. Therefore, if these are key organisms in the biofouling process, it may be possible to target on these fungi to prevent or delay membrane fouling. These results therefore suggest that it will valuable to better understand how these fungal groups contribute to biofouling and to rationally develop approaches that can be used to prevent the formation of fungal biofilms or to disperse mature fungal biofilms.

Chapter 5 Use of Nitric Oxide to Control Biofilm Formation in MBR

5.1 Introduction

Biofouling and its consequences of reduced performance and increased treatment costs limits the general adoption of MBRs as the preferred waste-water treatment option. Therefore, strategies must be explored to control biofouling in MBRs. A number of strategies have been trialed to reduce biofouling in MBRs, including modification of the membrane surface properties to reduce their fouling tendency (Nady et al., 2011). For example, modification of the polypropylene membrane surface by ozone treatment and graft polymerization with 2-hydroxy-ethyl methacrylate reduced membrane fouling and increased membrane permeability (Sainbayar, 2001). It has also been reported that antimicrobial properties were imparted to the membrane when the polyurethane membrane surface was modified by grafting of a *N*-halamine precursor and subsequent chlorine bleaching (Tan and Obendorf, 2007). Optimization of engineering operations has also been used to reduce biofouling in MBRs, such as splitting air bubbles into fine bubbles for aeration and larger coarse bubbles for fouling control (Phattaranawik, 2007), using intermittent permeation (Itoh.K;, 1995) and setting a critical flux (Field et al., 1995).

Chemical agents can kill microbes and remove biofouling materials from the membranes but overuse of chemicals can damage the polymeric membrane structure and can also lead to the environmental damage since such chemicals are typically toxic. Therefore, it is imperative to explore environmentally friendly biological methods to control biofouling. Nitric oxide (NO) is an intracellular signaling molecule that has recently been shown to disperse the biofilm (Barraud et al., 2006). The NO donor, PROLI NONOate, has been reported to disperse *Pseudomonas aeruginosa* PAO1 biofilms in the concentration range of 40 - 80 μM (Barnes et al., 2013). Therefore, this project aimed to investigate the application of NO as a means to control membrane biofouling in an MBR system. The NO donor compound, PROLI NONOate, was applied to the membrane module at different biofouling stages (low TMP stage and high TMP stage) to investigate the effect of PROLI NONOate on the reduction of TMP and fouling resistance on membrane.

5.2 Materials and Methods

5.2.1 Experimental MBR setup

A laboratory scale submerged MBR was operated to treat the artificial synthetic wastewater (TOC of 200 mg/mL) as described in Chapter 3. The MBR system was composed of an anoxic sludge tank and an aerobic sludge tank containing two separate membrane modules (Fig. 5.1a). The membrane modules were made with hollow fiber (HF) PVDF membranes (ZeeWeed 500, kindly provided by GE Singapore) and were assembled as a "curtain" style module. For the membrane pieces, one end was sealed and hung down into the sludge tank, which was the free end. The other ends of the hollow fiber membranes were open and sealed into a chamber that was linked to the suction pump (Fig. 5.1b).

Before the experiment, fresh activated sludge was collected from the Ulu Pandan wastewater treatment plant in Singapore and acclimated in artificial synthetic wastewater for 60 d before the start of the experiment. While running, the synthetic wastewater from the feedwater tank passed through the anoxic tank and aerobic tank and was utilized by the sludge biomass in the two tanks. The wastewater was then recycled from the aerobic tank to the anoxic tank to be further degraded. The purified water was subsequently separated from the sludge by the membrane module. The two modules were run with a constant flux, which was 15 Liters /m^2 h (LMH). The hydraulic retention time and sludge retention time for each MBR were maintained at approximately 10 h and 25 d respectively for the MBR. The MBR was run at a room temperature of 25 - 28 ^{o}C. The TMP was monitored automatically using a digital pressure gauge (Ashcroft). The TOC of the influent and permeate was measured using a multi N/C® 2100s (AnalytikJena) to monitor the MBR performance.

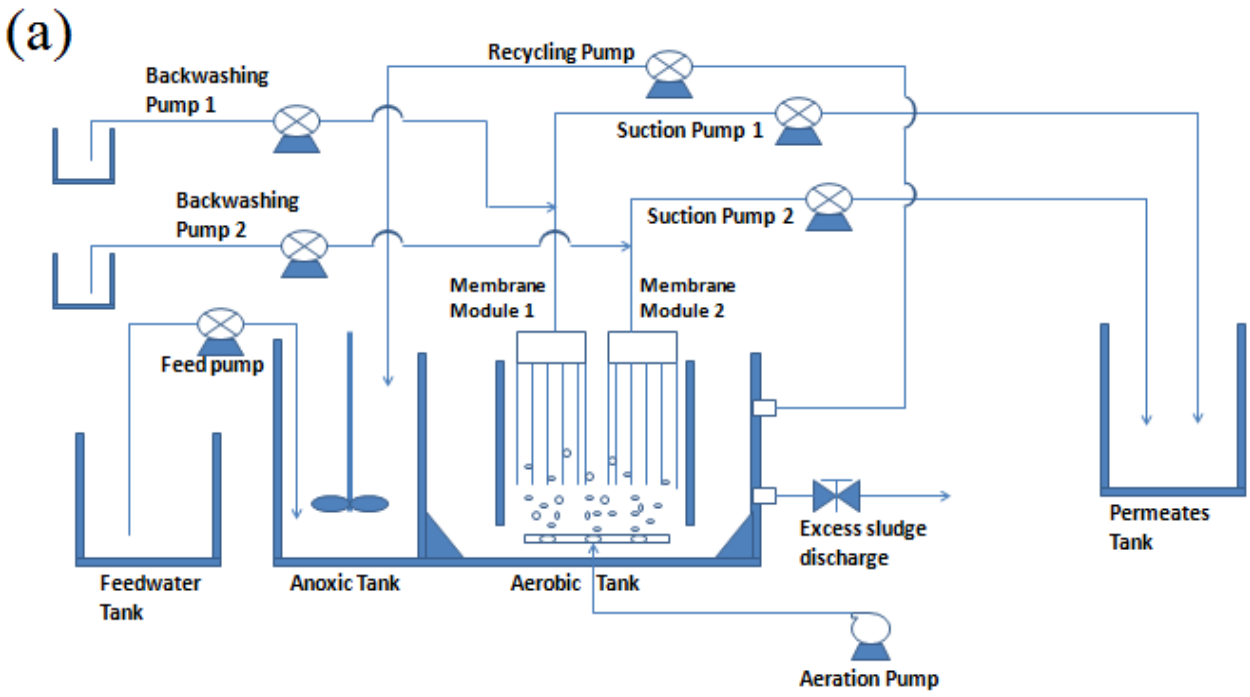

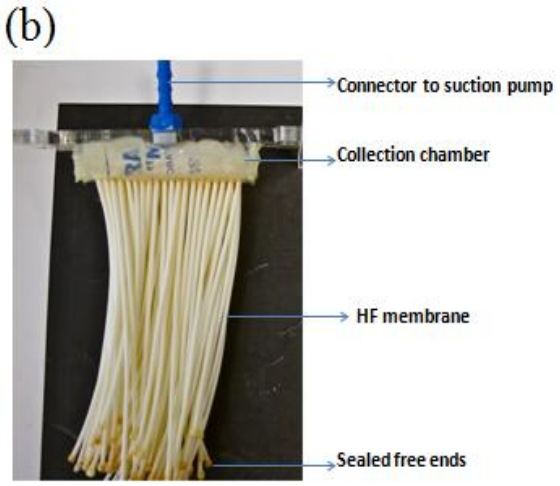

Fig. 5.1 The MBR system used in this project. (a) The schematic view of the internal submerged MBR. Two separated membrane modules were installed in the aerobic sludge tank. (b) The configuration of the "curtain" style HF membrane module.

5.2.2 PROLI dosing experiment

The effect of NO on membrane biofouling was tested using two approaches, the addition of the NO donor to the MBR system on a daily basis from the beginning of the experiment and the addition of the donor to the MBR after it had reached the maximum TMP.

For the continuous addition of the NO donor, the PROLI treatment was started from the beginning of the MBR operation. The treatment was performed on the membrane modules daily. The PROLI powder was dissolved into the diluted synthetic feed water (TOC of 10 mg/L), and adjusted to pH 8.5 - 9.0 to make the working solution. The PROLI treated module

and control module were taken out from the sludge tank and treated in two separate beakers. For the PROLI treated membrane module, the membrane was immersed in 80 μM PROLI in diluted synthetic feed water (pH 8.5 - 9.0) for 1 h. Dosing concentrations were based on previously published work (Barnes et al., 2013). For the control module, the membrane was immersed into the (TOC of 10 mg/L, adjusted pH 8.5 - 9.0) for 1 h. After treatment, the modules were returned to the MBR and operation was continued. The TMP and flux (Jw) were measured in pure water at room temperature before and after treatment. The fouling resistance was calculated using the TMP and flux in pure water based on the formula $R_f = (\Delta P - \Delta\pi)/\mu\ Jw - R_m$ (Vesilind et al., 1994). In the formula, the pressure differential (ΔP) and Jw are the measured TMP and flux. The osmotic pressure differential (Δπ) was 0 for the pure water here and μ is the viscosity of water at 25 - 28 ^{o}C. R_m is the resistance for the virginal membrane module.

To test the ability of the NO donor to remove an established fouling layer, the MBR system was operated until both membrane modules had reached the maximum TMP (85 - 90 kPa) after which time the donor was added. It should be noted that these experiments were separate from those described above where the NO donor was added daily, to avoid any confounding issues such as selection for NO insensitive communities. The membrane modules were taken out from the aerobic sludge tank and immersed into different beakers, which were filled with 500 mL diluted synthetic feed water (TOC of 10 mg/L, pH 7). For the PROLI treated membrane module, one backwashing pump was used to deliver 80 μM PROLI stock solution, dissolved in a 10 mM NaOH solution to prevent the spontaneous release of NO. The flow rate for the PROLI backwashing pump was 4 mL/min. Another backwashing pump, referred to here as the neutralizing pump, was used to deliver a 2.5 mM HCl solution at a flow rate of 16 mL/min. The two solutions were mixed before they entered the membrane module to neutralize the NaOH and to hence ensure there was no effect on the pH of the MBR. These flow rates and concentrations were verified to result in a neutral pH (data not shown), which allows for NO release from the PROLI NO donor. The untreated control module was treated in the same way, except that the 10 mM NaOH solution lacked the NO donor. The total flux for the backwashing was 30 $L.m^{-2}.h^{-1}$ for both the PROLI treated and control modules, which was twice the suction flux during the MBR operation.

5.2.3 Fluorescent staining and CLSM observation

Membrane pieces were collected to analyze microbial biomass by CLSM at different points along the transmembrane pressure (TMP) curve. The staining procedure, CLSM observation

and image process by IMARIS were the same as the protocols in section2.2.2-2.2.4 of Chapter 2. The significance in difference of biofouling components was examined by the T test.

5.2.4 DNA extraction

Total DNA from the biofouling community growing on the HF membranes as well as from the activated sludge was separately extracted by a modified CTAB-PEG protocol (Griffiths et al., 2000; Paithankar and Prasad, 1991), which was the same as described in section 3.2.2 of Chapter 3.

5.2.5 Pyrosequencing

The DNA was sequenced using the "454" pyrosequencing platform (Research and Testing Laboratory, Texas, US) (Handl et al., 2011) and two microbial communities, bacteria and fungi, were targeted. The primers selected for the bacterial PCR were Gray28F (5'-GAG TTT GAT CNT GGC TCAG-3') and Gray519R (5'-GTN TTA CNG CGG CKG CTG-3') (Baker et al., 2003). The primers selected for the fungal PCR were forward funSSUF (5'-TGGAGGGCAAGTCTGGTG-3') and reverse funSSUR (5'-TCGGCATAGTTTATGGTTAAG-3') (Foster et al., 2013). The number of reads for every sample was approximately 3,000.

5.2.6 Sequence process with MOTHUR

The pyrosequencing data was processed using MOTHUR (http://www.mothur.org/wiki/Main_Page) based on the Costello analysis pipeline (Costello et al., 2009; Schloss et al., 2009), which was the same as described in section3.2.4 of Chapter 3 and section 4.2.4 of Chapter 4.

5.2.7 Phylotype-based analysis with PRIMER 6

The community analysis based phylotype difference was processed by PRIMER 6 as described in section 3.2.6 in Chapter 3.

5.3 Results

5.3.1 The NO mediated biofilm control in an MBR system

5.3.1.1 The effect of PROLI on an established Biofilm Community at the High TMP stage

The MBR systems operated under a constant flux of 15 $L.m^{-2}.h^{-1}$ reached the maximum TMP (85 - 90 kPa) after 116 days and the fouling resistance (R_f) was 3.5×10^{10} m^{-1} for MBR-1 and 3.3×10^{10} m^{-1} for MBR-2 (Fig. 5.2a). Therefore, to determine if NO treatment could disperse the established fouling community, backwashing with the NO donor PROLI was initiated. In the first two days, H_2O was used for backwashing in both MBRs and the fouling resistance was 2.5×10^{10} m^{-1} for MBR-1 and 1.7×10^{10} m^{-1} for MBR-2 (Fig. 5.2a). MBR-1, which had a slightly higher fouling resistance, was selected for PROLI treatment and MBR-2 was used as the control MBR.

For the first 7 d of treatment, the fouling resistance was observed to increase for both the PROLI and control MBRs. At 126 d, representing 7 d of treatment, the fouling resistance for the PROLI treated MBR increased to 4.2×10^{10} m^{-1} while the fouling resistance for the control MBR increased to 4.1×10^{10} m^{-1} (Fig. 5.2). The Rf had increased 1.68 fold and 2.41 fold for the PROLI treated and the control MBRs respectively. This indicated that the increasing rate of R_f for the control MBR was higher than observed for the PROLI treated MBR. After the 9 d of treatment, the R_f for the control MBR was higher than the Rf for the PROLI treated MBR. After 37 d of treatment, the Rf after backwashing for the PROLI treated MBR only increased to 4.4×10^{10} m^{-1} while the Rf after backwashing for the control MBR increased up to 5.5×10^{10} m^{-1} (Fig. 5.2). Over the 37 d of treatment, the Rf for the PROLI treated MBR increased 1.49 fold in comparison to a 2.11 fold increase for the control MBR and the PROL was observed to reduce the Rf by 50%. This phenomenon indicated that back flushing PROLI into the membrane module could reduce the Rf and thus reduce the membrane fouling.

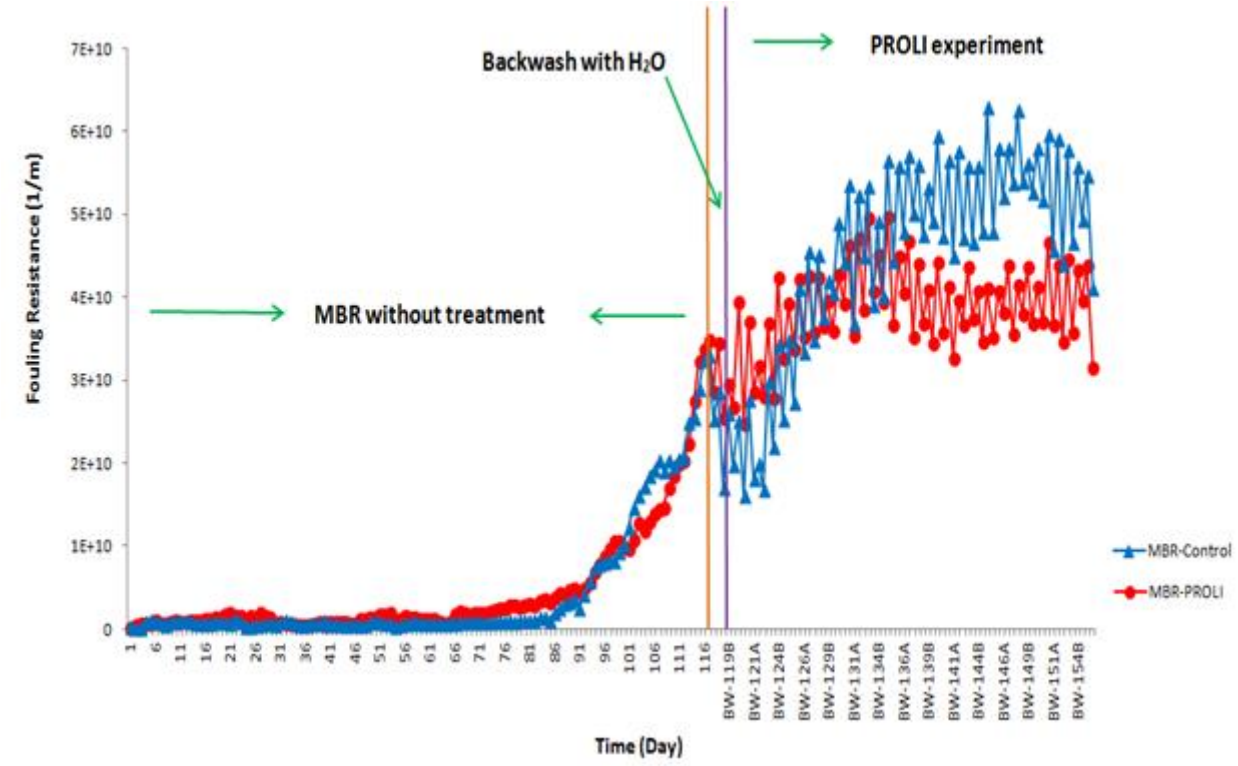

Fig. 5.2 The variation of membrane fouling resistance in the PROLI treated and control MBRs. The orange vertical line separates the experiment into two phases, where the first phase represents the normal operation of the MBR associated with fouling. The second phase of operation represents the effect of back flushing on membrane resistance. The purple vertical line separated the backwashing MBR time into two phases, "backwashing with H_2O" and "backwashing with PROLI".

5.3.1.2 The TMP increase was delayed by exposure to the NO donor PROLI

As discussed in the previous chapters, 15 kPa was considered to be the threshold TMP, below which, the system appears to be operating at a steady state. Above this threshold, the TMP enters an exponential jump stage, and increases rapidly to achieve the maximum TMP, 85 - 90 kPa, in a relatively short span of time. In these experiments, the effect of NO on preventing membrane fouling and the TMP jump was determined. For the control MBR, the system maintained operation in the low TMP stage (<15 kPa) for approximately 51 d before entering the jump stage after which time, the TMP rapidly rose to the maximum TMP (62 kPa) over the following 34 d (Fig. 5.3). In comparison, the PROLI treated MBR was observed to remain in the low TMP stage for the first 62 d before entering the jump phase. When the experiment was terminated on day 85, the PROLI treated MBR had only reached 42 kPa, representing a 32.3%

reduction in TMP compared to the untreated control. The average rates of TMP increase were 0.24 kPa/day for the PROLI treated MBR and 0.294 kPa/day for the control MBR in the steady TMP stage (3 - 15 kPa) and 1.17 kPa/day for the PROLI treated MBR and 1.38 kPa/day for the control MBR in the rapid increasing stage (>15 kPa). Thus the PROLI treatment was able to the maintain the MBR in the low TMP stage for 10 d longer than the untreated control and the NO treatment also resulted in a slower increase during the jump stage.

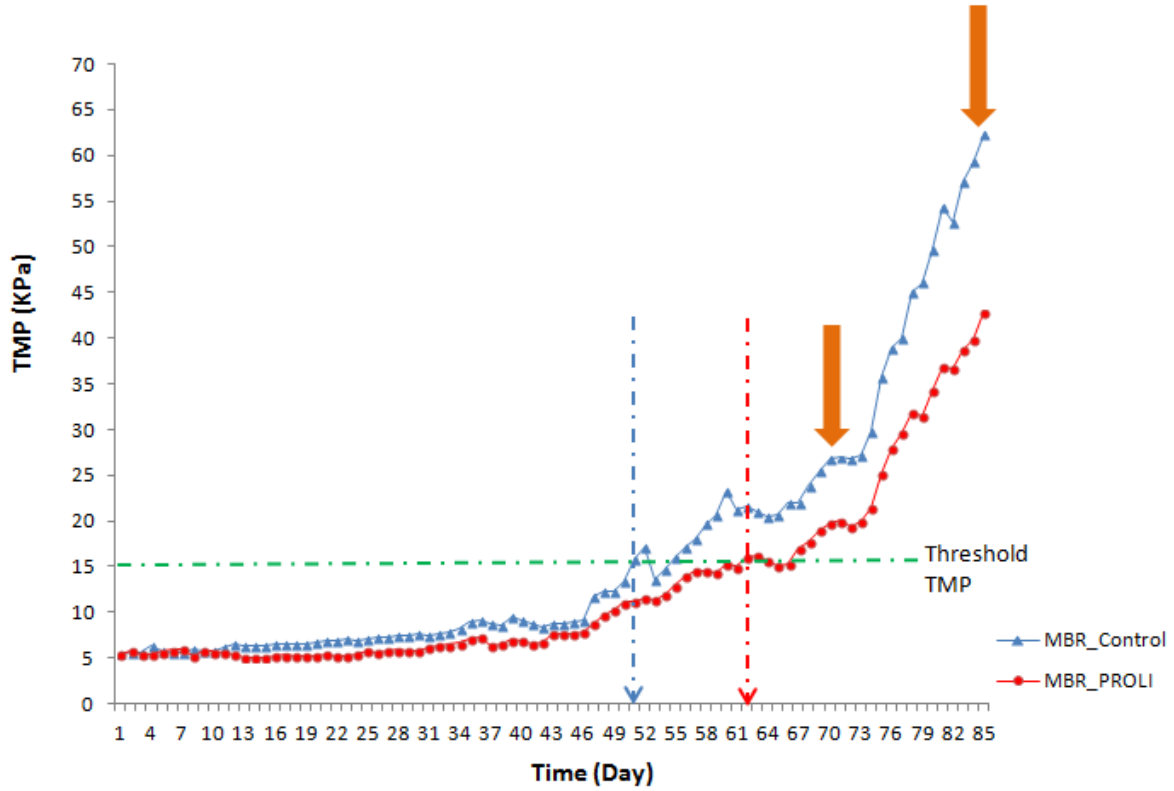

Fig. 5.3 The variations of TMP for the PROLI NONOate treated and control MBR. The horizontal dashed line indicates the threshold TMP between steady TMP stage and exponential increasing TMP stage. The blue arrow shows the time for the TMP in control MBR to reach the threshold value. The red arrow shows the time for the TMP in PROLI-treated MBR to reach the threshold value. The orange arrows show the time points when membrane samples were collected and analyzed for both MBRs.

Fouling resistance is a reflection of the accumulation of fouling layers on the membrane and therefore the effect of the PROLI treatment on the fouling resistance was determined here. It was found that the fouling resistance profiles for the PROLI treated MBR and control MBR

were almost the same in the first 46 d (Fig. 5.4), where the differences in fouling resistance between PROLI treated MBR and control MBR were in the range of -1.5×10^{8} m^{-1} to 1.13×10^{8} m^{-1} (Fig. 5.5). However, the membrane resistances for the control and PROLI treated MBRs diverged after 55 d, where the fouling resistance of the control module was higher than for the PROLI treated module (Fig. 5.4). The differences in fouling resistance before the treatment between the control MBR and PROLI treated MBRs were 2.3×10^{8} m^{-1} to 3.5×10^{9} m^{-1}, while the differences in fouling resistance after treatment were 1.3×10^{8} m^{-1} to 2.22×10^{9} m^{-1} (Fig. 5.5). At day 85, the fouling resistance was 7.56×10^{9} m^{-1} for the control module and 5.43×10^{9} m^{-1} for the PROLI treated module (Fig. 5.4). The efficiency of reduction for the fouling resistance was 28.2%.

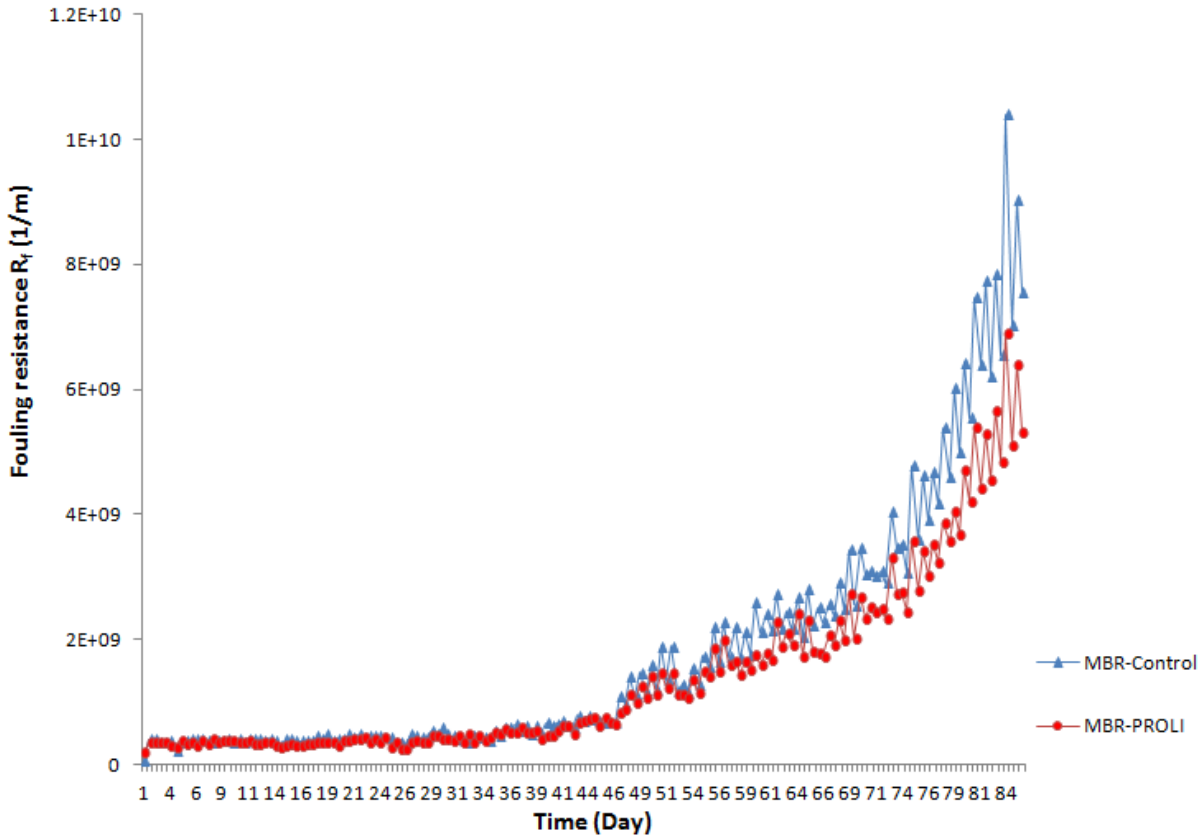

Fig. 5.4 The variation of fouling resistance (R_f) on membrane modules in the PROLI treated MBR and control MBR. The red circles show the Rf for the PROLI treated membrane module and blue triangles show the Rf of the control membrane module.

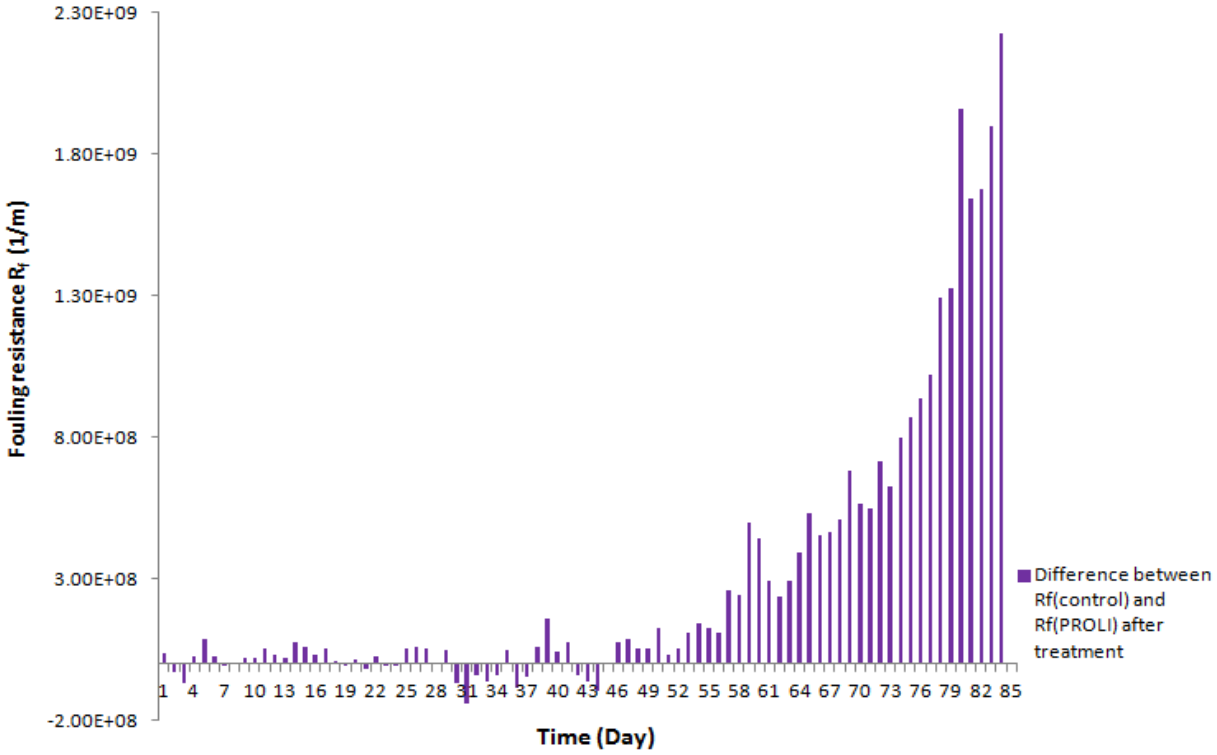

Fig. 5.5 The difference in Rf between Control MBR and PROLI treated MBRs after the daily treatment.

5.3.3 The effect of PROLI treatment on membrane biofilms

5.3.3.1 NO mediated reduction of biofilm constituents

In order to determine the effect of PROLI treatment on the biofilm, the biovolumes of the biofilm components on the membranes were quantified. Two time points were selected to compare the biovolume of biofilm components for the PROLI treated membranes (Fig. 5.3). The first time point was at day 71, when the TMP for the control module was 27 kPa and the TMP was 20 kPa for the PROLI treated module. The second time point was at the end of the experiment on day 85, when the TMP for the control module was 62 kPa while the TMP for PROLI treated module was 42 kPa. The biofilms were stained using fluorescent dyes that were specific for either proteins, α-polysaccharides, β-polysaccharides or total microbes (DNA stain) and captured by CLSM and the results were quantified as the volume (μm^3) of the specific component per membrane surface area (μm^2).

The biovolume of each biofilm component in the PROLI treated module was observed to be lower than the corresponding components in the untreated control MBR (Fig. 5.6). For

example at day 71, when the TMP of the PROLI treated MBR was 7 kPa lower than the control MBR, the biovolume of the proteins was 2.1 $\mu m^3/\mu m^2$ on the PROLI treated membrane and 3.4 $\mu m^3/\mu m^2$ on the control membrane, representing a 38.2% reduction as a consequence of PROLI treatment. Similarly, the biovolumes for the α-polysaccharides, β-polysaccharides and microbial cells were reduced 68.1%, 55% and 50% respectively for the PROLI treated MBR.

On day 85, the TMPs were 62 kPa and 42 kPa respectively for the control and PROLI treated MBRs. While the biovolumes for each component were observed to increase from day 71 to 85 in the control and NO treated MBRs (Fig. 5.6), the biovolumes for all components remained higher on the control MBR membranes than on the PROLI treated membranes. For example, the biovolume of the α-polysaccharides was 1.8 $\mu m^3/\mu m^2$ and 1.5 $\mu m^3/\mu m^2$ on the control and PROLI treated membranes respectively. The biggest difference in macromolecules on day 85 was for the protein component, which was 5.3 $\mu m^3/\mu m^2$ for the control membrane module and 3.3 $\mu m^3/\mu m^2$ for the PROLI treated membrane module ($p<0.05$). The differences in biovolume for the proteins and microorganisms were greater on day 85 than on day 71. At day 85, the biovolume for the microorganisms was 0.7 $\mu m^3/\mu m^2$ for the PROLI treated MBR and 1.8 $\mu m^3/\mu m^2$ for the control MBR ($p<0.05$). Thus, there was a 37.7% reduction in proteins and a 66.7% reduction in microorganisms after PROLI treatment. This may indicate that further treatment may result in additional reduction in the various fouling components. It was noted that the proteins were the most abundant component of the biofilm in both the untreated and PROLI treated modules (Fig. 5.6). This was consistent with the conclusion that the proteins were the most closely correlated macromolecule associated with the TMP rise and biofouling of the four components investigated (Chapter 2). The amount of DNA extracted on day 71 was 2.7 $\mu g/cm^2$ for the control membrane module and 2.3 $\mu g/cm^2$ for the PROLI treated module (Fig. 5.7). At day 85, 4.2 $\mu g/cm^2$ of DNA was extracted from the control membrane while 3.98 $\mu g/cm^2$ of DNA was extracted from the PROLI treated membrane (Fig. 5.7). However, the result of t test showed the *p* value was above 0.05, indicating the difference of extracted DNA was not significant.

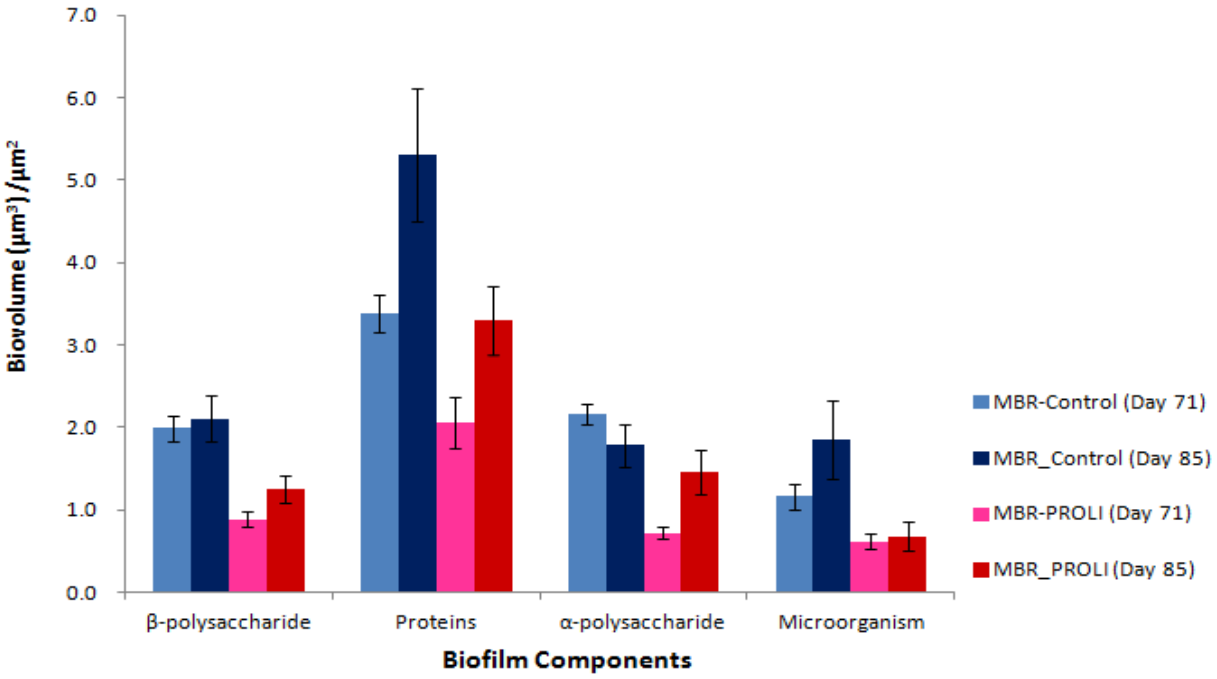

Fig. 5.6 The biovolume of biofilm components on membranes as visualized by confocal microscopy for the untreated control (blue) and PROLI treated (red) MBRs at days 71 and 85. The x-axis shows the different components of biofilms. Error bars are the standard error of the mean (n=30).

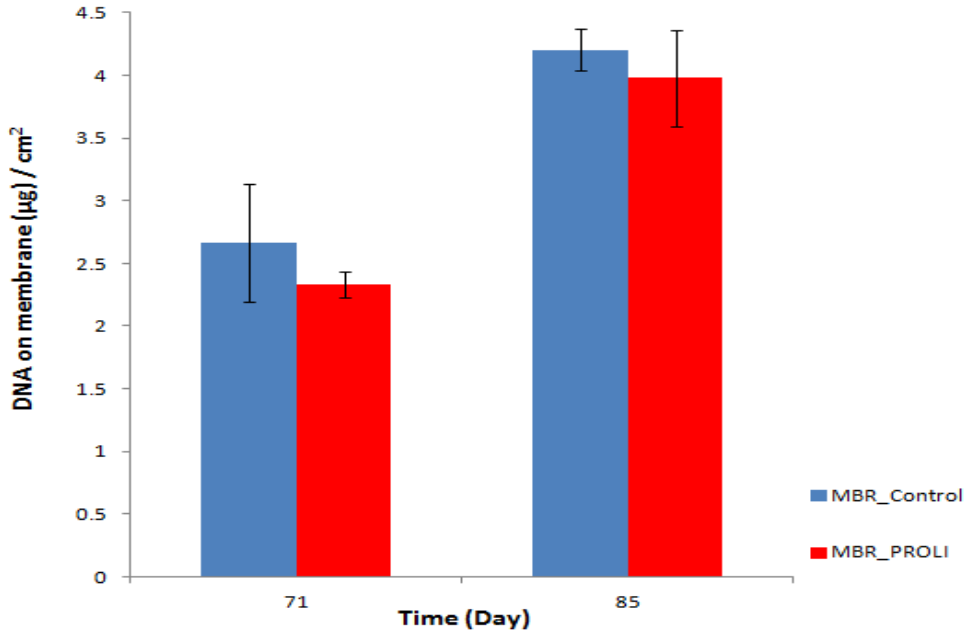

Fig. 5.7 The amount of DNA extracted from membranes for control and PROLI treated MBRs. The error bars are the standard error of the mean (n=3).

5.3.3.2 The effect of the PROLI treatment on the bacterial community

Nitric oxide has been shown to induce dispersal of bacteria from both single and mixed species biofilms (Barnes et al., 2013; Barraud et al., 2009a). It has recently been shown that some bacteria do not disperse in the presence of NO (Barnes et al., 2013) and therefore, the effect of PROLI treatment on the microbial communities was determined here. It was previously shown (Chapters 3 and 4) that there was a strong selection for a biofilm specific community relative to the sludge community. Not surprisingly, a comparison of the sludge and biofilm communities here showed similar differences in communities and this was true for both the control and PROLI treated MBRs (Fig. 5.8b). For example, the bacterial communities in the sludge at days 71 and 85, showed 74.3% similarity while the comparable biofilm communities showed 81.6% similarity. Thus, the bacterial communities were distinct for the sludge and biofilm (Fig. 5.8b). This indicated that establishment and selection of the biofilm specific community, which was derived from the sludge community, was similar for both the PROLI treated and control membranes.

The same groups of bacteria were found to dominate the treated and control biofilm communities on the two days tested, days 71 and 85 (Fig. 5.8a) and included: *Rhodobacterales*, *Actinomycetales*, *Rhodospirillales*, *Rhizobiales* and *Sphingobacteriales*. For example, the *Rhodobacterales* were the most dominant group in the PROLI treated biofilms at days 71 (28.53% in abundance) and 85 (32.88% in abundance) as well as in the control biofilms (32.04% in abundance day 71 and 28.63% in abundance day 85). These groups of bacteria accounted for 80.42% (PROLI treated) and 83.95% (control) of the bacterial communities at day 71 and 73.43% (PROLI treated) and 82.88% (control) of the total bacterial communities at day 85.

Closer examination indicated that there were some minor differences in the biofilm communities for the control and treated samples. The 85 d control biofilm were slightly different (18.33% in dissimilarity) from the rest of the biofilms, control or treated (Fig. 5.8b). This suggests that the PROLI treatment had a slight effect on the biofilm community composition as it developed from days 71 to 85.

Compared to the untreated bacterial community, six Orders of bacteria, including *Thiotrichales*, *Gemmatimonadales*, *Xanthomonadales*, *Rhodocyclales* and *Myxococcales*, had lower abundances on the PROLI treated membrane module at both day 71 and 85. For example, at day 85, the *Thiotrichales* accounted for 2.73% of bacterial community on control

membrane but only had an abundance of 0.16% on the PROLI treated membranes. This trend was also observed for *Gemmatimonadales* and *Xanthomonadales*, which had abundances of 1.12% and 1.16% on control membranes, while they were present on the PROLI treated membranes at lower abundances of 0.49% and 0.71% respectively. This phenomenon indicated that the abundance of these bacteria may be reduced in the biofilms due to the PROLI treatment to the membrane.

Additionally, some bacteria, such as *Rhizobiales* and *Actinomycetales*, were found to have higher abundances on the PROLI treated membranes at both days 71 and 85. The *Rhizobiales* accounted for 13.77% and 15.51% respectively in the PROLI treated biofilm community at days 71 and 85, while their abundances were 11.26% (*Rhizobiales*) and 11.08% (*Actinomycetales*) on the control membrane. Similarly, the abundance of *Actinomycetales* was also higher on PROLI treated membrane (25.91% at day 71 and 22.64% at day 85) than on the control membrane (20.96% at day 71 and 21.61% at day 85). This indicated the *Rhizobiales* and *Actinomycetales* may not be dispersed by PROLI treatment as dramatically as other bacteria, resulting in relative higher abundances for them in the PROLI treated biofilm community.

(a)

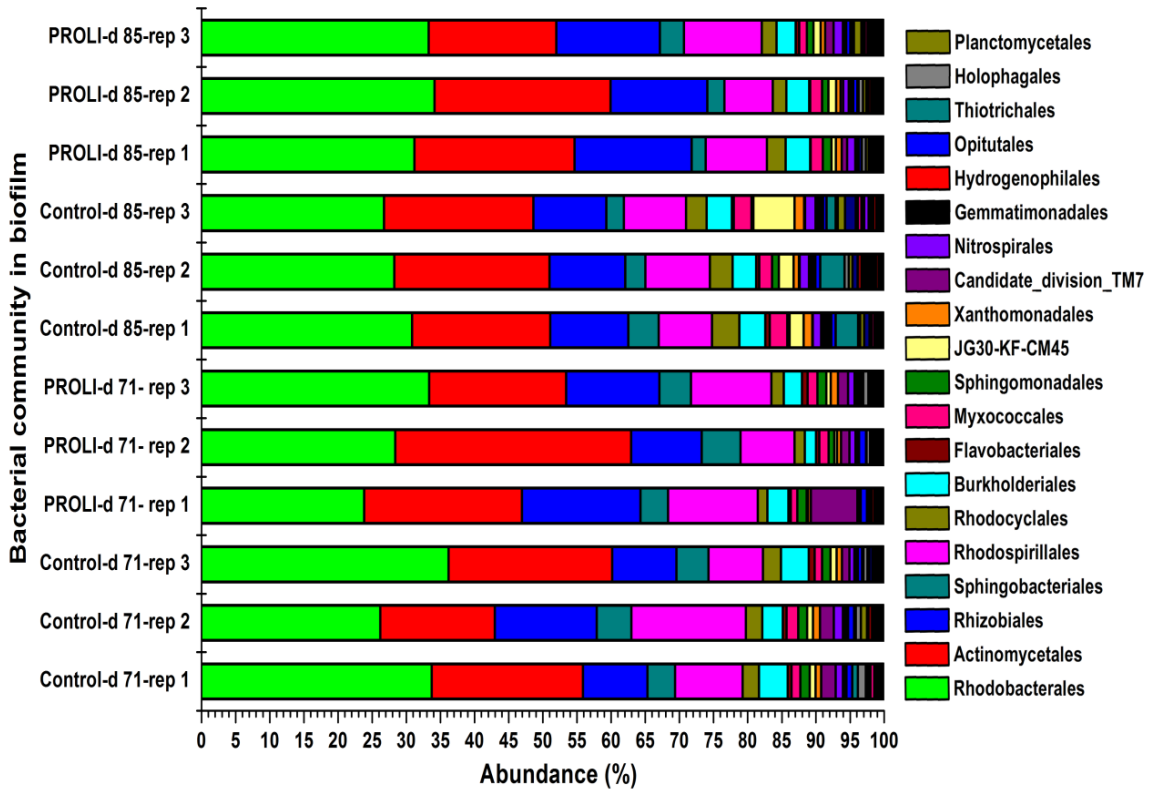

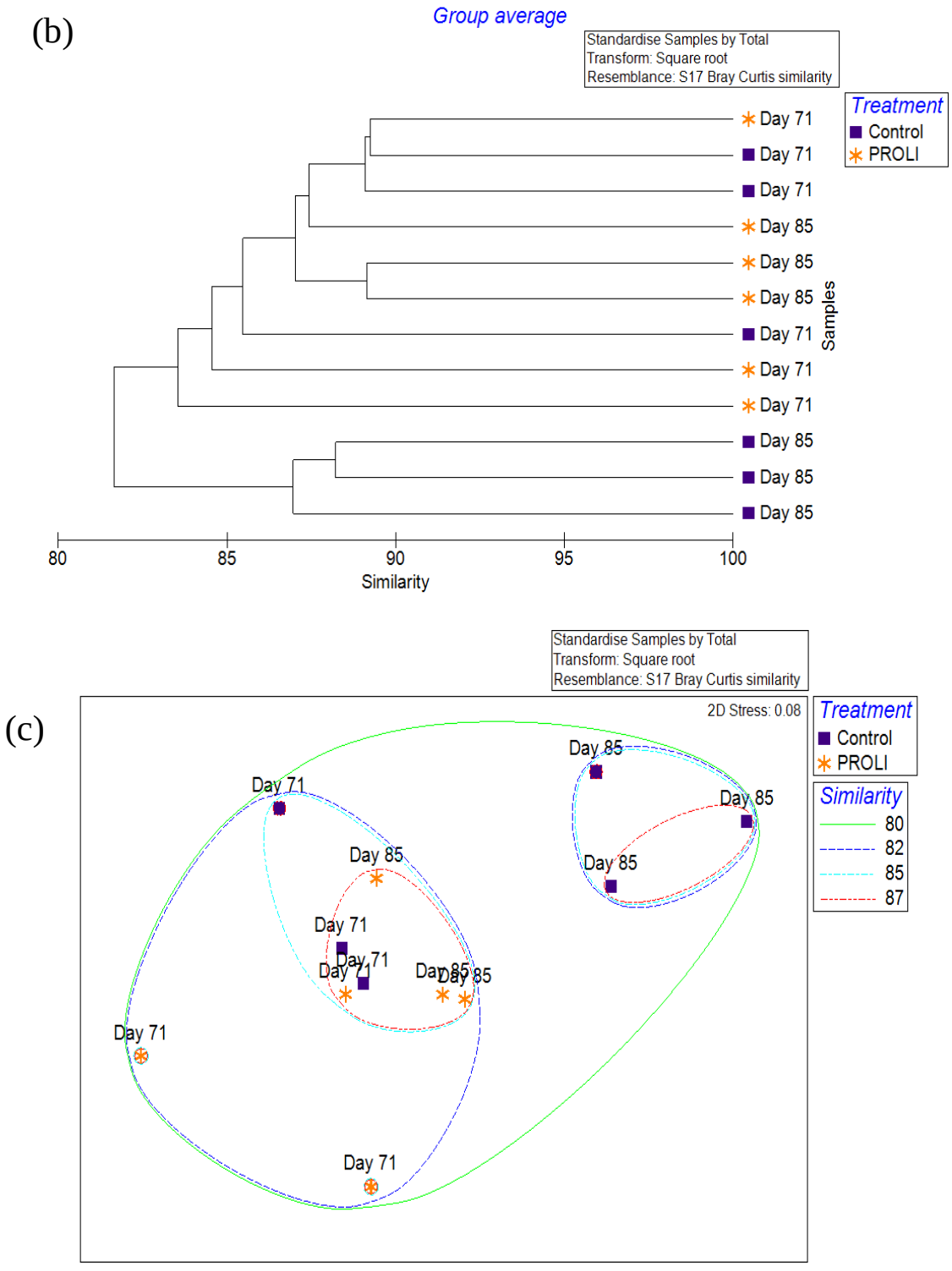

Fig. 5.8 (Continued from previous page) The bacterial communities in sludge and biofilm samples and their relationships based on the Bray-Curtis similarity. (a) The bacterial sludge and biofilm communities in the PROLI treated and control MBRs. (b) The phylogenetic tree for the bacterial communities in sludge and biofilms based on the Bray-Curtis similarity. (c) The NMDS plot for the bacterial communities in biofilm samples based on the Bray-Curtis similarity.

5.3.3.3 Change of fungal community responding to PROLI dosing

The difference in the fungal community was also compared for the PROLI treated and untreated biofilms. Not surprisingly, the sludge and biofilm communities were distinct from each other irrespective of treatment, with approximately 47.6% dissimilarity between biofilm and sludge samples (Fig. 5.9b). The fungal sludge communities were dominated by *Saccharomycetales*, *Hypocreales* and *Glomerales*, which accounted for 68.8% (seed sludge), 96.34% (sludge at day 71) and 95.46% (sludge at day 85) of the total fungal communities. For the biofilms, the fungal communities were considerably more divergent than the bacterial communities, showing 59.08% similarity between the PROLI and control modules. The top five most abundant fungi were *Hypocreales*, unclassified mitosporic_Ascomycota, *Saccharomycetales*, *Georgefischeriales* and *Glomerales*, which accounted for 88.36% (PROLI treated day 71) and 89.6% (PROLI treated day 85) and 95.07% (control day 71) and 93.21% (control day 85) of the total fungal biofilm communities.

The *Hypocreales* were found to have a high abundance (32.95%) in the control module but only accounted for 0.11% in the PROLI treated module at day 71. At day 85, the abundance of *Hypocreales* was 1.24% in the control module and 0.16% in the PROLI treated module. Given that there was a significant reduction in abundance in the group for the untreated control from day 71 to 85, it is difficult to be certain that the reduced percent composition for the PROLI was a consequence of the NO treatment or part of the natural community shift. Similarly, the *Glomerales* accounted for 1.75% of the biofilm community in the control module compared to 0.23% in the PROLI treated module at day 71 and 2.5% of fungal communities in biofilms in control module and 1.01% of the fungal biofilm community for the PROLI treated module at day 85. Members of the Order *Saccharomycetales* also decreased in biofilm abundance from 23.18% in the untreated biofilms to 3.48% in the PROLI treated samples on day 71. Similarly the abundance of this group was still lower in the PROLI treated biofilm (49.91%) than in the control biofilm (73.18%) on day 85, even though the abundance of *Saccharomycetales* increased in both the control and PROLI treated biofilms.

(a)

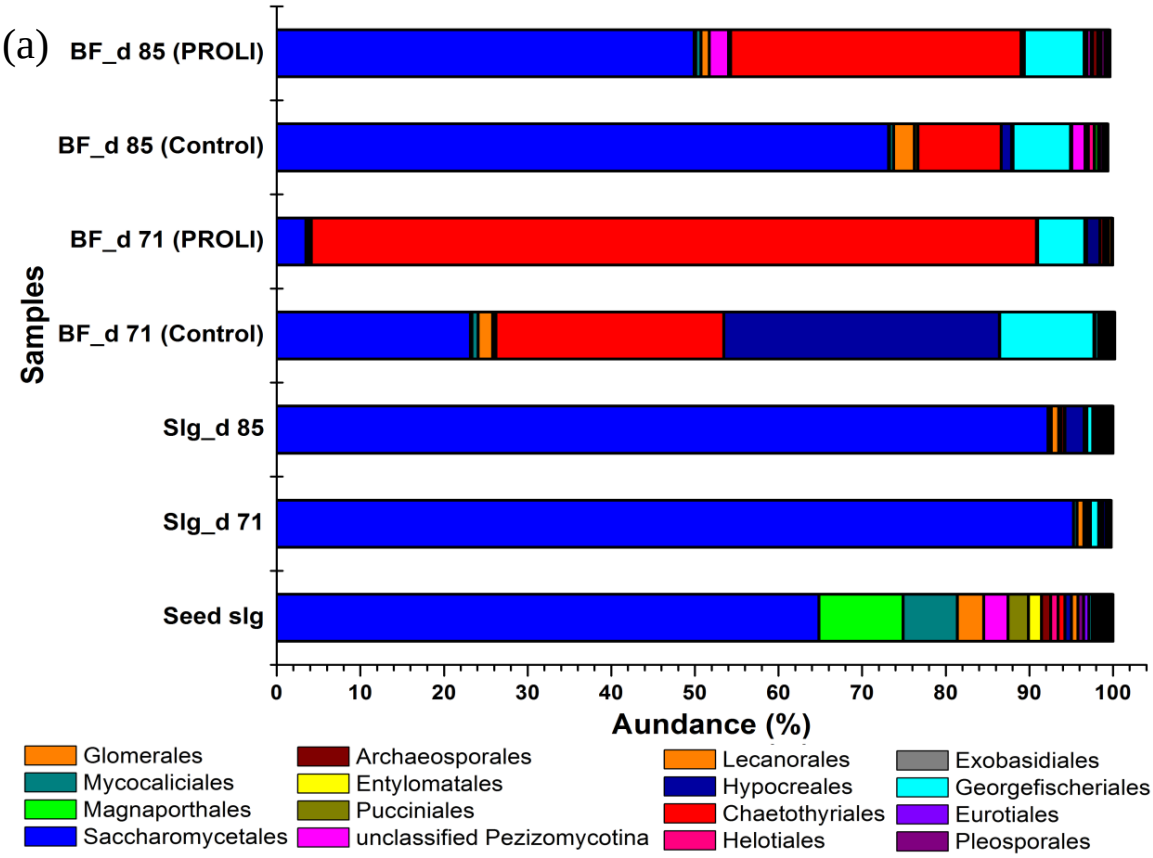
BF_d 85 (PROLI)
BF_d 85 (Control)
BF_d 71 (PROLI)
BF_d 71 (Control)
Slg_d 85
Slg_d 71
Seed slg
Samples
0 10 20 30 40 50 60 70 80 90 100
Aundance (%)
Glomerales
Mycocaliciales
Magnaporthales
Saccharomycetales
Archaeosporales
Entylomatales
Pucciniales
unclassified Pezizomycotina
Lecanorales
Hypocreales
Chaetothyriales
Helotiales
Exobasidiales
Georgefischeriales
Eurotiales
Pleosporales

(b)

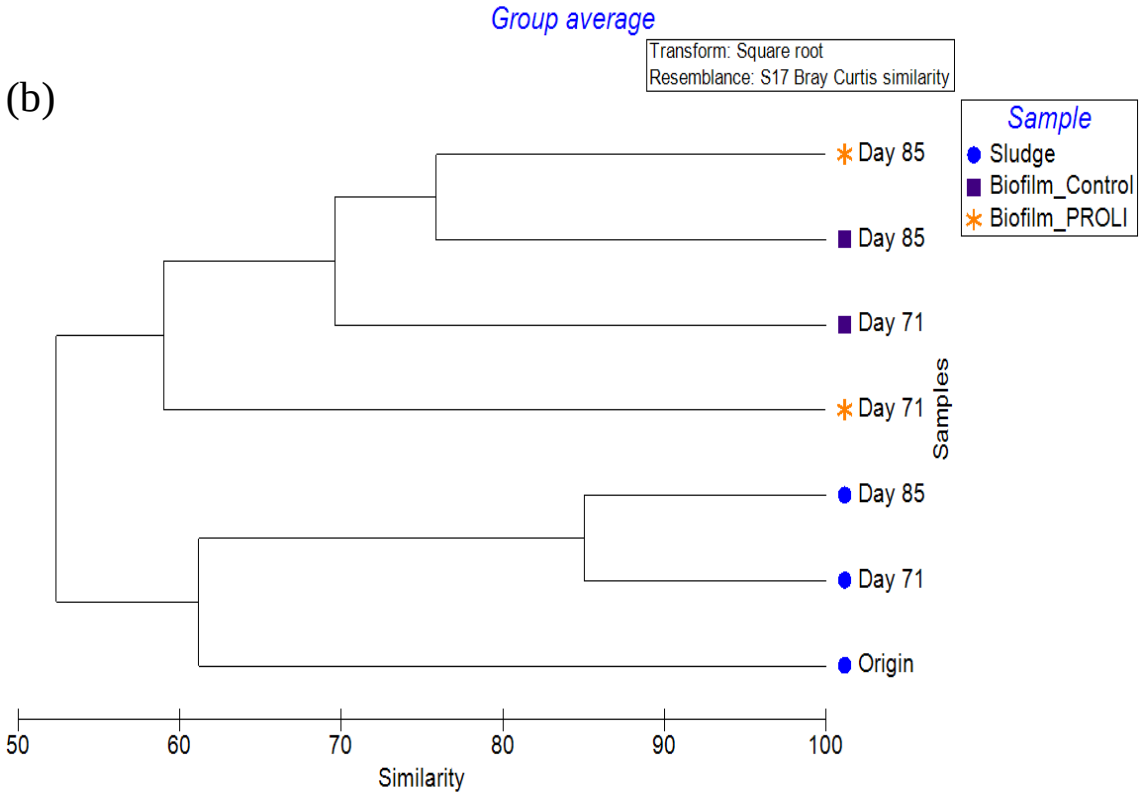
Group average
Transform: Square root
Resemblance: S17 Bray Curtis similarity
Sample
Sludge
Biofilm_Control
Biofilm_PROLI
Day 85
Day 85
Day 71
Day 71
Day 85
Day 71
Origin
Samples
50 60 70 80 90 100
Similarity

(c)

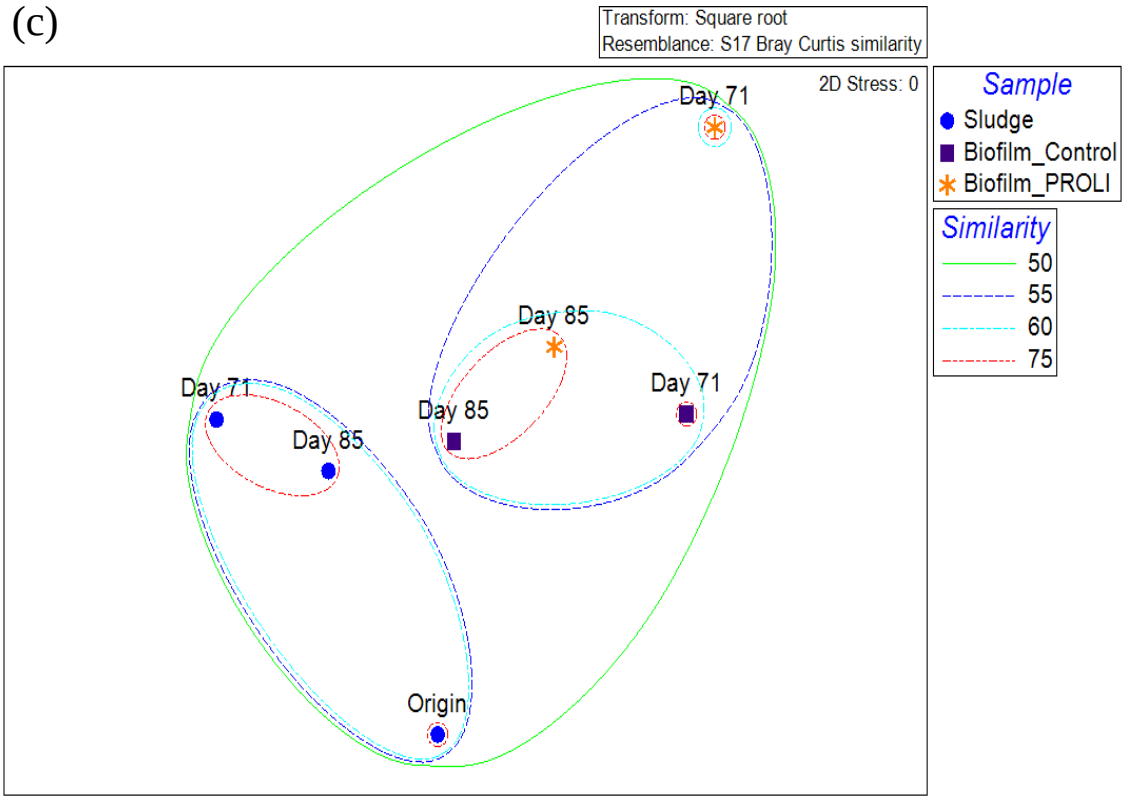

Fig. 5.9 (Continued from previous page) The fungal communities in sludge and biofilm samples and their relationships based on the Bray-Curtis similarity. (a) The fungal communities in sludge samples and biofilms in the PROLI treated module and control module. The abundances were the average values of the triplicate samples for the sludge and biofilms. (b) The phylogenetic tree for the fungal communities in (a) based on the Bray-Curtis similarity. (c) The NMDS plot for the fungal communities in (a) based on the Bray-Curtis similarity.

5.4 Discussion

In this study, the use of nitric oxide (NO) to induce biofilm dispersal was selected as a strategy to control biofouling in MBRs. The potential for NO to control biofilms in MBR systems was tested using two distinct approaches. The first was to disperse pre-established, mature biofilms that had developed during MBR operation and the second was to prevent biofilm accumulation by applying the NO from the beginning of the MBR operation. After backwashing the mature biofilms with PROLI NONOate for 37 d, the fouling resistance increased at a slower rate than was observed for the control MBR. Indeed, PROLI treatment resulted in a 50% (in pre-established biofilm dispersal experiment) and 28.2% (in the biofilm prevention experiment) reduction of fouling resistance. This indicated that backwashing of PROLI NONOate to the biofilms in the MBR could partially remove an established biofilm.

Similarly, treatment of the MBR from the beginning of the experiment with PROLI NONOate indicated that the formation of biofilm onto the membrane could not be blocked fully but could be substantially delayed. A replicate experiment, where the PROLI NONOate was used daily to treat the membrane module from the begining of operation also showed the same effect, delayed time to the TMP jump phase (data not shown). These observations were supported by the image based data which showed that NO treatment resulted in a reduction of biofilm biomass, for both cells (66.7% reduction) as well as macromolecules (e.g. 37.7% reduction for proteins). This finding is consistent with previous research, where a 30% reduction of microbial volume was observed when the biofilms were treated with 80 μM PROLI NONOate for 1 h (Barnes et al., 2013). It was noted that amount of extracted DNA was also lower in the PROLI NONOate treated biofilms than in the control biofilms, which is consistent with the CLSM result. However, the difference of extracted DNA was not significant (p>0.05), which was contrary to the CLSM data. This indicated the extracted material may contain some DNA that was not detected by the SYTO 63 staining. It was reported that the SYTO 63 is a cell permeable DNA binding dye and used to visualize cells (Douterelo et al., 2014). Therefore, some extracellular DNA may not be displayed by the CLSM observation but collected by the chemical extraction. This may explain why the data of CLSM observation and chemical extraction had different p values. In combination, these experiments strongly suggest that 80 μM PROLI NONOate can reduce the growth of biofilms in MBR and may therefore delay the TMP jump and hence increase the operational time of the MBR. In previous studies, biological methods based on the molecular signaling have been employed to control biofouling in MBR systems. It was reported that the Porcine kidney acylase I, which is a quenching enzyme of *N*-acyl homoserine lactone (AHL) autoinducers, can prevent biofouling (approximately 26% - 46% reduction in TMP) in MBR (Yeon et al., 2009a; Yeon et al., 2009b). The production of polysaccharides and proteins was reduced 87.7% and 86.9% respectively due to the application of immobilized acylase (Yeon et al., 2009a). Since the cost of the enzyme quenching strategy is very high, a quorum quenching enzyme producing bacterium, *Rhodococcus* sp. BH4, was entrapped into alginate beads and used to control biofouling in MBR. The data indicated that the time for TMP to increase to 70 kPa was delayed ten fold and the amounts of EPS and microorganisms were reduced 80% and 58.5% after the immobilized bacteria were applied to MBR (Kim et al., 2013). Thus, it is clear that the biological strategies, e.g. NO or anti quorum sensing approaches, can be successfully applied to control fouling of MBRs. However, the NO based biofouling prevention strategy was not as efficient as the commonly used chemical cleaning strategy, which was reported that treatment with the combination of 3000 mg/L NaClO and 500 mg/L NaOH reduced 81.8% of

TMP (Li et al., 2011) and treatment with 1000 mg/L citric acid recovered 90% of the membrane permeability in MBR (Yan et al., 2012). It has been shown previously that biofilms exposed to NO donor compounds were more susceptible to antimicrobial agents and removal from surfaces with surfactants. Therefore, NO treatment may be best complemented with traditional biofilm cleaning protocols, e.g. bleaching with low concentration of chlorine, to synergistically remove the biofilms and hence, alleviate the fouling problem.

While the NO treatment was able to delay the increase in biofilm biomass and the associated TMP, it was not able to prevent this phenomenon. Characterization of the biofilm communities indicated that the bacterial and fungal communities in the treated and untreated biofilms were quite similar, where the dominant microorganisms were *Rhodobacterales*, *Actinomycetales*, *Rhodospirillales*, *Rhizobiales* and *Sphingobacteriales* for bacterial community and *Hypocreales*, unclassified mitosporic_Ascomycota, *Saccharomycetales*, *Georgefischeriales* and *Glomerales* for fungal community. Based on the microbial community analysis in Chapters 3 and 4, bacteria including *Actinomycetales*, *Rhodospirillales*, *Rhizobiales* and *Sphingobacteriales* and fungi including *Hypocreales*, *Saccharomycetales* and *Glomerales* were the dominant biofilm forming microorganisms at high TMP. The PROLI NONOate treatment here did not significantly alter the microbial biofilm community composition, suggesting that the NO did not inhibit biofilm formation by specific microorganisms, but rather may be delay the increase in biofilm biomass by inducing dispersal in the community. This is supported by the image based data which demonstrated 66.7% and 37.7% reductions in microbes and protein on the membrane surface for the PROLI treated MBR.

While the overall biofilm community composition, bacteria or fungi, were not strikingly different in the control and treated MBRs, there were some subtle differences in both the bacterial and fungal communities after NO treatment. For example, the bacterial Orders of *Thiotrichales*, *Gemmatimonadales* and *Xanthomonadales* and fungal Orders of *Hypocreales* and *Glomerales* were reduced in abundance in the PROLI NONOate treated biofilms. The *Gemmatimonadales* and *Xanthomonadales* were reported in Chapter 3 to show increased biofilm abundance when the TMP increased. Similarly, the *Hypocreales* were shown to be key biofilm fungi when the TMP increased from low to high. In previous studies, the *Thiotrichales* and *Xanthomonadales* were found to compose the biofilms on membranes and involved in the sulfur oxidation in two-stage membrane biofilm reactors (Ontiveros-Valencia et al., 2014). And the *Xanthomonadales* were also a dominant microbial group of biofilm on caves (Porca

et al., 2012). Interestingly, these organisms were reduced in abundance in the PROLI treated biofilms in this study. This may suggest that these organisms are particularly sensitive to NO mediated dispersal and their removal from the biofilm may be important in the observed delay in TMP increase. Therefore, it will be of interest to track those specific organisms in future experiments by fluorescence *in situ* hybridization to determine their overall relationship to membrane fouling and the TMP rise.

In conclusion, the NO showed the potential to control membrane biofouling in MBRs through reducing the production of macromolecules in EPS, delaying the succession of community structure of microorganisms and dispersing some microbial groups selectively in this project. However, the biofouling behavior was not completely prevented, suggesting further studies are required to enhance the efficiency of NO treatment. For instance, increased biofilm inhibition may be achieved by optimizing the concentration and time of PROLI NONOate dosing. Additionally, alternative NO donors, such as sodium nitroprusside (SNP) and MAHMA NONOate, which exhibit different NO release kinetics may be better suited for the high organic content environment of the MBR (Barnes et al., 2013; Barraud et al., 2006; Barraud et al., 2009a; Miller and Megson, 2007). Furthermore, it may enhance the efficiency of biofouling removal through chemical treatment, e.g. chlorine bleaching, in combination with the NO treatment (Omer Elhag-Idris, 2006). As a result, this study has demonstrated the potential for the application of NO to control membrane biofouling in MBRs and may promote a wider implementation of MBR technology.

Chapter 6 Conclusions

In membrane bioreactors (MBR), the term biofouling refers to the undesirable deposition of a biological-layer on membrane surfaces that may block the membrane pores (Baker and Dudley, 1998). This reduces membrane permeability and increases the hydraulic resistance of the membrane (Sombatsompop et al., 2006). Thus, membrane fouling results in an increase of the transmembrane pressure (TMP) when operated at a constant flux or a decreased flux when operated at a constant pressure. Therefore, biofouling and its consequences restrict the widespread application of MBR technologies and it is essential to understand the biofouling process in order to develop effective strategies to reduce or prevent biofouling.

The composition of the biofouling layers has been intensively investigated (Meng et al., 2007) and has been shown to be comprised of a complex mixture of cells, polysaccharides and proteins that all contribute to the biofouling process (Le-Clech et al., 2007; Meng et al., 2007). However, few reports have investigated the correlation between the different biofouling components and the TMP increase and there is no current consensus regarding their specific contribution to the biofouling process. Therefore, the work presented here has developed a comprehensive investigation of the fouling process, through a combination of confocal microscopy based imaging of the biofilm stained with fluorophores that are specific for key macromolecules associated with fouling as well as cells and has also quantitatively described the fouling communities by 16S and ITS tagged sequencing.

6.1 Changes in biofouling layer in the process of TMP increase

As expected, when the MBR systems were operated at constant flux, the TMP was observed to eventually undergo a rapid increase until the system achieved its maximum pressure. The TMP variation curves were consistent across multiple experiments and consisted of two stages, a long-term, low TMP stage and a short-term, high TMP stage. These two stages were divided by a critical threshold TMP, 15 kPa, where the rate of TMP increase below this threshold was low (0.183 - 0.172 kPa/day). After approximately 80 - 87 d of operation in the low TMP stage, the MBR subsequently experienced a rapid TMP increase (2.143 - 2.778 kPa/day), also referred to as the TMP jump phase. This bimodal operation, of a low steady state operation followed by a rapid TMP increase has been previously observed, where, in a constant flux (10 $L.m^{-2}.h^{-1}$) MBR, the TMP increased at the rate of 0.864 kPa/day in the low TMP stage which increased dramatically to 86.4 kPa/day in the high TMP stage (Ognier et al., 2002). Given that

the TMP curve was clearly and reproducibly divided into these two stages, it was of particular interest to examine the changes in molecular and cellular fouling. Further, it was of interest to characterize the changes in the community composition in the context of these two phases in an attempt to identify the key contributor to the transition from steady state operation into the TMP jump phase.

In general, the biofilm and biopolymers were heterogeneously distributed on the membrane surface at low TMP. These were observed to form distinct clusters with open spaces between them. The biofilm, or the fouling layers, contained polysaccharides (α and β), proteins and microbial clusters at all of the time points tested and all four components were positively correlated (Pearson's correlation coefficient 0.7 - 0.95) with the TMP increase. During the first 20 d of MBR operation, where the pressure was still quite low (3 - 7 kPa), the α- and β-polysaccharides were found to dominate the biofouling layer. At the later stages of operation, the biofilm biomass was more evenly distributed across the membrane surface and was increased in thickness as measured by total biofilm biovolume. It was observed that the thickness of biofouling layers was 5 - 20 μm at 60 - 90 kPa relative to the thin biofouling clusters (1 - 5 μm) at 3 - 10 kPa (Figs. 2.4 and 2.5). Interestingly, as the MBR continued to operate, the percentage composition contributed by the proteins increased more than any of the other components when the TMP was below, but close to the threshold 15 kPa. The proteins were also proportionally the most abundant components in the biofilm in the later TMP jump stage. The higher protein abundance observed here was consistent with previous work, where the proteins accumulated preferentially in the biofouling layers of the MBR (Tian et al., 2012). Collectively, the data may indicate that the proteins were the dominant driver for the TMP increase in the MBR and, importantly, that they accumulate in the biofilm prior to the initiation of the jump stage.

In order to develop fouling control strategies, which should ideally target the key biopolymers or the organisms responsible for their production, it is necessary to better understand the origin of the proteins. With respect to polysaccharides, it has been suggested that there are essentially two sources that contribute to membrane fouling. These are the soluble polysaccharides, originating from the bulk solution, and the bound polysaccharides, which are directly produced by and tightly associated with the microbial cells in the biofilm biomass (Comte et al., 2006; Laspidou and Rittmann, 2002; Wang et al., 2009). Similarly, the proteins could either accumulate through their deposition from the liquid phase, e.g. soluble proteins, or could be produced at the membrane surface as a consequence of microbial growth and

biofilm formation and would be analogous to the bound polysaccharides. When the co-localization of the biopolymers and cells was investigated, there was a clear, strong correlation between the localization of the protein components, as well as the polysaccharides, with the cells present in the biofilm. This was most clearly demonstrated using the Mander co-localization coefficient, which indicated that 50% of the EPS co-localized with 80 - 90% microbial cells. This was confirmed by the visual observations, which also showed that the polysaccharides and proteins usually had larger biovolumes and enveloped the microbes. These observations strongly support the hypothesis here, that polysaccharides and proteins in the biofilm may be the secreted byproducts of the microbes on the membrane surface and are less likely to randomly deposit from the bulk liquid in this arrangement. It is important to note that two coefficients, Pearson correlation coefficient and Mander co-localization coefficient, were used. The Pearson correlation coefficient describes the distribution of fluorescent intensity for two objectives in one image and is especially suitable for the objectives with similar shape while the Mander colocalization coefficient measures the true level of co-localized pixels of two objectives in one image without the consideration of the shape (Dunn et al., 2011; Zinchuk and Zinchuk, 2001). This may explain why the Mander co-localization coefficient was higher than the Pearson correlation coefficient. If the microbial community is the source of the biopolymers associated with membrane fouling, then it becomes essential to understand the dynamics that drive microbial community organization in relation to the TMP jump.

6.2 The microbial community associated with the TMP jump

Another significant change in the biofouling layer that was apparent at the threshold pressure (15 kPa) was in the changes to the microbial community composition. It was interesting to note that microbial communities could essentially be divided into two distinct clusters. The microbial biofilm communities at the lowest TMP stage (5 - 7 kPa for the bacteria and 5 - 10 kPa for the fungi) were found to be most similar to each other and clustered into one group (Chapters 3 and 4, Fig.s 3.7 and 4.6), while biofilm communities at higher TMPs formed a separate distinct group. It was noted that the correation between the richness of biofilm bacterial community and TMP increase was not evident in this study. At the low TMP stage, the bacterial community on the membrane was comprised of *Sphingobacteriales*, *Rhodocyclales*, *Burkholderiales*, *Actinomycetales* and *Flavobacteriales* and the fungal community on the membrane was composed of *Glomerales*, *Mycocaliciales*, *Diversisporales*,

Saccharomycetales and *Archaeosporales*. Once the TMP increased to the threshold pressure, the bacterial biofilm community changed and was dominated by *Rhodospirillales*, *Sphingomonadales* and *Rhizobiales*. The fungal community at the higher TMP stages was dominated by *Saccharomycetales* and *Hypocreales*. It should be noted that these microbial groups may have different abundance in the repeated experiments of this study (Figs. 3.10). However, no matter the variation of the relative abundance, these microbial groups composed the dominant microorganisms in biofilms at low or high TMP in all the experiments. For the bacteria, the low pressure associated community shared a strong similarity with the sludge community and it was particularly clear that the developing biofilm was distinct from the sludge community. The fungal biofilm shared greater similarity with the sludge than the bacterial biofilm suggesting less selection for specialized biofilm forming organisms than that was observed for the bacteria. For the bacteria, the majority of the community shift occurred prior to the threshold TMP, 15 kPa and for the fungi, a more clear delineation of a biofilm specific community was apparent only after the TMP increased beyond the 15 kPa threshold pressure. Thus, it appears that the majority of the bacterial changes occur prior to the fungal community changes. These findings indicate that the change of microbial community may be one of the reasons for the change of TMP increasing rate in the operation of MBR.

6.3 Proposed model for biofilm formation, membrane fouling and increased TMP

Based on the results presented in Chapters 2 - 4, it is proposed that membrane fouling and the associated TMP jump is primarily a biofilm phenomenon. This is partly based on the observation that the biopolymers investigated here show a strong correlation and co-localization with the microbial cells. Community analysis data indicated that a subset of bacteria from the sludge comprise the early membrane colonizers and that these tend to be the non-dominant organisms in the sludge, suggesting these are biofilm specialists. This bacterial community changed dramatically over the initial TMP stages and became distinct from the sludge community further supporting the selection for biofilm specific bacteria. In contrast, the fungal community had a high degree of similarity to the sludge and the early biofilm colonizers represented the dominant fungi in the sludge. The delayed change in the fungal community, relative to the bacterial community could indicate that the bacteria are the primary membrane colonizers and that the fungi may require specific bacteria to be present in order to colonize the biofilm or that the bacteria condition the membrane such a way to allow for the fungi to better colonize. Such interactions between fungi and bacteria and the community composition changes would need to be validated by tracking the key organisms during biofilm

development. This would ideally be performed using Fluorescence *in situ* Hybridization (FISH) to not only demonstrate the key organisms are present in the biofilm at different time points during the MBR operation, but would also be used to quantify their relative proportions and could also be used to demonstrate co-localization of different organisms.

While the detailed community interactions and successional changes need to be verified here, these results and concepts are consistent with other published observations of changes in microbial communities. For example, it has been previously suggested that members of the *Sphingomonadales* are pioneer bacteria that initiate biofilm formation and flourish in the late biofilm in microfiltration and ultrafiltration based MBR systems (Calderón et al., 2011; Huang et al., 2008; Pang and Liu, 2006; Pang et al., 2005). This was in part consistent with the results in this study, which also showed that the *Sphingomonadales* were present, albeit in low abundance, in the biofilm at low TMP and became more prevalent in the biofilm at high TMP. It was also reported that the *Alphaproteobacteria* (represented here by *Rhodospirillales*, *Sphingomonadales*, *Rhizobiales*) increased in abundance in late biofilms in an MBR system (Lim et al., 2012). Similarly, the *Saccharomycetales* have also been reported to be an ubiquitous biofilm-associated fungal group (Ramage et al., 2009) and were also observed here to be key biofilm associated fungi. Community succession has also been studied extensively in oral biofilms (Kolenbrander, 2000), where specific bacteria are known to be the early colonizers, e.g. *Streptococci* (members of the *Lactobacillales*) and *Actinomyces* (members of the order *Actinomycetales*). These early colonizers are followed by bridging organisms, e.g. *Fusobacterium nucleatum*, that facilitate the subsequent colonization by organisms such as *Treponema denticola* (member of the order *Spirochaetales*) and *Porphyromonas gingivalis* (member of *Bacteroidetes*), which also happen to be the pathogens associated with dental disease. Similarly, the *Actinomycetales* were also shown here to be early membrane biofilm colonizers. This suggests that the *Actinomycetales* may generally be an early colonizer of biofilm communities. The *Bacteroidetes* (represented by *Sphingobacteriales* and *Flavobacteriales* in the results from this thesis) were observed to be the co-dominant organisms in the early biofilm and late biofilm in the MBR studied here, indicating the *Bacteroidetes* were also prevalent bacteria in the biofilm development.

Based on this model it is also proposed that the bacterial community undergoes a major community shift just prior to the threshold TMP, and this community shift is associated with an increased proportion of protein associated with the biofilm. The proteins may either be surface adhesions secreted by the community to adhere itself to the membrane, such as the

large amyloid fibrils that have been reported for a number of different bacteria and that have been reported in waste-water sludge (Larsen et al., 2007). Alternatively, the proteins could simply represent the bacterial cells, which are comprised of, among other polymers, proteins, in the cell membranes and cytoplasm. It has been reported that bacteria can be as much as 63% protein by dry weight compared to fungi or yeast which have been reported to be approximately 35% protein by dry weight (E Postma et al., 1989; Simon and Azam, 1989). The protein biovolume increased along the TMP curve in accordance with the cellular biovolume and hence may be contributed primarily from the bacterial cells with some contribution from the fungi.

6.4 Control of biofouling behavior using biological strategies

The results from Chapters 2 - 4 strongly suggest that the TMP rise is driven by the formation of microbial biofilms, and that the bacterial component may be the most relevant in the TMP increase given the relationship between the bacteria and the proteins which increased significantly just prior to the TMP jump. Many strategies have been developed to control biofilm formation on MBR membranes, such as modification of the membrane surface to make them toxic to the microorganisms or unsuitable for biofilm growth (Louie et al., 2006; Tan and Obendorf, 2007). Alternative strategies have focused on the removal the organic foulants through chemical cleaning after the biofilm becomes a problem (Al-Juboori and Yusaf, 2012; Kim et al., 2009; Nguyen et al., 2012). However, these efforts are not always effective since the bacterial biofilms can develop resistance to the surface modifications or disinfectants (Al-Juboori and Yusaf, 2012; Bridier et al., 2011). Furthermore, the over application of biocides and disinfectants, which are generally toxic compounds, also represent environmental risks (Guardiola et al., 2012). Therefore, an environmentally responsible biofouling control strategy is required.

As the proteins were the dominant macromolecule detected here, preliminary experiments were performed using proteinase K (40 μg/mL) with the expectation that digestion of the proteins would lead to a reduction of TMP and hence alleviate the fouling process. Interestingly protease treatment had no effect on the TMP or membrane resistance suggesting the protein was either not accessible to the protease K, the protease K was not specific for the types of proteins in the biofilm or that the proteins were not structural, but rather represented the microbial cells. Interestingly, DNase I treatment of *P. aeruginosa* biofilms has been shown to reduce or remove biofilms in the early stage of development (Whitchurch et al., 2002). However, when the biofilm was allowed to mature (84 h old) before the DNase I treatment

was applied, there was no effect on the biofilm. This suggested that even though the extracellular DNA was still present in the EPS, it may have been masked and hence protected by the other EPS components such as polysaccharides and thus it may be that the protein layer of the EPS observed in this study may similarly be protected from enzymatic degradation. This suggests that the control of biofouling should focus on controlling the bacterial community rather than focusing on a specific EPS component.

It has been reported that the application of low concentrations of nitric oxide (NO), released by the NO donor sodium nitroprusside (SNP), can cause the dispersal of *P. aeruginosa* biofilms (Barraud et al., 2006), where 24 h *P. aeruginosa* biofilms were reduced by 80%. Enhanced biofilm dispersal has also be been demonstrated where NO releasing silica nanoparticles reduced biofilm dispersal by 99% (Hetrick et al., 2009). Recently, another NO donor, PROLI NONOate, has been reported to disperse *P. aeruginosa* PAO1 biofilms (30% reduction in biovolume) in the concentration range of 5 - 80 μM (Barnes et al., 2013). NO has been shown to induce dispersal of a wide variety of microorganisms, including Gram-negative bacteria, e.g. *P. aeruginosa,* and *E. coli*, Gram-positive bacteria, e.g. *Staphylococcus aureus* and *Staphyolococcus epidermidis,* and fungi, e.g. *Candida albicans* (Barnes et al., 2013; Hetrick et al., 2009). Additionally, biofilms composed of mixed species on reverse osmosis (RO) membranes were also dispersed by NO treatment (Barraud et al., 2009a). It was subsequently determined that exposure to NO stimulated the activity of specific phosphodiesterases (PDEs) resulting in decreased levels of cyclic di-GMP (c-di-GMP), which is a second messenger molecule mediating the transition of living mode from planktonic to sessile biofilm for the bacteria (Barraud et al., 2009b). Therefore, in this project, the NO donor PROLI NONOate was dosed into the membrane module in the MBR system to determine if NO could reduce or prevent biofilm formation by the complex, multispecies biofilms on the hollow fiber membrane.

The ability of PROLI NONOate to control of biofouling was investigated by applying the donor under two different conditions. First, NO was continuously dosed into the system during operation starting at the low TMP stage. Secondly, the NO donor was back flushed through the hollow fiber membrane to remove the mature biofilm from the fouled membranes after the MBR has reached the high TMP stage. It was observed that the increase in fouling resistance was delayed in the PROLI treated membrane module for both sets of experiments. Compared to the untreated module, when the PROLI was applied at the low TMP stage, there was a 28.2% reduction of fouling resistance. Similarly, the addition of PROLI by

backwashing onto the membrane surface at the high TMP stage also caused a 50% reduction of fouling resistance. In combination, these results suggested that biofilm dispersal by NO can reduce fouling resistance in MBRs. These findings were supported by the simultaneous reduction of the biopolymers and cells on the membrane surface. The CLSM images showed that, when applying the PROLI NONOate at the low TMP stage, the biomass of biofouling components were all reduced. For example, there was a 66.7% reduction in microorganisms and a 37.7% reduction in the proteins. Since there were residual proteins and cells after NO treatment, this may explain why the fouling resistance was reduced but not prevented completely. The dispersal effect of PROLI NONOate had also been studied with pure culture biofilms, where a 30% reduction of microbial cells was observed when the biofilms were treated with 80 μM PROLI NONOate for 1 h (Barnes et al., 2013). This result was consistent with the findings reported here where the mixed microbial biofilm on the hollow fiber membranes were partly dispersed, indicating that NO can disperse not only the pure culture biofilms but also complex, mixed species biofilms. In contrast with the results presented in this thesis, the biofilm reduction efficiency of NO treatment was as high as 80% for the SNP induced dispersal of *P. aeruginosa* biofilms and 99% for the biofilm dispersal by the NO releasing silica nanoparticles (Barraud et al., 2006; Hetrick et al., 2009). One difference between the work presented here and previous studies is that the NO donor PROLI NONOate was tested here while other NO donors, such as SNP have been used. Since NO donors have different spontaneous NO release rates and these are often related to pH and temperature, the rate of NO release and peak amount of NO generated could have a dramatic influence on its ability to disperse microbial biofilms. For example, SNP has been reported to have a half-life of 1 - 2 min while the half-life for the PROLI NONOate is just 1.8 s at 37 ^{o}C (pH 7.4) (Friederich JA and Butterworth JF, 1995; Saavedra et al., 1996). Additionally, the communities to be dispersed from the MBR membranes were a complex mixture of bacteria and fungi. It was observed that the biofilms collected from the MBRs in this project were composed of at least 150 genera of bacteria and 25 genera of fungi in the microbial community. In contrast, much of the published work demonstrating the efficacy of NO has been performed using pure culture biofilms. These differences may explain the relatively low reduction efficiency of NO treatment in this project compared other published data. Indeed, it was reported that the exposure of 500 nM SNP resulted in 15% reduction of mixed species biofilms in water distribution system and 30% reduction of mixed species biofilms on RO membrane (Barraud et al., 2009a). However, combining the SNP treatment and chlorine disinfection can improve the reduction efficiency to the mixed species biofilms (94% reduction) (Barraud et al., 2009a). This suggested the reduction efficiency of biofilm by

PROLI NONOate may be enhanced in combination with the chemical treatment, e.g. chlorine disinfection and antibiotics killing.

In addition to NO, methods based on interfering with molecular signaling pathways, such as quorum quenching strategy, have been reported for the control of biofouling in MBRs. It was reported that the Porcine kidney acylase I, which is a quenching enzyme of *N*-acyl homoserine lactone (AHL) autoinducers, can prevent the biofouling behavior (approximately 26% - 46% reduction in TMP) in MBR (Yeon et al., 2009a; Yeon et al., 2009b). The production of polysaccharides and proteins was reduced 87.7% and 86.9% respectively due to the application of an immobilized acylase (Yeon et al., 2009a). Using alginate encapsulation of quorum quenching bacteria, *Rhodococcus* sp. BH4, it was shown that the time required for the TMP to increase to 70 kPa was delayed 10 fold and the amounts of EPS and microorganisms was reduced 80% and 58.5% respectively (Kim et al., 2013). In another study, encapsulation of *Escherichia coli* which producing N-acyl homoserine lactonase inside the lumen of microporous hollow fiber membrane increased 80 d of MBR operation (Oh et al., 2012). While previous studies did not assess the effect of such QS inhibitors on the relative community composition, it was observed here that NO treatment resulted in general dispersal of the microbial community, although some groups did not disperse to the same extent as others. For example, *Rhodospirillales*, *Rhizobiales* were observed to be enriched in the biofilms after NO dosing, while the relative abundances of *Gemmatimonadales* and *Xanthomonadales*, which were correlated with the TMP jump, were reduced after PROLI NONOate treatment. The results presented in this thesis suggest that NO can control MBR fouling and this could be improved through further optimization of the specific NO donor, the concentrations used as well as the dosing regime used.

6.5 Recommendations for the future works

Although much effort has been put in this study, it should be noted that the mechanisms of biofouling formation are still not completely clear and the efficiency of the biofouling prevention by NO is not as good as is needed for it to be commercially relevant. Therefore, more work is required to increase our knowledge of how biofouling occurs and to enhance anti-biofouling strategies such as the NO, so that they are viable alternatives to the use of toxic biocides. First, since the protein component is recognized as a dominant biopolymer during the TMP increase, it is necessary to elucidate the detailed compositions of the protein component. With this knowledge, the specific enzymes may be selected to break down the linkage of the proteins and other components, such as polysaccharides and bacteria. Second,

the key groups of bacterial and fungal communities have been revealed in this study. The next step may be focus how these organisms form the biofilms on membranes, such as through EPS production and their interactions with different microbial groups to facilitate mixed species biofilm formation. Third, it has been demonstrated that the QS signals were involved in the TMP increase of MBR (Yeon et al., 2009b). Thus, it may be valuable to investigate the diversity of the QS signals and whether the QS signals changed at different stage of biofouling process. Fourth, the effect of NO treatment on the biofouling control may be improved through optimizing the delivery of NO donor compound, selecting alternative NO donor compounds and compare their effect and combining the NO treatment with the traditional chemical cleaning methods, e.g. lower concentration of sodium hypochlorite.

References

Ahn, S., Congeevaram, S., Choung, Y.K., Park, J., 2008. Enhanced phenol removal by floating fungal populations in a high concentration phenol-fed membrane bioreactor. Desalination 221, 494-501.

Al-Juboori, R.A., Yusaf, T., 2012. Biofouling in RO system: Mechanisms, monitoring and controlling. Desalination 302, 1-23.

Almeida, C., Azevedo, N.F., Santos, S., Keevil, C.W., Vieira, M.J., 2011. Discriminating Multi-Species Populations in Biofilms with Peptide Nucleic Acid Fluorescence *In Situ* Hybridization (PNA FISH). PLoS ONE 6, e14786.

Avsar, Y., Batibay, A., 2010. Ozone application as an alternative method to the chemical treatment technique for textile wastewater. Fresenius Environ. Bull. 19, 2788-2794.

Awad, M.F., Kraume, M., 2010. The occurrence of fungi in activated sludge from MBRs. WASET 71, 561-564.

Awad, M.F., Kraume, M., 2011. Keratinophilic fungi in activated sludge of wastewater treatment plants with MBR in Berlin, Germany. Mycology 2, 276-282.

Bai, X., Wu, F., Zhou, B., Zhi, X., 2010. Biofilm bacterial communities and abundance in a full-scale drinking water distribution system in Shanghai. J. Water Health 8, 593-600.

Baker, B.J., Tyson, G.W., Goosherst, L., Banfield, J.F., 2009. Insights into the diversity of eukaryotes in acid mine drainage biofilm communities. Appl. Environ. Microbiol. 75, 2192-2199.

Baker, G.C., Smith, J.J., Cowan, D.A., 2003. Review and re-analysis of domain-specific 16S primers. J Microbiol Methods 55, 541-555.

Baker, J.S., Dudley, L.Y., 1998. Biofouling in membrane systems -- A review. Desalination 118, 81-89.

Bal, A.S., Dhagat, N.N., 2001. Upflow anaerobic sludge blanket reactor - A Review. Indian J. Environ. Health 43, 1-83.

Barnes, R.J., Bandi, R.R., Wong, W.S., Barraud, N., McDougald, D., Fane, A., Kjelleberg, S., Rice, S.A., 2013. Optimal dosing regimen of nitric oxide donor compounds for the reduction of *Pseudomonas aeruginosa* biofilm and isolates from wastewater membranes. Biofouling 29, 203-212.

Barnes, R.J., Bandi, R.R., Chua, F., Low, J.H., Aung, T., Barraud, N., Fane, A.G., Kjelleberg, S., Rice, S.A., 2014. The roles of *Pseudomonas aeruginosa* extracellular polysaccharides in biofouling of reverse osmosis membranes and nitric oxide induced dispersal. J. Membr. Sci. 466, 161-172.

Barraud, N., Hassett, D.J., Hwang, S.H., Rice, S.A., Kjelleberg, S., Webb, J.S., 2006. Involvement of nitric oxide in biofilm dispersal of *Pseudomonas aeruginosa*. J. Bacteriol. 188, 7344-7353.

Barraud, N., Storey, M.V., Moore, Z.P., Webb, J.S., Rice, S.A., Kjelleberg, S., 2009a. Nitric oxide-mediated dispersal in single- and multi-species biofilms of clinically and industrially relevant microorganisms. Microbial Biotech 2, 370-378.

Barraud, N., Schleheck, D., Klebensberger, J., Webb, J.S., Hassett, D.J., Rice, S.A., Kjelleberg, S., 2009b. Nitric oxide signaling in *Pseudomonas aeruginosa* biofilms mediates phosphodiesterase activity, decreased cyclic di-GMP levels, and enhanced dispersal. J Bacteriol 191, 7333-7342.

Bergheim, A., Sanni, S., Indrevik, G., Hølland, P., 1993. Sludge removal from salmonid tank effluent using rotating microsieves. Aquacult. Eng. 12, 97-109.

Bernier, S.P., Lebeaux, D., DeFrancesco, A.S., Valomon, A., Soubigou, G., Coppée, J.-Y., Ghigo, J.-M., Beloin, C., 2013. Starvation, together with the SOS response, mediates high biofilm-specific tolerance to the fluoroquinolone ofloxacin. PLoS Genet. 9, e1003144.

Bojsen, R.K., Andersen, K.S., Regenberg, B., 2012. *Saccharomyces cerevisiae* - a model to uncover molecular mechanisms for yeast biofilm biology. FEMS Immunol. Med. Microbiol. 65, 169-182.

Bridier, A., Briandet, R., Thomas, V., Dubois-Brissonnet, F., 2011. Resistance of bacterial biofilms to disinfectants: A review. Biofouling 27, 1017-1032.

Calderón, K., Rodelas, B., Cabirol, N., González-López, J., Noyola, A., 2011. Analysis of microbial communities developed on the fouling layers of a membrane-coupled anaerobic bioreactor applied to wastewater treatment. Bioresour. Technol. 102, 4618-4627.

Cantrell, K.B., Szogi, A.A., Hunt, P.G., Vanotti, M.B., 2007. Effect of solid separation and composting on the energy content of swine manure, 2007 ASABE Annual International Meeting, Minneapolis, MN.

Chandrasekar, P.H., Manavathu, E.K., 2008. Do *Aspergillus* species produce biofilm? Future Microbiol. 3, 19-21.

Chen, M.Y., Lee, D.J., Tay, J.H., 2006a. Extracellular polymeric substances in fouling layer. Sep. Sci. Technol. 41, 1467-1474.

Chen, M.Y., Lee, D.J., Tay, J.H., Show, K.Y., 2007. Staining of extracellular polymeric substances and cells in bioaggregates. Appl Microbiol Biotechnol 75, 467-474.

Chen, M.Y., Lee, D.J., Yang, Z., Peng, X.F., Lai, J.Y., 2006b. Fluorecent staining for study of extracellular polymeric substances in membrane biofouling layers. Environ. Sci. Technol. 40, 6642-6646.

Chen, X., Suwarno, S.R., Chong, T.H., McDougald, D., Kjelleberg, S., Cohen, Y., Fane, A.G., Rice, S.A., 2013. Dynamics of biofilm formation under different nutrient levels and the effect on biofouling of a reverse osmosis membrane system. Biofouling 29, 319-330.

Cho, B.D., Fane, A.G., 2002. Fouling transients in nominally sub-critical flux operation of a membrane bioreactor. J. Membr. Sci. 209, 391-403.

Cho, J., Song, K.G., Chung, T.H., 2005. Quantitative analysis of biological effect on membrane fouling in submerged membrane bioreactor. Water Sci. Technol. 51, 9-18.

Cicek, N., 2003. A review of membrane bioreactors and their potential application in the treatment of agricultural wastewater. Can. Biosyst. Eng. 45, 637-649.

Clarke, K.R., 1993. Non-parametric multivariate analyses of changes in community structure. Aust J Ecol 18, 117-143.

Clarke, K.R., Gorley, R.N., 2006. PRIMER v6: User manual/tutorial. PRIMER-E Ltd, Plymouth.

Comte, S., Guibaud, G., Baudu, M., 2006. Biosorption properties of extracellular polymeric substances (EPS) resulting from activated sludge according to their type: Soluble or bound. Process Biochem. 41, 815-823.

Costello, E.K., Lauber, C.L., Hamady, M., Fierer, N., Gordon, J.I., Knight, R., 2009.

Bacterial community variation in human body habitats across space and time. Science 326, 1694-1697.

da Silva, E.S., Feres, M., Figueiredo, L.C., Shibli, J.A., Ramiro, F.S., Faveri, M., 2014. Microbiological diversity of peri-implantitis biofilm by Sanger sequencing. Clin. Oral Implants. Res. 25, 1192-1199.

de Nys, R.W., A. D.; Konig, G. M.; Sticher, O.,, 1993. New halogenated furanones from the marine alga *Delisea pulchra* (cf. fimbriata). Tetrahedron 49, 11213-11220.

Douterelo, I., Sharpe, R., Boxall, J., 2014. Bacterial community dynamics during the early stages of biofilm formation in a chlorinated experimental drinking water distribution system: implications for drinking water discolouration. J Appl. Microbiol. 177, 286-301.

Dunn, K.W., Kamocka, M.M., McDonald, J.H., 2011. A practical guide to evaluating colocalization in biological microscopy. AM J. Physiol.-Cell PH. 300, C723-C742.

E Postma, C Verduyn, W A Scheffers, Dijken, J.P.V., 1989. Enzymic analysis of the crabtree effect in glucose-limited chemostat cultures of *Saccharomyces cerevisiae*. Appl. Environ. Microbiol. 55, 468-477.

Field, R.W., Wu, D., Howell, J.A., Gupta, B.B., 1995. Critical flux concept for microfiltration fouling. J. Membr. Sci. 100, 259-272.

Foster, M.L., Dowd, S.E., Stephenson, C., Steiner, J., Suchodolski, J.S., 2013. Characterization of the fungal microbiome (mycobiome) in fecal samples from dogs. Vet Med Int 2013, 8.

Fowler, J., Cohen, L., Jarvis, P., 1998. Practical statistics for field biology. John Wiley & Sons Ltd, p83-89 pp.

Friederich JA, Butterworth JF, 1995. Sodium nitroprusside: twenty years and counting. Anesth. Analg. 81, 152-162.

Gao, D.-W., Wen, Z.-D., Li, B., Liang, H., 2013a. Membrane fouling related to microbial community and extracellular polymeric substances at different temperatures. Bioresour. Technol. 143, 172-177.

Gao, D., Fu, Y., Ren, N., 2013b. Tracing biofouling to the structure of the microbial community and its metabolic products: A study of the three-stage MBR process. Water Res. 47, 6680-6690.

Gillings, M.R., Holley, M.P., Selleck, M., 2006. Molecular identification of species comprising an unusual biofilm from a groundwater treatment plant. Biofilms 3, 19-24.

Griffiths, R.I., Whiteley, A.S., O'Donnell, A.G., Bailey, M.J., 2000. Rapid method for coextraction of DNA and RNA from natural environments for analysis of ribosomal DNA- and rRNA-based microbial community composition. Appl. Environ. Microbiol. 66, 5488-5491.

Guardiola, F.A., Cuesta, A., Meseguer, J., Esteban, M.A., 2012. Risks of using antifouling biocides in aquaculture. Int. J. Mol. Sci. 13, 1541-1560.

Hai, F.I., Yamamoto, K., Nakajima, F., Fukushi, K., 2011. Bioaugmented membrane bioreactor (MBR) with a GAC-packed zone for high rate textile wastewater treatment. Water Res. 45, 2199-2206.

Hai, F.I., Yamamoto, K., Nakajima, F., Fukushi, K., Nghiem, L.D., Price, W.E., Jin, B., 2013. Degradation of azo dye acid orange 7 in a membrane bioreactor by pellets and attached growth of *Coriolus versicolour*. Bioresour. Technol. 141, 29-34.

Handl, S., Dowd, S.E., Garcia-Mazcorro, J.F., Steiner, J.M., Suchodolski, J.S., 2011. Massive parallel 16S rRNA gene pyrosequencing reveals highly diverse fecal bacterial and fungal communities in healthy dogs and cats. FEMS Microbiol. Ecol. 76, 301-310.

Hentzer, M., L. Eberl, M. Givskov, 2005. Transcriptome analysis of *Pseudomonas aeruginosa* biofilm development: anaerobic respiration and iron limitation. Biofilms 2, 37-61.

Hentzer, M.W., H.; Andersen, J. B.; Riedel, K.; Rasmussen, T. B.;, Bagge, N.K., N.; Schembri, M. A.; Song, Z. J.; Kristoffersen, P.;, Manefield, M.C., J. W.; Molin, S.; Eberl, L.; Steinberg, P.;, Kjelleberg, S.H., N.; Givskov, M.,, 2003. Attenuation of *Pseudomonas aeruginosa* virulence by quorum sensing inhibitors. EMBO J. 22, 3803-3815.

Her, N., Amy, G., Plottu-Pecheux, A., Yoon, Y., 2007. Identification of nanofiltration membrane foulants. Water Res. 41, 3936-3947.

Hetrick, E.M., Shin, J.H., Paul, H.S., Schoenfisch, M.H., 2009. Anti-biofilm efficacy of nitric oxide-releasing silica nanoparticles. Biomaterials 30, 2782-2789.

Huang, L.N., De Wever, H., Diels, L., 2008. Diverse and distinct bacterial communities induced biofilm fouling in membrane bioreactors operated under different conditions. Environ. Sci. Technol. 42, 8360-8366.

Huang, Y., Zeng, Y., Yu, Z., Zhang, J., Feng, H., Lin, X., 2013. In silico and experimental methods revealed highly diverse bacteria with quorum sensing and aromatics biodegradation systems--a potential broad application on bioremediation. Bioresour Technol 148, 311-316.

Huber, B.R., K.; Hentzer, M.; Heydorn, A.; Gotschlich, A.; Givskov, M.; Molin, S.; Eberl, L.;, 2001. The cep quorum-sensing system of *Burkholderia cepacia* H111 controls biofilm formation and swarming motility. Microbiology-Sgm 147, 2517-2528.

Hulsmans, A., Joris, K., Lambert, N., Rediers, H., Declerck, P., Delaedt, Y., Ollevier, F., Liers, S., 2010. Evaluation of process parameters of ultrasonic treatment of bacterial suspensions in a pilot scale water disinfection system. Ultrasonics sonochem. 17, 1004-1009.

Hwang, B.-K., Lee, C.-H., Chang, I.-S., Drews, A., Field, R., 2012. Membrane bioreactor: TMP rise and characterization of bio-cake structure using CLSM-image analysis. J. Membr. Sci. 419–420, 33-41.

Itoh.K;, T.T.H.T., 1995. Crossflow filtration of baker's yeast with periodical stopping of permeation flow and bubbling. Biotechnol. Bioeng. 47, 401-404.

Ivnitsky, H., Katz, I., Minz, D., Volvovic, G., Shimoni, E., Kesselman, E., Semiat, R., Dosoretz, C.G., 2007. Bacterial community composition and structure of biofilms developing on nanofiltration membranes applied to wastewater treatment. Water Res. 41, 3924-3935.

Iyer, L.M., Anantharaman, V., Aravind, L., 2003. Ancient conserved domains shared by animal soluble guanylyl cyclases and bacterial signaling proteins. BMC genomics 4, 5-12.

J. Buffle, G.G.L., 1995. Characterization of aquatic colloids and macromolecules. 1. Structure and behavior of colloidal material. Environ. Sci. Technol. 29, 2169-2175.

J. Moghadasi, H.M.-S., M. Jamialahmadi, and A. Sharif, 2007. Scale deposition in porous media and their removal by EDTA injection ECI Engineering Conferences International Symposium Series, Heat Exchanger Fouling and Cleaning VII, pp. 57-

70.

J. Rubio, Rosa, J.J., 2007. Flotation in water and wastewater treatment and reuse: recent trends in Brazil. Int. J. Environ. Pollut. 30, 193.

James, H., Ghannoum, M., Jurevic, R., 2011. The story of biofilms. J Invas Fungal Infect 5, 37-42.

Janga, N., Ren, X., Kim, G., Ahn, C., Cho, J., Kim, I.S., 2007. Characteristics of soluble microbial products and extracellular polymeric substances in the membrane bioreactor for water reuse. Desalination 202, 90-98.

Jangkorn, S., Kuhakaew, S., Theantanoo, S., Klinla-or, H., Sriwiriyarat, T., 2011. Evaluation of reusing alum sludge for the coagulation of industrial wastewater containing mixed anionic surfactants. J Environ Sci 23, 587-594.

Jiao, Y., D'Haeseleer, P., Dill, B.D., Shah, M., Verberkmoes, N.C., Hettich, R.L., Banfield, J.F., Thelen, M.P., 2011. Identification of biofilm matrix-associated proteins from an acid mine drainage microbial community. Appl. Environ. Microbiol. 77, 5230-5237.

Keener, N.G.C.J.P., 2004. The role of the biofilm matrix in structural development . Math. Med. Biol. 21, 147-166.

Khan, R., Bhawana, P., Fulekar, M.H., 2013. Microbial decolorization and degradation of synthetic dyes: A review. Rev. Environ. Sci. Biotechnol. 12, 75-97.

Kim, D., Jung, S., Sohn, J., Kim, H., Lee, S., 2009. Biocide application for controlling biofouling of SWRO membranes — an overview. Desalination 238, 43-52.

Kim, S.R., Oh, H.S., Jo, S.J., Yeon, K.M., Lee, C.H., Lim, D.J., Lee, J.K., 2013. Biofouling control with bead-entrapped quorum quenching bacteria in membrane bioreactors: Physical and biological effects. Environ Sci Technol 47, 836-842.

Kiuru, H.J., 2001. Development of dissolved air flotation technology from the first generation to the newest (third) one (DAF in turbulent flow conditions). Water Sci. Technol. 43, 1-7.

Kolenbrander, P.E., 2000. Oral microbial communities: Biofilms, interactions, and genetic systems. Annu. Rev. Microbiol. 54, 413-437.

Kubota, H., Senda, S., Tokuda, H., Uchiyama, H., Nomura, N., 2009. Stress resistance of biofilm and planktonic *Lactobacillus plantarum* subsp. plantarum JCM 1149. Food Microbiol. 26, 592-597.

Lan, W., Li, H., Wang, W.D., Katayama, Y., Gu, J.D., 2010. Microbial community analysis of fresh and old microbial biofilms on Bayon Temple sandstone of Angkor Thom, Cambodia. Microb. Ecol. 60, 105-115.

Larsen, P., Nielsen, J.L., Dueholm, M.S., Wetzel, R., Otzen, D., Nielsen, P.H., 2007. Amyloid adhesins are abundant in natural biofilms. Environ. Microbiol. 9, 3077-3090.

Laspidou, C.S., Rittmann, B.E., 2002. A unified theory for extracellular polymeric substances, soluble microbial products, and active and inert biomass. Water Research 36, 2711-2720.

Latasa, C., Solano, C., Penadés, J.R., Lasa, I., 2006. Biofilm-associated proteins. C. R. Biol. 329, 849-857.

Lazar, E.E., Wills, R.B., Ho, B.T., Harris, A.M., Spohr, L.J., 2008. Antifungal effect of gaseous nitric oxide on mycelium growth, sporulation and spore germination of the postharvest horticulture pathogens, *Aspergillus niger*, *Monilinia fructicola* and *Penicillium italicum*. Lett Appl. Microbiol. 46, 688-692.

Le-Clech, P., Chen, V., Fane, A.G., 2006. Fouling in membrane bioreactors used in wastewater treatment. J. Membr. Sci. 284, 17-53.

Le-Clech, P., Marselina, Y., Ye, Y., Stuetz, R.M., Chen, V., 2007. Visualisation of polysaccharide fouling on microporous membrane using different characterisation techniques. J. Membr. Sci. 290, 36-45.

Le Clech, P., Jefferson, B., Chang, I.S., Judd, S.J., 2003. Critical flux determination by the flux-step method in a submerged membrane bioreactor. J. Membr. Sci. 227, 81-93.

Lee, C.H., Park, P.K., Lee, W.N., Hwang, B.K., Hong, S.H., Yeon, K.M., Oh, H.S., Chang, I.S., 2008. Correlation of biofouling with the bio-cake architecture in an MBR. Desalination 231, 115-123.

Lei, F., Xiufen, L., Jian, C., 2009. Fouling behavior of extra-cellular polysaccharide produced by micrococcus luteus during dead-end microfiltration, International conference on energy and environment technology, pp. 353-356.

Li, J., Yu, D., Wang, D., 2011. Experimental test for high saline wastewater treatment in a submerged membrane bioreactor. Desalin. Water Treat. 36, 171-177.

Li, M., Cheng, X., Guo, H., 2013. Heavy metal removal by biomineralization of urease producing bacteria isolated from soil. Int. Biodeter. Biodegr. 76, 81-85.

Lim, S., Kim, S., Yeon, K.M., Sang, B.I., Chun, J., Lee, C.H., 2012. Correlation between microbial community structure and biofouling in a laboratory scale membrane bioreactor with synthetic wastewater. Desalination 287, 209-215.

Lin, J.C.T., Lee, D.J., Huang, C., 2010. Membrane fouling mitigation: Membrane cleaning. Sep. Sci. Technol. 45, 858-872.

Liu, H., Fang, H.H., 2002. Extraction of extracellular polymeric substances (EPS) of sludges. J. Biotechnol. 95, 249-256.

Liu, R., Yu, Z., Guo, H., Liu, M., Zhang, H., Yang, M., 2012. Pyrosequencing analysis of eukaryotic and bacterial communities in faucet biofilms. Sci. Total Environ. 435-436, 124-131.

López-Ribot, J.L., 2005. Candida albicans biofilms: More than filamentation. Curr. Biol. 15, R453-R455.

Louie, J.S., Pinnau, I., Ciobanu, I., Ishida, K.P., Ng, A., Reinhard, M., 2006. Effects of polyether–polyamide block copolymer coating on performance and fouling of reverse osmosis membranes. J. Membr. Sci. 280, 762-770.

Lynch, M.J., Swift, S., Kirke, D.F., Keevil, C.W., Dodd, C.E.R., Williams, P., 2002. The regulation of biofilm development by quorum sensing in *Aeromonas hydrophila*. Environ. Microbiol. 4, 18-28.

Ma, L., Wang, J., Wang, S., Anderson, E.M., Lam, J.S., Parsek, M.R., Wozniak, D.J., 2012. Synthesis of multiple *Pseudomonas aeruginosa* biofilm matrix exopolysaccharides is post-transcriptionally regulated. Environ Microbiol 14, 1995-2005.

Madaeni, S.S., Saedi, S., Rahimpour, F., Zereshki, S., 2009. Optimization of chemical cleaning for removal of biofouling layer. Chem Prod Process Model 4, Art. No.: 16.

Melin, T., Jefferson, B., Bixio, D., Thoeye, C., De Wilde, W., De Koning, J., van der Graaf, J., Wintgens, T., 2006. Membrane bioreactor technology for wastewater treatment and reuse. Desalination 187, 271-282.

Meng, F., Zhang, H., Yang, F., Liu, L., 2007. Characterization of cake layer in submerged membrane bioreactor. Environ. Sci. Technol. 41, 4065-4070.

Meng, F., Chae, S.-R., Drews, A., Kraume, M., Shin, H.-S., Yang, F., 2009. Recent advances in membrane bioreactors (MBRs): Membrane fouling and membrane material. Water Res 43, 1489-1512.

Meng, F., Liao, B., Liang, S., Yang, F., Zhang, H., Song, L., 2010. Morphological visualization, componential characterization and microbiological identification of membrane fouling in membrane bioreactors (MBRs). J. Membr. Sci. 361, 1-14.

Miller MB, B.B., 2001. Quorum sensing in bacteria. Annu. Rev. Microbiol. 55, 165-199.

Miller, M.R., Megson, I.L., 2007. Recent developments in nitric oxide donor drugs. Br. J. Pharmacol. 151, 305-321.

Miura, Y., Watanabe, Y., Okabe, S., 2007. Membrane biofouling in pilot-scale membrane bioreactors (MBRs) treating municipal wastewater: Impact of biofilm formation. Environ. Sci. Technol. 41, 632-638.

Moxon, E.R., Kroll, J.S., 1990. The role of bacterial polysaccharide capsules as virulence factors. Curr. Top. Microbiol. Immunol. 150, 65-85.

Mutamim, N.S.A., Noor, Z.Z., Hassan, M.A.A., Yuniarto, A., Olsson, G., 2013. Membrane bioreactor: Applications and limitations in treating high strength industrial wastewater. Chem. Eng. J. 225, 109-119.

Nadell, C.D., Xavier, J.B., Levin, S.A., Foster, K.R., 2008. The Evolution of Quorum Sensing in Bacterial Biofilms. PLoS Biol. 6, e14.

Nguyen, T., Roddick, F.A., Fan, L., 2012. Biofouling of water treatment membranes: A review of the underlying causes, monitoring techniques and control measures. Membranes 2, 804-840.

O'Toole G, K.H., Kolter R., 2000. Biofilm formation as microbial development. Annu. Rev. Microbiol. 54, 49-79.

Ognier, S., Wisniewski, C., Grasmick, A., 2002. Membrane fouling during constant flux filtration in membrane bioreactors. Membr. Technol. 2002, 6-10.

Oh, H.S., Yeon, K.M., Yang, C.S., Kim, S.R., Lee, C.H., Park, S.Y., Han, J.Y., Lee, J.K., 2012. Control of membrane biofouling in MBR for wastewater treatment by quorum quenching bacteria encapsulated in microporous membrane. Environ. Sci. Technol. 46, 4877-4884.

Omer Elhag-Idris, G.E., 2006. Controlling biofilm formation in industrial water treatment systems. Ultrapure Water 23, 38-42.

Ontiveros-Valencia, A., Tang, Y., Zhao, H.P., Friese, D., Overstreet, R., Smith, J., Evans, P., Rittmann, B.E., Krajmalnik-Brown, R., 2014. Pyrosequencing analysis yields comprehensive assessment of microbial communities in pilot-scale two-stage membrane biofilm reactors. Environ. Sci. Technol. 48, 7511-7518.

Paithankar, K.R., Prasad, K.S.N., 1991. Precipitation of DNA by polyethylene-glycol and ethanol. Nucleic Acids Res 19, 1346-1346.

Pang, C.M., Liu, W.T., 2006. Biological filtration limits carbon availability and affects downstream biofilm formation and community structure. Appl. Environ. Microbiol. 72, 5702-5712.

Pang, C.M., Hong, P., Guo, H., Liu, W.T., 2005. Biofilm formation characteristics of bacterial isolates retrieved from a reverse osmosis membrane. Environ. Sci. Technol. 39, 7541-7550.

Parsek, M.R.V., D. L.; Hanzelka, B. L.; Cronan, J. E.; Greenberg, E.P., 1999. Acyl

homoserine-lactone quorum-sensing signal generation. Proc. Natl. Acad. Sci., USA 96, 4360-4365.

Phattaranawik, J.F., A. G.; Pasquier, A. C. S.; Bing, W.;, 2007. Membrane bioreactor with bubble-size transformer: Design and fouling control. AIChE J 53, 243-248.

Piasecka, A., Souffreau, C., Vandepitte, K., Vanysacker, L., Bilad, R.M., de Bie, T., Hellemans, B., de Meester, L., Yan, X., Declerck, P., Vankelecom, I.F.J., 2012. Analysis of the microbial community structure in a membrane bioreactor during initial stages of filtration. Biofouling 28, 225-238.

Pinto, A.J., Raskin, L., 2012. PCR Biases Distort Bacterial and Archaeal Community Structure in Pyrosequencing Datasets. PLoS ONE 7, e43093.

Ponnusamy, K., Paul, D., Sam Kim, Y., Kweon, J.H., 2010. 2(5H)-Furanone: A Prospective strategy for biofouling-control in membrane biofilm bacteria by quorum sensing inhibition. Braz. J. Microbiol. 41, 227-234.

Porca, E., Jurado, V., Zgur-Bertok, D., Saiz-Jimenez, C., Pasic, L., 2012. Comparative analysis of yellow microbial communities growing on the walls of geographically distinct caves indicates a common core of microorganisms involved in their formation. FEMS Microbiol. Ecol. 81, 255-266.

Porter, J.E., 2010. The activated sludge process of sewage treatment (1921). Kessinger Publishing, p 122 pp.

Pruesse, E., Quast, C., Knittel, K., Fuchs, B.M., Ludwig, W., Peplies, J., Glöckner, F.O., 2007. SILVA: A comprehensive online resource for quality checked and aligned ribosomal RNA sequence data compatible with ARB. Nucleic Acids Res 35, 7188-7196.

Puspitasari, V., Granville, A., Le-Clech, P., Chen, V., 2010. Cleaning and ageing effect of sodium hypochlorite on polyvinylidene fluoride (PVDF) membrane. Sep. Purif. Technol. 72, 301-308.

Raja, C.E., Omine, K., 2012. Characterization of boron resistant and accumulating bacteria *Lysinibacillus fusiformis* M1, *Bacillus cereus* M2, *Bacillus cereus* M3, *Bacillus pumilus* M4 isolated from former mining site, Hokkaido, Japan. J. Environ. Sci. Health A Tox. Hazard Subst. Environ. Eng. 47, 1341-1349.

Ramage, G., Rajendran, R., Sherry, L., Williams, C., 2012. Fungal Biofilm Resistance. Int. J. Microbiol. 2012, 14.

Ramage, G., Mowat, E., Jones, B., Williams, C., Lopez-Ribot, J., 2009. Our current understanding of fungal biofilms. Crit. Rev. Microbiol. 35, 340-355.

Rasmussen, T.B.B., T.; Skindersoe, M. E.; Hentzer, M.;, Kristoffersen, P.K., M.; Nielsen, J.; Eberl, L.; Givskov, M.,, 2005. Screening for quorum-sensing inhibitors (QSI) by use of a novel genetic system, the QSI selector. J. Bacteriol. 187, 1799-1814.

Ravi, S., Pierce, C., Witt, C., Wormley Jr, F.L., 2009. Biofilm formation by *Cryptococcus neoformans* under distinct environmental conditions. Mycopathologia 167, 307-314.

Regev-Shoshani, G., Crowe, A., Miller, C.C., 2013. A nitric oxide-releasing solution as a potential treatment for fungi associated with tinea pedis. J. Appl. Microbiol. 114, 536-544.

Ren, D.S., J. J.; Wood, T. K.,, 2002. Inhibition of biofilm formation and swarming of *Bacillus subtilis* by (5Z)-4-bromo-5-(bromomethylene)-3-butyl-2(5H)-furanone. Lett. Appl. Microbiol. 34, 293-299.

Reverchon, S.C., B.; Deshayes, C.; Doutheau, A.; Cotte-Pattat, N., 2002. New synthetic analogues of N-acyl homoserine lactones as agonists or antagonists of transcriptional regulators involved in bacterial quorum sensing. Bioorg. Med. Chem. Lett. 12, 1153-1157.

Rosenberger, S., Laabs, C., Lesjean, B., Gnirss, R., Amy, G., Jekel, M., Schrotter, J.C., 2006. Impact of colloidal and soluble organic material on membrane performance in membrane bioreactors for municipal wastewater treatment. Water Res. 40, 710-720.

Saavedra, J.E., Southan, G.J., Davies, K.M., Lundell, A., Markou, C., Hanson, S.R., Adrie, C., Hurford, W.E., Zapol, W.M., Keefer, L.K., 1996. Localizing antithrombotic and vasodilatory activity with a novel, ultrafast nitric oxide donor. J. Med. Chem. 39, 4361-4365.

Sainbayar, A.K., J. S.; Jung, W. J.; Lee, Y. S.; Lee, C. H., 2001. Application of surface modified polypropylene membranes to an anaerobic membrane bioreactor. Environ. Technol. 22, 1035-1042.

Salim, S., Gilissen, L., Rinzema, A., Vermuë, M.H., Wijffels, R.H., 2013. Modeling microalgal flocculation and sedimentation. Bioresour. Technol. 144, 602-607.

Sant'Anna, F.H., Almeida, L.G., Cecagno, R., Reolon, L.A., Siqueira, F.M., Machado, M.R., Vasconcelos, A.T., Schrank, I.S., 2011. Genomic insights into the versatility of the plant growth-promoting bacterium *Azospirillum amazonense*. BMC genomics 12, 409.

Schloss, P.D., Westcott, S.L., Ryabin, T., Hall, J., Hartmann, M., Hollister, E., Weber, C., 2009. Introducing mothur: open-source, platform-independent, community-supported software for describing and comparing microbial communities. Appl Environ Microbiol 75, 7537-7541.

Show, K.Y., Lee, D.J., Pan, X., 2013. Simultaneous biological removal of nitrogen-sulfur-carbon: Recent advances and challenges. Biotechnol. Adv. 31, 409-420.

Simon, M., Azam, F., 1989. Protein content and protein synthesis rates of planktonic marine bacteria. Mar. Ecol. Prog. Ser. 501, 201-213.

Sombatsompop, K., Visvanathan, C., Ben Aim, R., 2006. Evaluation of biofouling phenomenon in suspended and attached growth membrane bioreactor systems. Desalination 201, 138-149.

Sponza, D.T., 2002. Extracellular polymer substances and physicochemical properties of flocs in steady and unsteady-state activated sludge systems. Process Biochem. 37, 983-998.

Tan, K., Obendorf, S.K., 2007. Development of an antimicrobial microporous polyurethane membrane. J Membr Sci 289, 199-209.

Tardieu, E., Grasmick, A., Geaugey, V., Manem, J., 1998. Hydrodynamic control of bioparticle deposition in a MBR applied to wastewater treatment. J. Membr. Sci. 147, 1-12.

Tian, Y., Li, Z., Chen, L., Lu, Y., 2012. Role of extracellular polymeric substances (EPSs) in membrane fouling of membrane bioreactor coupled with worm reactor. Bioresour. Technol. 123, 566-573.

Tran T, B.B., Gray S, Hoang M, Ostarcevic E., 2007. An autopsy study of a fouled reverse osmosis membrane element used in a brackish water treatment plant. Water Res. 41, 3915-3923.

Vanysacker, L., Boerjan, B., Declerck, P., Vankelecom, I.F., 2014. Biofouling ecology as a

means to better understand membrane biofouling. Appl. Microbiol. Biotechnol. 98, 8047-8072.

Veerasamy, D., Supurmaniam, A., Nor, Z.M., 2009. Evaluating the use of in-situ ultrasonication to reduce fouling during natural rubber skim latex (waste latex) recovery by ultrafiltration. Desalination 236, 202-207.

Vesilind, P.A., Peirce, J.J., Weiner, R.F., 1994. Environmental engineering. Butterworth Heinemann, 545 pp.

Viessman, J.W., Hammer, M.J., Perez, E.M., Chadik, P.A., 2008. Water Supply and Pollution Control. Prentice Hall, 864 pp.

Wang, L.K., Hung, Y.T., Lo, H.H., Yapijakis, C., 2004. Handbook of industrial and hazardous wastes treatment. Taylor & Francis, 1368 pp.

Wang, X.-M., Li, X.-Y., Huang, X., 2007. Membrane fouling in a submerged membrane bioreactor (SMBR): Characterisation of the sludge cake and its high filtration resistance. Sep. Purif. Technol. 52, 439-445.

Wang, Z., Wu, Z., Tang, S., 2009. Extracellular polymeric substances (EPS) properties and their effects on membrane fouling in a submerged membrane bioreactor. Water Res. 43, 2504-2512.

Wang, Z., Zheng, Y., Xiao, Y., Wu, S., Wu, Y., Yang, Z., Zhao, F., 2013. Analysis of oxygen reduction and microbial community of air-diffusion biocathode in microbial fuel cells. Bioresour. Technol. 144, 74-79.

Wei, Q., Ma, L.Z., 2013. Biofilm matrix and its regulation in *Pseudomonas aeruginosa*. Int J Mol Sci 14, 20983-21005.

Whitchurch, C.B., Tolker-Nielsen, T., Ragas, P.C., Mattick, J.S., 2002. Extracellular DNA required for bacterial biofilm formation. Science 295, 1487.

Wu, K., Wang, H., Liu, R., Zhao, X., Liu, H., Qu, J., 2011. Arsenic removal from a high-arsenic wastewater using in situ formed Fe-Mn binary oxide combined with coagulation by poly-aluminum chloride. J. Hazard. Mater. 185, 990-995.

Xia, S., Li, J., He, S., Xie, K., Wang, X., Zhang, Y., Duan, L., Zhang, Z., 2010. The effect of organic loading on bacterial community composition of membrane biofilms in a submerged polyvinyl chloride membrane bioreactor. Bioresour. Technol. 101, 6601-6609.

Xu, H., Liu, Y., 2011. Control and cleaning of membrane biofouling by energy uncoupling and cellular communication. Environ. Sci. Technol. 45, 595-601.

Yan, X., Bilad, M.R., Gerards, R., Vriens, L., Piasecka, A., Vankelecom, I.F.J., 2012. Comparison of MBR performance and membrane cleaning in a single-stage activated sludge system and a two-stage anaerobic/aerobic (A/A) system for treating synthetic molasses wastewater. J. Membr. Sci. 394–395, 49-56.

Yang, C., Zhang, W., Liu, R., Li, Q., Li, B., Wang, S., Song, C., Qiao, C., Mulchandani, A., 2011. Phylogenetic diversity and metabolic potential of activated sludge microbial communities in full-scale wastewater treatment plants. Environ. Sci. Technol. 45, 7408-7415.

Yeon, K.M., Lee, C.H., Kim, J., 2009a. Magnetic enzyme carrier for effective biofouling control in the membrane bioreactor based on enzymatic quorum quenching. Environ Sci Technol 43, 7403-7409.

Yeon, K.M., Cheong, W.S., Oh, H.S., Lee, W.N., Hwang, B.K., Lee, C.H., Beyenal, H.,

Lewandowski, Z., 2009b. Quorum sensing: A new biofouling control paradigm in a membrane bioreactor for advanced wastewater treatment. Environ Sci Technol 43, 380-385.

Yu, J., Baek, Y., Yoon, H., Yoon, J., 2013. New disinfectant to control biofouling of polyamide reverse osmosis membrane. J. Membr. Sci. 427, 30-36.

Zhang, K., Choi, H., Dionysiou, D.D., Oerther, D.B., 2008. Application of membrane bioreactors in the preliminary treatment of early planetary base wastewater for long duration space missions. Water Environ. Res. 80, 2209-2218.

Zhang, K., Choi, H., Wu, M., Sorial, G.A., Dionysiou, D., Oerther, D.B., 2007. An ecology-based analysis of irreversible biofouling in membrane bioreactors. Water Sci Technol 55, 395-402.

Zinchuk, V., Zinchuk, O., 2001. Quantitative colocalization analysis of confocal fluorescence microscopy images, Curr. protoc. cell biol. John Wiley & Sons, Inc.

Appendix A The supplementary information for Chapter 3

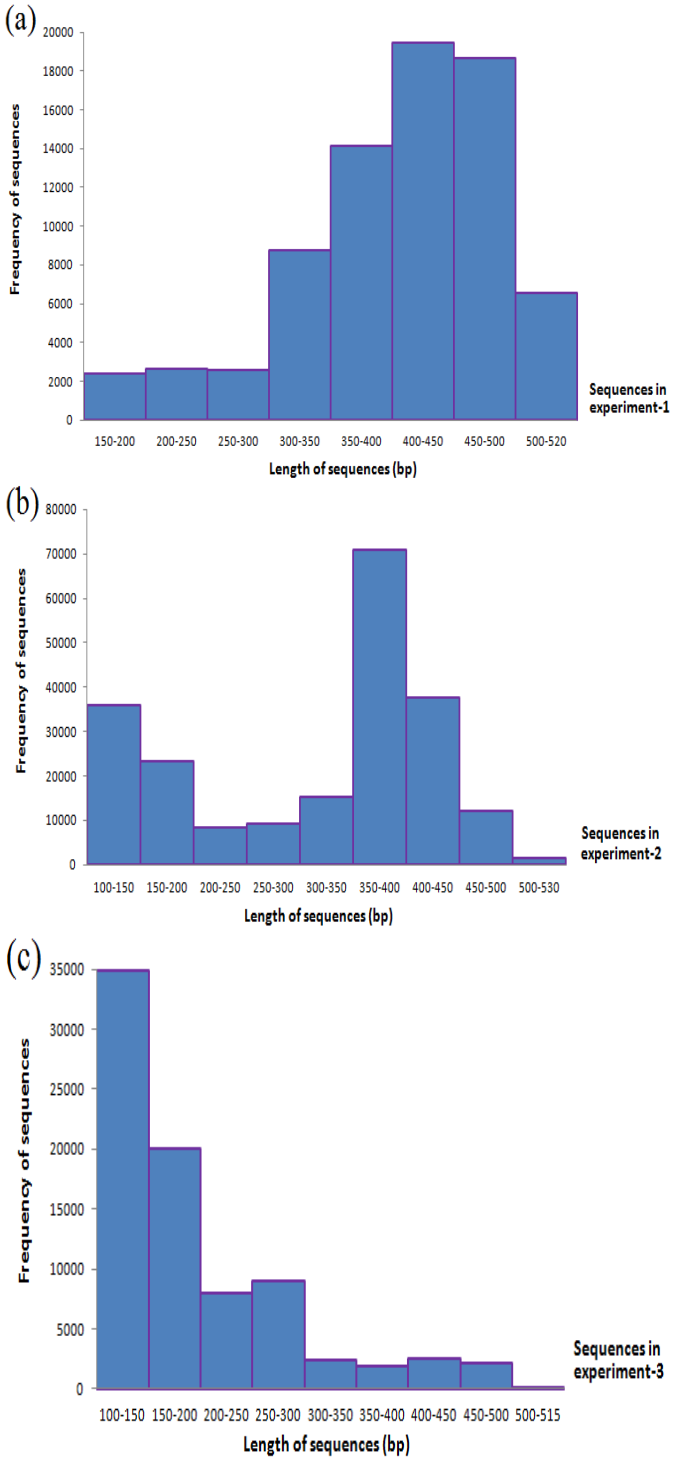

Fig. S3.1 The distribution of sequences in the sequence package in experiment-1 (a), experiment-2 (b) and experiment-3 (c) after the sequence process with MOTHUR.

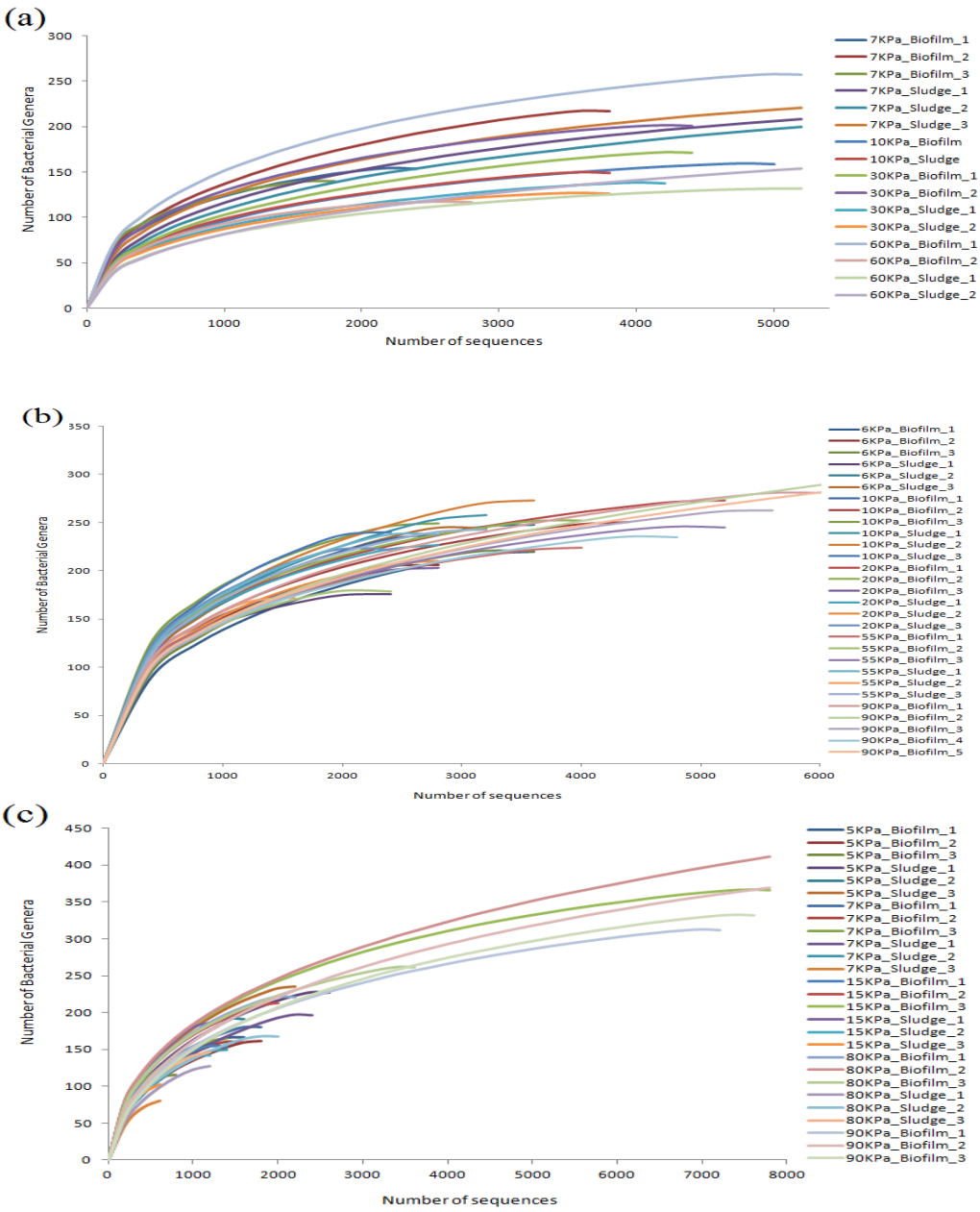

Fig. S3.2 The rarefaction curves for the bacterial community in sludge and biofilm in experiment-1 (a), experiment-2 (b) and experiment-3 (c). The "x" axis shows the sequence number in the datasets. The "y" axis shows the number of bacterial genera identified from the sequences, as calculated using the software package "MOTHUR" with the "rarefaction.single" command.

(a)

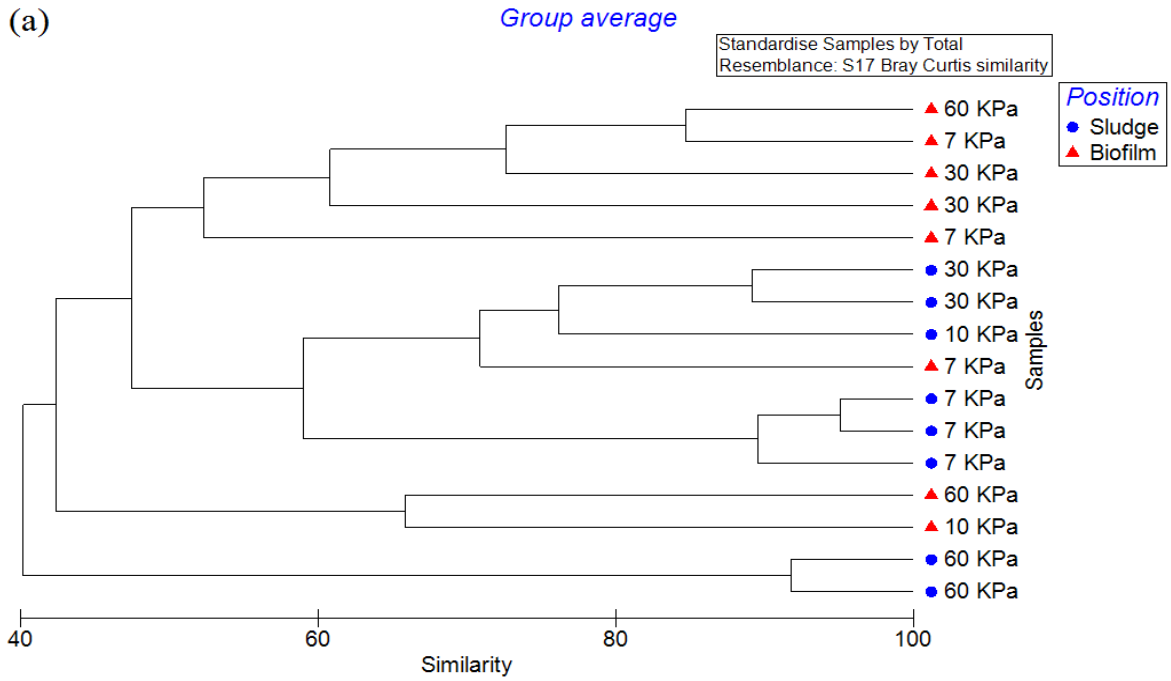
Group average
Standardise Samples by Total
Resemblance: S17 Bray Curtis similarity
Position
Sludge
Biofilm
60 KPa
7 KPa
30 KPa
30 KPa
7 KPa
30 KPa
30 KPa
10 KPa
7 KPa
7 KPa
7 KPa
7 KPa
60 KPa
10 KPa
60 KPa
60 KPa
Samples
40
60
80
100
Similarity

(b)

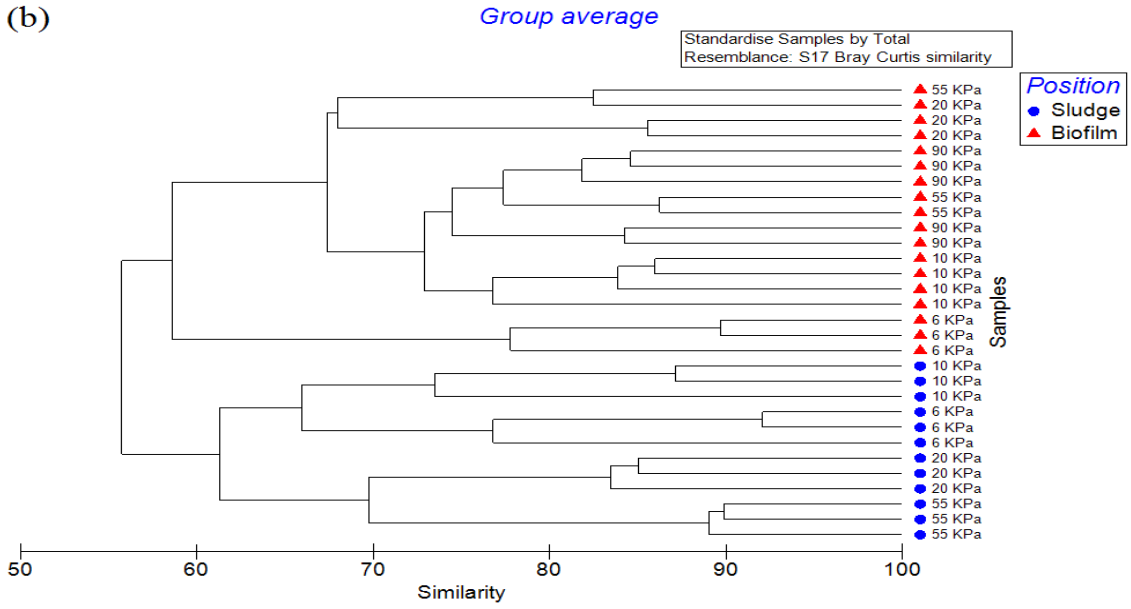
Group average
Standardise Samples by Total
Resemblance: S17 Bray Curtis similarity
Position
Sludge
Biofilm
55 KPa
20 KPa
20 KPa
20 KPa
90 KPa
90 KPa
90 KPa
55 KPa
55 KPa
90 KPa
90 KPa
10 KPa
10 KPa
10 KPa
10 KPa
6 KPa
6 KPa
6 KPa
10 KPa
10 KPa
10 KPa
6 KPa
6 KPa
6 KPa
20 KPa
20 KPa
20 KPa
55 KPa
55 KPa
55 KPa
Samples
50
60
70
80
90
100
Similarity

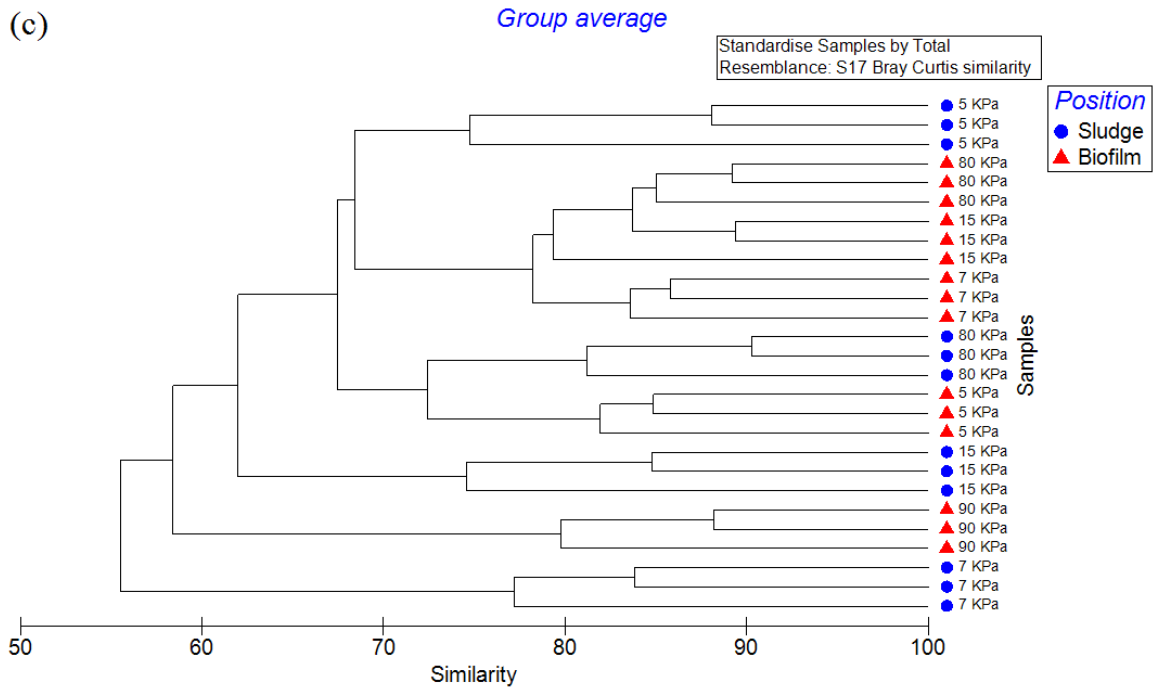

Fig. S3.3 (Continued from previous page) The phylogenetic tree at the Order level for biofilms and activated sludge samples in the experiment-1 (a), experiment-2 (b) and experiment-3 (c). The Bray-Curtis similarity between samples was calculated with the raw abundance data. The blue circles represent the bacterial communities in the sludge, and the red triangles represent the bacterial communities in the biofilms. The relationships amongst samples were displayed based on the Bray-Curtis similarity between bacterial communities.

(a)

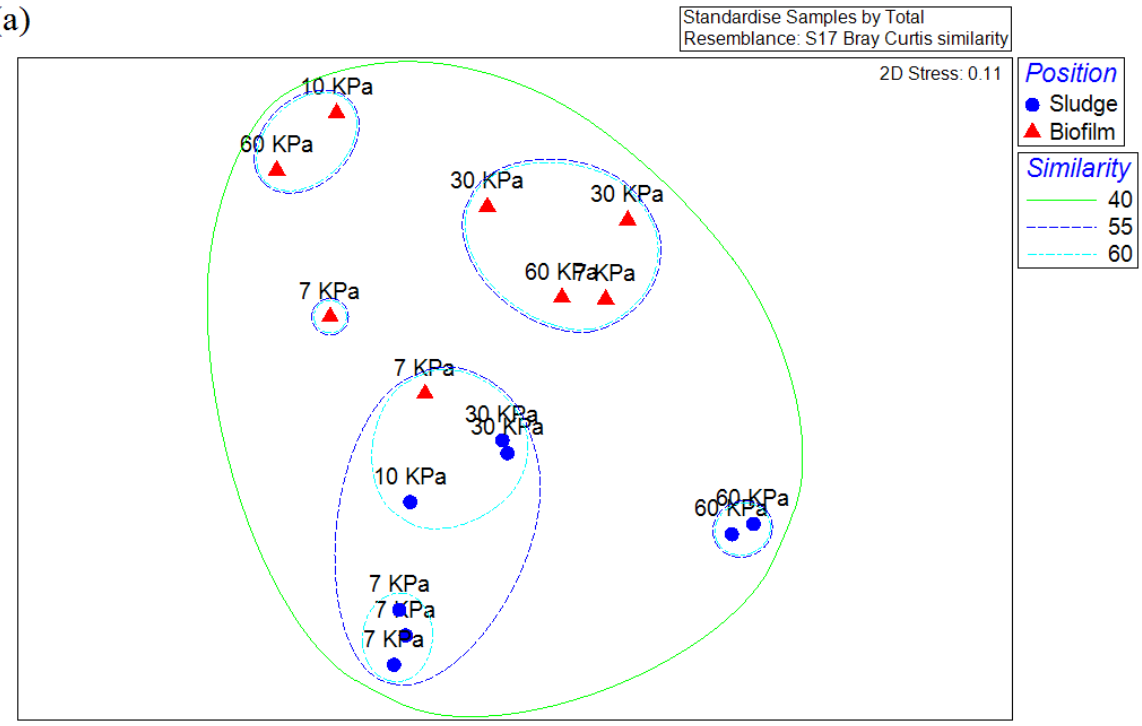
Standardise Samples by Total
Resemblance: S17 Bray Curtis similarity
2D Stress: 0.11
Position
Sludge
Biofilm
Similarity
40
55
60
10 KPa
60 KPa
30 KPa
30 KPa
60 KPa
7 KPa
7 KPa
7 KPa
30 KPa
30 KPa
10 KPa
60 KPa
60 KPa
7 KPa
7 KPa
7 KPa

(b)

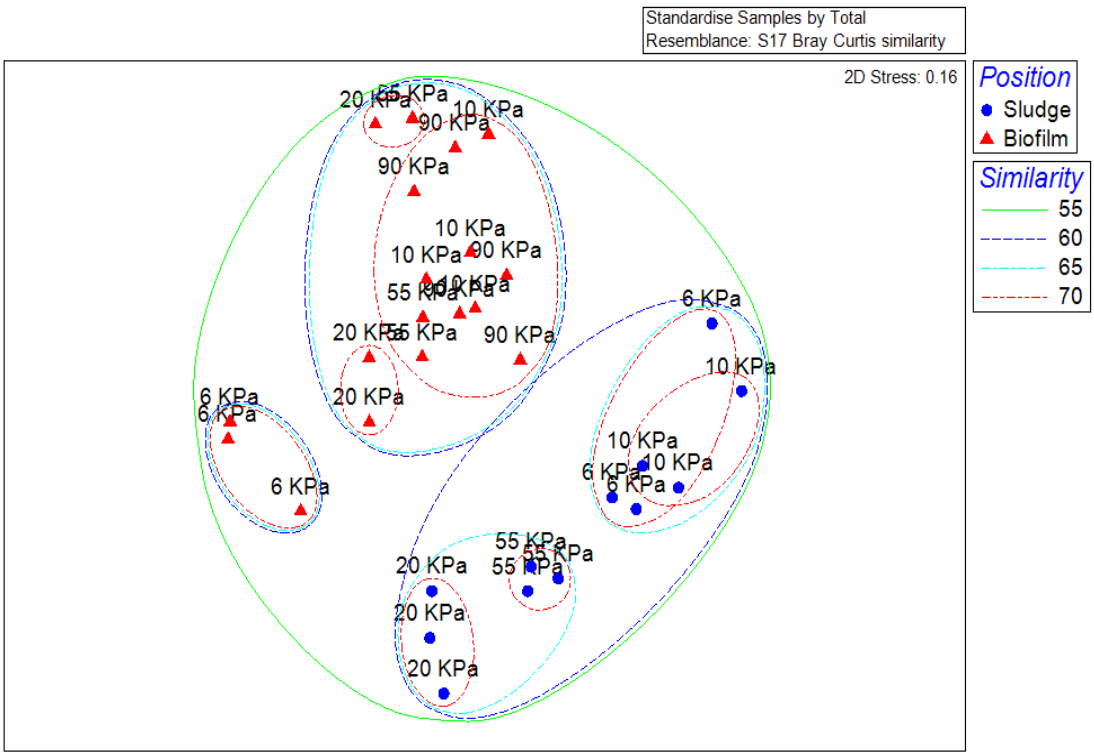
Standardise Samples by Total
Resemblance: S17 Bray Curtis similarity
2D Stress: 0.16
Position
Sludge
Biofilm
Similarity
55
60
65
70
20 KPa
10 KPa
90 KPa
90 KPa
10 KPa
10 KPa
90 KPa
55 KPa
20 KPa
55 KPa
90 KPa
20 KPa
6 KPa
6 KPa
6 KPa
6 KPa
10 KPa
10 KPa
6 KPa
6 KPa
55 KPa
55 KPa
55 KPa
20 KPa
20 KPa
20 KPa

(c)

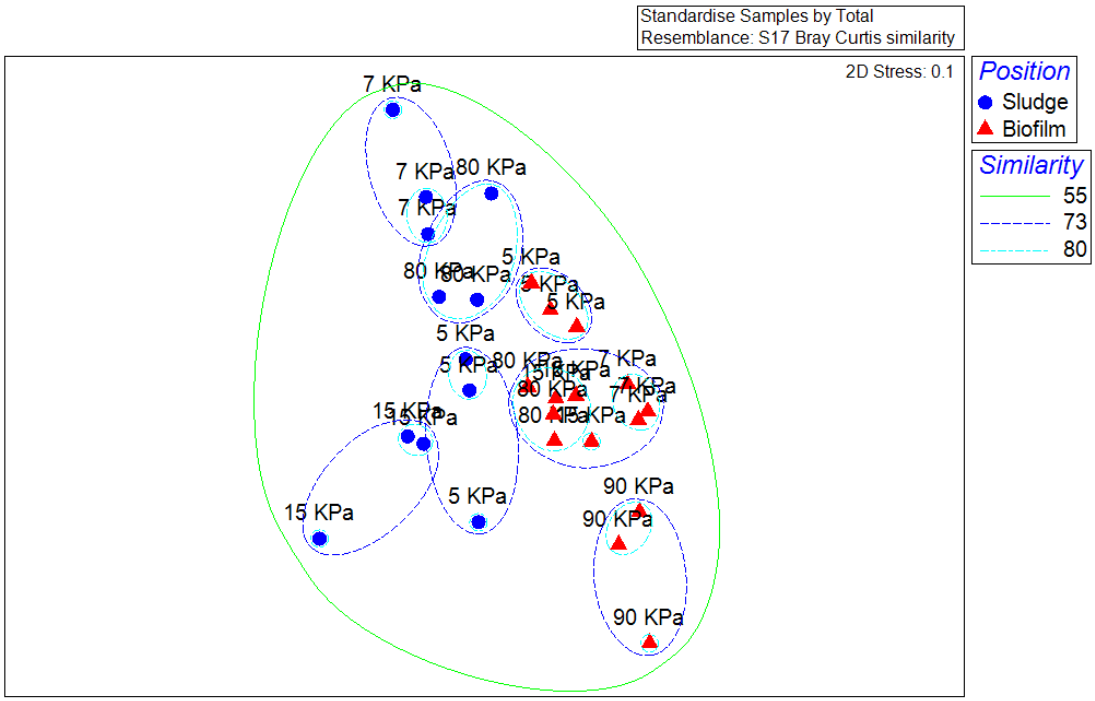

Fig. S3.4 (Continued from previous page) The NMDS analysis at the Order level for biofilms and activated sludge samples for experiment-1 (a), experiment-2 (b) and experiment-3 (c). The Bray-Curtis similarity between samples was calculated with the raw abundance data. The blue circles represent the bacterial communities in sludge, and the red triangles represent the bacterial communities in biofilms. The dotted lines show the average Bray-Curtis similarities between samples, where the colored lines indicate different percentage similarities.

Appendix B The supplementary information for Chapter 4

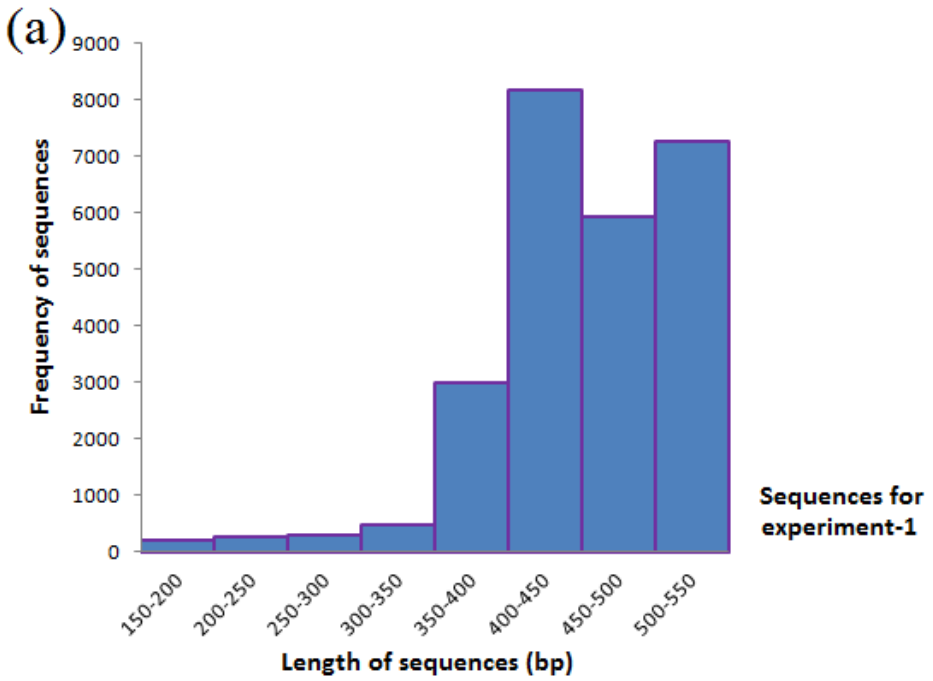

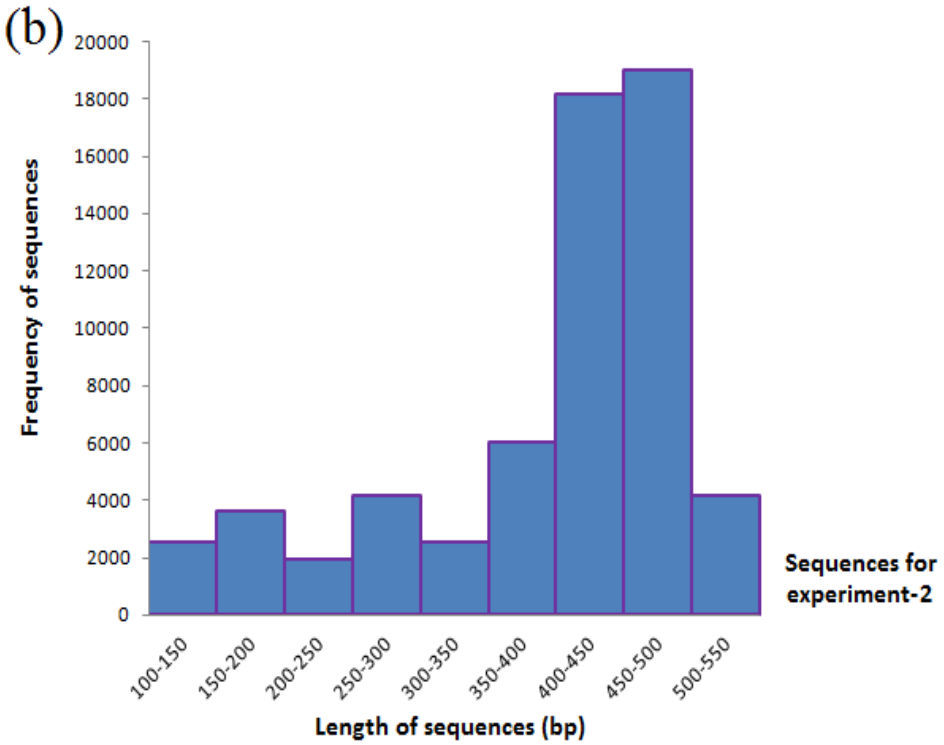

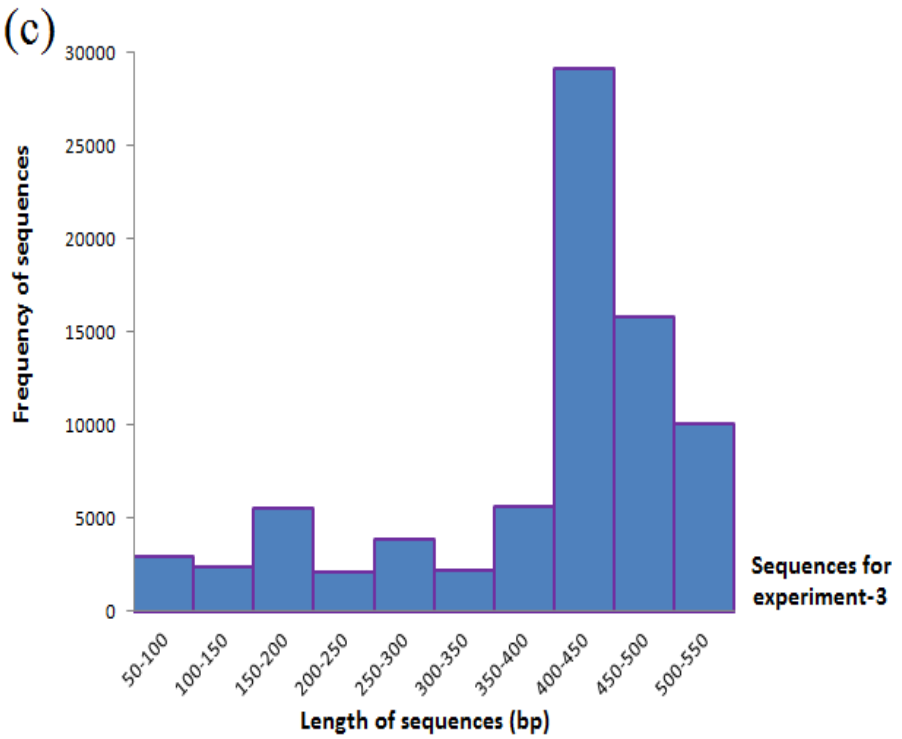

Fig. S4.1 (Continued from the previous page) The frequency of sequences for the samples in the triplicate experiments, experiment-1 (a), experiment-2 (b), and experiment-3 (c). The "x" axis shows the sequence read lengths. The "y" axis shows the number of the sequences with different sequence lengths.

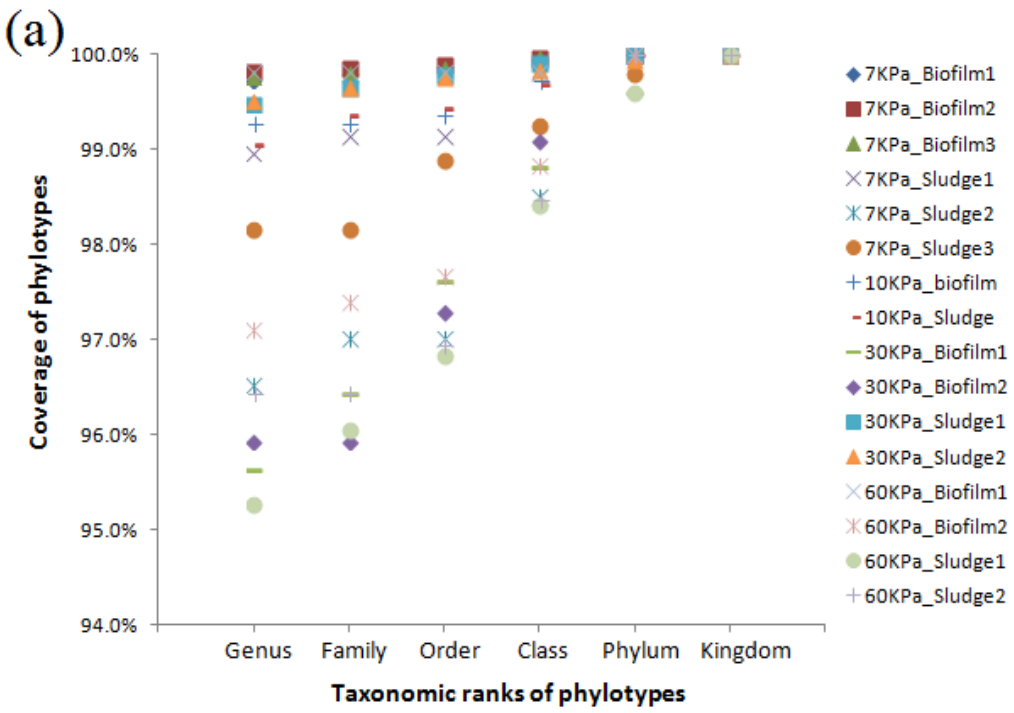

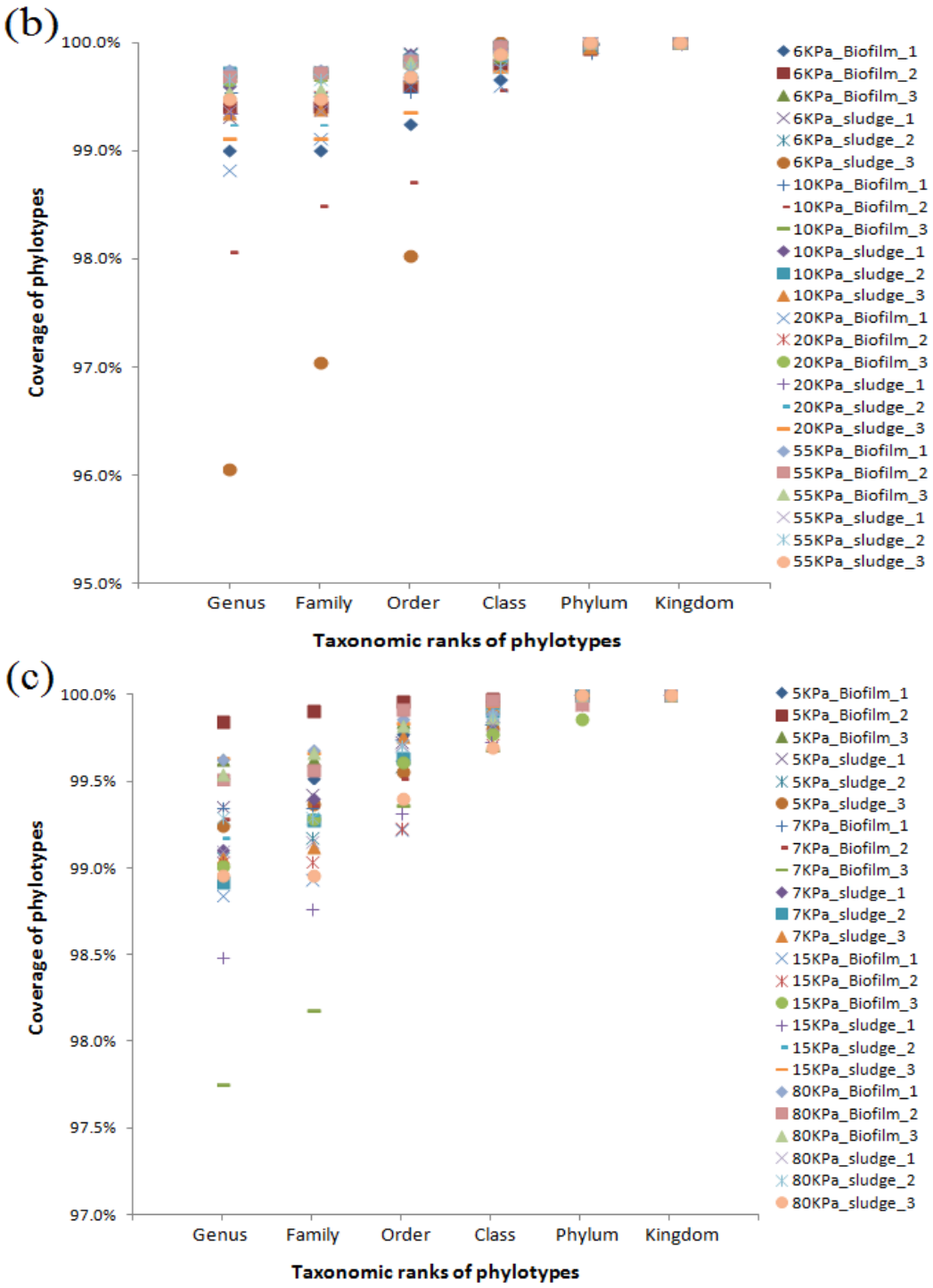

Fig. S4.2 (Continued from the previous page) The coverage of fungal phylotypes at different taxonomic ranks for experiment-1 (a), experiment-2 (b) and experiment-3 (c). The coverage values were calculated using the "summary.single" command of MOTHUR. The x-axis shows the taxonomic ranks for the phylotypes in the datasets. The y-axis shows the percent coverage of phylotypes at different taxonomic ranks.

(a)

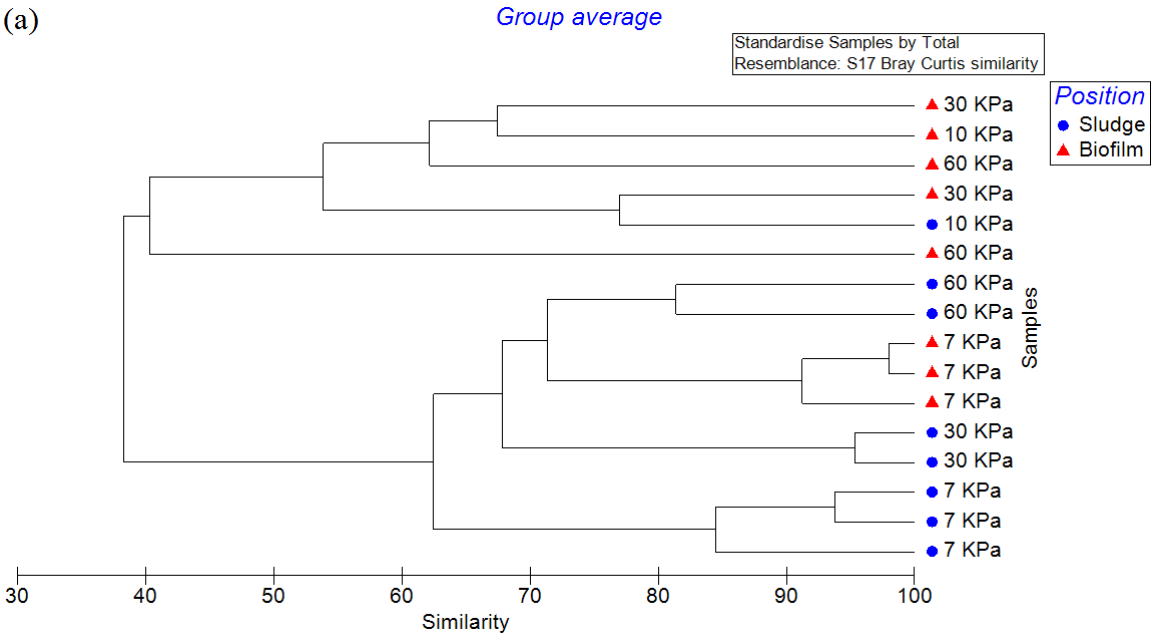
Group average
Standardise Samples by Total
Resemblance: S17 Bray Curtis similarity
Position
Sludge
Biofilm
30 KPa
10 KPa
60 KPa
30 KPa
10 KPa
60 KPa
60 KPa
60 KPa
7 KPa
7 KPa
7 KPa
30 KPa
30 KPa
7 KPa
7 KPa
7 KPa
Samples
30
40
50
60
70
80
90
100
Similarity

(b)

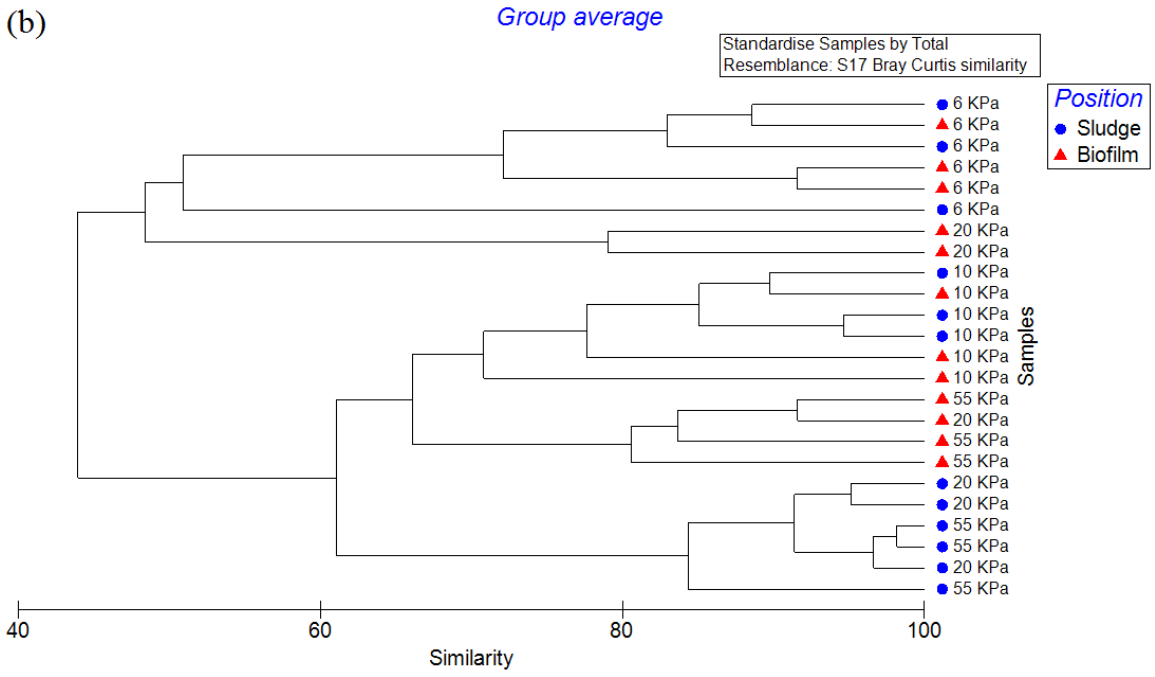
Group average
Standardise Samples by Total
Resemblance: S17 Bray Curtis similarity
Position
Sludge
Biofilm
6 KPa
6 KPa
6 KPa
6 KPa
6 KPa
6 KPa
20 KPa
20 KPa
10 KPa
10 KPa
10 KPa
10 KPa
10 KPa
10 KPa
55 KPa
20 KPa
55 KPa
55 KPa
20 KPa
20 KPa
55 KPa
55 KPa
20 KPa
55 KPa
Samples
40
60
80
100
Similarity

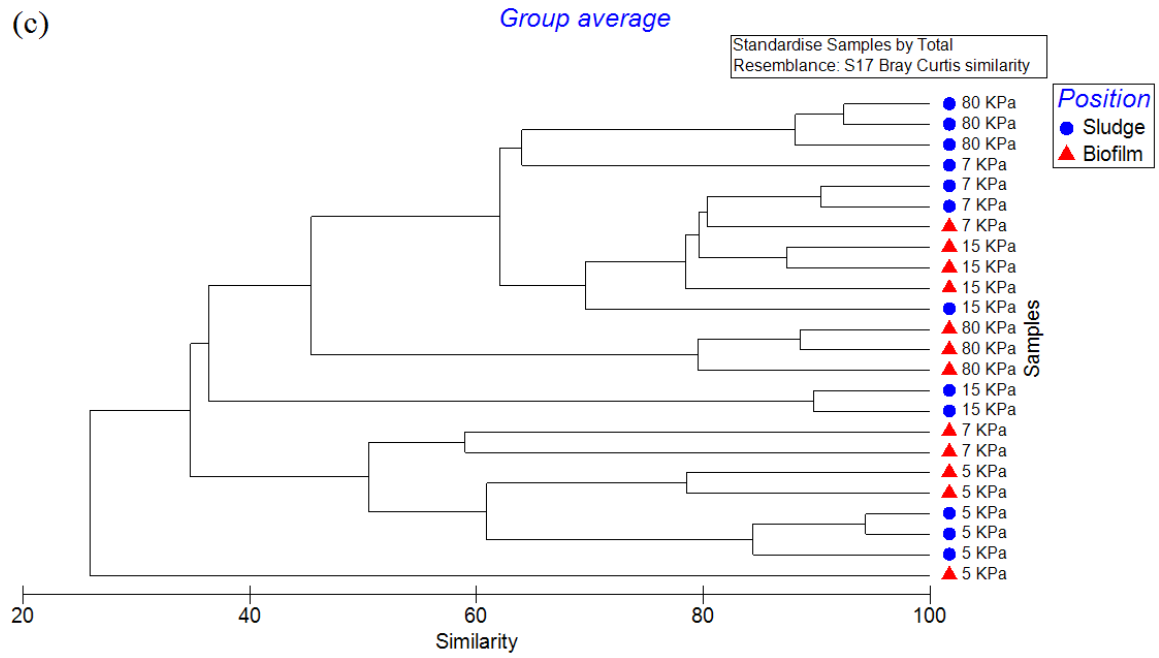

Fig. S4.3 (Continued from previous page) The phylogenetic tree at the Order level for fungi identified in the MBR system in experiment-1 (a), experiment-2 (b) and experiment-3 (c). The blue circles represent the fungal communities in the sludge, and the red triangles represent the fungal communities in the biofilms. The relationships amongst samples were displayed based on the Bray-Curtis similarity between fungal communities which was calculated with the raw abundance data.

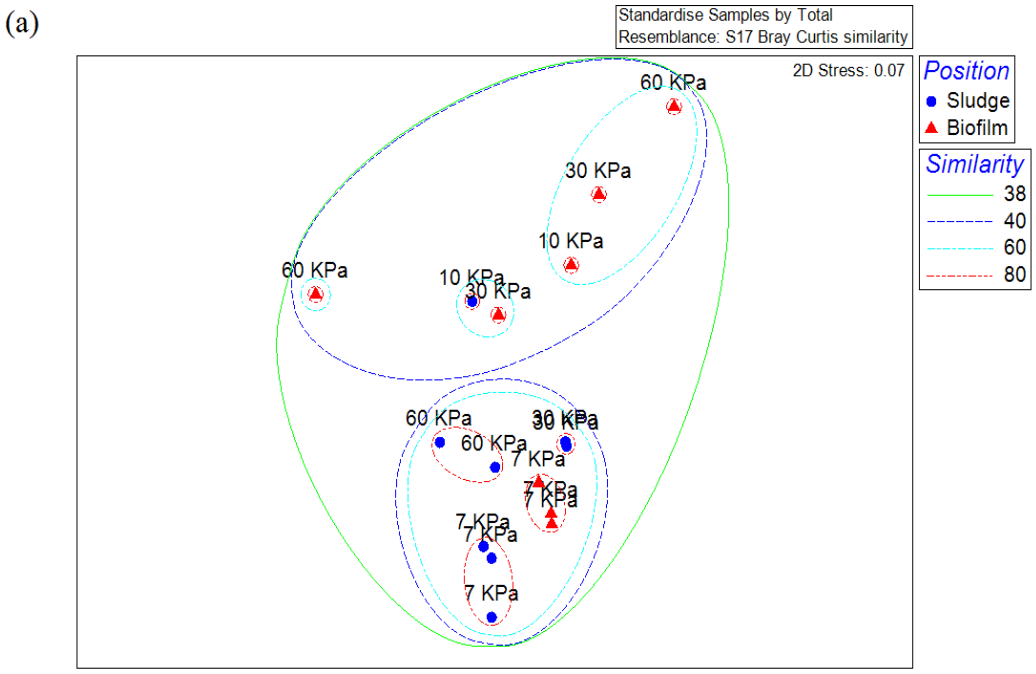

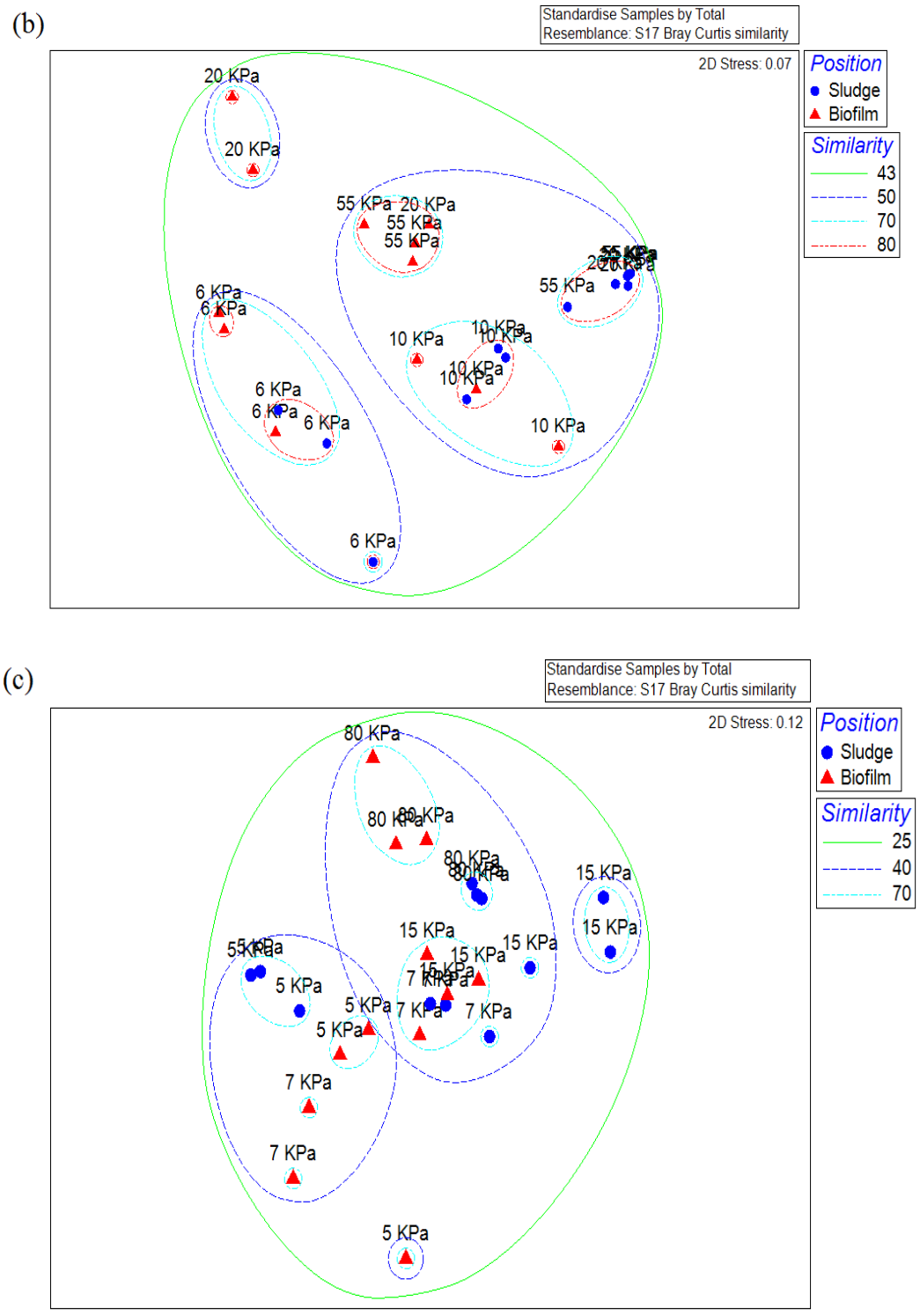

Fig. S4.4 (Continued from the previous page) The NMDS analysis at the Order level for biofilms and activated sludge samples the experiment-1 (a), experiment-2 (b) and experiment-3 (c). The blue circles represent the fungal communities in the sludge, and the red triangles represent the fungal communities in biofilms. The dotted lines show the average Bray-Curtis similarities between samples, where the colored lines indicate different percentage similarities. The Bray-Curtis similarity was calculated with the raw abundance data

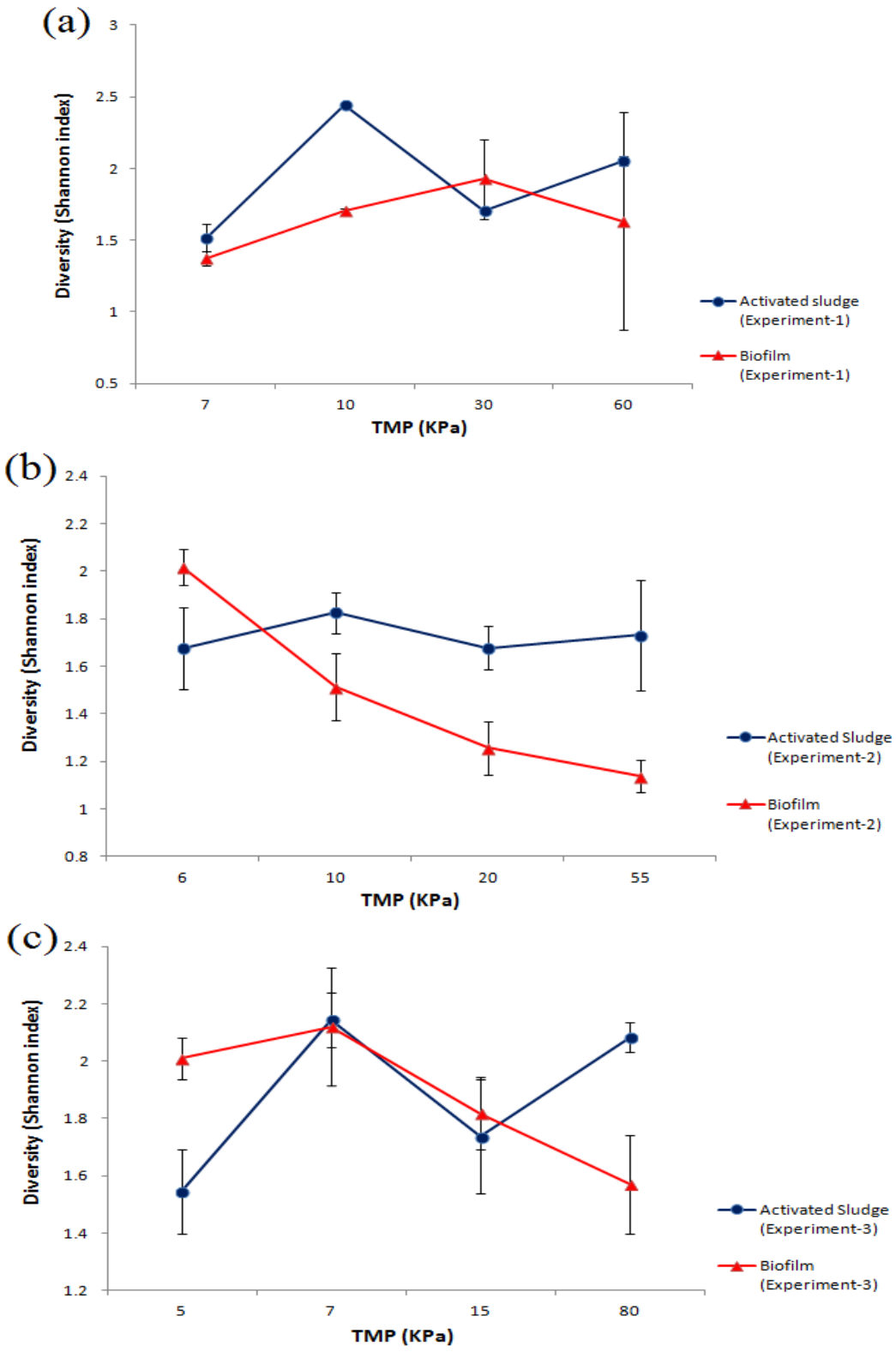

Fig. S4.5 The Shannon diversity of the fungal communities in both activated sludge and biofilm in experiment-1 (a), experiment-2 (b) and experiment-3 (c).

Appendix C The supplementary information for Chapter 5

(a)	Day 71	Day 85
PROLI Treated	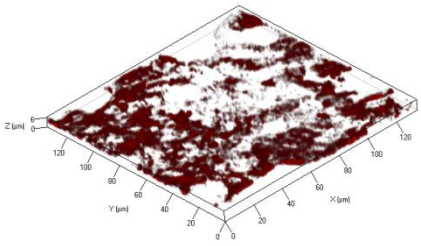	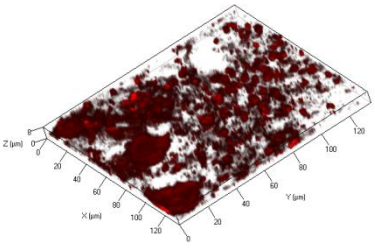
Control	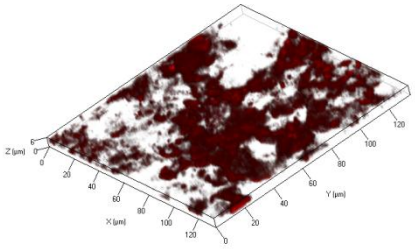	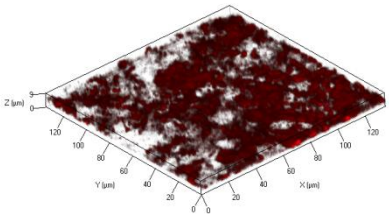

(b)	Day 71	Day 85
PROLI Treated	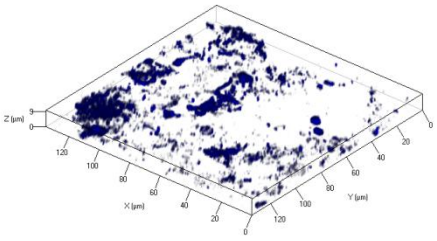	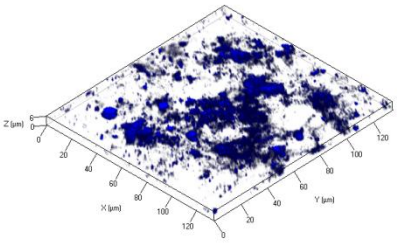
Control	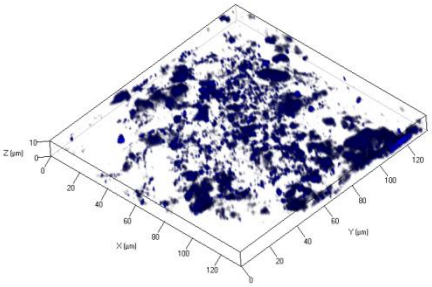	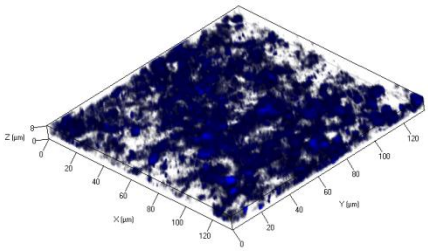

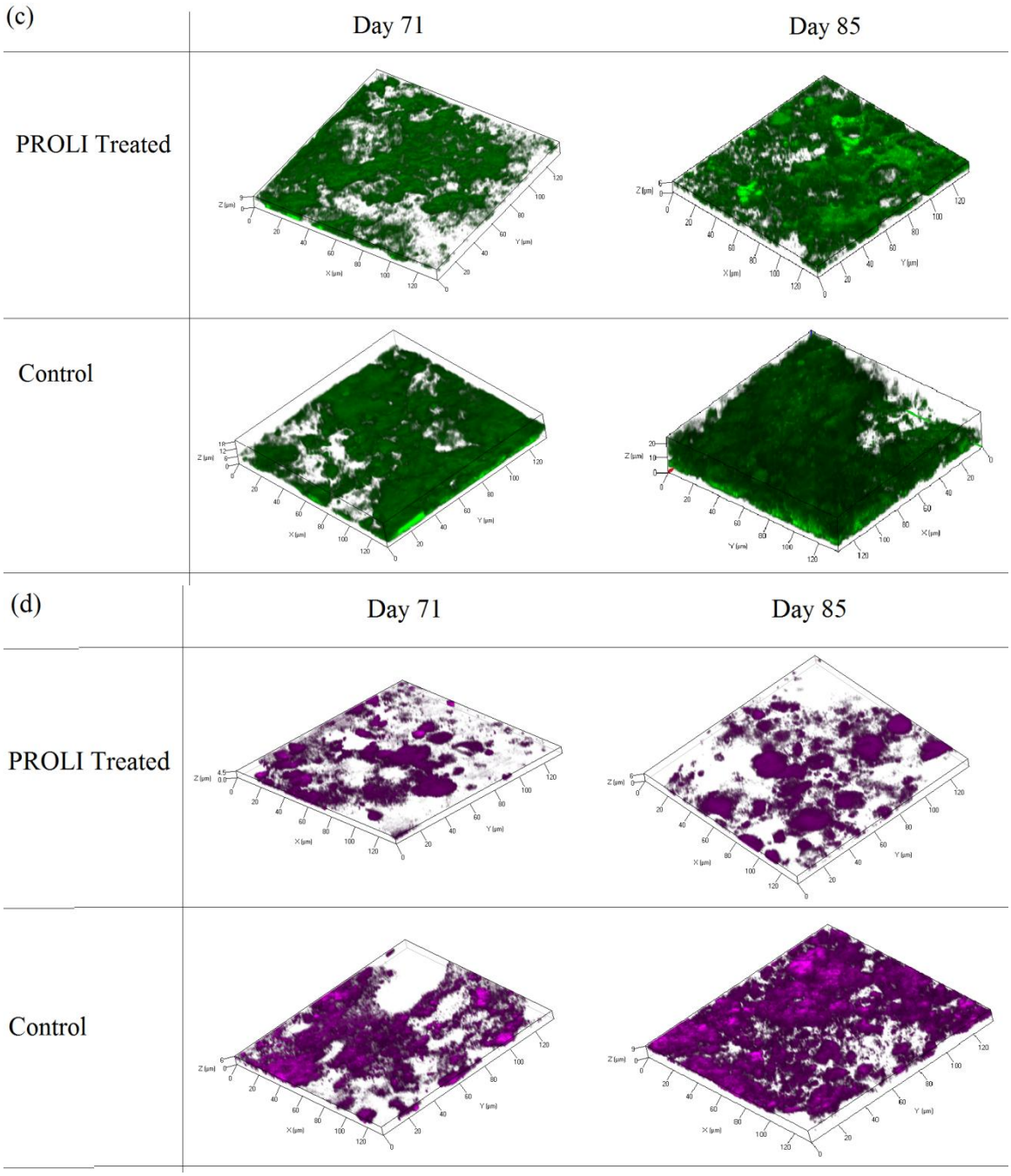

Fig. S5.1 (Continued from previous page) The 3D CLSM images of biofouling components on the PROLI NONOate treated membrane and control membrane. The α-polysaccharides (a) are shown in red, the β-polysaccharides (b) are shown in blue, the proteins (c) are shown in green and the microorganisms (d) are shown in purple. All images are top down projects of 3-D reconstructions of the biofilm. The total magnification for the images was 630×.

Appendix D Quantification of biofilm microbial communities by qPCR

In chapter 3 and 4, the community compositions of bacteria and fungi were studied. Here, we quantified the populations of archaea, bacteria and fungi in the biofilm and activated sludge by qPCR during the MBR operation in experiment-3 and 3 respectively. To facilitate the analysis, the quantity of each microbial group was normalized to the copy number of microbial populations per 1 ng DNA.

Methods and materials

The real time quantitative PCR (qPCR) was performed in a LightCycler 480II system with white LightCycler 96-well Plate (Roche Applied Science). Triplicate samples were used to determine the quantity of DNA copies in biofilm and sludge. The PCR reactions was amplified and tested in a 20 µl reaction system containing 10 µl LightCycler 480 Probes Master (Roche Applied Science), 2 µl forward primer (10 µM), 2 µl reverse primer (10 µM), 2 µl fluorescent TaqMan probe (10 µM), 1 µl DNA template and 3 µl MilliQ water. The primers and probes used in qPCR are listed in the Table 1. A two-step amplification procedure, annealing and extension, was performed, which included one cycle of predenaturation at 95 ℃ for 10 min, 50 cycles of denaturation step at 95 ℃ for 10 sec and simultaneous annealing and extension step at 60 ℃ for 30 sec. The control DNA templates for the standard curves were extracted from *Escherichia coli* K12 (for bacteria), *Saccharomyces cerevisiae* (for fungi), and *Methanobacterium formicicum*, *Methanobrevibacter arboriphilicus*, *Methanospirillum hungatei*, *Methanomicrobium mobile*, *Methanosarcina acetivorans*, *M. barkeri*, *M. mazei* and *Methanosaeta concilli* (for archaea).

Results

The populations of archaea, bacteria and fungi in the biofilm and activated sludge were quantified by qPCR during the MBR operation in experiment-3 and 3 respectively. To facilitate the analysis, the quantity of each microbial group was normalized to the copy number of microbial populations per 1 ng DNA.

Quantity of microbial community in biofilm and sludge.

In experiment-2, the quantities of total bacterial community were observed to maintain at a range of $0.7 \times 10^5 – 2.6 \times 10^5$/ng in the biofilms and $3.3 \times 10^5 – 1.2 \times 10^6$/ng in the sludge across the MBR operation (Fig. Sd1). Similarly, the quantities of fungal communities were $4.9 \times 10^3 – 6.7 \times 10^3$/ng and $6.8 \times 10^3 – 1.3 \times 10^4$/ng in biofilm and sludge respectively (Fig. Sd1).

It was noted that both the bacterial and fungal communities had more populations in activated sludge in comparison with the biofilm samples, indicating the bacteria and fungi had more contributions to compose the microbial community of sludge than the biofilm. The similar variations of bacterial and fungal populations were observed in experiment-3 (Fig. Sd1). The quantities of archaea communities were maintained relative stable in biofilm and sludge in the two experiments, except for the test at 8 kPa at 56 d (Fig. Sd1). The members of archaea were a bit higher in sludge ($2.3 \times 10^2 – 2.1 \times 10^4$/ng) than in biofilm ($0.7 \times 10^2 – 1.0 \times 10^3$/ng) in experiment-2, while no significant difference was observed in the quantities of archaea between the biofilm and sludge in experiment-3, where the populations of archaea were $1.6 \times 10^2 – 1.6 \times 10^3$/ng in biofilm and $0.3 \times 10^2 – 2.4 \times 10^3$/ng in sludge.

Relative abundance of bacteria, fungi and archaea in biofilm and sludge

Compared between the 3 microbial communities, the bacteria were the most abundant community in biofilm (77.8 – 98.4%) and sludge (95.9 – 99.6%) across the whole process of TMP increase, while the fungi were the second abundant community in biofilm (1.5 – 22.1%) and sludge (0.4 – 3.6%) followed by the archaea community (0.01 – 1.1% in biofilm and 0.03 – 1.62% in sludge) in the both experiment-2 and 3 (Fig. Sd2). This indicated that the bacteria dominated the majority of microbial populations in biofilm and sludge in the biofouling process. Additionally, the fungi were observed to contribute more in composing the biofilm community (2.3 – 6.9% in experiment-2, 1.5 – 22.1% in experiment-3) relative to the sludge community (0.6 – 3.6% in experiment-2, 0.3 – 2.2% in experiment-3), indicating the fungi may play a more important role in constructing the biofilm community rather than the sludge community.

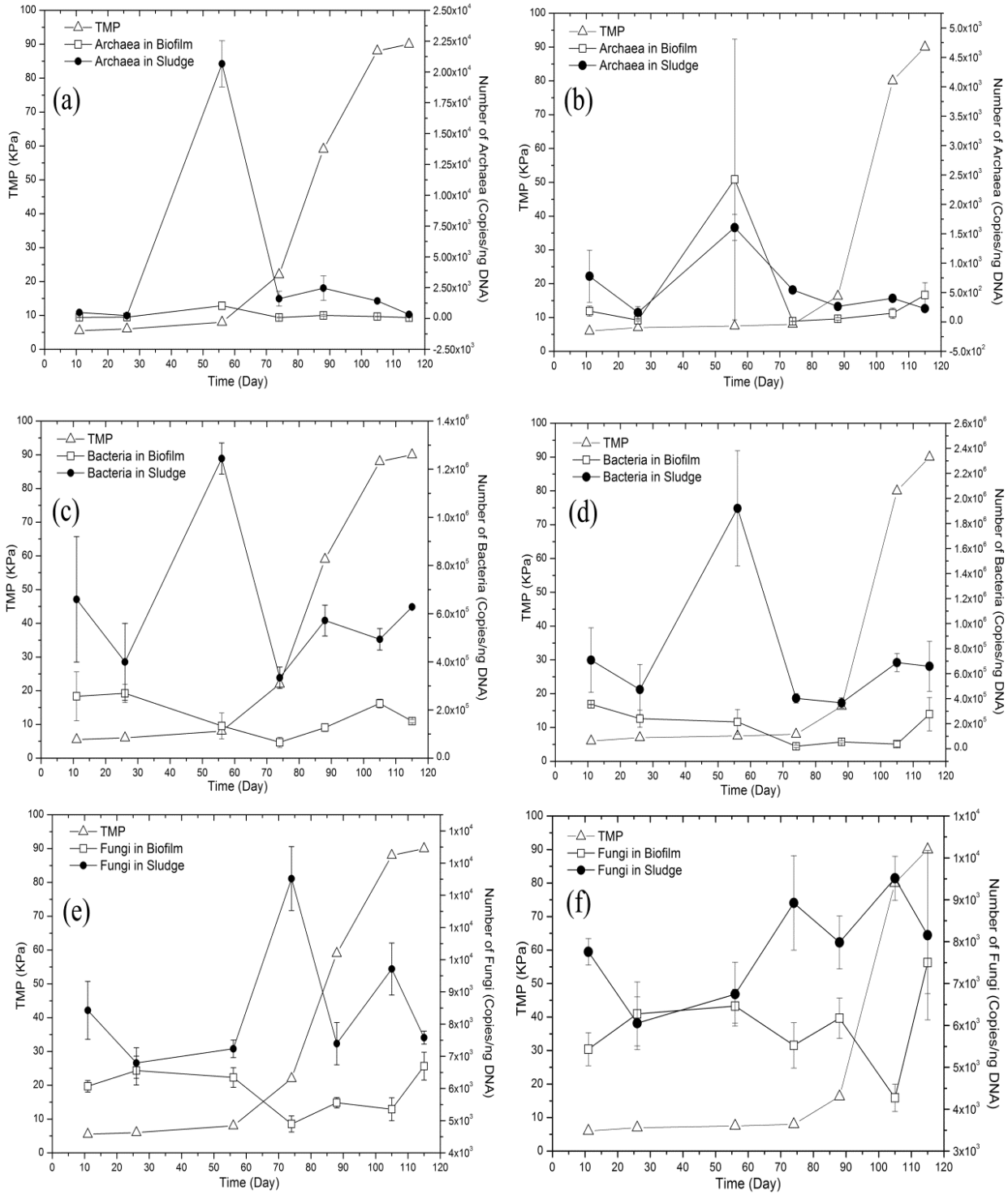

Fig. Sd1 The number of microbial populations in biofilm and activated sludge during the MBR operation. The left "y" axis shows the TMP at different time. The right "y" axis shows the population of archaea, bacteria and fungi in experiment-2 (a, c, e) and experiment-3 (b, d, f) respectively. The values are the average number of the triplicate samples. The error bars are the standard errors of the mean (n=3).

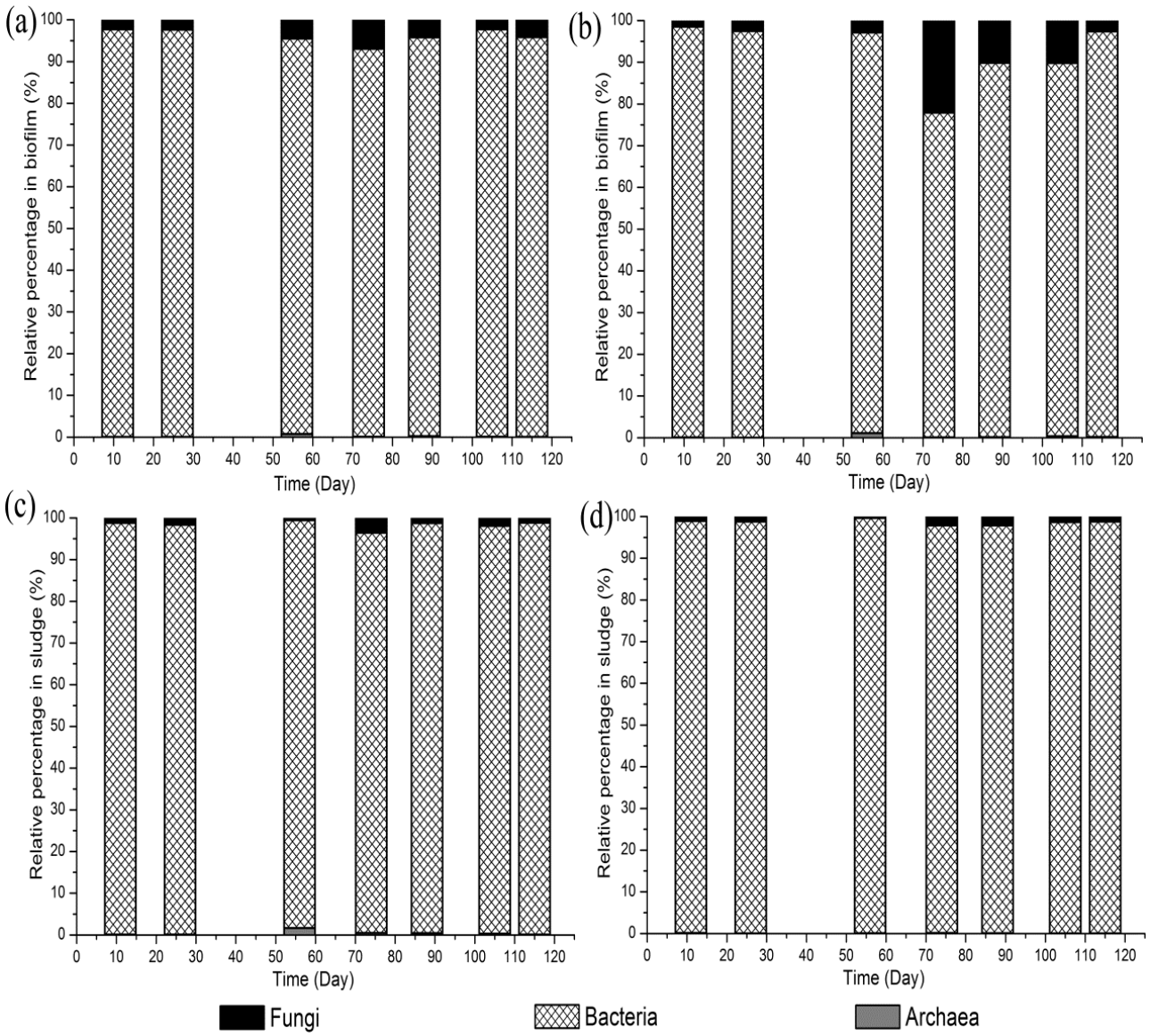

Fig. Sd2 The relative percentage of archaea, bacterial and fungal communities in biofilm and sludge during the MBR operation. The microbial communities were tested in separated experiment-2 (a, c) and experiment-3 (b, d).

Publications

Journal articles

Jinxue Luo, Jinsong Zhang, Xiaohui Tan, Diane McDougald, Guoqiang Zhuang, Anthony G Fane, Staffan Kjelleberg, Yehuda Cohen, Scott A Rice. (2014) The Correlation between biofilm biopolymer comsposition and membrane fouling in submerged membrane bioreactors (MBRs). Biofouling 30(9), 1093-1110

Jinxue Luo, Jinsong Zhang, Xiaohui Tan, Diane McDougald, Guoqiang Zhuang, Anthony G Fane, Staffan Kjelleberg, Yehuda Cohen, Scott A Rice. (2015) Characterization of the archaeal community fouling a membrane bioreactor. Journal of Environmental Sciences, doi:10.1016/j.jes.2014.07.025.

Jinxue Luo, Jinsong Zhang, Xiaohui Tan, Diane McDougald, Guoqiang Zhuang, Anthony G Fane, Staffan Kjelleberg, Yehuda Cohen, Scott A Rice. (2015) The application of nitric oxide to control biofouling of membrane bioreactors. Microbial Biotechnology (Accepted)

Conference Abstracts and Posters

Luo J. X., Rice S. A., Zhang J. S., Fane A. G., McDougald D., Cohen Y., (2011) Unveiling of bacterial community in membrane biofouling of a submerged MBR through pyrosequencing, in "Membrane Science and Technology 2011". Singapore. p. 67.

Luo J.X., Zhang J.S., Fane, A.G., McDougald D., Cohen Y., Rice S.A. (2013) Successional changes in the microbial community compositions of a membrane bioreactor during fouling, in “2nd International Conference on Water Research”. Singapore. p. 223.